



저작자표시-비영리-변경금지 2.0 대한민국

이용자는 아래의 조건을 따르는 경우에 한하여 자유롭게

- 이 저작물을 복제, 배포, 전송, 전시, 공연 및 방송할 수 있습니다.

다음과 같은 조건을 따라야 합니다:



저작자표시. 귀하는 원저작자를 표시하여야 합니다.



비영리. 귀하는 이 저작물을 영리 목적으로 이용할 수 없습니다.



변경금지. 귀하는 이 저작물을 개작, 변형 또는 가공할 수 없습니다.

- 귀하는, 이 저작물의 재이용이나 배포의 경우, 이 저작물에 적용된 이용허락조건을 명확하게 나타내어야 합니다.
- 저작권자로부터 별도의 허가를 받으면 이러한 조건들은 적용되지 않습니다.

저작권법에 따른 이용자의 권리는 위의 내용에 의하여 영향을 받지 않습니다.

이것은 [이용허락규약\(Legal Code\)](#)을 이해하기 쉽게 요약한 것입니다.

[Disclaimer](#)

공학박사 학위논문

**Influence of Internal Curing with  
Superabsorbent Polymer on  
Properties of Ultra-High  
Performance Concrete**

고흡수성 수지에 의한 내부양생이 초고성능  
콘크리트의 특성에 미치는 영향

2017 년 2 월

서울대학교 대학원

건축학과

강 성 훈



**Abstract****Influence of Internal Curing with  
Superabsorbent Polymer on  
Properties of Ultra-High  
Performance Concrete**

Kang, Sung-Hoon  
Department of Architecture and Architectural Engineering  
College of Engineering  
Seoul National University

The internally cured ultra-high performance concrete (UHPC) using superabsorbent polymer (SAP) is developed in this study. The use of SAP has been met with a great interest for a low water to cement ratio (w/c) concrete as a price-competitive shrinkage reducing admixture. Because the developed concrete contains the water reservoir such as SAP, its self-desiccation and resulting autogenous shrinkage can be prevented without external water supply. However, SAP can absorb water or an ionic solution while its volume is expanded up to hundreds or tens of times compared to that of dry state. Thus, along with the formation of reservoirs, large pores that can contribute to the reduction of

mechanical performance are additionally formed within the UHPC; but this reduction is compensated due to the promoted hydration reaction by the released water from the reservoirs. In addition, moisture contents of UHPC is increased due to the water supply, which completely prevent the risk of cracking associated with self-desiccation or autogenous shrinkage. It is also confirmed that increasing the moisture contents is another factor in the strength reduction. However, due to the changed pore structure of UHPC by the swollen SAP particles, the drying speed of UHPC is accelerated; the strength reduction due to high moisture contents can also be avoided by this acceleration. Consequently, the water entrainment using SAP can completely solve the cracking risk of UHPC without the deterioration of mechanical performance, workability and price competitiveness.

The amount of the required extra water to prevent the self-desiccation can be designed based on previous theories. However, the ideal result that the risk is solved without any adverse effect on strength or workability of UHPC only happens when this amount is accurately absorbed by the reservoir, SAP. In other words, if SAP absorbs a water less or more than the designed amount, mechanical performance or workability should be decreased, respectively. Therefore, the optimal SAP proportion can be determined only if SAP's water absorption and retain capacities within the concrete are fully understood. The understanding these capacities is also crucial to investigate water absorption and release behaviors of SAP in low w/c concrete that have not been fully explained yet. These complex behaviors are described in this study. As a first step, the method to measure the absorbency of SAP in various cement-based solutions is newly suggested. This method includes a centrifugal process to

remove excess solution that can cause inaccurate measurement. Depending on the monovalent ion concentrations under the given  $\text{Ca}^{2+}$  concentration in a cementitious materials, the absorption kinetics of SAP is drastically altered. This result underlines the risk of underestimation on absorption capacity of SAP. The suggested method and cement-based solutions can be used to reasonably and efficiently determine the amount of extra water prior to the mix design for internal curing (IC) purpose. Furthermore, the investigated ion-dependent characteristics herein can not only enhance the understanding of the absorption kinetics of SAP, but also contribute to the development of hydrogel products for concrete.

In addition to these findings, the effects of ion composition and the concentration of cement-based solutions on the retention capacities of SAP are investigated. The ion concentration history and absorbency test of SAP verify that a reduction in long-term absorption occurs from an irreversible ion exchange between  $\text{Ca}^{2+}$  and the anionic groups of SAP; thus, the  $\text{Ca}^{2+}$  concentration in a solution is a decisive factor for the absorption and retention capacities. Furthermore, this reduction of absorption is also highly dependent on the concentrations of the other ions in the solution (i.e., mono valent ions). The retention capacity is improved as the total ion concentration, which is influenced by these concentrations, increases because a higher total ion concentration indicates a weaker osmotic pressure (driving force of absorption of SAP), which reduces the maximum absorbency along with the effect of the trapped  $\text{Ca}^{2+}$  in SAP. With the help of herein determined ionic factors for the prepared cement-based solutions, the complicated absorption and retention behaviors of SAP in concrete can be understood.

Characteristics of pore structure of internally cured UHPC are rigorously investigated by 3D computed tomography as well as mercury intrusion porosimetry analysis (MIP). Pores from SAP are successfully separated from others such as entrapped pores based on the 3D image processing method. Measured total porosity of UHPC with and without SAP is 2.5% and 6.0%, respectively, which means that a significant increase in volume due to the large pores is actually confirmed by CT analysis. In other words, the volume expansion of SAP produces additional large size pores in UHPC which can reduce the mechanical performance. However, the MIP analysis provides the evidence that the reduced strength can be compensated; hydration products are additionally formed due to IC, which reduces capillary voids associated with strength. The reason for the contradictory results of the two methods is that the pore sizes that can be detected by them are different. By using these two methods, both hydration promotion by IC and large size pores formed by swollen SAP particles can be verified in this study.

Based on the confirmed results (such as the absorption and retention capacity of SAP, the effectiveness of IC on the improvement of degree of hydration, and change of pore structure), the characteristics of hydration reaction, shrinkage, internal relative humidity (RH) and mechanical performance are investigated. Considering the practicality of the developed concrete, these investigations were divided into precast UHPC containing heat treatment (HT) and field-cast UHPC. Firstly, fundamental shrinkage characteristics of heat-treated UHPC is understood and shrinkage and cracking problems under HT using SAP is mitigated. The HT accelerates the hydration of UHPC, including pozzolanic reaction, which causes additional self-

desiccation. Consequently, UHPC experiences severe shrinkage during the HT period. However, this study successfully verifies that the increased shrinkage due to HT can be fundamentally resolved by applying SAP-based IC method. The accurately performed experiments herein can help to further understand the shrinkage characteristics of heat-treated UHPC, and be used to broaden its application.

In addition, the effects of IC by SAP on the properties of field-cast UHPC are investigated. Hydration heat, internal relative humidity (RH), compressive strength, and shrinkage are accurately measured over time. The influence of moisture content is set as the main parameter to analyze the complex interdependent relationship. The promotion of hydration reaction and mitigation of self-desiccation by IC are closely related to the internal RH history. Maintaining a high internal RH by IC causes loss of strength. However, this loss can be recovered because the internal RH is decreased again when the internally cured UHPC is exposed to a dry air of field curing condition. That is, the drying speed of the concrete is accelerated due to the changed pore structure by SAP. When considering the two conflicting humidity-related effects on shrinkage and strength, sealed curing for the first 7 d is suggested as a reasonable way, and is also recommended by specifications for field-cast concretes.

In this study, the shrinkage and cracking problems of UHPC are fundamentally solved by water entrainment or IC method using SAP. This method does not cause any loss in price competitiveness and usability of the concrete. In addition, the newly proposed methods (for measuring absorption

behavior of SAP in concrete, shrinkage of heat treated UHPC, internal RH history within concrete) also can be used for new discoveries in other studies. In addition, the firstly verified experimental results of this study (SAP's water retention capacity in low w/c concrete, severe shrinkage of heat-treated UHPC and its solution, and rapid drying characteristics and recovery of strength by it) can contribute to promotion of the practical use of IC in the field of concrete.

**Keywords : Ultra-high performance concrete, internal curing, water entrainment, superabsorbent polymer, material property, self-desiccation, autogenous shrinkage**

**Student Number : 2010-30158**

# Contents

<b>Abstract</b> .....	<b>i</b>
<b>Contents</b> .....	<b>vii</b>
<b>List of Tables</b> .....	<b>x</b>
<b>List of Figures</b> .....	<b>xi</b>
<b>List of Abbreviations</b> .....	<b>xvi</b>
<b>Chapter 1. Introduction</b> .....	<b>1</b>
1.1 Ultra-high performance concrete (UHPC) .....	1
1.2 Internal curing and its necessity for UHPC .....	7
1.3 Scope .....	12
1.4 Objective.....	13
1.5 Organization .....	14
<b>Chapter 2. Water entrainment properties of superabsorbent polymer (SAP)</b> .....	<b>17</b>
2.1 Introduction .....	17
2.2 Literature review on application of SAP for concrete .....	21
2.3 Basic principles of internal curing.....	24
2.4 SAP used in this study .....	32
2.5 Design of extra water.....	35

**Chapter 3. Absorption kinetics and retention capacity of SAP in cementitious materials..... 37**

3.1 Absorption kinetics of SAP in low water to cement ratio concrete ..... 37

    3.1.1 Introduction ..... 37

    3.1.2 Materials and methods..... 44

    3.1.3 Results and discussion..... 52

    3.1.4 Summary and concluding remarks ..... 83

3.2 Absorption and retention capacities of SAP depending on ion concentration ..... 87

    3.2.1 Introduction ..... 87

    3.2.2 Materials and methods..... 90

    3.2.3 Results ..... 94

    3.2.4 Discussion..... 106

    3.2.5 Summary and concluding remarks ..... 121

**Chapter 4. Hydration reaction and microstructure..... 125**

4.1 Introduction ..... 125

4.2 Materials and methods..... 129

    4.2.1 Sample preparation..... 129

    4.2.2 Test methods..... 132

4.3 Results and discussion ..... 134

    4.3.1 Literature study on heat evolution by cement hydration ..... 134

    4.3.2 X-ray diffraction (XRD) analysis ..... 136

    4.3.3 Scanning electron microscope (SEM) analysis ..... 138

    4.3.4 Pore structure by 3D-computed tomography (CT) analysis ..... 139

    4.3.5 Pore-size distribution and total porosity by mercury intrusion porosimetry (MIP) and 3D-CT analysis ..... 151

4.4 Summary and concluding remarks ..... 156

---

<b>Chapter 5. Properties of internally cured ultra-high performance concrete (UHPC) .....</b>	<b>157</b>
5.1 Precast UHPC .....	157
5.1.1 Introduction .....	157
5.1.2 Experiment methods .....	160
5.1.3 Results and discussion .....	166
5.1.4 Summary and concluding remarks .....	192
5.2 Field-cast UHPC .....	194
5.2.1 Introduction .....	194
5.2.2 Experiment methods .....	201
5.2.3 Results and discussion .....	205
5.2.4 Summary and concluding remarks .....	234
<b>Chapter 6. Conclusions .....</b>	<b>237</b>
<b>References .....</b>	<b>241</b>
<b>Appendix A. SEM images of raw materials and UHPC samples .....</b>	<b>268</b>
<b>초    록 .....</b>	<b>273</b>

## List of Tables

Table 3-1 Ion concentration of used superplasticizer by ICP-OES analysis .....	45
Table 3-2 Mix proportion and ion concentration of solutions .....	46
Table 3-3 Comparison of SAP absorbencies determined by tea-bag and slump flow methods .....	81
Table 3-4 Ionic concentration and strength of solutions.....	92
Table 4-1. Mix proportion of developed ultra-high performance concrete (UHPC).....	131
Table 4-2 Oxide compositions of raw materials (wt.%).....	131

## List of Figures

Fig. 1-1 Variation of relative density as a function of water and air contents.....	4
Fig. 1-2 Physical and chemical lubricating mechanisms by silica fume (a) and superplasticizer (b).....	5
Fig. 1-3 Pantheon in Rome, the world's largest unreinforced dome ....	11
Fig. 1-4 Schematic illustration of internal curing.....	12
Fig. 1-5 Organization of thesis .....	15
Fig. 2-1 Volume expansion of SAP after absorbing tap water.....	19
Fig. 2-2 Schematic illustration of volume change of SAP in cementitious materials .....	20
Fig. 2-3 Volumetric phase distribution of cement paste as a function of degree of hydration at $w/c=0.36$ (a) and $w/c=0.36+0.06$ (b).....	26
Fig. 2-4 Design extra water theoretically required to prevent self-desiccation of cement paste with or without silica fume.....	31
Fig. 2-5 SEM images of SAP_AA (a) and SAP_AM (b).....	32
Fig. 2-6 Particle size distribution (a) and cumulative distributions (b) of SAPs .....	34
Fig. 3-1 Tea-bag method using various solutions.....	51
Fig. 3-2 Absorbency of SAPs in distilled water and solution A as a function of centrifugation time.....	53
Fig. 3-3 Relationship between absorbencies without centrifugation and excess solution: Results including (a) and excluding (b) distilled water .....	55
Fig. 3-4 Absorbency of SAPs in distilled water (a) and solution A (a) with standard deviation.....	57
Fig. 3-5 Ion concentration ratio of cement filtrate with (a) or without (b) silica fume as a function of $w/c$ .....	60
Fig. 3-6 Variation of ion concentration due to silica fume addition as function of $w/c$ (a), and effect of PCE to water ratio on ion concentration of cement based solution ( $w/c = 0.4$ ) with (b) or without (c) silica fume	

.....	62
Fig. 3-7 Structure of swollen polyacrylate SAP .....	66
Fig. 3-8 Effect of w/c on absorption kinetics of SAP in cement filtrates: without silica fume (a) and with silica fume (b).....	69
Fig. 3-9 Effect of silica fume addition on absorbency of SAPs in cement filtrates: w/c = 2 (a) and 4 (b).....	72
Fig. 3-10 Effect of PCE on absorbency of SAPs in cement filtrates of w/c = 0.4.....	73
Fig. 3-11 Effect of additional monovalent ions ( $\text{Na}^+$ , $\text{K}^+$ and $\text{OH}^-$ ) on absorbency of SAPs in cement filtrates.....	74
Fig. 3-12 Slump spread value of UHPC with or without SAPs .....	80
Fig. 3-13 Effect of the monovalent ion concentration ( $\text{Na}^+$ and $\text{Cl}^-$ ) on the absorbencies of SAP_AA (a) and SAP_AM (b): the absorbencies in Sol. 1 and Sol. 2 are scaled down by 1/9 and 1/3, respectively.....	98
Fig. 3-14 Effect of the cation charge number ( $\text{Na}^+$ vs. $\text{Ca}^{2+}$ ) on the absorption kinetics of SAP_AA (a) and SAP_AM (b) at a cation concentration of $24.5 \pm 0.8$ mM .....	100
Fig. 3-15 Effect of $\text{Ca}^{2+}$ concentration (1.6 mM vs. 21.9 mM) on the absorption kinetics of SAP at a total ion concentration of $982.5 \pm 12.3$ mM .....	102
Fig. 3-16 Effect of the $\text{Na}^+$ concentration on the absorption kinetics of SAP_AA (a) and SAP_AM (b) at a $\text{Ca}^{2+}$ concentration of $22.5 \pm 1.5$ mM in the solutions.....	104
Fig. 3-17 Effect of the monovalent cation concentration on the absorption kinetics of SAP_AA (a) and SAP_AM (b) at a $\text{Ca}^{2+}$ concentration of $20.3 \pm 2.3$ mM in the cement filtrates.....	105
Fig. 3-18 SAP absorbency at 1 min at a $\text{Ca}^{2+}$ concentration of $20.8 \pm 2.8$ mM as a function of the total ion concentration.....	107
Fig. 3-19 Relationship between the initial (at 10 min) and long-term (at 180 min) absorbencies of SAP_AA .....	107
Fig. 3-20 Average absorption speed (AAS) between 0-10 min and 60- 180 min of SAP_AA (a) and SAP_AM (b) as a function of the total ion concentration .....	109
Fig. 3-21 Change of the ion concentration in solutions caused by ion	

trapping or releasing by SAP_AA (a) and SAP_AM (b) .....	112
Fig. 3-22 Schematic of the initial absorbency-dependent ionic cross-linking effect and retention capacity of polyacrylate SAP in cement-based solutions: with a high initial absorbency (a) and with a low initial absorbency (b) .....	116
Fig. 3-23 Total ion concentration and ionic strength of cement pore solutions (w/c=0.4 and 0.5) during long-term (a) and early (b) ages based on five ions ( $\text{Na}^+$ , $\text{K}^+$ , $\text{Ca}^{2+}$ , $\text{SO}_4^{2-}$ , and $\text{OH}^-$ ).....	119
Fig. 4-1 Multi-scale pore network in a hydrated cement paste .....	128
Fig. 4-2 Particle size distributions of raw materials used in developed UHPC .....	130
Fig. 4-3 Typical hydration heat curve of cement paste.....	135
Fig. 4-4 Results of XRD analysis of cement and UHPC pastes: X-ray Rietveld analysis of AA_0.255 (a), and quantitative results of all samples (b) .....	137
Fig. 4-5 SEM images of internally cured UHPC (AM_0.275).....	138
Fig. 4-6 2D-CT images with different threshold values .....	139
Fig. 4-7 3D-rendering images of UHPC with SAP (left) and pores/fibers segmentation (right).....	140
Fig. 4-8 Fiber orientation analysis of Ref_0.215 on vertical (top) and horizontal (bottom) directions .....	141
Fig. 4-9 Orientation of steel fibers on vertical (top) and horizontal (bottom) directions .....	143
Fig. 4-10 Cumulative distributions of pore volumes with different threshold values (20, 25, 30, 35, and 40/256) .....	145
Fig. 4-11 Computed total porosity as a function of segmentation threshold .....	146
Fig. 4-12 Pore number as a function of volume .....	147
Fig. 4-13 Scatter distribution of measured surface areas and volumes from pores.....	147
Fig. 4-14 3D-rendering images of Ref_0.215 (UHPC), AM_0.275 (UHPC_SAP), and only SAP pores in AM_0.275 .....	148
Fig. 4-15 Normalized distribution of computed pore anisotropy .....	150

List of Figures

---

Fig. 4-16 Distribution of  $I_{22} / I_{11}$  and  $I_{33} / I_{11}$  of pores in Ref\_0.215 (left) and only SAP pores in AM\_0.275 (right)..... 150

Fig. 4-17 Distribution of measured closest distance of all pores in Ref\_0.215 and SAP pores in AM\_0.275 ..... 151

Fig. 4-18 Pore size distribution of UHPC by MIP (a) and 3D-CT (b) methods..... 154

Fig. 4-19 Total porosity of UHPC by MIP and 3D-CT methods..... 155

Fig. 5-1 Free strain measurement for shrinkage test (a) and curing program for heat treated UHPC (b)..... 161

Fig. 5-2 Modified FreshCon system by this study (a), preparation of device for “time zero” (b), and measured UPV of sample over time (c) ..... 163

Fig. 5-3 Heat flow of hydration (a) and cumulative heat (b) of UHPC cured under 20 °C for 2 days then successively under 60 °C for 3 days ..... 167

Fig. 5-4 Heat flow of hydration (a) and cumulative heat (b) of UHPC cured under 20 °C for 2 days then successively under 90 °C for 2 days ..... 168

Fig. 5-5 Heat flow of hydration (a) and cumulative heat (b) of UHPC during heat treatment period..... 171

Fig. 5-6 Section of specimen used for shrinkage test of UHPC..... 173

Fig. 5-7 Shrinkage behaviors of heat treated UHPC: Ref\_0.215 (a), Ref\_0.255 (b). TS before 7 d was determined by the average of SS\_1<sup>st</sup> and SS\_2<sup>nd</sup>. ..... 176

Fig. 5-8 Shrinkage behaviors of heat treated UHPC during the first 6 days ..... 178

Fig. 5-9 Sealed shrinkage at the end of heat treatment (negative value indicates expansion) ..... 183

Fig. 5-10 Strain rates of heat treated UHPC during the first 6 days: Ref\_0.215 (a), Ref\_0.255 (b) ..... 188

Fig. 5-11 Sealed and drying shrinkages of UHPC at 28 days (bold numbers on the chart mean total shrinkages) ..... 191

Fig. 5-12 Specimen for internal RH of UHPC (a) and accuracy test of RH sensor (b)..... 203

---

Fig. 5-13 Heat flow (a) and cumulative heat of hydration (b).....	206
Fig. 5-14 Internal RH histories of UHPC under air-dry curing condition (20 °C and RH 60%) (a), and water curing condition (20 °C) (b).....	209
Fig. 5-15 Early-age shrinkage behavior of three replicates for each specimen ( $\nabla$ symbols indicate defined time zero points from UPV measurement).....	214
Fig. 5-16 Total and autogenous shrinkages of designed UHPC: Ref_0.215 (a), Ref_0.255 (b) .....	216
Fig. 5-17 Autogenous and drying shrinkages of UHPC at 28 days under air-dry curing condition (bold numbers on each chart mean total shrinkages).....	221
Fig. 5-18 Strain rates of UHPC: Ref_0.215 (a), Ref_0.255 (b).....	222
Fig. 5-19 Compressive strength development of UHPC under air-dry curing condition (20 °C and RH 60%) (a), and water curing condition (20 °C) (b).....	224
Fig. 5-20 Compressive strength ratios of 28 d to 7 d (a), air-dry curing to water curing (b) .....	226
Fig. 5-21 Compressive strength change based on decreased internal RH by evaporation between 7 d and 28 d (a) and increased internal RH by water curing (b) .....	233

## List of Abbreviations

AAS	Average absorption speed
AS	Autogenous shrinkage
ASTM	American Society for Testing and Materials
CT	Computed tomography
CTE	Coefficient of thermal expansion
DEF	Delayed ettringite formation
DS	Drying shrinkage
DSP	Densified small particles
EA	Expansive agent
ESR	Equilibrium swelling ratio
HPC	High performance concrete
HPM	High-performance mortar
HT	Heat treatment
IS	Ionic strength
MDF	Macro defect free
MIC	Monovalent ion concentration
MIP	Mercury intrusion porosimetry
PCE	Polycarboxylate-ether
RH	Relative humidity
RPC	Reactive powder concrete
SEM	Scanning electron microscope
SF	Silica fume
SIFCON	Slurry infiltrated fibered concrete
SPPL	Superplasticizer
SRA	Shrinkage reducing agent
SS	Sealed shrinkage
TIC	Total ion concentration
TS	Total shrinkage
UHPC	Ultra-high performance concrete
UPV	Ultra-pulse velocity
XRD	X-ray diffraction

# Chapter 1. Introduction

## 1.1 Ultra-high performance concrete (UHPC)

Ultra-high performance concrete (UHPC) exhibits outstanding compressive strength (over 150 MPa), durability, and ductile behavior under tension owing to its incorporated metallic fibers (Association Française De Génie Civil (AFGC), 2013; Korea Concrete Institute (KCI), 2012; Japan Society of Civil Engineers (JSCE), 2004). By considering various applications, including architectural non-structural components, a recently revised recommendation has classified UHPC as concrete with a strength of over 130 MPa that contains specific types of fibers, such as synthetic fibers (Toutlemonde & Delort, 2016).

Developments in concrete technology have progressed remarkably over the last 30 years. These developments have mostly focused on improving concrete strength (Vande Voort, Suleiman & Sritharan, 2008). In the 1980s, there were some pioneering studies on the improvements in this area. Densified small particles (DSPs) were developed via the compact granular matrix concept using silica fume and superplasticizers (Bache, 1981). Very hard aggregates were also incorporated into DSPs to further increase their compressive strength. The bending strength of concrete has been increased (by more than 150 MPa) by incorporating polymers into cement paste, forming macro defect free (MDF) paste (Kendall, Howard, Birchall, Pratt, Proctor & Jefferis, 1983). The ductility of state-of-the-art concrete has been increased by adding steel fibers as in the

slurry infiltrated fibered concrete (SIFCON) (Lankard, 1984). The preferential characteristic these materials, along with the potential of the minimum defect strategy of concrete fabrication contributed the emergence of UHPC (Vande Voort *et al.*, 2008).

The basis of the material composition of the current iteration of UHPC originally comes from the development of reactive powder concrete (RPC), which was developed in the 1990s (Richard & Cheyrezy, 1995). Since then, UHPC has been commercialized globally. State-of-the-art commercial UHPC products follow the same composition and curing methods as RPC 200, whose compressive strength is approximately  $200 \pm 30$  MPa; the following five principles were established to insure the outstanding performance of RPC (Richard & Cheyrezy, 1995).

- Improve the homogeneity by eliminating coarse aggregates.
- Ensure the mix proportion is compactly composed by applying packing density theory as well as keeping the water to cement ratio (w/c) extremely low.
- Enhance the microstructure by undertaking heat treatment (HT) (generally 90 °C for 48 h) or autoclave curing (if necessary).
- Prevent brittle failure, and increase ductility and tensile strength by incorporating short steel fibers (generally 13 mm in length) into the concrete.

- Maintain optimized mixing and casting procedures.

The most influential factor that contributes to the development of UHPC over 150 MPa, is the packing density (De Larrard & Sedran, 1994). Unlike previous generations of concrete, the ultra-high strength of RPC was achieved by maximizing the density using small particles (less than 400  $\mu\text{m}$  instead of the usual 10-20 mm). The packing density is defined as the volume ratio of the sum of solid particles to a container which encloses the particles. The relative density is the ratio of the density of a real mixture to the density of ideal mixture in which no air and water are included. These defined densities are directly related to the compressive strength and elastic modulus of concrete. Fig. 1-1 shows the value of the relative density of RPC mixtures as a function of the water to binder ratio (w/b) and air content (Richard & Cheyrezy, 1995). This graph explains the influence of relative density on the mechanical properties of RPC or UHPC. In fresh UHPC, non-solid materials (e.g. liquid and air) are classified as voids, and thus the void fraction is defined as the sum of the air and water volume in the concrete. At the theoretical optimum w/b point (point B) the maximum relative density is achieved. If the w/b is decreased below this point the water content in the concrete reduces, however the air content increases due to the loss of flowability, causing a decrease in density. When the w/b increases above the optimal value, the air content decreases due to the improved flowability, however the increased water content decreases the density. In practice the optimum point is not at the point B, but between points B and D, when taking into account the hydration reaction and workability of UHPC (Richard & Cheyrezy, 1995).

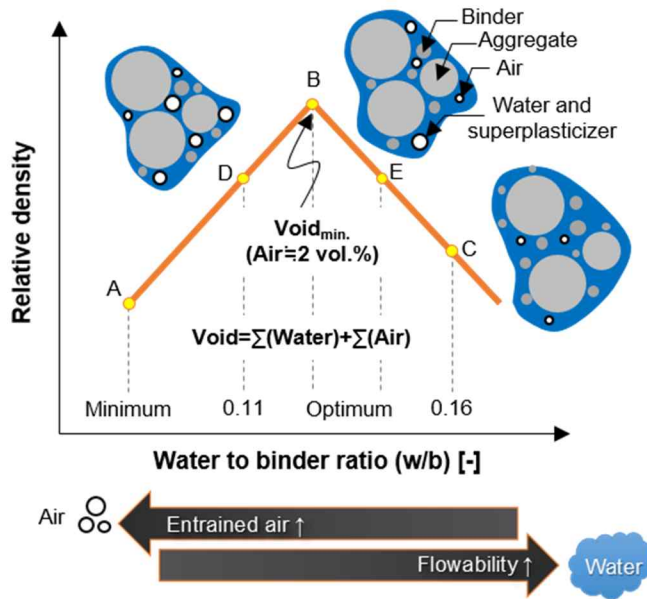


Fig. 1-1 Variation of relative density as a function of water and air contents  
(Richard & Cheyrezy, 1995)

Fresh UHPC has superior flowability and self-compacting ability in spite of its extremely low w/c. This offers another advantage in the field of architecture, i.e., designers or architects can express any desired shape and texture (and even color by using a pigment) precisely in real structures. Both physical effects of micro particles (such as silica fume and silica flour), and chemical effects of polycarboxylate (PCE) type superplasticizer (SPPL) control the flowability mechanism of UHPC. The physical mechanism of flowability is illustrated in Fig. 1-2 (a). Globular silica fume particles, located between other solids such as cement, silica flour, and silica sand, can be described as acting like ball bearings (Sugano, 2008). The ball bearing effect is dependent on the degree of dispersion. In preliminary tests, fresh UHPC with non-densified silica

fume displayed a 43.7% higher slump spread value than UHPC with densified silica fume. Thus, non-densified silica fume was adopted for the optimized mix proportion of UHPC in this study. The chemical effect can be explained by the elastostatic repulsive forces of electric double layers (Fig. 1-2 (b)), and steric hindrance by side chains of PCE type SPPL (Tue, Ma & Orgass, 2008). These forces and hindrances interrupt and delay the attraction of cement particles to one another.

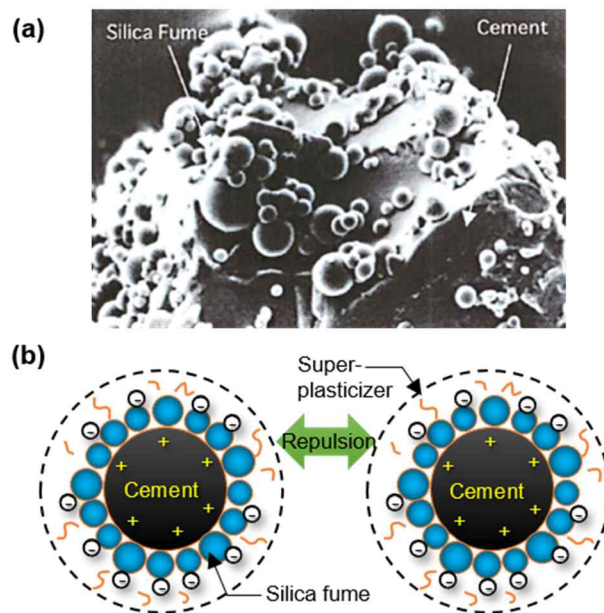


Fig. 1-2 Physical and chemical lubricating mechanisms by silica fume (a) and superplasticizer (b)

(Sugano, 2008)

Based on the principles of the composition of RPC, this study successfully developed a UHPC using raw materials available in the Korean domestic

market. The UHPC has a compressive strength of 150-200 MPa and a direct tensile strength of more than 10 MPa, depending on curing temperatures (20-90 °C). A compressive strength of even 300 MPa was possible by varying the raw materials and curing temperature (200 °C). However, practically temperatures over 100 °C are undesirable, therefore, temperatures of 20-90 °C were considered for the developed UHPC. The optimized w/c and w/b ratio for the UHPC was 0.215 and 0.172, respectively, which is slightly higher than the w/c of RPC 200 (0.15-0.19) and the recommended w/b in Fig. 1-1. During the development process, one concern of this study was the price competitiveness of the concrete, thus, the maximum size of the fine aggregates and the SPPL (solid contents) to cement ratio (SPPL/c) were determined as 2 mm and 1.2%, respectively. The size and ratio for RPC 200 were 0.4 mm and 1.6-1.9%, respectively. It can be safely inferred that a larger amount of water was required to achieve the superior flowability because of the relatively large aggregates and low SPPL/c. Therefore, the compressive strength of UHPC (150-200 MPa) was 20-30 MPa lower than that of RPC 200 (170-230 MPa).

Aside from the outstanding performances of fresh and hardened UHPC, problems arise due to the compact composition and low w/c condition, as well as the HT. In the case of UHPC, a large proportion of the total shrinkage (TS) is owed to autogenous shrinkage (AS) (Vande Voort *et al.*, 2008; Japan Society of Civil Engineers (JSCE), 2004; Zhang, Tam & Leow, 2003). The silica fume addition and low w/c conditions accelerate the self-desiccation and resultant AS (Lura, Jensen & Van Breugel, 2003; Jensen & Hansen, 1996). This is because the chemical shrinkage, the driving force of AS, is accelerated because of the pozzolanic reaction that occurs due to the inclusion of silica fume ( $6 \text{ cm}^3 / 100$

g of cement vs. 22 cm<sup>3</sup> / 100 g of silica fume); this phenomenon also results in a finer pore structure (Bentz & Jensen, 2004). The pozzolanic reaction highly depends on the curing temperature (Maruyama & Teramoto, 2013; Vande Voort *et al.*, 2008; Zanni, Cheyrezy, Maret, Philippot & Nieto, 1996; Richard & Cheyrezy, 1995); specifically, the HT accelerates the reaction between the silica fume and portlandite (Schachinger, Hilbig & Stengel, 2008). This causes a change in the microstructure due to the additional formation of C-S-H (Richard & Cheyrezy, 1995). Thus, as a result of the short HT period, the UHPC can exhibit better performance at an earlier stage of curing (< 7 d). However, the degree and rate of AS are also increased due to the acceleration of the pozzolanic reaction and densification of the pore structure as a result of the HT (Jiang, Yang, Wang, Zhou & Ma, 2014; Maruyama & Teramoto, 2013; Mounanga, Baroghel-Bouny, Loukili & Khelidj, 2006; Japan Society of Civil Engineers (JSCE), 2004; Loukili, Chopin, Khelidj & Le Touzo, 2000).

## **1.2 Internal curing and its necessity for UHPC**

Over the last few decades, advancements on concrete admixtures such as silica fume and superplasticizer allowed for the reduction in w/c with proper workability, leading to the production of high performance concrete (HPC) and UHPC (Wang, Zhou, Peng, Liu & Hu, 2009). Although it successfully increased mechanical strength by reducing these low w/c concrete, additional shrinkage that is not usually observed in concrete with a high w/c, raised a new problem (Jensen & Hansen, 2001b). This additional shrinkage is mainly due to

the self-desiccation of concrete and becomes significant as the w/c decreases. This AS makes the concrete vulnerable to early age cracking (Lura *et al.*, 2003), especially in UHPC when following mix proportion is used: more than 600kg/m<sup>3</sup> of cement, 0.15~0.25 of silica fume ratio, and w/c less than 0.3 (Dudziak & Mechtcherine, 2008; Eppers & Müller, 2008).

In general, shrinkage reducing agent (SRA) and expansive agent (EA) have been traditionally used together to reduce AS (Yoo, Banthia & Yoon, 2015; Meddah, Suzuki & Sato, 2011). However, not only these materials are the factors that increase the material cost of low w/c concrete like UHPC, but also the mechanisms related to the shrinkage reductions by the two materials (e.g., reduction of surface tension and expansive reaction, respectively) are not fundamental treatments for AS. The driving force of AS is the self-desiccation that occurs in the low w/c (< 0.4) condition (Jensen & Hansen, 2001b; Powers & Brownyard, 1948). The desiccation and resulting AS are directly related to the decrease of internal relative humidity (RH) (Maruyama & Teramoto, 2013; De La Varga, Castro, Bentz & Weiss, 2012; Kosmatka, Kerkhoff & Panarese, 2011; Jiang, Sun & Wang, 2005; Lura, Van Breugel & Maruyama, 2001). However, as a fundamental treatment, to diffuse external water into the concrete by using traditional methods (e.g. water or spray curing) is very challenging and unrealistic because the low w/c concrete has compact internal structure and low permeability, as well (Justs, Wyrzykowski, Bajare & Lura, 2015).

Therefore, porous lightweight aggregate (LWA) has been extensively studied as an IC agent due to its competitive price and its benefits in concrete durability (Bentz & Weiss, 2011). For instance, IC by LWA has been effectively

and economically used to enhance the durability of HPC for bridge deck structures (Cusson, Lounis & Daigle, 2010). However, compressive and tensile strengths of low w/c concrete can be decreased due to LWA (Jensen, 2013; Bentz & Weiss, 2011). Recently developed HPC and UHPC incorporates a maximum aggregate size of less than 13mm and 1mm, respectively; thus, the use of large size porous aggregate can cause the loss of mechanical properties. In particular, average diameter of the aggregate is quite larger than the maximum particle size of UHPC ( $< 1$  mm) (Kang, Hong & Moon, 2016d; Kang, Gyephel, Hong & Moon, 2015; Richard & Cheyrezy, 1995). From early 2000, there has been vigorous studies on the application of superabsorbent polymer (SAP) to reduce AS by using IC (Jensen & Hansen, 2002, 2001b). When considering the compact composition of UHPC (Richard & Cheyrezy, 1995), thus, IC by superabsorbent polymer (SAP) is the most promising way to solve the shrinkage problems of UHPC (Justs *et al.*, 2015; Snoeck, Jensen & De Belie, 2015a; Jensen & Hansen, 2002, 2001b) because its size is less than the maximum particle size of UHPC.

In 2010, for the first time, the American Concrete Institute defined IC as “supplying water throughout a freshly placed cementitious mixture using reservoirs, via pre-wetted lightweight aggregates, that readily release water as needed for hydration or to replace moisture lost through evaporation or self-desiccation” (Bentz & Weiss, 2011). Three years later, the definition was revised to a “process by which the hydration of cement continues because of the availability of internal water that is not part of mixing water” (American Concrete Institute, 2013). This revision indicates that IC is the process to promote cement hydration; strictly speaking, the method to mitigate the self-

desiccation was originally named as water entrainment by Jensen and Hansen in 2001 (Jensen & Hansen, 2001b). However, both IC and water entrainment are closely related since their prerequisite conditions, keeping internal RH high by additionally supplied moisture, are exactly same. Thus, both of terms, IC and water entrainment, can be used especially for SAP incorporated low w/c concrete in which the additional water is supplied by SAP to increase the RH. Based on these reviews, IC or water entrainment can be classified as referring to cementitious materials that satisfy the following requirements.

- The material contains reservoirs that can absorb and retain water.
- The reservoirs can retain the absorbed extra water (not mixing water) for several days, but this water can be released to the surrounding material later.
- The released water is used to increase the degree of hydration and to mitigate self-desiccation in a low w/c material.

IC of concrete has been used without recognition for centuries. If porous LWA is included in a concrete mixture, IC or water entrainment is automatically possible. Thus, the history of lightweight concrete matches that of IC (Bentz & Weiss, 2011). For instance, it has been identified that IC was used in the construction of the Pantheon (A.D. 126), in which LWA was used to reduce the weight of the dome (Fig. 1-3). The use of LWA and the resulting IC possibly helped to accelerate the typically slow hydration reaction of lime-pozzolan cement (Narayanan, 2016). Nevertheless, the concept of IC or water

entrainment has been studied and has developed as an emergent concrete technology during this century. Also in this period, very low w/c concrete ( $w/c < 0.3$ ), such as UHPC, has been widely researched and thus it has been necessary to develop a new technology to mitigate severe shrinkage of the concrete (Jensen & Hansen, 2002, 2001b).



Fig. 1-3 Pantheon in Rome, the world's largest unreinforced dome  
(Narayanan, 2016)

The concept of IC is expressed simply but clearly in Fig. 1-4. Most parts of the concrete can be kept in a saturated state due to the water reservoirs (Bentz & Weiss, 2011). Although this concept originated from IC by LWA, it has recently been expanded to other materials with absorption capacity, thanks to developments in material science. Examples of absorbing materials include SAP, micro sized porous particles (e.g., rice husk ash), and nano or micro sized porous fibers (e.g., wood fibers). Due to the developments in micro and nanotechnology, IC is becoming a core technology in concrete material science, allowing the hydration reaction of cementitious materials to proceed slowly

over a long time due to the supply of water.

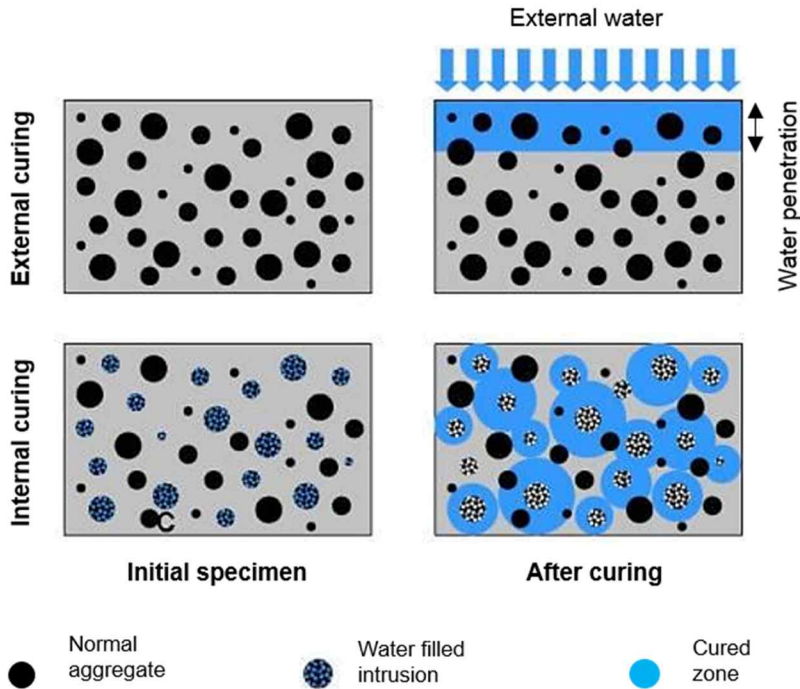


Fig. 1-4 Schematic illustration of internal curing  
(Bentz & Weiss, 2011)

### 1.3 Scope

Previous studies have proven the effectiveness of IC to improve the durability of concrete, without consideration of the fresh and hardened performances. Although IC can promote the hydration reaction and reduce shrinkage and cracking risks, practically IC is not beneficial if the essential performances of the concrete, such as strength and workability, are not guaranteed. A low w/c concrete has the advantages of outstanding mechanical

performances, flowability, watertightness, and durability. The advantages are the reasons why low w/c concretes should be used, despite the high price. If IC cannot guarantee these advantages, it will not be a competitive method compared to traditional methods such as SRA and EA. Furthermore, the compressive strength of concrete has been increased remarkably over the last 30 years, but the applications for ultra-high strength (or performance) concrete for structures have rarely been reported (Vande Voort *et al.*, 2008). This is mainly due to its extremely high price. Thus, when using a new material such as SAP to improve the performance of such concrete, it is essential that the economic feasibility be reviewed.

## **1.4 Objective**

The main purposes of this study are to investigate the principles of IC using SAP in low w/c concrete, and the effects of IC on the material properties of UHPC. Although it has been confirmed that IC can effectively mitigate AS of UHPC (Justs *et al.*, 2015; Dudziak & Mechtcherine, 2008), the mechanism of absorption and release of water by SAP within the concrete and its impact on the mechanical properties, as well as the material price, have not been satisfactorily examined. In this research IC is applied to UHPC without any loss of the performances. The impact of IC is physically and chemically investigated, while considering feasibility, practicality and price competitiveness.

## 1.5 Organization

Fig. 1-5 shows the organization of this thesis that is composed of five chapters. To achieve the research objective, the chapters are connected each other. First of all, two main key words of the research, UHPC and IC were reviewed with their definition in Chapter 1. Previous studies and their limitations are reviewed in Chapter 2. In this chapter, two different types of SAP are selected and extra water to cement ratio ( $w_e/c$ ) for each SAP is designed based on the literature study of the previous principles. Next, experiments on SAP and UHPC are widely conducted to find the evidences of IC. In Chapter 3, ab-and de-sorption principles of the selected two SAPs in low  $w/c$  concrete are experimentally investigated, i.e., the driving force of IC by SAP is experimentally verified. In addition, the water retention capacity of the SAPs in UHPC is confirmed, which can support to explain the mitigation of self-desiccation of UHPC due to IC. Chapter 4 microstructure and pore system of UHPC are rigorously analyzed. The UHPC samples are designed according to the optimized mix proportion of the developed UHPC and the predetermined SAP type and  $w_e/c$  in Chapter 2. The changes of microstructure and pore system due to SAP addition are investigated to obtain evidences of internal curing. Lastly, effects of IC using SAP on the materials properties of UHPC are verified in Chapter 5 which is the final stage to achieve the objective. The promotion of hydration reaction, prevention of self-desiccation and shrinkage behavior are directly connected to the ab-and desorption kinetics and water retention capacity of SAP. In addition, the change of mechanical properties and drying speed are closely related to the densification of microstructure and change of pore structure as confirmed in Chapter 4.

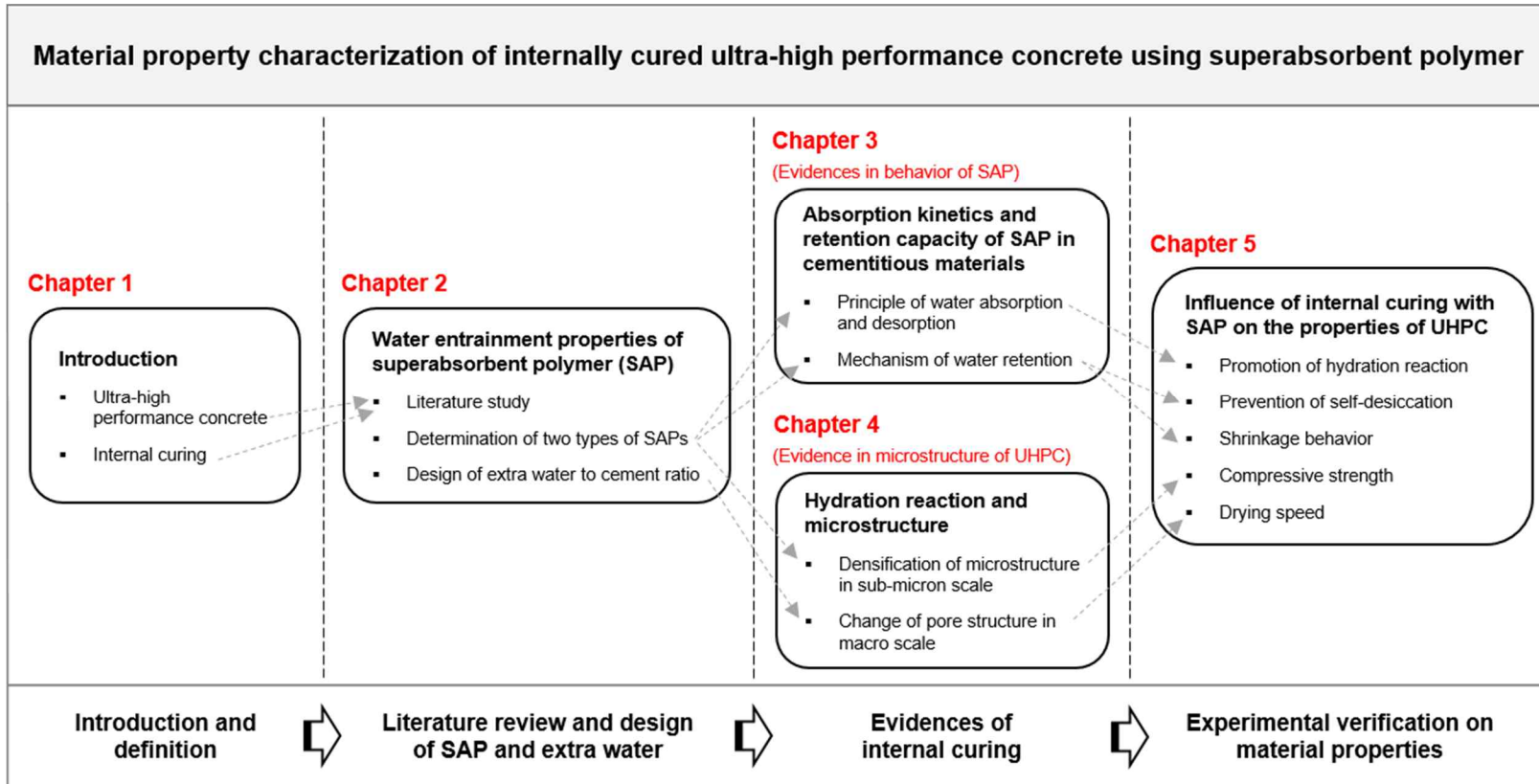


Fig. 1-5 Organization of thesis



## Chapter 2. Water entrainment properties of superabsorbent polymer (SAP)

### 2.1 Introduction

Superabsorbent polymer (SAP) is a material that can absorb water (or solution) up to thousand times of its own weight, due to its hydrophilic network structure (Zohuriaan-Mehr & Kabiri, 2008). Chemically, because SAPs possess an ionic nature and interconnected structure, they are defined as cross-linked polyelectrolytes (Buchholz, 1996). Such absorption capacity enables SAP to be used as an admixture or additive for concrete in a number of different uses. One possibility is to use an IC agent, which can effectively mitigate the autogenous shrinkage that is a major problem in concrete with low water to cement (w/c) ratio (Snoeck *et al.*, 2015a; Mechtcherine, Gorges, Schroefl, Assmann, Brameshuber, Ribeiro, Cusson, Custódio, Da Silva & Ichimiya, 2014; Jensen & Hansen, 2002, 2001b). It has been reported that IC using SAP is effective at reducing the severe autogenous shrinkage of low w/c concrete or mortar including high performance concrete (HPC), and ultra-high performance concrete (UHPC) (Justs *et al.*, 2015; Kang *et al.*, 2015; Mechtcherine & Reinhardt, 2012; Schröfl, Mechtcherine & Gorges, 2012; Jensen & Hansen, 2002).

The advantages of SAP as an IC agent is related to its high water absorbing ability, leading to a reduction in the autogenous shrinkage, with an extremely small required quantity (typically 0.3-0.6 wt.% of cement) and low cost. Since

the volume of SAP expands up to few millimeters once it absorbs water (Fig. 2-1), it can affect the workability of concrete during the mixing stage (Fig. 2-2 (a) and (b)). While releasing the absorbed water, SAP can compensate the decreased the internal RH of concrete due to the self-desiccation. However, after releasing the absorbed water back into the cement matrix, the volume of the SAP will decrease and leave its pore space in concrete (Fig. 2-2 (c)). The changed pore structure can affect the freeze-thawing resistance of concrete. In addition, the contracted SAP will re-absorb water and re-expand if additional water is supplied. This behavior can be explained as the crack self-healing and sealing effects (Snoeck, Van Tittelboom, Steuperaert, Dubruel & De Belie, 2014b). In summary, the SAP will play an important role in most water-related phenomena (including workability, strength, durability, crack-healing or sealing, and hydration) during the entire lifetime of concrete.

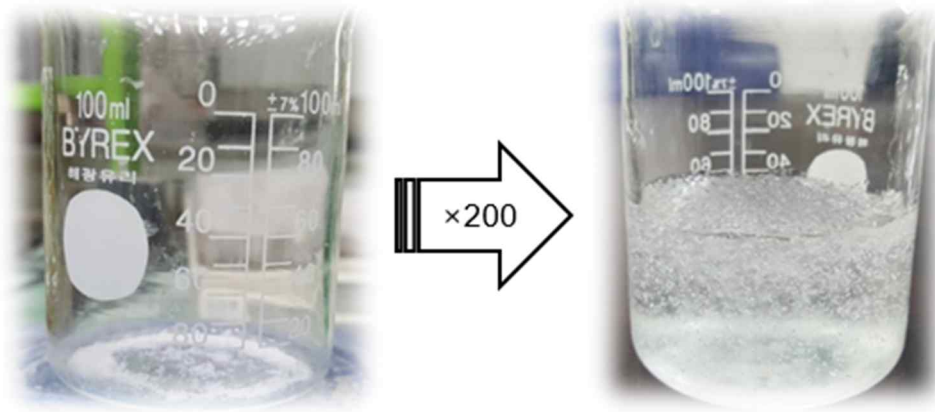


Fig. 2-1 Volume expansion of SAP after absorbing tap water

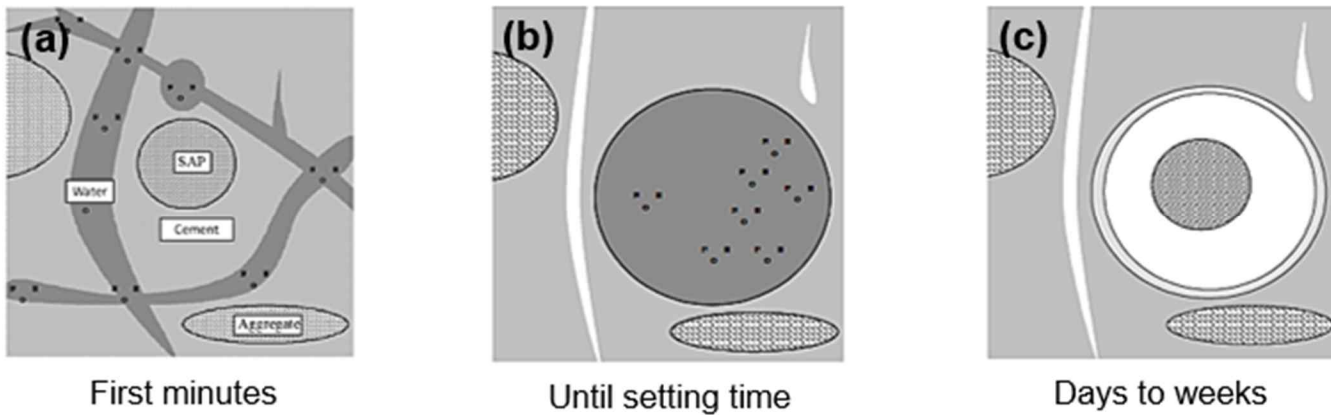


Fig. 2-2 Schematic illustration of volume change of SAP in cementitious materials  
(Mönnig, 2009)

## 2.2 Literature review on application of SAP for concrete

In early 2000s, it was firstly proved by Jensen and Hansen that the water entrainment using SAP is effective to reduce AS of low w/c cementitious materials (Jensen & Hansen, 2002, 2001b). The AS of high performance mortar (w/c=0.3) was successfully reduced by this method. The internal RH of the mortar was decreased to 80% at 21 d, while two mortars with SAPs (0.3% and 0.6% by weight of cement) maintained the RH above 95% at the same time. As a result, two mortars did not experience any shrinkage during the first 21 d, but the other mortar without SAP experienced a severe AS of 3,700  $\mu\text{m}/\text{m}$  during the same period. Nonetheless, the water cured mortars with SAP showed significant strength loss, i.e., the compressive strength was decreased by 19% at 28 d due to the addition of SAP and extra water.

The effect of SAP addition on the compressive strength of concrete is also main topic in the field of IC. This is because that the strength is the main property of concrete and especially superior strength is the main feature of HPC or UHPC. Currently, contradictory claims have been raised about the effect of SAP on the compressive strength of concrete. As a conclusion of the study, Craeye et al., mentioned that the addition of SAP causes severe losses in strength and elastic modulus of concrete (Craeye, Geirnaert & De Schutter, 2011). However, the opposite conclusion was raised by Hasholt et al., i.e., the strength loss impossibly occurs when the optimum portion of SAP is added into a concrete with the accurately designed extra water (Hasholt, Jensen, Kovler & Zhutovsky, 2012). Kolver also have supported this conclusion, i.e., he

mentioned that the strength loss can be avoid if the SAP and extra water are accurately deigned, and mixing, placing, and curing are conducted with the optimized methods (Mechtcherine & Reinhardt, 2012). To support this conclusion, evidences were presented; there are experimental results in which the 28 d compressive strength was slightly increased despite the addition of SAP. The reason of the increase was due to the increase of the final degree of hydration by internal curing. In spite of the several positive results (i.e., strength increase by internal curing), unfortunately, the majority studies have reported the strength loss up to 30% when SAP is added into a concrete.

Previously, the feasibility of SAP as a shrinkage reducing agent for UHPC was confirmed (Dudziak & Mechtcherine, 2008). Without SAP, AS of UHPC was 500-700  $\mu\text{m}/\text{m}$  at 28 d. However, this shrinkage was decreased to less than 200  $\mu\text{m}/\text{m}$  by IC using SAP. This result has confirmed that the IC is one of the most promising method to solve the severe shrinkage and early age cracking problems of UHPC. However, there was a strength loss of UHPC (up to 13%) due to the addition of SAP. Recently, Just et al. also investigated the effect of IC using SAP on the material characteristics of UHPC (Justs *et al.*, 2015). Above all, they firstly verified the additional formation of hydration product, portlandite in voids induced by SAP particles. As expected the IC was effective to reduce AS of UHPC. However, they could not prevent the strength loss of UHPC due to SAP addition; at 2 d, 28 d and 365 d, the compressive strengths of UHPC were decreased by 16-33%, 9-19% and 7-13%, respectively compared with the control specimen. Although the decreased strength was tend to increase with curing age due to the IC effect, the UHPC with SAP and extra water could not recover the decreased portion of strength.

At this point, therefore it is necessary to study the material properties of the internally cured UHPC systematically, including shrinkage reduction as well as the recovery of reduced mechanical performance by IC effect. Furthermore, previous studies only selected one type of SAP, acrylic acid or acrylamide type for the IC of UHPC, i.e., the effect of the SAP type on the internal curing of UHPC has not been examined, yet. The most widely used commercial SAPs are made from acrylic acid and acrylamide monomers. Acrylic acid and acrylamide type SAP have also been studied as suitable for the internal curing of concrete. In the study by Schröfl et al., the impact of anionicity and cross-link density of SAP on the IC effect of low w/c mortar was investigated (Schröfl *et al.*, 2012). The study has reported that especially the IC effect for reducing AS is decreased as the anionicity of SAP is increased. Between the two types, the anionicity is higher in acrylic acid SAP than that in acrylamide SAP. This means that undoubtedly the acrylamide SAP is the most suitable type, considering only the internal curing effect of UHPC. However, this situation can be changed by taking into account the economic feasibility, as well. The price of acrylamide SAP is much higher (almost 10 times in the case of this thesis) than that of acrylic acid SAP. Even if acrylamide SAP has excellent performance due to relatively low anionicity, its low price competitiveness can be an obstacle for practical use of IC using SAP. Therefore, the shrinkage and mechanical properties of internally cured UHPCs need to be compared using two commercial SAPs, considering the internal curing effect and economic feasibility of SAPs.

## 2.3 Basic principles of internal curing

In 1948, to describe the phase distribution of cement pastes, Powers and Brownyard established an empirical model based on the previous 12 years of research (Powers & Brownyard, 1948). After that (in 2001), Jensen and Hansen developed the basic theory of IC and water entrainment by reinterpreting the previous model (Jensen & Hansen, 2001b). According to the Powers' model, the water in cement paste can be divided into three types. First, capillary water, also known as free water, is the only water that can be consumed for cement hydration. The internal RH of a cementitious materials is determined by the quantity of this type water and thus, the amount is a key factor influencing self-desiccation and its mitigation. Second, gel water is defined as physically bounded water in a gel solid. When 1 g of cement is hydrated, 0.19 g of gel water is produced. This type water can be evaporated only under low RH conditions (i.e.,  $RH < 30\%$ ). The third is chemically bound water; 0.23 g of the water is produced when 1 g of cement is hydrated. This water never evaporates, but can be lost when the hydration product is decomposed at high temperatures (i.e., 105-1,000 ° C) (Aligizaki, 2006; Jensen & Hansen, 2001b).

The volume of the hydration products is smaller than the sum of unhydrated cement and the mixing water. Therefore, as cement hydration proceeds (i.e., degree of hydration increases), inevitably the void fraction increases and volume of the paste decreases. This type of volume reduction is called chemical shrinkage. Variations in the volume composition of cement pastes as a function of degree of hydration were classified into five categories

by Powers and Brownyard (Powers & Brownyard, 1948). Each category has been presented as the following equations, using a constant initial porosity which can be determined by the mix proportion.

$$V_{cs} = 0.20(1 - p)\alpha \quad (2-1)$$

$$V_{aw} = p - 1.32(1 - p)\alpha \quad (2-2)$$

$$V_{gw} = 0.60(1 - p)\alpha \quad (2-3)$$

$$V_{gs} = 1.52(1 - p)\alpha \quad (2-4)$$

$$V_{uc} = (1 - p)(1 - \alpha) \quad (2-5)$$

In Eqs. (2-1) to (2-5),  $V_{cs}$ ,  $V_{aw}$ ,  $V_{gw}$ ,  $V_{gs}$  and  $V_{uc}$  are the volume fractions related to chemical shrinkage, capillary water, gel water, gel solid and unhydrated cement, respectively.  $\alpha$  and  $p$  are the degree of hydration and initial porosity (at  $\alpha = \alpha_0$ ), respectively. To calculate  $p$ , the equation  $p = V_{aw,0} = (w/c)/(w/c + \rho_w/\rho_c)$  can be used. In this equation, the densities of cement ( $\rho_c$ ) and water ( $\rho_w$ ) are assumed to be 3,150 kg/m<sup>3</sup> and 1,000 kg/m<sup>3</sup>, respectively.

By plotting the five equations, a phase distribution diagram for cement pastes can be drawn such as that found in Fig. 2-3 (a).

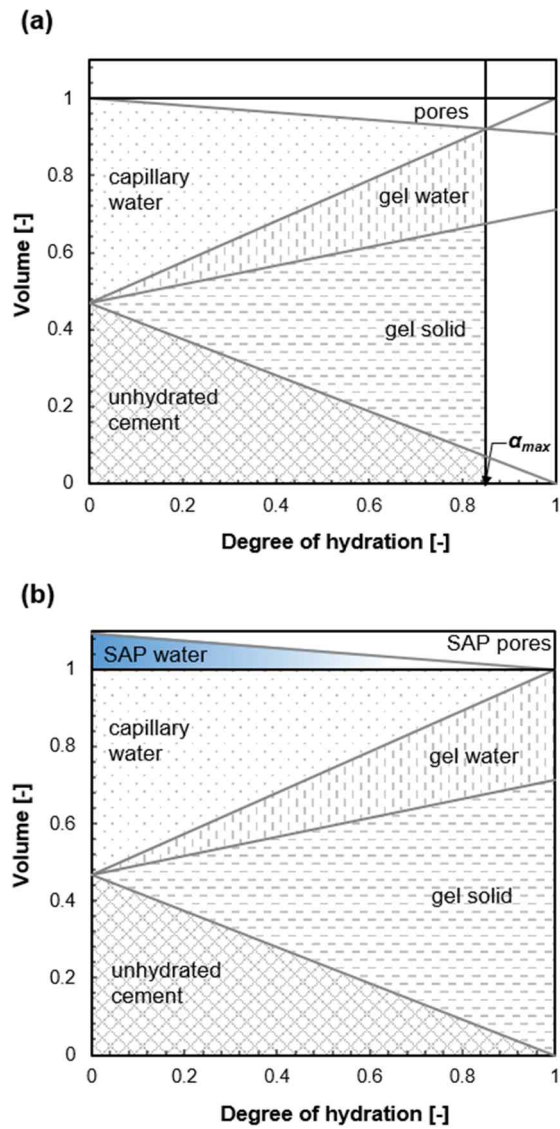


Fig. 2-3 Volumetric phase distribution of cement paste as a function of degree of hydration at  $w/c=0.36$  (a) and  $w/c=0.36+0.06$  (b)

(Assmann, 2013)

Fig. 2-3 (a) shows the phase distribution of a low  $w/c$  (0.36) cement paste

(Assmann, 2013). Since we know the w/c of the paste, the volume ratios of water and cement at  $\alpha = \alpha_0$  can be found using their densities. As hydration progresses (i.e.,  $\alpha \rightarrow \alpha_{max}$ ), the volumes of unhydrated cement and capillary water in the paste decrease, whereas those of gel water and gel solid increase. In addition, the porosity of the paste increases as the chemical shrinkage proceeds. Based on Powers' model, a complete hydration reaction is impossible (i.e.,  $\alpha_{max} < 1$ ) in this paste. On top of this, self-desiccation occurs under the condition of  $w/c < 0.42$  (Jensen & Hansen, 2001b; Powers & Brownyard, 1948), and thus, the unhydrated cement remains and the capillary water is entirely consumed at  $\alpha_{max}$ . There are two reasons why hydration processes of cementitious materials stop: a lack of available water, and a lack of space where additional hydration products can be produced. The second reason is more dominant for low w/c conditions. In summary, we know the volume ratio of capillary water at  $\alpha_0$ , and the fact that all the water is consumed by cement hydration at  $\alpha_{max}$ . Thus, the final volume reduction or void (at  $\alpha_{max}$ ) can be estimated using w/c information along with the knowledge of the chemical shrinkage, i.e., 6.4 ml of volume reduction when 1 g of cement is hydrated. Based on this, the design equation for IC water can be derived.

$$V_{gw} + V_{gs} + V_{uc} = 1, \text{ at } \alpha = \alpha_{max} \quad (2-6)_1$$

$$\begin{aligned} 0.6(1-p)\alpha_{max} + 1.52(1-p)\alpha_{max} \\ + (1-p)(1-\alpha_{max}) = 1 \end{aligned} \quad (2-6)_2$$

$$\alpha_{m\ ax} = \frac{p}{1.1(1-p)} \quad (2-6)_3$$

First of all, the volume of cement paste at  $\alpha_{m\ ax}$  can be expressed as the sum of  $V_{gw}$ ,  $V_{gs}$  and  $V_{uc}$  (Eq. (2-6)<sub>1</sub>) (Jensen & Hansen, 2001b). By substituting Eqs. (2-3)-(2-5) into Eq. (2-6)<sub>1</sub>, the maximum degree of hydration ( $\alpha_{m\ ax}$ ) can be derived as a function of the initial porosity ( $p$ ) (see Eq. (2-6)<sub>3</sub>). Eq. (2-6)<sub>3</sub> shows that  $\alpha_{m\ ax}$  can be predicted using the initial porosity (or w/c) information.

For low w/c paste, additionally supplied water can contribute to the increase of  $\alpha_{m\ ax}$  up to 1. According to Powers' model, a completed hydration reaction (i.e.,  $\alpha_{m\ ax} = 1$ ) is possible in low w/c pastes ( $w/c > 0.36$ ) if additional water is supplied as shown in Fig. 2-3 (b). Self-desiccation occurs when cement hydration proceeds while consuming water, reducing the capillary water quantity. If this reduction can be instantly compensated for from water reservoirs such as SAP, the desiccation can be prevented. Eq. (2-7) is based on this concept. In this equation,  $V_{ew,0}$  is the volume of IC water necessary to prevent the self-desiccation.

$$\begin{aligned} V_{ew,0} &= V_{cs,\alpha_{m\ ax}} = 0.2(1-p)\alpha_{m\ ax} = 0.18p \\ &= 0.18V_{aw,0} \end{aligned} \quad (2-7)_1$$

$$\therefore \frac{V_{ew,0}}{V_{av,0}} = 0.18 \quad (2-7)_2$$

Eq. (2-7)<sub>2</sub> reveals that the minimum ratio of IC water to capillary water to prevent the desiccation of low w/c cement paste is 18%. In other words, the design w<sub>e</sub>/c is 18% of the w/c value. From this, the design equation shown in Eq. (2-8) can be obtained.

$$\frac{w_e}{c} = 0.18 \times \frac{w}{c}, \text{ for } \frac{w}{c} \leq 0.36 \quad (2-8)$$

In addition, since the complete hydration reaction ( $\alpha_{max} = 1$ ) is possible due to the IC when w/c > 0.36, the total water to cement ratio (w<sub>t</sub>/c = (w+w<sub>e</sub>)/c) need not be designed over 0.42. Therefore, another design equation can be expressed, as shown in Eq. (2-9).

$$\frac{w_e}{c} = 0.42 - \frac{w}{c}, \text{ for } 0.36 \leq \frac{w}{c} \leq 0.42 \quad (2-9)$$

Two years after Jensen and Hansen published the concept of water entrainment for cement paste (Jensen & Hansen, 2001b), Lura developed another extended model (Lura, 2003). The basic concept remains the same as

the previous model, but the new model reflects the fact that the ratio of chemical shrinkage by silica fume (22 cm<sup>3</sup> / 100 g) is much higher than that by cement (6 cm<sup>3</sup> / 100 g) (Assmann, 2013; Bentz & Jensen, 2004; Lura, 2003). Since the majority of low w/c concretes or mortars contain silica fume, this new model can be used more widely in practice than the previous model. As can be seen in Eqs. (2-10) and (2-11), the necessary w<sub>e</sub>/c to achieve  $\alpha_{max} = 1$  depends on both the w/c and silica fume to cement ratio (sf/c).

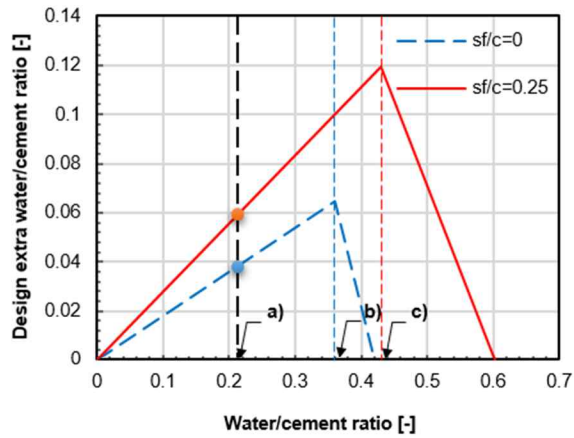
$$\frac{w_e}{c} = \frac{0.2 + 0.69 (sf / c)}{1.12 + 0.88 (sf / c)} \times \frac{w}{c}, \quad (2-10)$$

$$\text{for } \frac{w}{c} \leq [0.36 + 0.28 (sf / c)]$$

$$\frac{w_e}{c} = [0.42 + 0.73 (sf / c)], \quad (2-11)$$

$$\begin{aligned} \text{for } [0.36 + 0.28 (sf / c)] &\leq \frac{w}{c} \\ &\leq [0.42 + 0.73 (sf / c)] \end{aligned}$$

Using Eqs. (2-10) and (2-11), w<sub>e</sub>/c as a function of w/c can be drawn, as shown in Fig. 2-4. This diagram can be used to design the required extra or IC water theoretically, as well as practically.



**a)** w/c of the developed UHPC

**b) and c)** minimum w/c ratios of internally cured concrete for  $a_{max}=1$  when sf/c ratios are 0 and 0.25, respectively.

Note: red and blue points on the graphs indicate the design extra water/cement ratio for the developed UHPC

Fig. 2-4 Design extra water theoretically required to prevent self-desiccation of cement paste with or without silica fume (Lura, 2003; Jensen & Hansen, 2001b)

## 2.4 SAP used in this study

Two types of SAPs, namely poly acrylic acid type (SAP\_AA) and poly acrylic acid-co-acrylamide type (SAP\_AM) were selected for this study (Fig. 2-5). The poly acrylic acid type is one of the most commonly used commercial types of SAP (Buchholz, 1994), mainly used for personal hygiene products such as diapers. This material has been successfully used for decades due to its productivity, safety and suitability for diapers, along with low unit price and excellent absorption capacity. However, this particular material is not optimal for all fields requiring SAPs, such as agriculture, horticulture, and construction. The covalently crosslinked poly acrylic acid-acrylamide type has been found to be more efficient in terms of IC of concrete, and therefore has been successfully used in these fields (Zhu, Barney & Erk, 2015; Schröfl *et al.*, 2012; Siritwatwechakul, Siramanont & Vichit-Vadakan, 2012).

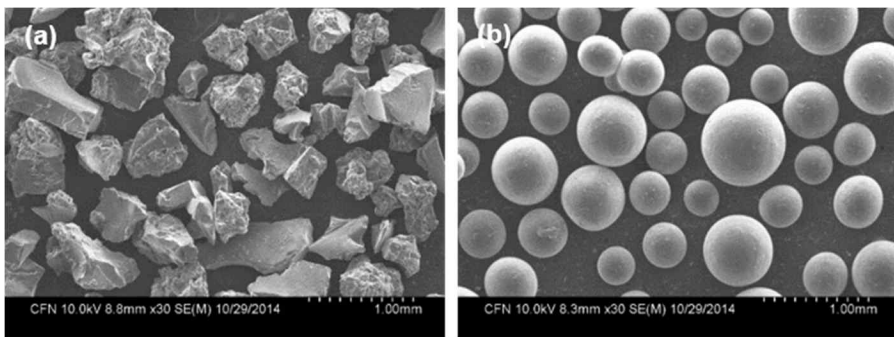


Fig. 2-5 SEM images of SAP\_AA (a) and SAP\_AM (b)

Both SAPs are derived from acrylic monomers (Zohuriaan-Mehr & Kabiri,

2008), and as such they possess ionic properties. However, their shapes and methods of manufacture differ. Due to manufacturing differences, the anionic group density of SAP\_AA is higher than that of SAP\_AM. SAP\_AA, a cross-linked sodium polyacrylate hydrogel, is manufactured by solution polymerization which is more advantageous for mass production (Kiatkamjornwong, 2007) and makes the material an irregular shape. Due to this method, the present carboxylic acid groups (-COOH) are partially neutralized with a strong alkali such as sodium hydroxide and swiftly mixed with a cross-link agent, generating heat and forming an elastic gel. This gel is sieved to the desired size after undergoing drying and pulverizing (Zohuriaan-Mehr & Kabiri, 2008). On the other hand, SAP\_AM is copolymerized by a partially neutralized acrylic acid monomer and acrylamide with the cross-link agent. Unlike SAP\_AA, because it is manufactured by an inverse suspension polymerization that does not include pulverization, SAP\_AM possesses a perfect globular shape. The adhesiveness is removed by the dispersing agent and lubricating agent, producing particles that are perfectly individually separated (Chem Tech Co. Ltd., 2003).

The anionic group density of SAP\_AA is higher than that of SAP\_AM because of the difference in their manufacturing processes. However, the particle size distributions of two SAPs both range from 100  $\mu\text{m}$  to 700  $\mu\text{m}$  (Fig. 2-6). Due to this similarity, we can disregard the influence of particle size on the absorption kinetics in this study. In such particle distributions in general, gel-blocking (i.e., blocking of solution flow among SAP particles due to the reduction of permeability caused by swelled SAP particles) is ineffective, because this behavior is prominent in small particles ( $< 100 \mu\text{m}$ ) (Mechtcherine

& Reinhardt, 2012). Thus, it is safe to assume that all the SAP particles here can be in contact with the solution inside the tea-bag.

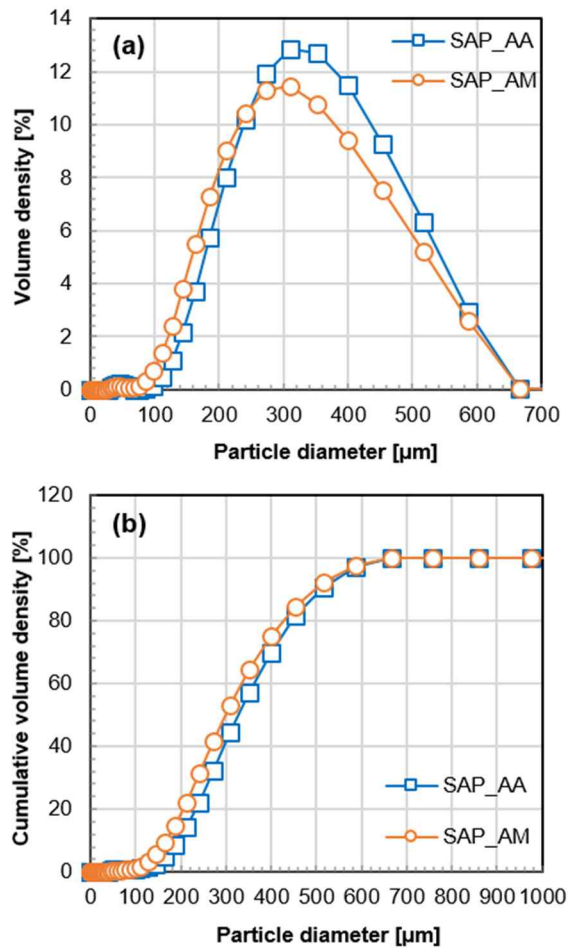


Fig. 2-6 Particle size distribution (a) and cumulative distributions (b) of SAPs

## 2.5 Design of extra water

Extra water for IC of low w/c concrete can be easily estimated by using Eqs. (2-8)-(2-11). As presented in Section 1, the UHPC developed in this study has a w/c ratio of 0.215, thus the  $w_e/c$  is determined as 3.87% or 5.98% using Eq. (2-8) or (2-10), respectively (refer to two points on Fig. 2-4). Based on this estimation, 4% and 6%  $w_e/c$  ratios were determined for internally cured UHPCs. The reason that not one ratio but two ratios were estimated, was to consider the different absorption capacities of the two SAPs presented in Section 2.3.

Aside from the design of extra water, it is very challenging to make SAP in concrete capable of absorbing the required amount of extra water and to confirm this amount after absorption. As a first step of this study, slump flow tests according to the ASTM standard (ASTM C1611 / 1611m, 2014) were conducted in order to determine the amount of SAP that can absorb the required water in UHPC. After several trials the required SAP to cement ratios (SAP/c) were determined as 0.4% for SAP\_AA (with 4% of  $w_e/c$ ), and 0.3% for SAP\_AM (with 6% of  $w_e/c$ ). These ratios also mean that the absorption capacity of SAP\_AM in UHPC is twice that of SAP\_AA. Remarkably, the optimized extra water and SAP ratios not only satisfied the basic principles of water entrainment for preventing self-desiccation, but also did not result in loss of the UHPC's workability during the slump flow tests.

Other cases such as 6% of  $w_e/c$  for SAP\_AA and 4% of  $w_e/c$  for SAP\_AM were excluded due to the different absorption capacity of the SAPs. If 6% of  $w_e/c$  was designed for SAP\_AA, 0.6% of SAP\_AA/c should be required. In this

case, a significant decrease in the mechanical performance was expected due to the formation of additional pores caused by the SAP. On the other hand, if 4% of  $w_e/c$  was designed for SAP\_AM, 0.2% of SAP\_AM/c should be required. With these values the amount of SAP particles added would be too low; the spacing between the particles in the concrete would be too far, which could limit the diffusion range of moisture. Consequently, the effect of IC was expected to decline in both cases.

The mentioned decreases in mechanical performance and shrinkage reduction capacity were actually confirmed in the preliminary test that was conducted to determine SAP/c for the internally cured UHPC. Compared with the UHPC\_0.4% & 4% (SAP\_AA/c &  $w_e/c$ ), the UHPC\_0.6% & 6% showed 25% lower AS (from 737  $\mu\text{m}/\text{m}$  to 553  $\mu\text{m}/\text{m}$ ), but 28 d compressive and flexural tensile strengths were decreased by 4% and 21% respectively. On the other hand, the strengths of the UHPC\_0.2% & 4% (SAP\_AM/c &  $w_e/c$ ) were increased by 11% and 9%, respectively compared with the UHPC\_0.3% & 6%. However, AS was significantly increased by 190% (from 279  $\mu\text{m}/\text{m}$  to 810  $\mu\text{m}/\text{m}$ ).

## **Chapter 3. Absorption kinetics and retention capacity of SAP in cementitious materials**

### **3.1 Absorption kinetics of SAP in low water to cement ratio concrete**

#### **3.1.1 Introduction**

Section 3.1 contains information regarding the method for manufacturing artificial pore solutions, and the procedure for measuring the SAP absorbency including the suggested tea-bag method. Also it covers the results of the experiments, as well as discussions regarding the following three sub-topics: 1) review of the problems in the existing tea-bag method and the verification of the proposed method's reliability, 2) ion concentration of the artificial pore solution cement filtrate, and 3) the absorption kinetics of SAP based on the ion concentration in the artificial pore solution.

When mixing concrete, SAP absorbs and stores water, which will be used for IC, while forming water-filled inclusions. To successfully mitigate AS, certain amounts of IC water which can be estimated based on the models presented in Section 2 (Snoeck *et al.*, 2015a; Jensen & Hansen, 2001b; Powers & Brownyard, 1948), need to be determined to ensure the intended effect; this water should be provided to the concrete by SAP in advance. However, this design is possible only when the absorption and release kinetics of SAP inside the concrete are well known. In other words, in order to utilize SAP as an IC agent, the understanding and prediction of SAP's absorption capacity in cement

pore solution must first be established (Justs *et al.*, 2015; Jensen & Hansen, 2001b). Moreover, since the SAP's absorption capacity also influences the effectiveness of IC (Schröfl *et al.*, 2012), predicting the absorption kinetics can be useful with regard to select the type of commercially available SAPs and manufacture of a new SAP for concrete application (Siriwatwechakul *et al.*, 2012).

Two situations can arise when the SAP's absorption capacity is mispredicted. First, SAP can absorb more water than planned during the mixing of concrete if the absorption capacity is underestimated. In this case, the free water required for target slump or slump flow value can be absorbed by SAP, causing severe reduction of workability. Also, when SAP has not reached equilibrium swelling at the time of measurement, even if the target level is satisfied, severe workability loss can occur due to the increasing absorption of SAP beyond that point (Esteves, 2010). The second situation involves the overestimation of the absorption capacity. In this case, due to the extra water added with SAP, the w/c of concrete after mixing exceeds its designed value. This increase can cause unwanted strength loss, and can even lead to problems in structural safety. The compressive strength loss by such overestimation has been demonstrated previously (Craeye *et al.*, 2011), with Hasholt *et al.* (Hasholt *et al.*, 2012) noting the problems with this behavior. As a new additive for concrete, another promising function of SAP is that it can enhance the freeze-thawing resistance by forming pores of intended size distribution within the concrete (Hasholt, Jensen & Laustsen, 2015). As the final pore size matches the swelled SAP size inside the concrete, SAP's absorption kinetics or swelling behavior should be considered in advance, to obtain an effective mix design for

the enhancement of freeze-thawing resistance.

Although the ability to predict SAP's absorbency is essential for its applications in both IC and freeze-thawing resistance, existing prediction methods are not sufficiently accurate to be used for the design of an internally cured concrete. For example, an indirect method (tea-bag method) showed SAP absorbency more than double the SAP absorbency derived using a direct method (slump flow method) in which actual mortar was used (Snoeck *et al.*, 2015a; Snoeck, Velasco, Mignon, Van Vlierberghe, Dubruel, Lodewyckx & De Belie, 2015b; Snoeck, Schaubroeck, Dubruel & De Belie, 2014a). Such differences indicate that the solution and conditions used in the tea-bag method are quite different from those of actual cement based materials (Snoeck *et al.*, 2014a). These indirect methods have their own advantage in that they are easily used for estimation of the absorbency and absorption kinetics of SAP. However, in order to obtain desirable results, understanding the complex absorption kinetics of SAP is essential. For instance, various factors such as particle size distribution, anionicity and cross-link density of SAP, temperature and ion concentration of external solution, and pressure applied to the SAP can all complicate these absorption kinetics. Because of the influence of such factors on the SAP absorbency and absorption kinetics, current indirect methods alone are not sufficient for accurately considering these factors (Hasholt *et al.*, 2015; Mechtcherine & Reinhardt, 2012).

In addition, the use of supplementary cementitious materials such as silica fume (SF) can change the ionic characteristic of cement pore solutions (Mechtcherine & Reinhardt, 2012; Lura, Lothenbach, Miao, Ye & Chen, 2010).

### Chapter 3. Absorption kinetics and retention capacity of SAP in cementitious materials

Not accounting for such changes when using indirect methods can also be a source of inaccuracy (Pourjavadi, Fakoorpoor, Hosseini & Khaloo, 2013). SF is generally added to HPC and UHPC in order to fill up the pores between aggregates (Schröfl *et al.*, 2012), or to promote a strong pozzolanic reaction (Page & Vennesland, 1983). Because the addition of SF can reduce the workability, superplasticizer (SPPL) should be added (Schröfl *et al.*, 2012). In particular, polycarboxylate-ether (PCE) type SPPL (which is capable of steric hindrance between cement particles) is the most effective and is typically used with SF (Lesti, Ng & Plank, 2010). Moreover, the w/c of these concretes is fairly low, and the mixing rates of silica fume to cement ratio (sf/c) and superplasticizer to cement ratio (SPPL/c) are considerably high. For instance, UHPCs developed in Europe have w/c=22-28%, sf/c=16.2-31.4%, SPPL/c=3.1-5.2%, and SPPL/w=13.6-18.7% (Schmidt & Fehling, 2005). SPPL, which appears as an aqueous solution, is generally mixed with water prior to mixing of the concrete, where it affects the ion concentration of the cement or concrete pore solution (Lothenbach, Winnefeld & Figi, 2007). Therefore, the influence of SF and PCE included in low w/c concretes on the SAP absorption kinetics should be understood in advance, and these factors need to be tested when predicting the absorbency using indirect methods.

Several direct methods use actual concrete or mortar for the measurement of absorbency. First, images of SAP included pores within hardened concrete can be measured, and the volume increase ratios are calculated from this information [7]. Second, the slump flow or spread value of fresh concrete with SAP can be calculated during the planned time. The purpose of this measurement is to decide the amount of water to be added to the fresh concrete

until the same target value as the fresh concrete without SAP is obtained (Schröfl *et al.*, 2012). However, it is difficult to use these direct methods for preliminary tests in practical fields.

The most common method used to determine SAP absorbency in the polymer industry is the gravimetric tea-bag method (Buchholz, 1994). This method is simple, rapid, and has been used in the field of personal care due to its sufficient reproducibility (Mechtcherine & Reinhardt, 2012; Zohuriaan-Mehr & Kabiri, 2008; Pourjavadi & Mahdavinia, 2006). This has also been used as an indirect method for cement based materials. Although this tea-bag method is simple and rapid, potential excess solution cannot be effectively removed. Therefore, there is some inherent inaccuracy in its measurement (Esteves, 2015). The excess solution is a summation of the solution trapped between swelled SAP particles and the solution smeared on the surface of the particles and tea-bag. In the field of cement based materials, the excess solution is commonly removed with dry cloth, in order to improve measurement accuracy (Zhu *et al.*, 2015; Schröfl *et al.*, 2012). However, the effectiveness of this practice has yet been verified. Another treatment for removing excess solution is to suspend the tea-bag, and wait until the excess solution drops by its own weight (Zohuriaan-Mehr & Kabiri, 2008). However, this treatment is clearly inappropriate for cement based materials, because if the SAP is not in a state of equilibrium swelling, this solution can be reabsorbed into SAP over time, or the solution already absorbed by the SAP can be released. Because of this, removal of the excess solution must be conducted immediately after removing the tea-bag out of solution, followed by measurement of the weight.

When determining the SAP's absorption kinetics for cement based materials using the tea-bag method, there are other major factors affecting the test's accuracy, including difference between the artificial pore solution and real cement pore solution. A method for directly deducing the real pore solution includes the extraction of a small amount ( $10^0$ – $10^1$  mL) of the solution after pressurizing the sample (Lothenbach *et al.*, 2007; Andersson, Allard, Bengtsson & Magnusson, 1989). Although the analysis of ion concentration of the pore solution is doubtlessly possible using such amount, much time and effort are required for obtaining a sufficient amount of pore solution ( $10^2$ – $10^3$  mL) for the tea-bag method, raising questions of method efficiency. The artificial pore solution can be manufactured based on the analyzed ion concentration of real pore solution. However, since the pre-conditions for various ions included in the cement pore solution to be dissolved in the aqueous solution are complex, the reproducibility of this method is questionable. Therefore, in the case of the tea-bag method for cement based materials, cement and water having a mass 4 to 10 times the weight of cement were mixed prior to filtration (cement filtrate) (Schroefl, Mechtcherine, Vontobel, Hovind & Lehmann, 2015; Snoeck *et al.*, 2015a; Snoeck *et al.*, 2014a; Schröfl *et al.*, 2012; Siriwatwechakul, Siramanont & Vichit-Vadakan, 2010). However, the ion concentration of such a filtrate and its reproducibility is yet to be specifically and precisely analyzed.

In the cement and concrete fields, because the actual conditions cannot be replicated using indirect methods (such as the tea-bag method), systematic analysis and reasonable test methods are required for the solutions used for the actual prediction and evaluation of absorption kinetics of SAP. For the

### Chapter 3. Absorption kinetics and retention capacity of SAP in cementitious materials

systematic analysis, the problem of excess solution in the tea-bag method, the difficulty of simulating artificial pore solutions, and the effects of additional admixtures (SF and PCE type SPPL) are among the various factors related to the SAP absorption kinetics, and should be carefully studied in advance. In addition, the issues of existing methods as mentioned above should be reviewed when suggesting potential test methods.

Based on this information, a modified tea-bag method for cement based materials is suggested in this study. By using the method, the absorption kinetics was measured and analyzed while considering the conditions of pore solutions in low w/c concrete. By reviewing the problems of existing issues, this modified method involves removing the excess solution as the method used in the polymer industry. Prior to the use of this method on deciding the SAP absorbency, the reproducibility was evaluated. To reflect the ion composition and concentration of cement pore solution, a cement filtrate is manufactured. During manufacturing, the influence of the admixture is also examined. The ion concentration changes of the filtrate due to the influence of admixture and w/c are precisely analyzed by inductively coupled plasma - optical emission spectroscopy (ICP-OES). This analysis leads to the manufacture of an artificial pore solution that can reasonably reproduce the ion concentration of cement pore solutions. Finally, the SAP absorbency decided by the tea-bag method (indirect method) was compared with the absorbency predetermined by the slump spread method (direct method).

### **3.1.2 Materials and methods**

#### **3.1.2.1 Tea-bag method**

##### ***1) Materials***

The cement filtrate used in the tea-bag method was made using cement, silica fume (SF), distilled water, and superplasticizer (SPPL). The properties and chemical composition of the materials for low w/c concrete are presented in Section 4. The pH of the distilled water was measured as 6.46, while the PCE type SPPL's pH was 4.47. To determine the solid contents in the SPPL, 2 g of aqueous SPPL was placed in a drying furnace of  $105 \pm 1$  °C for 4 h (Lothenbach *et al.*, 2007). The measured solid contents were  $30 \pm 0.65\%$ , matching the manufacturer's data (30%). In this study, the name SPPL was defined by the form of aqueous solution sold by the manufacturer, and the name PCE was used to define the 30% solid contents dissolved within. The ion concentration of SPPL was analyzed by the ICP-OES as shown in Table 3-1. The results showed that  $\text{Na}^+$  and  $\text{S}^{2-}$  are mainly featured, while multivalent cations like  $\text{Ca}^{2+}$ ,  $\text{Mg}^{2+}$  and  $\text{Al}^{3+}$  are present at negligible concentrations ( $< 1$  mM).

Table 3-1 Ion concentration of used superplasticizer by ICP-OES analysis

Elements	Na	K	Ca	Mg	Al	Fe	Si	S
<b>Ion concentration [mM]</b>	72.57	5.54	0.28	0.05	0.004	0.03	0.03	34.82

### ***2) Preparation of cement based solutions***

During the preparation of the cement filtrate, SF and PCE were added in order to realistically reflect the ion concentration of pore solution in low w/c concrete. In addition, to investigate the dilution effect of ions (i.e., caused by the inclusion of large amounts of water compared to the real pore solution), the different w/c ratios of the filtrates were prepared as 1, 2, 4, and 10. The name, mix proportion of the solutions, and the cement filtrates are presented in Table 3-2.

Chapter 3. Absorption kinetics and retention capacity of SAP in cementitious materials

Table 3-2 Mix proportion and ion concentration of solutions

Solution name	w/c	sf/c	PCE/w	Ion concentration by ICP-OES [mM]								pH
				Na	K	Ca	Mg	Al	Fe	Si	S	
Solution A	n.a	n.a	0%	35.50	169.17	0.02	0.000	0.007	0.004	0.268	10.66	13.14
Mixing water [0%]*	n.a	n.a	0%				Not conducted				6.46	
Mixing water [2%]**	n.a	n.a	2.12%				Not conducted				4.44	
Mixing water [4%]**	n.a	n.a	4.24%	9.78	1.16	0.23	0.014	0.006	0.006	0.016	4.26	4.43
Filt.[1][SF:X][0%]	1	0	0%	15.06	124.75	15.37	0.000	0.001	0.007	0.027	52.81	13.07
Filt.[1][SF:O][0%]	1	0.25	0%	23.70	136.22	11.05	0.000	0.001	0.010	0.060	57.41	13.04
Filt.[2][SF:X ][0%]	2	0	0%	8.14	65.25	23.09	0.000	0.001	0.003	0.021	31.32	12.95
Filt.[2][SF:O][0%]	2	0.25	0%	10.96	68.53	20.98	0.000	0.001	0.003	0.035	31.42	12.95
Filt.[4][SF:X][0%]	4	0	0%	4.34	30.98	25.90	0.000	0.001	0.003	0.015	20.68	12.85
Filt.[4][SF:O][0%]	4	0.25	0%	5.83	31.89	23.90	0.000	0.001	0.004	0.033	21.00	12.85

Chapter 3. Absorption kinetics and retention capacity of SAP in cementitious materials

Table 3-2 Mix proportion and ion concentration of solutions (cont.)

Solution name	w/c	sf/c	PCE/w	Ion concentration by ICP-OES [mM]								pH
				Na	K	Ca	Mg	Al	Fe	Si	S	
Filt.[4][SF:X][2%]	4	0	2.12%	11.50	31.29	42.27	0.368	1.764	0.910	2.933	27.85	12.67
Filt.[4][SF:O][2%]	4	0.25	2.12%	12.09	32.16	30.95	0.294	1.204	0.590	3.175	24.01	12.67
Filt.[4][SF:X][4%]	4	0	4.24%	16.15	30.24	57.57	0.553	1.966	1.329	5.430	30.00	12.49
Filt.[4][SF:O][4%]	4	0.25	4.24%	16.58	30.78	40.92	0.486	0.573	0.889	4.975	21.98	12.5
Filt.[4][SF:X][4%]@***	4	0	4.24%	40.93	256.98	37.70	0.857	2.339	2.324	7.201	25.17	13.46
Filt.[4][SF:O][4%]@***	4	0.25	4.24%	40.35	257.30	33.03	0.667	1.979	1.638	6.747	24.90	13.46
Filt.[10][SF:X][0%]	10	0	0%	2.11	11.88	12.33	0.003	0.003	0.009	0.199	12.06	12.23
Filt.[10][SF:O][0%]	10	0.25	0%	2.53	11.98	12.57	0.003	0.003	0.007	0.239	12.92	12.29

\* Distilled water

\*\* Distilled water with superplasticizer

\*\*\* “@” symbol indicates additional dissolutions of sodium hydroxide and potassium hydroxide.

### Chapter 3. Absorption kinetics and retention capacity of SAP in cementitious materials

First, Solution A (not a cement filtrate) was manufactured by dissolving KOH, NaOH, Na<sub>2</sub>SO<sub>4</sub>, and Ca(OH)<sub>2</sub> powders in distilled water as described in the previous study (Addari, Elsener & Rossi, 2008). The purpose of this solution was to simulate the ion concentration of concrete pore solution in the long term. This does not coincide with the purpose of this study which considers the absorption kinetics of SAP wherein the ion concentration of fresh concrete is mainly of interest. As can be seen in Table 3-2, Solution A has a negligible Ca<sup>2+</sup> concentration (0.02 mM), and contains primarily monovalent cations such as Na<sup>+</sup> (35 mM) and K<sup>+</sup> (169 mM). Therefore, Solution A was used in the preliminary test stage for the evaluation of SAP absorption kinetics and a reliable review of tea-bag methods in the strong alkali solutions (pH > 13) comprised of only monovalent cations.

Next, total 14 types of cement filtrates were manufactured, and labeled based on the combination of Filt.[w/c][SF:O/X][PCE/W]. [w/c] refers to the water to cement ratio, while [SF:O] or [SF:X] denotes the addition of 25% silica fume into the cement or not. [PCE/W] refers to the PCE to water ratio (0%, 2.12%, 4.24%) of the mixing water. The 4.24% of PCE/w, in accordance with the mix proportion of the developed UHPC as presented in Section 4, was determined by considering basic w/c (0.243, including water in SPPL) with PCE/c (0.012, only solid contents) and additional w/c (0.04, w<sub>e</sub>/c of AA\_0.255). Because mixing water [0%] is identical to distilled water, the ion concentration was not measured. Mixing water [2%] also does not require measurement, as its concentration of main ions can be estimated from the results of mixing water [4%] which has twice the PCE/w. Based on the analysis results of Table 3-2, the primary ions present in mixing water [4%] are Na<sup>+</sup> and S<sup>2-</sup> (i.e., the same as

SPPL). However, the concentrations were reduced to 9.78 mM and 4.26 mM respectively, due to dilution effects. In addition, due to the presence of SPPL, the two mixing waters of [2%] and [4%] are both acidic. Such ion concentrations demonstrate that the ionic condition of mixing water mixed with PCE type SPPL is totally different from that of pure water. Finally, the symbol “@” included in the name denotes additional sodium hydroxide and potassium hydroxide dissolved in the filtrate. This additional dissolution was conducted in order to compensate for very low monovalent ion concentrations ( $\text{Na}^+$ ,  $\text{K}^+$  and  $\text{OH}^-$ ) resulting from dilution effects.

For the tea-bag method, each filtrate was manufactured at a mass 1,000 – 1,500 × the weight of dry SAP. First, cement with or without SF was mixed with mixing water for 10 min while preventing the particles from subsiding. Filter papers were then used to filter those particles > 3 μm size (top 95% of cumulative cement particle size distribution) through 5 stages (filtering by 25 μm, 12 μm, 8 μm, 5 μm, and 3 μm). When particles are present in solution during the tea-bag method, they can reduce measurement accuracy by coating the surface of the tea-bag or SAP particles. Samples including the “@” symbol in their names were additionally dissolved with sodium hydroxide and potassium hydroxide powders after passing through 5 μm size filter paper. Particles left over from dissolution were filtered with 3 μm size filter paper, along with the cement particles. The filtrate prepared by this procedure was directly used for pH measurement (calibrated by pH 4, 7, and 10 buffer solutions) and tea-bag method. Additionally, 0.45 μm size Teflon filter was used to conduct ICP-OES analysis of 10–15 mL vacuum filtrated solutions. The temperature of all solutions was maintained at 20±1 °C.

Because the absorption of IC water by SAP is effective in fresh concrete (Hasholt *et al.*, 2012), all procedures involving the filtrates were conducted within 7 h of cement mixing, confirmed with no rapid changes of ion concentrations in the cement pore solution (Lothenbach & Winnefeld, 2006). Furthermore, the experimental solutions were all sealed and stored to avoid any changes in ion concentration due to carbonation. Based on these procedures, the concentration of the main ions ( $\text{Na}^+$ ,  $\text{K}^+$ ,  $\text{S}^{2-}$  and  $\text{Ca}^{2+}$ ) and pH are measured and listed in Table 3-2. The influence of each factor on the ion concentrations of the cement filtrate will be discussed later.

### ***3) Test procedure***

The SAP absorption kinetics are determined according to the modified tea-bag method. First, to manufacture the tea-bag, an electronic scale (precision of  $\pm 0.1$  mg) is used to put 0.1 g ( $W_0$ ) of dry SAP particles into a tea-bag ( $85 \times 75$  mm<sup>2</sup> size) made of polyethylene and polypropylene fabric, which was then sealed. Next, the tea-bags are completely submerged in a container of solution (see Fig. 3-1). After a predetermined time, the tea-bags are then removed and the liquid on the surface of the tea-bag is lightly wiped with a dry cloth, after which the weight of the swelled tea-bag ( $W_1$ ) is measured. After measuring  $W_1$ , the tea-bags are mounted on the inner wall of a perforated cylindrical spin dryer container, and the excess solution is then removed by the centrifuge operated at 1000 rpm. Finally, the tea-bag weight ( $W_2$ ) after centrifugation is measured. Absorbency is determined by the weight of solution absorbed by the unit weight

(1 g) of dry SAP,  $(W_2 - W_0)/W_0$ , while the excess solution ratio is calculated by the absorbency reduced by the centrifugation,  $(W_1 - W_2)/W_0$ . When calculating the absorbency, the weight of the tea-bag itself (measured prior to the experiment) is deducted from  $W_1$  or  $W_2$ . At the 1, 10, 30, 60, and 180 min, the absorbency is monitored and recorded to obtain an absorption kinetics curve.



Fig. 3-1 Tea-bag method using various solutions

### **3.1.2.2 Slump spread measurement for evaluating absorbency of SAP**

To evaluate the influence of SAP addition to the flowability of low w/c concrete (UHPC), the slump spread value was measured at the 5, 10, and 20 min after the addition of water. This mix proportion was selected based on the experimental result that shrinkage was effectively mitigated without diminished flowability and strength loss, which will be rigorously reviewed and discussed in Section 5. Mixing and the slump spread measurement of the concrete were conducted according to the optimized method (in Section 4) and ASTM standards (but without impact of flow table) (ASTM, 2014), respectively. The slump spread value was recorded as the average between the maximum

diameter and its perpendicular diameter of spread.

### **3.1.3 Results and discussion**

#### **3.1.3.1 Evaluation of suggested modified method**

Above all, this study suggests a modified tea-bag method which is suitable for the purpose of cement based materials, based on the review of known problems of existing tea-bag methods. In order to prevent absorbency overestimation due to excess solution, the suggested method includes a centrifugal process utilizing a spin dryer. In the polymer industry, this process is used not only to remove excess solution, but also to measure the retention capacity of SAP absorbency after centrifugation (Buchholz, 1994; Nagorski, 1994). By using this process in the tea-bag method, we propose that more accurate and realistic absorbency measurements in cement based solutions can be possible (Zohuriaan-Mehr & Kabiri, 2008).

##### ***1) Excess solution depending on centrifugation time and SAP type***

To evaluate the correlation between solution absorbed by SAP and excess solution, distilled water and Solution A (which does not include multivalent cations) were used. Fig. 3-2 shows the SAP absorbency at 30 min as a function of centrifugation time. In Section 3, circular points denote results of SAP\_AM, while rectangular points denote those of SAP\_AA.

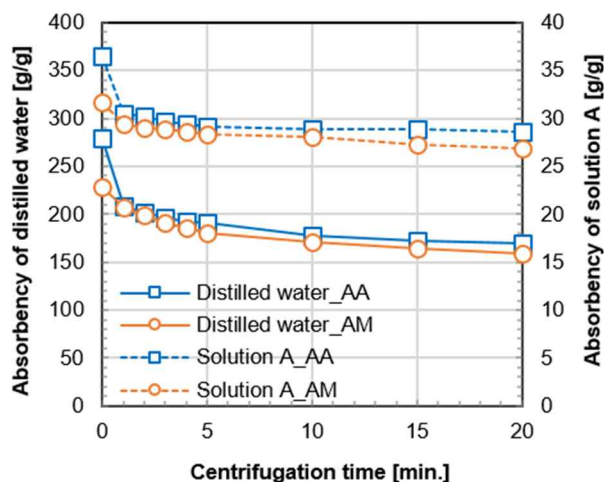


Fig. 3-2 Absorbency of SAPs in distilled water and solution A as a function of centrifugation time

In all cases, the dewatering rate was the fastest during the first minute, after which the rate decreases and then maintains a constant value (Fig. 3-2). The constant release from the tea-bag between 1–20 min is possibly the solution absorbed by SAP, rather than the excess solution to be removed. SAP containing large amounts of water has a fast dewatering speed due to the influence of pressure. Generally, the more water absorbed per unit weight of dry SAP, the greater the centripetal force developed at a given rotation speed, leading to increase the applied pressure on SAP. Along with the removal of excess solution, this centrifugal process can be also used to evaluate the retention capacity of SAP absorbency under pressure (Nagorski, 1994). However, since the pressure-

dependent dewatering or water release of SAP is outside the scope of this study, it will not be examined further.

Based on the obtained results, the centrifugal time was determined as 1 min. Along with this determination, this study suggests that the removal of excess solution including that in the tea-bag can be reasonably conducted by centrifugation without loss of SAP absorbency. This also considers the negligible amount of dewatered Solution A after the first minute. In addition, it is clear that the strong alkaline solution containing cations is more similar to the cement pore solution or filtrate than the distilled water. Therefore, it is herein concluded that the SAP dewatering trend by using the centrifugal process for more than 1 min under the condition of distilled water does not need to be considered.

Without using the centrifugal process, the SAP\_AA absorbency is higher than the SAP\_AM absorbency in both solutions. However, the amount of water removed during the first minute is larger for SAP\_AA than for SAP\_AM. Therefore, after the centrifugation, both SAPs show similar absorbency. Fig. 3-3 shows the correlation between the SAP absorbency determined without the centrifugation and excess solution ratio; this relationship was derived by using all 118 results of the tea-bag method in this study. The excess solution ratio also increases proportionally as more solutions are absorbed into SAP. This is because the ratio increases along with the increased space between particles wherein the excess solution can be trapped.

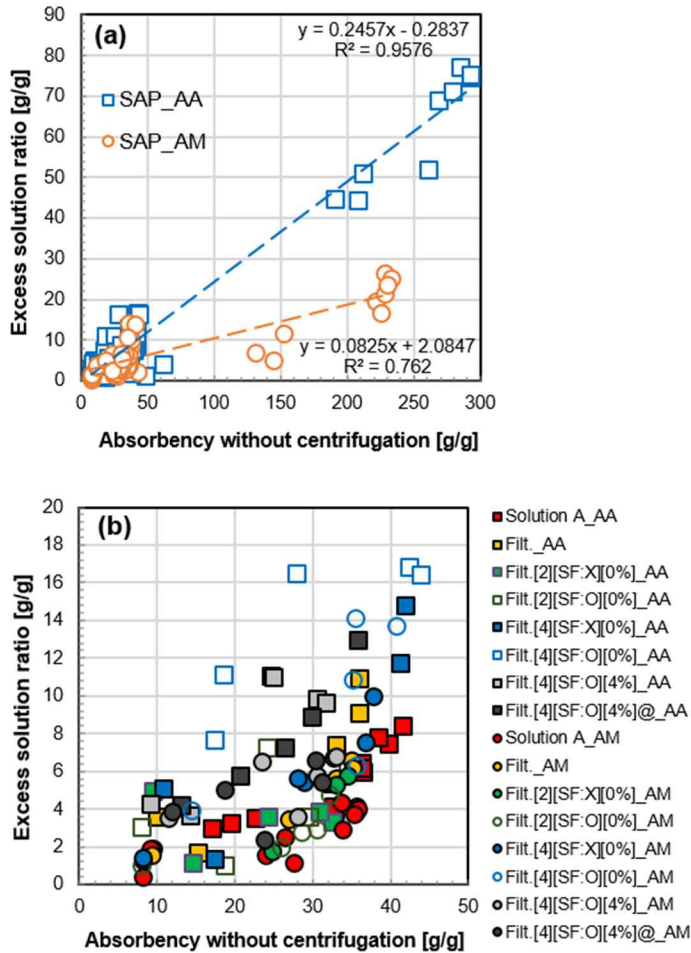


Fig. 3-3 Relationship between absorbencies without centrifugation and excess solution: Results including (a) and excluding (b) distilled water

The excess solution ratios after the one-minute dewatering process are  $25 \pm 13\%$  for SAP\_AA and  $16 \pm 8\%$  for SAP\_AM on average. This is due to the difference in type and shape between the SAPs. The inside of the tea-bag after removing the excess solution showed that unlike SAP\_AM, which could still be individually separated even after swelling, the SAP\_AA seemed to easily block excess solution due to the coagulation of SAP particles after swelling,

along with its irregular shape. In such conditions, conventional tea-bag methods without considering the trapped excess solution cannot be accurate. Moreover, if the excess solution is not completely removed in the tea-bag method, the SAP absorbency can be easily overestimated. The risk of such overestimation depends on the shape and type of the SAP, and thus the risk in irregular SAP\_AA is higher than that of the globular SAP\_AM.

## ***2) Reproducibility of the modified tea-bag method***

To evaluate the reproducibility of the suggested tea-bag method, the SAP absorption kinetics were measured in triplicate for each set of conditions. Accounting for few-second error (< 3 s) from submerging the tea-bag in the solution or removing it, the absorbency and standard deviation for each trial is shown in Fig. 3-4. Both the distilled water and Solution A showed enhanced reproducibility as the absorption time increased. Since the absorption speed of SAP is faster at the initial state, the influence of the few-second tolerance on the absorbency can be quite noticeable. As a consequence, the variation in absorbency was 10% at the 10 min and lower than 4% after the 30 min, which are acceptable. However, since the coefficient showed a highest value (up to 25%) at the first minute, the reproducibility was less than ideal in terms of tolerance. If the absorption time is accurately observed during evaluation, the proposed tea-bag method is reproducible. Therefore, the SAP absorbency for each timeline within a cement filtrate was determined by the measurement value of a single tea-bag considering the efficiency of the experiment.

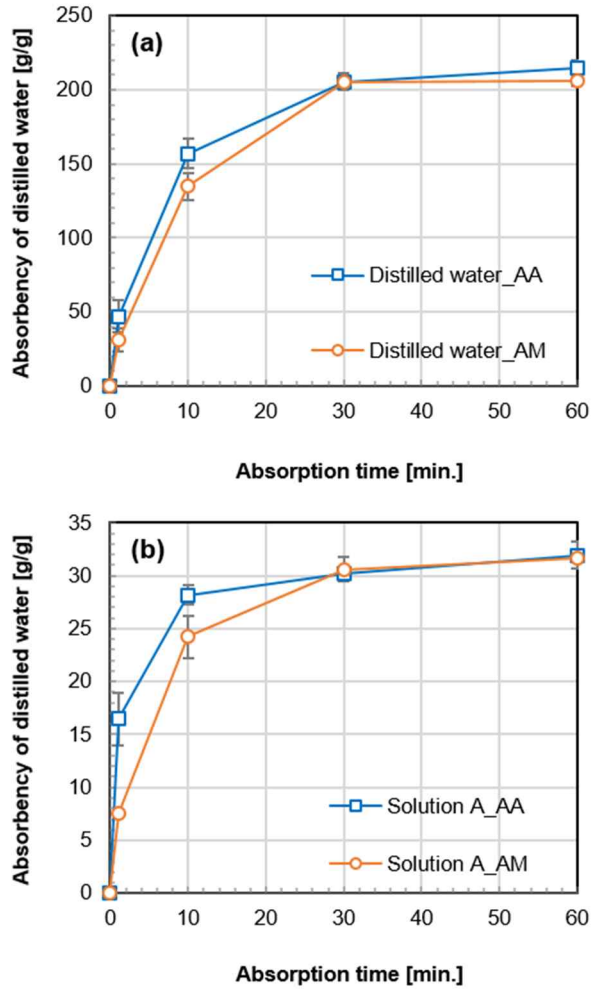


Fig. 3-4 Absorbency of SAPs in distilled water (a) and solution A (a) with standard deviation

Compared to distilled water, the absorbency of SAPs in Solution A was reduced to 1/7 due to the influence of monovalent ions (Fig. 3-4). However, regardless of the SAP type, the equilibrium swelling (or absorbency) and absorption kinetics did not largely differ in each solution, and swelling reduction was also not observed. In terms of absorption speed, SAP\_AA is faster up the 10 min, while SAP\_AM is faster at 10–30 min. After the 30 min,

both SAPs show nearly identical absorbency and absorption kinetics.

### **3.1.3.2 Ion concentration of cement filtrate**

Prior to discussing the ion concentration in the cement filtrate, the ion composition and concentration of the cement pore solution must first be understood. When OPC is mixed with water,  $K^+$ ,  $Na^+$ , and  $SO_4^{2-}$  are quickly dissolved.  $Ca^{2+}$  is also dissolved from free lime, alite ( $C_3S$ ), and belite ( $C_2S$ ) (Hewlett, 2010). The clinker phases ( $C_3S$ ,  $C_2S$ ,  $C_3A$ ,  $C_4AF$ ) and sulfates in OPC, cause the cement pore solution to become a strong alkali solution during hydration (Lesti *et al.*, 2010). Among the various ions dissolved in the pore solution, those with the highest concentrations are  $Na^+$ ,  $K^+$ ,  $Ca^{2+}$ ,  $OH^-$ , and  $SO_4^{2-}$  (Zhu *et al.*, 2015; Mechtcherine & Reinhardt, 2012). Because of these ions, the pore solution becomes an electrolyte solution (2-3%) (Lesti *et al.*, 2010; Rechenberg & Sprung, 1983), and the concentration of ions changes depending on the hydration time (Mechtcherine & Reinhardt, 2012; Lothenbach & Winnefeld, 2006). During the induction or dormant period, the hydration speed is very slow, and the concentration is maintained to levels similar to the initial stage. After that, the  $Ca^{2+}$  concentration rapidly reduces due to portlandite precipitation and AFt formation (Hewlett, 2010). The  $SO_4^{2-}$  concentration also starts to decline due to AFt formation and the adsorption of sulfate on the surface of C-S-H phase (Hewlett, 2010). Along with  $Ca^{2+}$ ,  $Al^{3+}$  is another ion that can decisively influence the SAP absorption kinetics (Zhu *et al.*, 2015). However, its concentration in this instance ( $< 0.01$  mM) is maintained at a very

low during the entire hydration period (Hewlett, 2010).

### ***1) Effects of water to cement ratio on ion concentration***

Fig. 3-5 shows the ion concentration ratio of major ions as well as the pH for different w/c values of the cement filtrates. The ion concentration ratio is defined as the ratio of each ion concentration present in the base filtrate (w/c = 1). Due to the dilution effects, the concentrations of Na<sup>+</sup>, K<sup>+</sup>, and SO<sub>4</sub><sup>2-</sup> decrease as w/c increases regardless of the SF addition. Such effects are also relevant to OH<sup>-</sup>, so the pH decreases as w/c increases.

On the other hand, the decreasing trend of Ca<sup>2+</sup> ion concentration was only apparent in the w/c range of 4–10. Within the w/c range of 1–4, even though more water was included, the Ca<sup>2+</sup> concentration in the filtrate increases; this increase of concentration is because the solubility Ca<sup>2+</sup> in the cement pore solution is pH-dependent (Bonen & Sarkar, 1995; Moragues, Macias & Andrade, 1987). In other words, when the pore solution's pH decreases, the Ca<sup>2+</sup> concentration increases and vice versa. The Ca<sup>2+</sup> concentration in the solution is inversely proportional to the OH<sup>-</sup> concentration as shown in Frattini's curve, which has been confirmed in both the artificial pore solution and the cement pore solution (Moragues *et al.*, 1987; Rechenberg & Sprung, 1983). The w/c range of 1–4 applicable to the cement filtrate also indicates that the pH change by dilution effects contributes to the overall Ca<sup>2+</sup> concentration (Fig. 3-5).

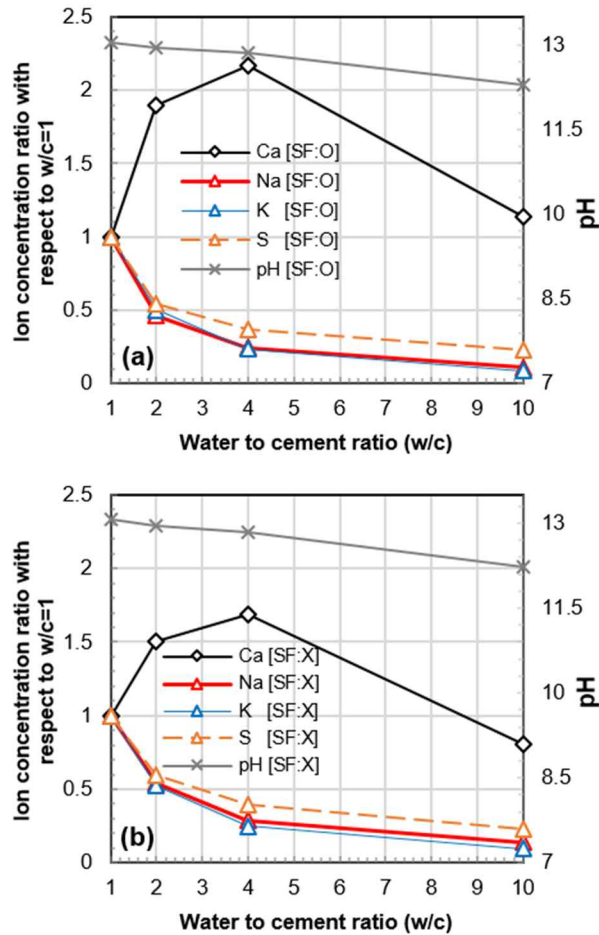


Fig. 3-5 Ion concentration ratio of cement filtrate with (a) or without (b) silica fume as a function of w/c

When w/c is held constant, the  $\text{Ca}^{2+}$  concentration decreases along with SF addition; this decrease is even more prominent when w/c is low (Fig. 3-6 (a)). Therefore,  $\text{Ca}^{2+}$  concentration as w/c increases is more prominently increased in the filtrate when SF is included (Fig. 3-5).

***2) Effects of silica fume and PCE additions on ion concentration***

Although the addition of SF has a minimal effect on the pH of the filtrate, it induces changes to the concentrations of the main ions ( $\text{Na}^+$ ,  $\text{K}^+$ ,  $\text{SO}_4^{2-}$ , and  $\text{Ca}^{2+}$ ) under various conditions (Fig. 3-6 (a)). Within the w/c range of 1–10, the ion concentrations of  $\text{Na}^+$ ,  $\text{K}^+$ , and  $\text{SO}_4^{2-}$  increased by 20–57%, 1–9%, and 2–9% respectively, due to the addition of SF, while the  $\text{Ca}^{2+}$  concentration decreased by up to 28%. As mentioned earlier, the change of ion concentration caused by the addition of SF is more prominent in the mixture of low w/c values. One reason why SF addition can change the ion concentration of cement pore solution is because SF adsorbs water in competition with the cement (Mechtcherine, Secieru & Schröfl, 2015); such adsorption can reduce the effective w/c. During the manufacture of the filtrate, the same amount of SF was included regardless of the w/c value. Therefore, at low w/c values, such adsorption can obviously affect changes in the ion concentration. Similarly, in previous studies examining the ion concentration of cement pore solution ( $w/(c+sf)=0.4-0.56$  with  $sf/c=0.2$ ), the addition of SF clearly affected changes in the aqueous phase of the cement system and the concentration of main ions (Larbi, Fraay & Bijen, 1990).

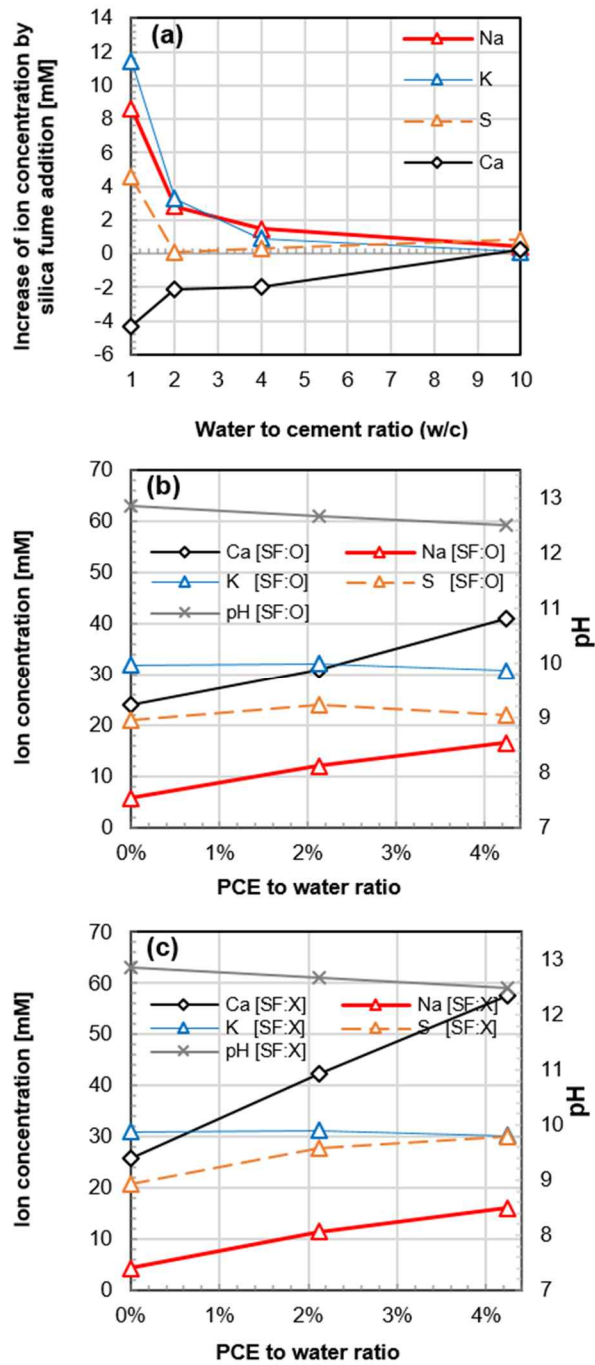


Fig. 3-6 Variation of ion concentration due to silica fume addition as function of w/c (a), and effect of PCE to water ratio on ion concentration of cement based solution (w/c = 0.4) with (b) or without (c) silica fume

Meanwhile, the pH of the filtrate decreased as the ratio of PCE in the mixing water increases (Fig. 3-6 (b)), because the acidic SPPL was added to the mixing water. While the  $K^+$  concentration was maintained at a constant level regardless of the PCE/w, the concentration of  $Na^+$  and  $Ca^+$  increased proportionally. Also, the  $S^{2-}$  concentration tends to increase. SPPL itself contains  $Na^+$  and  $S^{2-}$ , so as the PCE/w increases, the concentration of these ions in the filtrate also increases. In the cement pore solution ( $w/c = 0.4$ ), similarly, although new complexation does not form with the ions included in the pores solution due to the addition of PCE type SPPL, the  $Na^+$  concentration in the pore solution increases by about 10% because SPPL itself contains  $Na^+$  (Lothenbach *et al.*, 2007). Moreover, in this study, it was also confirmed that the increase of the  $Na^+$  concentration is proportional to the PCE/w.

This study experimentally verified that the  $Ca^{2+}$  concentration in the filtrate could increase proportionally depending on the PCE contents. This increase arises not because of a direct supply from SPPL (as in the case for  $Na^+$ ), but because of indirect factors such as the decreased pH in the filtrate (after mixing with PCE). Two filtrates having PCE/W of 4.24% (Filt.[4][SF:X][4%], Filt.[4][SF:O][4%]), contain more water than real cement pore solutions. However, they possess higher  $Ca^{2+}$  concentration (41-57 mM) than the pore solutions. Both the cement pore solution ( $w/c=0.5$ ) within 7 h of manufacture (Lothenbach & Winnefeld, 2006) and cement pore solution including SF at 10 min (Larbi *et al.*, 1990) had  $Ca^{2+}$  concentrations  $< 25$  mM. The  $Ca^{2+}$  concentration of the cement filtrates I this study is ranged within that of UHPC

(30–62 mM) (Plank, Schroefl, Gruber, Lesti & Sieber, 2009). This high  $\text{Ca}^{2+}$  concentration of the two filtrates is due to decreased pH by  $\text{OH}^-$  dilution effects and the addition of  $\text{H}^+$  (from acidic SPPL).

The concentration of major two ions ( $\text{Na}^+$ ,  $\text{K}^+$ ) in the filtrate is far lower than that in the cement pore solution within 7 h limit ( $\text{Na}^+$ : 26–30 mM,  $\text{K}^+$ : 320–360 mM) (Lothenbach & Winnefeld, 2006). The concentration of monovalent cations in the pore solution is in the range of 350–390 mM, while the concentration in the two filtrates was only 47 mM. The pH value of the filtrates was approximately 12.5, lower than that of the cement pore solutions (i.e., higher than 13) (Larbi *et al.*, 1990). In short, the dilution effect of cement filtrate by the addition of large amount water only affects the concentrations of major four ions ( $\text{Na}^+$ ,  $\text{K}^+$ ,  $\text{SO}_4^{2-}$ , and  $\text{OH}^-$ ), while the  $\text{Ca}^{2+}$  concentration in the filtrate ( $w/c = 4$ ) is higher than in the cement pore solution. Therefore, without proper treatment, when the cement filtrate ( $w/c = 4.3$  or 10) is used in the tea-bag method, either the influence of the four ions on SAP absorption kinetics can be severely underestimated due to the dilution effect, or the influence of divalent cations can be severely overestimated.

### ***3) Additional dissolution of monovalent ions ( $\text{Na}^+$ , $\text{K}^+$ , $\text{OH}^-$ )***

Comparing the ion concentrations within the cement pore solution,  $\text{Na}^+$ ,  $\text{K}^+$ , and  $\text{OH}^-$  ions were dissolved in the two filtrates (Filt.[4][SF:X][4%], Filt.[4][SF:O][4%]) to reflect the influence of SF and PCE. The concentrations of  $\text{Na}^+$  and  $\text{K}^+$  increased from 16 mM and 30 mM to 40 mM and 257 mM

respectively, due to additional dissolution. The pH increased from 12.5 to 13.46 as the  $\text{OH}^-$  was also dissolved. Because of this, the  $\text{Ca}^{2+}$  concentration decreased from 40.9–57.6 mM to 33.0–37.7 mM. The decreased  $\text{Ca}^{2+}$  concentration remains in the range of UHPC, which can mitigate the risk of misleading absorption kinetics based on high  $\text{Ca}^{2+}$  concentration. Although it is an artificial treatment, an artificial pore solution similar to the cement or concrete pore solution can be manufactured; by using this solution along with the suggested tea-bag method, the SAP absorption kinetics can be realistically predicted and evaluated.

### **3.1.3.3 Absorption kinetics of superabsorbent polymers in various ionic solutions of cement filtrates**

When the SAP comes into contact with water or aqueous solutions, the hydrophilic groups (carboxylate and carboxylamide) draw in the water or solution, while the inside of the SAP forms an electrolyte solution because the cations (e.g.  $\text{Na}^+$  or  $\text{K}^+$ ) in SAP are released into the water, as shown in Fig. 3-7 (Wang, Yang, Cheng, Wu & Liang, 2015; Zhu *et al.*, 2015). Osmotic pressure is developed due to the difference of total ion concentration between the inside of the SAP and the external solution, making the absorption continuous. Therefore, the higher the ion concentration of the external solution, the lower the SAP absorbency (Mechtcherine & Reinhardt, 2012). In the SAP network, which is grid-like due to cross-linking, absorption is proceeded along with volume expansion due to the electrostatic repulsion by the anionic groups such

as carboxyl groups (Jignesh H. Trivedi, 2015). However, when commercial SAP absorbs cations with a solution, a charge screening effect occurs due to irreversible ionic exchange between the absorbed cations and anionic groups. As this weakens the electrostatic repulsion, the SAP absorption capacity is reduced. Moreover, since additional ionic cross-links are formed as a result of the ion exchange, the SAP cross-link density increases. SAP can effectively absorb the solution under external pressure thanks to its grid-like cross-linked structure. Therefore, cross-linking is an essential factor for the performance of SAPs. However, although a higher cross-link density leads to better absorption capacity under external pressure, the maximum absorbency decreases (Pourjavadi, Soleyman, Ghasemzadeh & Salimi, 2010; Jensen & Hansen, 2001b; Shimomura & Namba, 1994; Flory, 1953). Therefore, ionic cross-linking effect is a main factor for decreased absorption capacity of SAP.

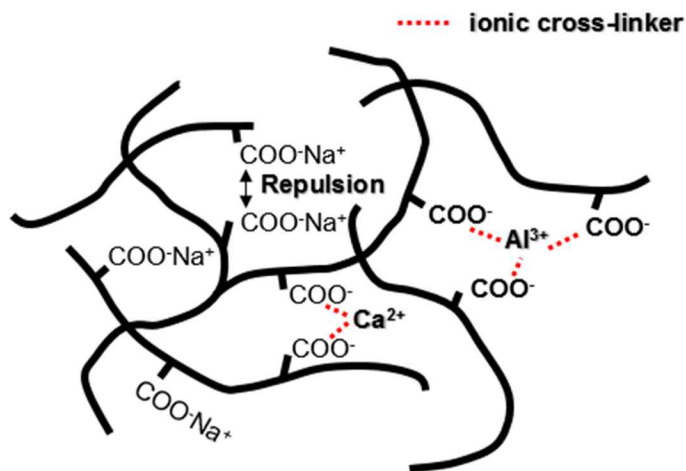


Fig. 3-7 Structure of swollen polyacrylate SAP  
(Zhu *et al.*, 2015)

In the case of concrete pore solutions, irreversible ion exchange occurs between the cations dissolved from cement and anionic groups within commercial SAP (Shimomura & Namba, 1994). The cations are eventually connected through charge screening effect and ionic cross-linking effect, which are major factors contributing to the decreased absorbency. Such effects depend on the type and concentration of cations included in the solution (Zhu *et al.*, 2015; Schröfl *et al.*, 2012). In particular,  $\text{Ca}^{2+}$  contributes to both the SAP absorption capacity and kinetics, and in this regard is the most important among those ions present in the cement pore solution (Schröfl *et al.*, 2012; Lesti *et al.*, 2010). These multivalent cations form intermolecular complexes or ionic cross-links along with the anionic groups inside the SAP (Jignesh H. Trivedi, 2015). The factors, which can decrease SAP absorption capacity caused by the ions present in the concrete pore solution, can be summarized in three steps (Pourjavadi *et al.*, 2013). First, the osmotic pressure decreases due to the high total ion concentration of the pore solution. Second, a charge screening effect arising from the cations decreases the anionic-anionic repulsion. Lastly, ionic cross-linking effects are developed by the multivalent cations (such as  $\text{Ca}^{2+}$ ), leading to increased SAP cross-link density.

Based on the experimental parameters of w/c, sf/c, and PCE/w in these cement filtrates, changes in ion concentration were quantitatively verified by ICP-OES analysis. Because these factors can influence the SAP absorbency and absorption kinetics in cement based materials, the effects of these parameters along with the additional dissolution of monovalent ions on the absorbency and kinetics were investigated and discussed using the suggested tea-bag method.

***1) Absorption kinetics in cement filtrate as a function of water to cement ratio***

Using Fig. 3-8, it is possible to observe the influence of cement filtrates' w/c on absorption kinetics of SAP. As w/c increases from 1 to 4, the initial absorbency (up to 30 min) increases, while the long-term absorbency (30 min to 180 min) decreases. As mentioned previously, the concentration of four main ions ( $\text{Na}^+$ ,  $\text{K}^+$ ,  $\text{SO}_4^{2-}$ , and  $\text{OH}^-$ ) in the filtrate decreases, as w/c increases. Such a decrease in concentration increases the osmotic pressure (Schröfl *et al.*, 2012) and mitigates charge screening effects (Jignesh H. Trivedi, 2015), which in turn causes an increase of the initial absorbency. Changes of the absorption kinetics in the filtrate based on the increased w/c can also be confirmed (Fig. 3-8). As w/c increases, the swelling reduction is accelerated after 30 min, thus the long-term absorption kinetics is changed. Such changes in the swelling reduction and absorption kinetics arise due to multivalent cations like  $\text{Ca}^{2+}$ , rather than from monovalent cations or anions (Zhu *et al.*, 2015; Schröfl *et al.*, 2012). Through the result in Fig. 3-4, it is confirmed that the SAP absorption kinetics is not changed by concentration of monovalent cations. The monovalent cations absorbed by SAP along with water deprotonate with only one anionic group, while the divalent cations can deprotonate with two anionic groups (Zhu *et al.*, 2015). Since the cross-link density of SAP is increased while shrinking due to the deprotonation of  $\text{Ca}^{2+}$ , not only the water flow into SAP is blocked but also the swelling reduction occurs. This can change the absorption kinetics of SAP. In addition, because such increases and shrinkage occur mainly on the surface

of SAP (Jignesh H. Trivedi, 2015; Pourjavadi & Mahdavinia, 2006), SAP becomes more hardened (Zhu *et al.*, 2015).

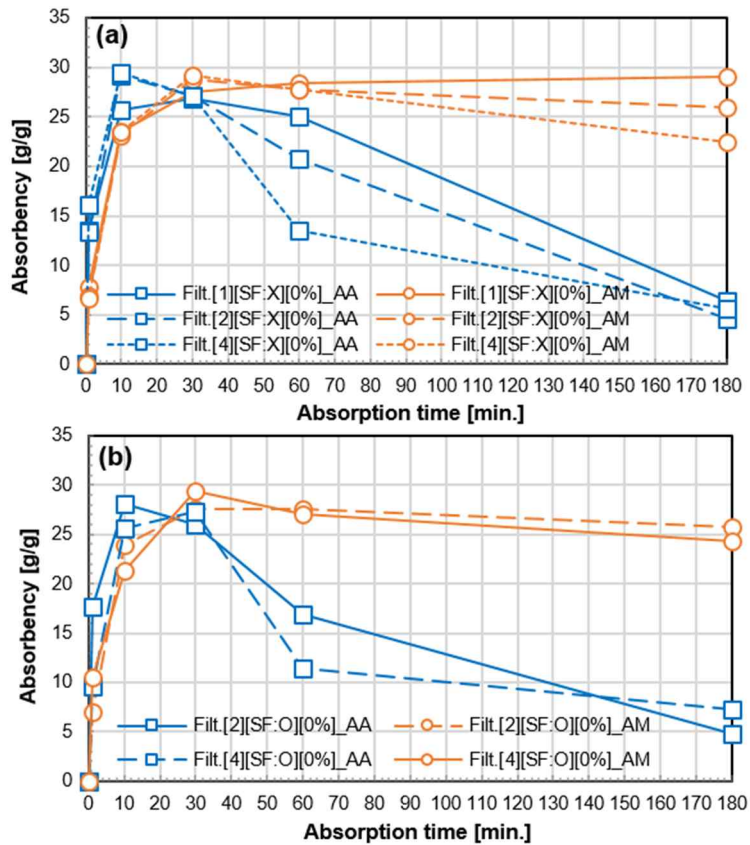


Fig. 3-8 Effect of w/c on absorption kinetics of SAP in cement filtrates: without silica fume (a) and with silica fume (b)

SAP\_AA is more sensitive than SAP\_AM in terms of absorbency and absorption kinetics based on the cation concentration in the filtrate, (Fig. 3-8). The initial absorbency of SAP\_AA is higher than that of SAP\_AM; the same trend was also shown in the aqueous solution containing only monovalent cations (Fig. 3-4). However, the long-term absorption kinetics are completely

different from this. After the 30 min, the absorbency of SAP\_AA becomes far lower than the absorbency of SAP\_AM due to the constant swelling reduction. The absorbency of SAP\_AA at the 180 min ranges from 4.5–7.3, which is about 17–30% that of SAP\_AM (which has an absorbency of 22.5–29.1). Therefore, the long-term absorbency of SAP\_AA is clearly influenced by  $\text{Ca}^{2+}$  due to its higher anionic group density.

Previously, Siriwatwechakul et al. (Siriwatwechakul *et al.*, 2010) measured cation absorbency of SAP by using a cement filtrate ( $w/c = 10$ ). As the acrylic acid present in the SAP (copolymerized acrylic acid and acrylamide type) increases, the amount of cations absorbed by SAP also increased. Although the filtrate was used to consider the various cations present in the cement pore solution, the measured cations absorbency did not distinguish the different types of cations present. Using a solution containing 25 mM  $\text{Ca}^{2+}$  (aside from the cement filtrate), Zhu et al. (Zhu *et al.*, 2015) reported that as the acrylic acid ratio of SAP (copolymerized acrylic acid and acrylamide type) increases, the amount of  $\text{Ca}^{2+}$  trapped by SAP increases, eventually leading to swelling reduction. In a solution containing various cations, assuming that there are no interactions between the cations, it can be concluded that the swelling reduction of SAP\_AA occurs more noticeably as the amount of  $\text{Ca}^{2+}$  trapped therein is much greater.

***2) Effects of silica fume and PCE additions into cement filtrate on absorption kinetics***

Fig. 3-9 shows the absorption kinetics of SAP as a function of SF addition. As mentioned in Section 3.2, the concentrations of  $\text{Na}^+$ ,  $\text{K}^+$ , and  $\text{SO}_4^{2-}$  in the cement filtrate increased as a result of SF addition, while the  $\text{Ca}^{2+}$  concentration decreased. However, the degrees of this increase and decrease were negligible when compared with other influential factors (w/c, PCE/w). The measurement results from the tea-bag method showed that SF addition affected the SAP absorbency, albeit to a lesser degree than expected compared to other factors. The absorbency of both types of SAP decreased slightly before the 60 min due to SF addition, as the concentration of monovalent cations increased. Beyond that point however, the absorbency was decreased again by SF addition, showing a value equal to or above that of the filtrate without SF addition at the 180 min. A decrease of  $\text{Ca}^{2+}$  concentration contributes to such increased long-term absorbency.

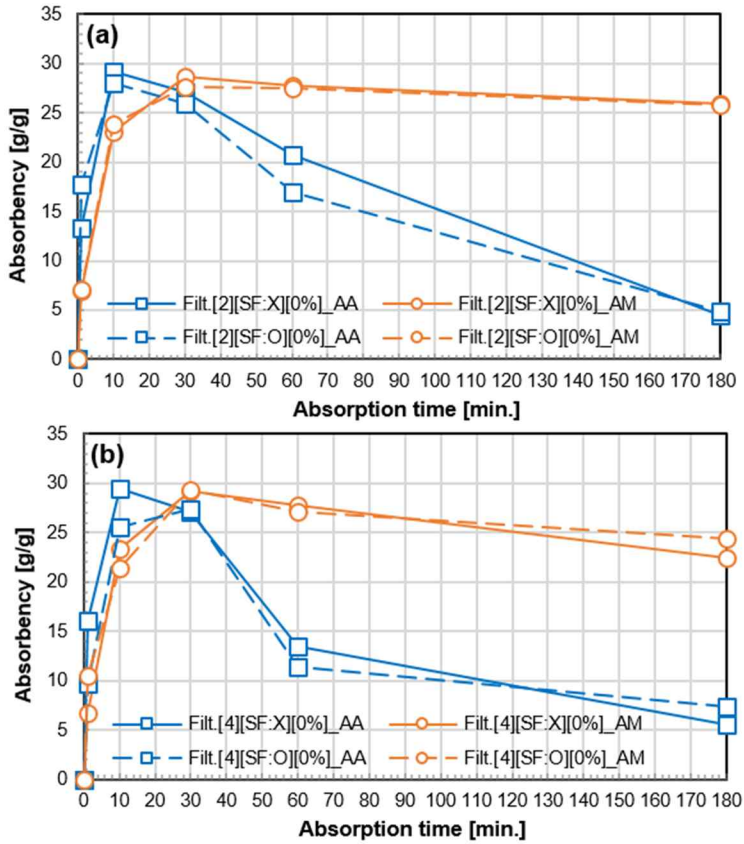


Fig. 3-9 Effect of silica fume addition on absorbency of SAPs in cement filtrates: w/c = 2 (a) and 4 (b)

The absorption kinetics of SAP that is influenced by PCE addition can be predicted using the ion concentration of the cement filtrate and the absorbency of SAP, because as the PCE contents increase, both the concentrations of  $\text{Na}^+$  and  $\text{Ca}^{2+}$  increased. In addition, the concentrations of these ions were already shown to influence both the initial and long-term absorbency. SAP\_AA, which has a higher anionic group density, is expected to be more sensitive to cation concentrations in filtrate. As can be seen in Fig. 3-10, the SAP absorption kinetics based on PCE addition reflect such predictions. Over the entire 180

min period, the absorbency decreased due to PCE addition. In particular, the increase of cation concentration prior to the 60 min was significant for the swelling reduction. For the absorbency at 180 min, while PCE addition did not negatively influence SAP\_AM, SAP\_AA absorbency decreased by 45% due to the increase of  $\text{Ca}^{2+}$  concentration.

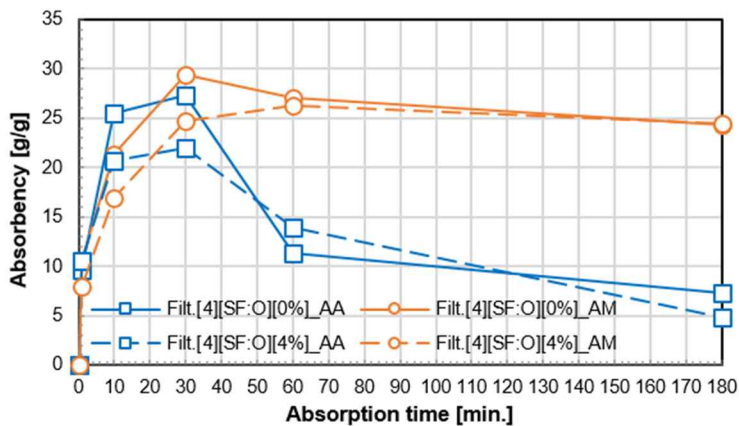


Fig. 3-10 Effect of PCE on absorbency of SAPs in cement filtrates of  $w/c = 0.4$

### 3) *Change of absorption kinetics by additional dissolution of monovalent ions ( $\text{Na}^+$ , $\text{K}^+$ , $\text{OH}^-$ ) into cement filtrate*

Since the  $w/c$  for cement filtrate can reach 10 times that of concrete, the absorption kinetics of SAP in a cement filtrate can be completely different from the actual kinetics in a cement pore solution. Fig. 3-11 shows the absorption kinetics under two conditions of cement filtrates in which additional sodium hydroxide and potassium hydroxide were dissolved. To investigate the influence of the ion compensation (by additional dissolution) on the absorption kinetics, the absorption kinetics without the compensation were also examined. Due to the additional dissolution, the SAP\_AM absorbency decreases during

the first 60 min, but after then, the absorbency increased by 5% again until 180 min. The decrease of initial absorbency was mainly attributed to the increased concentration of dissolved monovalent ions ( $\text{Na}^+$ ,  $\text{K}^+$  and  $\text{OH}^-$ ), while the increase of long-term absorbency was mainly attributed to the decrease of  $\text{Ca}^{2+}$  concentration (from 41 mM to 33 mM).

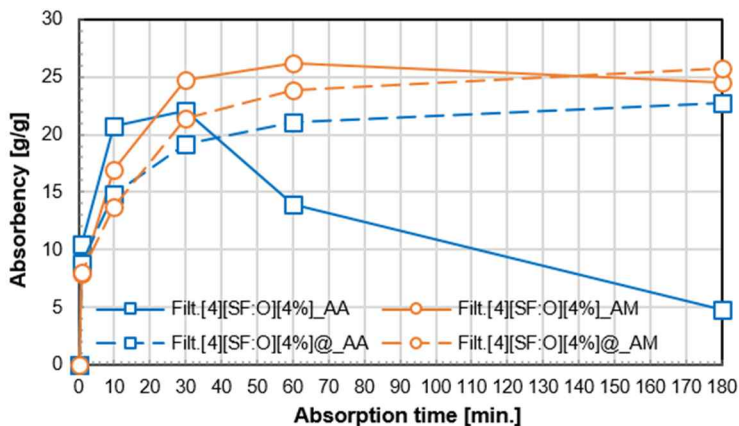


Fig. 3-11 Effect of additional monovalent ions ( $\text{Na}^+$ ,  $\text{K}^+$  and  $\text{OH}^-$ ) on absorbency of SAPs in cement filtrates

Meanwhile, the additional dissolution of monovalent ions not only reduces the initial SAP\_AA absorbency within 30 min, but also completely changes the absorption kinetics beyond that point in time. In the cement filtrate without additional dissolution (Filt.[4][SF:O][4%]), SAP\_AA released 78% of the absorbed solution from 30 min to 180 min. Such swelling reduction due to presence of multivalent cations in the solution, is commonly reported as absorption kinetics of SAP having high anionic group density (Mechtcherine *et al.*, 2015; Schroefl *et al.*, 2015; Zhu *et al.*, 2015; Schröfl *et al.*, 2012). However, cement filtrate with additional dissolution (Filt.[4][SF:O][4%]@) showed no

swelling reduction until 180 min in the case of SAP\_AA. Rather, an additional 18% of solution (based on 30 min absorbency) was absorbed by this SAP from 30 min to 180 min. The decrease of  $\text{Ca}^{2+}$  concentration cannot be the sole reason for such dramatic changes in absorption kinetics as in the case of SAP\_AM; despite its decreased value (8 mM), the  $\text{Ca}^{2+}$  concentration of this filtrate is still high level (33 mM). Rather, the absorption kinetics of SAP\_AA in the filtrate is similar to that in Solution A (Fig. 3-4), in which only monovalent ions were dissolved. Inside of SAP\_AA which containing Solution A, although charge screening effects may be present, ionic cross-linking effect is less likely. Therefore, the dramatic change in absorption kinetics of SAP\_AA is likely due to the mitigation of ionic cross-linking effect due to the reduced influence of multivalent cations.

The phenomenon that acrylic acid or polyacrylate type SAP like SAP\_AA (having a high density of anionic group) maintains its initial absorbency up to 180 min without swelling reduction due to the additional dissolution of monovalent ions under the condition of high  $\text{Ca}^{2+}$  concentration (such as cement base solution), has not been reported. In this study, severe swelling reduction of SAP\_AA under the real pore solution condition ( $\text{Ca}^{2+} > 25$  mM) was experimentally confirmed. In addition, it is newly confirmed that  $\text{Ca}^{2+}$  ions in cement filtrate affect the absorption kinetics of SAP depending on the concentration of monovalent ions.

Based on the new experimental results, this study reveals that the degree of underestimation is dependent on the ion composition and concentration in artificial solutions especially when measuring absorbency of polyacrylate SAP

using the tea-bag method. In two cement filtrates (Filt.[4][SF:X][4%], Filt.[4][SF:O][4%]), the  $\text{Ca}^{2+}$  concentration to total cation concentration was 43–51%. However, due to additional dissolution, the ratio greatly decreased to 9.7–10.8%, and even that in the real pore solution within 7 h is much lower, i.e., 5.3–5.8% (Lothenbach & Winnefeld, 2006). Therefore, when using filtrates in the tea-bag method, the determined absorption kinetics may be completely different from those within the pore solutions. If the ion composition and concentration are not realistically simulated in the artificial pore solution, the performance of SAP (especially polyacrylate types) as IC agent can be significantly underestimated. Regardless of the SAP type, due to the overestimation of the initial absorbency based on dilution effects, a large amount of extra water can be designed in the design step.

As mentioned previously, the addition of both SAP\_AA (with 4% of extra water) and SAP\_AM (with 6% of extra water) into low w/c concrete (UHPC) can decrease AS. Such performance related IC is completely different from the absorption capacity of SAPs in a cement filtrate without ion compensation (Fig. 3-10). The reason that these SAPs can effectively mitigate AS is because they are still absorbing water until the beginning of severe AS (Hasholt *et al.*, 2012; Schröfl *et al.*, 2012; Jensen & Hansen, 2002). Although the absorbency around 12 h, which is known as time zero, was not measured, if SAP\_AA had already released most of the absorbed water by 180 min (as in the case of filtrate without this compensation), the mitigation of AS by IC would be impossible. In other words, inside the concrete, when SAP had already released most of the absorbed water during the induction period (e.g. < 7 h), the AS behavior of this concrete after time zero should be similar to that of the concrete without SAP (with 4%

higher w/c). However, the totally different AS behavior shows that ion composition and concentration of cement filtrate is different from that of the low w/c concrete pore solution. Similar results were also found by Schroefl et al. (Schroefl *et al.*, 2015); two types of SAPs (relative anionicity: SAP 1 > SAP 2) had their absorption kinetics measured using a tea-bag method. As a result, SAP 1 inside the cement filtrate (w/c = 4.3) showed an absorbency close to zero at 9 h due to severe swelling reduction, while the absorbency of SAP 2 at the same time was approximately 30.

Although it is difficult to perfectly explain sorption kinetics of SAPs due to different observations (e.g. pressure effect in mortar) when using an indirect method (tea-bag method) or a direct method (neutron radiography method with cement paste), unlike the clashing absorption kinetics in cement filtrates, the desorption kinetics of SAPs (studied using neutron radiography) were not dramatically different from those measured inside the cement pastes (Schroefl *et al.*, 2015). The measurement of AS resulted in the expansion of mortar with additional SAP 1 (= SAP B) for 24 h up to approximately 100  $\mu\text{m}/\text{m}$ , unlike the significant AS during early ages (< 24 h) in two mortars without SAP (w/c = 0.30, 0.36) (Schröfl *et al.*, 2012). At 7 d, the AS was measured as nearly zero. The mortar with SAP 2 (= SAP D) (w/c = 0.36) also showed no shrinkage behavior until the 7 d, after expansion up to 300  $\mu\text{m}/\text{m}$  for 24 h. This mortar, due to the higher absorption capacity of SAP 2, contained more extra water than SAP 1.

In the measured AS behavior, the current study especially focuses on the shrinkage during an early age (< 48 h). In the case of low w/c concrete, the

majority of the AS (> 50%) occurs during this period. Therefore, the mitigation of severe AS by IC using SAP is mostly effective during this age (Kang *et al.*, 2015; Schroefl *et al.*, 2015; Schröfl *et al.*, 2012), even though the anionicity of SAP is high such as polyacrylate type.

According to Trtik *et al.* (Trtik, Münch, Weiss, Herth, Kaestner, Lehmann, Lura & Brameshuber, 2010), the volume of SAP (produced by inverse suspension polymerization) in a low w/c (0.25) cement paste including PCE type SPPL, did not decrease during the first 4 h. After contact with mixing water, the degree of swelling reached 90% at 30 min, and 100% at 3 h, and did not decrease until the 4 h. In the artificial pore solution suggested in our study, the absorbencies at 30 min of both SAPs were 83–84% those of the absorbencies at 180 min; only slightly different (6–7%) was confirmed compared with the neutron tomography results (Trtik *et al.*, 2010). Such difference is expected due to the limitations of indirect methods as mentioned previously, but is allowable in this instance.

As confirmed in this study, the absorption kinetics of polyacrylate based SAP varies based on the cation composition and concentration, in solutions containing various types of ions. This new result can contribute not only to the understanding of absorption kinetics in concrete pore solutions, but also the selection and development of appropriate SAP materials suitable for IC. Since this type of SAP has been successfully optimized for commercial products in previous years (Jensen & Hansen, 2001b; Buchholz, 1994), the production of cement based materials can be efficiently performed with numerous advantages including economic feasibility, productivity, and safety.

#### **3.1.3.4 Comparison of SAP absorbencies based on suggested tea-bag method and slump spread method for low water to cement concrete**

SAP absorbency determined using the tea-bag method and the artificial pore solution was compared with that determined using the slump spread method. Fig. 3-12 shows the change of slump spread values over time, which are respectively different in terms of SAP type, ratio, and water to cement ratio. When both the SAP and extra water are not mixed (Ref\_0.215), no decrease of slump spread value was observed in the initial 10 min, after which there was a slight decrease until the 20 min. This decrease occurred because of the cement hydration and evaporation on the surface of concrete (Fehling, Schmidt, Walraven, Leutbecher & Fröhlich, 2014). However, the Ref\_0.255 whose w/c is 4% higher than Ref\_0.215, showed no decrease of fluidity because a sufficient amount of water for securing a high slump spread value (250 mm) was added without SAP. However, when SAPs are added to the UHPC, the fluidity certainly decreases depending on their absorption capacity.

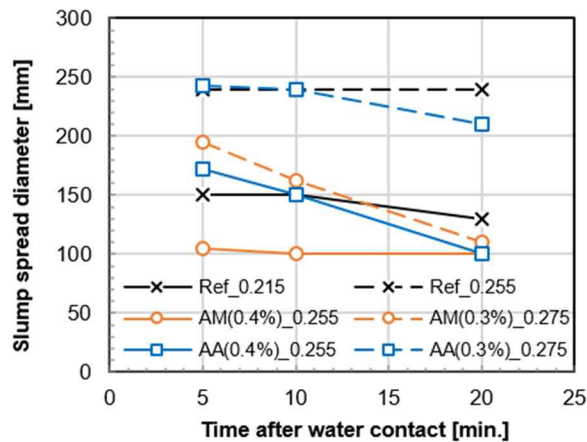


Fig. 3-12 Slump spread value of UHPC with or without SAPs

By comparing the slump spread values of the samples each other, the SAP absorbency at each time point could be measured. Such measurements are possible because the amount of water absorbed by SAP within concrete directly affects the spread value. It has been confirmed that the spread value of UHPC decreases as w/c is decreased (Wille, Naaman & Parra-Montesinos, 2011). When determining the absorbency by this method, other factors which can affect the spread value (e.g., shape of swelled SAP particles, decrease of density or self-weight) are not considered.

The SAP\_AA absorbency at 5 min is less than 10, because the slump spread value of AA (0.4%)\_0.255 (w/c and SAP/c are 0.255 and 0.4%, respectively) is higher than that of the Ref\_0.215. Because the value at 10 min is same with that of Ref\_0.215, the absorbency at this point is 10. Finally, since the sample absorbed entire extra water as well as a part of capillary water at the 20 min, the value is lower than Ref\_0.215; thus, the absorbency is more than

10. However, at this time, SAP\_AA does not absorb water more than 20 times its own weight (dry state), because the slump spread value of AA (0.3%)<sub>0.275</sub> is much higher than that of Ref<sub>0.215</sub> for 20 min.

The absorbency of SAP at each time, as determined by both slump spread method and tea-bag method, are summarized in Table 3-3. Compared to the slump spread method, the tea-bag method showed higher SAP\_AA absorbency before 20 min, while SAP\_AM absorbency was lower after the 5 min. Such differences between the determined absorbencies are also dependent on the shape and type of SAP. The influence of the shape and type of SAP on the tea-bag method was already discussed, and their influence on the slump spread is discussed below.

Table 3-3 Comparison of SAP absorbencies determined by tea-bag and slump flow methods

Type of SAP	Test method	Absorbency [g/g]				
		1 min	5 min	10 min	20 min	30 min
SAP_AA	Modified tea-bag method	8.80	11.50	14.87	17.02	19.16
	Slump spread method	-	< 10	10	10 to 20	-
SAP_AM	Modified tea-bag method	7.97	10.54	13.75	17.56	21.37
	Slump spread method	-	10 to 20	≅ 20	> 20	-

Absorbencies at 5 and 20 min by the tea-bag method are obtained from linear regression shown in Fig. 3-11.

Gray cells indicate matched results between two methods.

Although we are comparing the tea-bag method with the most commonly used direct method (slump spread method), this slump spread method has its own limitations in terms of the accuracy of absorbency measurement; the rheology of fresh concrete, which is directly related to the slump spread value, depends not only on the amount of free water used for determining the absorbency, but also on the cement hydration, size and shape of aggregate, and self-weight of concrete. Moreover, SAP addition independently changes the density (Azarijafari, Kazemian, Rahimi & Yahia, 2016), yield stress, plastic viscosity, particle shape and size distribution of concrete (Mechtcherine *et al.*, 2015). When the swelled SAP is regarded merely in terms of aggregates, those closer to a globular shape (SAP\_AM) can better lower the yield stress and plastic viscosity of fresh concrete compared to those with irregular shapes (SAP\_AA) (Wallevik & Wallevik, 2011). This allows for a higher slump spread value to be induced, and as these factors can affect the rheology or flowability, they reduce the accuracy in determining absorbency.

On the other hands, realistic condition that is difficult to be simulated using the tea-bag method can be reflected in the slump spread method. Additional factors to consider in terms of the absorption kinetics are the influences of the pressure and dispersibility of SAP in concrete; which can be reflected in the slump spread method (e.g., in a mixing process). As mentioned, the uniform dispersibility in concrete is more effective in the case of SAP\_AM than in SAP\_AA. Therefore, SAP\_AM has better conditions for absorbing the pore solution. However, predicting and evaluating the SAP absorbency or absorption kinetics using the slump spread method is very laborious (Hasholt *et al.*, 2015) and inefficient. In order to measure the absorbency over a given time period,

the mixing and slump spread test should be conducted individually. In general, the slump spread value of low w/c concrete constantly decreases regardless of the addition of SAP. Therefore, measurements after working time (e.g. longer than 30 to 60 min) are inaccurate or sometimes impossible. Finally, the influence of admixtures such as SF and SPPL on the absorbency cannot be considered, because they themselves decisively affect the cement hydration and slump spread value.

Although the limitations of these two experimental methods are unavoidably neglected, the suggested tea-bag method was used to reduce the gaps between the absorbencies determined by the slump spread method. In some time periods, the absorbencies determined by the two methods matched perfectly. Therefore, the tea-bag method and artificial pore solution suggested in this study can contribute to reducing the amount of trial and error that goes into such measurements when utilized for preliminary test for determining the amount of extra water in the mix design for IC.

### **3.1.4 Summary and concluding remarks**

In this section, a newly designed tea-bag method and cement filtrate were used to determine SAP absorbency inside cement based materials, and to better understand the absorption kinetics. When determining the SAP absorbency using tea-bag methods, the risk of overestimation due to the excess solution (trapped between SAP particles or smeared on the tea-bag and surface of the particles) was verified. The amount of excess solution was determined using the dewatering process by centrifugation for 1 min. Analysis of the excess

### Chapter 3. Absorption kinetics and retention capacity of SAP in cementitious materials

solution showed that the greater the absorption of solution with SAP, the more excess solution was present. The SAP\_AM, which has a globular shape, contained less excess water compared to the SAP\_AA, having an irregular shape. The average excess solution ratios were 25% in SAP\_AA and 16% in SAP\_AM; these numbers can reduce the accuracy in determining the absorbency, thus they must be exempted from the tea-bag method.

The ion concentration of cement filtrates, commonly used as artificial pore solutions in the tea-bag method for cement based materials, was quantitatively investigated. The major interest of this study was the influence of additional w/c and admixtures (silica fume and polycarboxylate-ether type superplasticizer) on the ion concentration of the filtrates. Between the w/c ratios of 1-10, the concentration of major four ions ( $\text{Na}^+$ ,  $\text{K}^+$ ,  $\text{SO}_4^{2-}$ , and  $\text{OH}^-$ ) of the filtrate was decreased as w/c increases due to dilution effects. However, the  $\text{Ca}^{2+}$  concentration increased because of the decreasing  $\text{OH}^-$  concentration.

The change of ion concentration influenced both the SAP absorbency and the absorption kinetics. As w/c of the filtrate increases, the initial absorbency (within 30 min) increases. This is because the osmotic pressure decreases due to the decreased concentration of the four ions and the mitigation of charge screening effects. However, the long-term absorbency decreased from that time to the 180 min because  $\text{Ca}^{2+}$  concentration increased, which contributes to the formation of additional ionic cross-linkers among the anionic groups inside the SAP. The swelling reduction of SAP, which is related to the concentration of multivalent cations, is also related to the internal anionic groups. Therefore, the swelling reduction was more dramatic in SAP\_AA, which has the higher

anionic group density.

The addition of SF could slightly change the ion concentration of the filtrate, but its influence on the absorption kinetics was negligible. Due to the mixing of acid type SPPL, both the concentrations of the  $\text{Na}^+$  and  $\text{Ca}^{2+}$  inside the filtrate increased. This in turn decreased both the initial and long-term absorbencies of SAPs. Therefore, the influence of SPPL when measuring the SAP absorption kinetics for low w/c concrete have to be considered.

To manufacture artificial pore solutions realistically, sodium hydroxide and potassium hydroxide were dissolved into the filtrate ( $w/c = 4$ ) in which the influences of SF and SPPL were also reflected. This additional dissolution was conducted to compensate for the concentration of monovalent ions ( $\text{Na}^+$ ,  $\text{K}^+$ , and  $\text{OH}^-$ ) due to the dilution effect. By this compensation, the concentrations of main ions in concrete pore solution could be simulated the artificial pore solution using cement filtrate. The  $\text{Ca}^{2+}$  concentration of the cement filtrate itself is one source of severe swelling reduction of polyacrylate based SAP (SAP\_AA). However, in a filtrate having the same condition, when the concentration of monovalent ions is higher, such reduction did not occur. Multivalent cations such as  $\text{Ca}^{2+}$  can trigger reduced absorbency due to ionic cross-linking effects. However, rather than the absolute  $\text{Ca}^{2+}$  concentration, the relative ratio regarding the concentration of monovalent ions is more likely to influence the SAP absorption kinetics, which has not been previously demonstrated. Based on this new result, the present study points out the risk of underestimating the absorption capacity due to the ion composition and concentration of cement filtrate, when the polyacrylate based SAP for the IC of

### Chapter 3. Absorption kinetics and retention capacity of SAP in cementitious materials

concrete is used in the tea-bag method. Such risk occurs because this kind of SAP in the filtrate is unrealistically influenced by multivalent cations such as  $\text{Ca}^{2+}$ , greatly reduces absorption capacity.

Finally, the SAP absorbency determined using the suggested artificial pore solution and the modified tea-bag method was compared to the absorbency determined using the slump spread method. Although it is difficult to conclude that the slump spread method is more accurate, the reflection of realistic conditions in the indirect method (tea-bag method) brings it closer to the direct method. The reflected conditions include the removal of excess solution, the simulation of ion concentrations by admixtures (SF, PCE) and the ion compensation. By using these solutions and methods, the SAP absorbency and absorption kinetics in low w/c concrete pore solutions can be reasonably predicted and evaluated.

Predicting the SAP absorbency and absorption kinetics is decisive in the mix design for internally cured concrete, because the strength or workability can be decreased depending on the amount of extra water as well as the absorbency. In these circumstances, the tea-bag method and artificial pore solution suggested in this study can be easily, efficiently, and reasonably used for determining type and amount of SAP before the mix design. The absorption kinetics of polyacrylate based SAP are especially dependent on the ratio of concentration between multivalent cation and the others. This new finding can help to understand the absorption kinetics of SAP in a real cement or concrete pore solution, and can contribute to the development of commercial products for IC.

## **3.2 Absorption and retention capacities of SAP depending on ion concentration**

### **3.2.1 Introduction**

In Section 3.2, the influence of the ion composition and concentration on the absorption kinetics of SAP is systematically investigated to understand the absorption capacity and behavior of SAP within cement-based solutions, such as cement pore solutions or filtrates. Various ionic solutions and cement filtrates are manufactured; then, the SAP absorbency in those solutions is accurately measured. All solutions and filtrates are quantitatively analyzed to obtain accurate ion concentration information and history. This history is measured to verify the effect of  $\text{Ca}^{2+}$  in the external solution on the absorption kinetics of SAP. Based on the measured absorbency and history results, a conceptual model is suggested to explain the reason why the water retention capacity of polyacrylate hydrogel, one of the most widely used commercial hydrogels, is especially sensitive to the ion composition and concentration. Lastly, the retention capacity in the low w/c concrete is discussed.

Predicting the SAP absorptivity and absorption kinetics in a concrete is a crucial factor in the mix design for internally cured concrete. To successfully alleviate the AS, a necessary amount of IC water should be precisely determined by a theoretic models (presented in Section 2) to prevent self-desiccation; then, this water should be absorbed and released by SAP properly in the concrete with the correct timing (Hasholt *et al.*, 2015; Snoeck *et al.*, 2015a; Hasholt *et al.*, 2012; Jensen & Hansen, 2001b). Therefore, the

absorptivity and absorption kinetics in the concrete should be accurately predicted to use SAP for IC without any side effect.

The concentration and composition of the cement filtrate, which is commonly used for the artificial solution, are totally different from the real solutions because of the dilution effect (Kang, Hong & Moon, 2016a). This effect occurs because the typically used w/c of 4-10 for the filtrate is more than 10 times higher than that of the solutions. In particular, this effect dominantly attributes to decrease the concentration of monovalent cations and anions, rather than multivalent cations (Kang *et al.*, 2016a). This indicates the possibility of an inaccuracy because the absorptivity and absorption kinetics of SAP are dominantly affected by the composition and concentration of ions in solution (Kang *et al.*, 2016a).

For hygiene products, a 0.9% NaCl solution, which can represent urine, is typically used to measure the absorptivity of SAP for disposable diapers (Pourjavadi *et al.*, 2010; Nagorski, 1994). Unlike this simple ionic solution, cement pore solutions contain various ions with different concentrations (Hewlett, 2010). Among them, the concentrations of the five ions ( $\text{Na}^+$ ,  $\text{K}^+$ ,  $\text{Ca}^{2+}$ ,  $\text{SO}_4^{2-}$ , and  $\text{OH}^-$ ) are the highest, but the  $\text{Ca}^{2+}$  concentration is the lowest among the five during the entire curing time (Lothenbach, Le Saout, Gallucci & Scrivener, 2008; Lothenbach & Winnefeld, 2006). Previously, the ion concentration history of two real cement pore solutions (w/c=0.4 and 0.5) were quantitatively analyzed using inductively coupled plasma-optical emission spectroscopy (ICP-OES) and a pH electrode (Lothenbach *et al.*, 2008; Lothenbach & Winnefeld, 2006). As a result, the top five ion concentrations of

### Chapter 3. Absorption kinetics and retention capacity of SAP in cementitious materials

the pore solution ( $w/c=0.4$ ) during the induction period were  $78.5\pm 3.1$  mM,  $402.0\pm 5.5$  mM,  $20.5\pm 1.0$  mM,  $174.8\pm 5.0$  mM, and  $162.5\pm 5.0$  mM for  $\text{Na}^+$ ,  $\text{K}^+$ ,  $\text{Ca}^{2+}$ ,  $\text{SO}_4^{2-}$  and  $\text{OH}^-$ , respectively (Lothenbach *et al.*, 2008), and those of the pore solution ( $w/c=0.5$ ) were  $28.1\pm 1.2$  mM,  $350.0\pm 14.1$  mM,  $22.2\pm 1.1$  mM,  $152.1\pm 7.8$  mM, and  $135.6\pm 23.5$  mM, respectively (Lothenbach & Winnefeld, 2006). The concentrations of the other ions were negligible ( $< 1$  mM) in the two solutions. Meanwhile, the absorption kinetics of SAP is dependent on the cation charge number of an external solution (Zhu *et al.*, 2015; Schröfl *et al.*, 2012). Schröfl *et al.* (Schröfl *et al.*, 2012) investigated the effect of the anionic group density and cross-linking density of SAP on the efficiency of the IC. As a result, the absorption capacity of SAP with a higher anionic group density was remarkably decreased in the presence of  $\text{Ca}^{2+}$  in the ionic solutions or cement filtrates ( $w/c=4.3$ ). Including this result, recent studies simply reported the responsibility of this ion to change the absorption kinetics and to decrease the absorption capacity of SAP in the solutions or filtrates (Zhu *et al.*, 2015; Schröfl *et al.*, 2012).

Although the absorption capacity and kinetics of SAP are known to be dependent on the ion concentration and charge number, the effects of the ion composition on the capacity and kinetics and its interdependency have not been investigated. In particular, the roles of the four major ions in the pore solutions are not understood. Therefore, a clear explanation of the absorption kinetics of SAP in cementitious materials is required by investigating these roles and the ion composition effect. Moreover, the factors that can cause a misestimation of the absorptivity of SAP when using an artificial pore solution should be addressed by experiments.

In section 3.1, contrasting absorption kinetics results were shown between two types of cement filtrates. In the basic cement filtrate ( $w/c=4$ ), the polyacrylate hydrogel (or acrylic acid SAP) released most of the absorbed solution after 30 min of absorption time because of the severe swelling reduction, while this reduction did not occur in the modified cement filtrate simulating a low  $w/c$  concrete pore solution. As a result, the hydrogel absorbed more solutions even after 30 min of absorption time because of the increased amount of monovalent ions ( $\text{Na}^+$ ,  $\text{K}^+$ , and  $\text{OH}^-$ ). Although, this long-term retention (or absorption) behavior is likely to occur in the low  $w/c$  concrete during the induction period, the reason for the contrasting results is not fundamentally understood. Thus, it is necessary to study the effect of not only  $\text{Ca}^{2+}$ , but also the other major four ions on the swelling reduction and retention capacity of SAP.

### **3.2.2 Materials and methods**

#### **3.2.2.2 Preparation of ionic solutions**

Various ionic solutions were manufactured by dissolving  $\text{NaCl}$ ,  $\text{KCl}$ , and  $\text{Ca}(\text{NO}_3)_2$  powders into the two basic solutions, such as distilled water and cement filtrate. To avoid the effect of the pH change on the  $\text{Ca}^{2+}$  concentration, powders that did not include  $\text{H}^+$  and  $\text{OH}^-$  were selected. The  $\text{Ca}^{2+}$  concentration is inversely proportional to the pH of the cement-based solutions (Kang *et al.*, 2016a; Bonen & Sarkar, 1995; Moragues *et al.*, 1987; Rechenberg & Sprung, 1983). Thus, to investigate the effect of the concentrations of the other ions

### Chapter 3. Absorption kinetics and retention capacity of SAP in cementitious materials

(monovalent cations and anions) at a given  $\text{Ca}^{2+}$  concentration, which is one of the main objective of this study, the ion concentration of the solutions were designed by controlling these powders. After the solutions were prepared, the pH was measured by using a pH electrode (calibrated by pH 4, 7, and 10 buffer solutions), and the concentrations of the four ions ( $\text{Na}^+$ ,  $\text{K}^+$ ,  $\text{Ca}^{2+}$ , and  $\text{SO}_4^{2-}$ ) were quantitatively analyzed by ICP-OES. Although the concentrations of  $\text{Cl}^-$  and  $\text{NO}_3^-$  (which dissolved along with the cations) could not be analyzed directly, these concentrations could be estimated from the molecular formulas of the raw materials and the analysis results of the cation concentrations.

Table 3-4 shows the measured cation concentrations and pH of all solutions and filtrates. It is reasonable to assume that Sol. 1, equal to distilled water, does not contain any ions. Sol. 2 and Sol. 7 include 25.3 mM and 482.7 mM of  $\text{Na}^+$  with  $\text{Cl}^-$ , respectively. The four solutions (Sols. 3-6) have different total monovalent ion concentrations by  $\text{Na}^+$ ,  $\text{Cl}^-$ , and  $\text{NO}_3^-$ , at a given  $\text{Ca}^{2+}$  concentration ( $22.5 \pm 1.5$  mM). Filt. 1, an actual cement filtrate ( $w/c=4$ ), is the base cement filtrate according to the previous method in Section 3.1. Filts. 2-4 are the modified filtrates with different total monovalent ion concentrations at a  $\text{Ca}^{2+}$  concentration of  $20.3 \pm 2.3$  mM. This  $\text{Ca}^{2+}$  concentration was originally from the base filtrate.

Table 3-4 Ionic concentration and strength of solutions

Solution name	Ion concentration [mM]			pH	Total Ion Concentration, TIC [mM]	Ionic Strength, IS [mM]
	Na <sup>+</sup>	K <sup>+</sup>	Ca <sup>2+</sup>			
<b>Sol.1</b>	-	-	-	6.5	-	-
<b>Sol.2</b>	25.3	0.0	0.1	7.1	50.8	25.5
<b>Sol.3</b>	0.2	0.0	23.7	6.2	71.3	71.1
<b>Sol.4</b>	24.4	0.0	22.9	6.1	117.6	93.2
<b>Sol.5</b>	114.2	0.0	22.9	5.8	297.1	182.9
<b>Sol.6</b>	464.4	0.2	21.9	6.4	994.8	530.2
<b>Sol.7</b>	482.7	0.2	1.6	6.8	970.3	487.4
<b>Filt.1</b>	4.3	30.4	22.5	12.4	103.6	120.0
<b>Filt.2</b>	15.0	156.6	22.5	12.4	376.3	256.5
<b>Filt.3</b>	24.8	261.9	21.8	12.4	607.4	370.9
<b>Filt.4</b>	46.6	490.3	18.0	12.4	1104.7	613.9

SO<sub>4</sub><sup>2-</sup> concentrations of Sol. 1-7 and Filt. 1-4 are analyzed at 0 mM and 23 mM, respectively.

Total ion concentration and ionic strength are estimated by considering both the dissolved ions (Na<sup>+</sup>, K<sup>+</sup>, Ca<sup>2+</sup>, Cl<sup>-</sup>, NO<sub>3</sub><sup>-</sup>) and major ions in the cement filtrate (Na<sup>+</sup>, K<sup>+</sup>, Ca<sup>2+</sup>, SO<sub>4</sub><sup>2-</sup>, OH<sup>-</sup>).

It is confirmed in Table 3-4 that the intended Ca<sup>2+</sup> concentrations (18-24 mM) of all solutions and filtrates are similar to those of fresh cement pore solutions (w/c=0.4 and 0.5), 19-24 mM (Lothenbach *et al.*, 2008; Lothenbach & Winnefeld, 2006). The pH of the solutions (Sols. 1-7) ranged from 5.8 to 7.1. In addition, the OH<sup>-</sup> concentrations of the filtrates (Filt. 1-4) ranged between

22.4 mM and 24.5 mM, which correspond to the measured pH values. The total ion concentration (TIC) and ionic strength (IS) were also calculated to examine the SAP absorption kinetics as a function of the osmotic pressure and equilibrium swelling ratio (ESR). In this calculation, the five ions ( $\text{Na}^+$ ,  $\text{K}^+$ ,  $\text{Ca}^{2+}$ ,  $\text{SO}_4^{2-}$ , and  $\text{OH}^-$ ) along with the additionally dissolved anions ( $\text{Cl}^-$ ,  $\text{NO}_3^-$ ) were considered. Among them, the concentration of  $\text{SO}_4^{2-}$  dissolved from cement was measured as 23 mM in all filtrates.

### **3.2.2.3 Absorbency test**

The absorptivity and absorption kinetics of SAP were determined using the modified tea bag method, which can effectively remove unabsorbed excess solutions. To measure the absorbency, a tea bag that included 0.1 g of dry SAP was submerged into a waterproof container filled with 100 mL of a solution immediately after the container was sealed. After the measurements, each solution in the container was vacuum filtered using a 0.45  $\mu\text{m}$  polytetrafluoroethylene (PTFE) filter to analyze the ion concentration by ICP-OES. The purpose of this analysis was to investigate the trapped or released cations by SAP during the absorption time. This ion absorbency is defined by the increased or decreased ion concentration in the 100 mL solution by 0.1 g of dry SAP.

### 3.2.3 Results

#### 3.2.3.1 Total Ion Concentration (TIC) and Ionic Strength (IS)

The TIC of a solution is the sum of all ionic concentrations, irrespective of the ionic charge numbers. Thus, the TICs of the solutions listed in Table 3-4 proportionally increased with respect to the total monovalent ion concentration. The total monovalent cation concentrations of Sol. 6 and Sol. 7 are the same ( $485.5 \pm 1.05$  mM), but the TIC of Sol. 6 is 3% higher than that of Sol. 7 because of the two additional dissolved anions ( $2 \times \text{NO}_3^-$ ) with one cation ( $\text{Ca}^{2+}$ ). However, the IS considers the charge numbers as well as the ion concentrations. Thus, despite the same TIC values, IS can vary depending on the multivalent ion concentration to TIC ratio. For instance, with similar TICs (3% difference), the IS of Sol. 6 is 9% higher than that of Sol. 7 because of the higher  $\text{Ca}^{2+}$  concentration to TIC ratio.

The TIC of an external solution affects the osmotic pressure, which is the driving force for the SAP absorption. This can be fully explained by the Van't Hoff equation (Eq. (3-1)). Based on the equation and the analysis results in Table 3-4, the increase of the TIC by the monovalent ions weakens the driving force; thus, the initial absorbency of SAP is decreased.

$$\Pi = CRT \quad (3-1)$$

Where,  $\Pi$ ,  $C$ ,  $R$  and  $T$  are the osmotic pressure [atm], the concentration of solute ions in solution [mol], gas constant [ $0.0821$  L atm mol<sup>-1</sup>]

<sup>1</sup> K<sup>-1</sup>], and the absolute temperature [K].

Meanwhile, the IS represents the equilibrium swelling ratio (ESR) of SAP. This can be explained by the Flory equation (Eq. (3-2)) which defines the absorbency of SAP (Flory, 1953). According to the equation, the ESR ( $q_m$ ) decreases as the IS ( $S^*$ ) increases (and vice versa). In other words, the ESR can be changed by multivalent ion concentration to the TIC ratio. This means that the possibility of change in the absorption capacity depends on the ion composition of a solution. Furthermore, the denominator of Eq. (3-1) ( $V_0/v_e$ ) indicates the cross-linking density of SAP (Shimomura & Namba, 1994). By using this, both the decrease of the ESR based on the cross-linking density of SAP and the loss of long-term absorbency caused by the formation of the additional ionic cross-linkers can be reflected. The presence of multivalent cations in a solution results in a low absorption capacity because of the additionally formed ionic cross-linkers within the SAP (Zhu *et al.*, 2015; Pourjavadi *et al.*, 2013; Schröfl *et al.*, 2012; Shimomura & Namba, 1994).

$$q_m^{5/3} = \frac{[i/2v_u S^{*1/2}]^2 + [(1/2 - \chi_1)/v_1]}{V_0/v_e} \quad (3-2)$$

Where,  $q_m$  is the equilibrium swelling ratio,  $i/v_u$  is the concentration of fixed charge referred to the un-swollen network,  $S^*$  is the ionic strength of external solution,  $\chi_1$  is the interaction parameter between the polymer network and the solvent,  $v_1$  is the molar volume of solvent,  $v_e$  is the effective number of chains in the network, and  $V_0$  is the volume of the un-swollen

network.

The first term in the right side of Eq. (3-1) indicates the contribution of ionic charges in the network ( $i/v_u$ ) and in the solution ( $S^*$ ). The second term represents the contribution of the affinity between the network and the external solution. As presented in Table 3-4, the main variables of the various ionic solutions or cement pore solutions with a given type of SAP, are TIC and IS; these variables depend on the ionic condition of the solutions. Based on the ESR of Eq. (3-1), the main two parameters that should be considered in this chapter are  $S^*$  and  $V_0/v_e$  because other parameters in the equation are not depend on the ionic condition of the solutions. The parameter,  $V_0/v_e$ , which is related to the ionic cross-linking density, can vary as a function of concentration of the multivalent cation in the solution. Because the osmotic pressure between polymer network and external solution is balanced at an equilibrium swelling stage (i.e., additional absorption or swelling is not allowed to occurs), TIC, the main parameter of the osmotic pressure, should not be considered as a main variable at this stage. In other words, TIC which is related to the driving force of absorption, should be considered to discuss the only initial absorption (or desorption) of SAP, while IS should be considered to explain the maximum absorption or swelling of SAP. However, when two ionic solutions having monovalent ions only are compared each other to investigate the effect of maximum (or equilibrium) swelling of SAP based on the ion concentration of the solutions, the TIC can be considered as a main parameter because IS is exactly half of TIC only in this case.

### **3.2.3.2 Effect of the monovalent ion concentration on the SAP absorbency**

Fig. 3-13 shows the absorption kinetics of SAP as a function of TIC, influenced by the monovalent ion concentration (MIC). To provide a clear presentation, the absorbencies of Sol. 1 and Sol. 2 were scaled down by 1/9 and 1/3, respectively. In all solutions of Sol. 1, Sol. 2, and Sol.7, the absorbency of SAP\_AA is slightly higher than that of SAP\_AM. Regardless of the type of SAP, the initial absorption speed and the maximum absorbency decreased to 1/3 of the original value (Sol.1) as the TIC and IS of the solution increased from 0 mM to 50.8 mM and 25.5 mM, respectively (Sol. 1 vs. Sol. 2). The speed and absorbency again decreased to 1/3 of the original value (Sol.2), as TIC and IS additionally increased by 919.4 mM and 461.9 mM, respectively (Sol. 2 vs. Sol. 7). The increase of TIC or MIC contributed to the decrease of the absorption speed and absorbency, but it did not change the absorption kinetics because the multivalent cations were not included in the solutions. This absorbency result can also be theoretically supported by Eq. (3-1) for the osmotic pressure and Eq. (3-2) for the ESR; the initial absorption speed and the maximum absorbency decreased because of the reduced osmotic pressure and ESR, respectively, without the change of the cross-linking density of the SAP. Moreover, the results show that the charge screening effect caused by the presence of monovalent cations (Pourjavadi *et al.*, 2013) does not change the absorption kinetics.

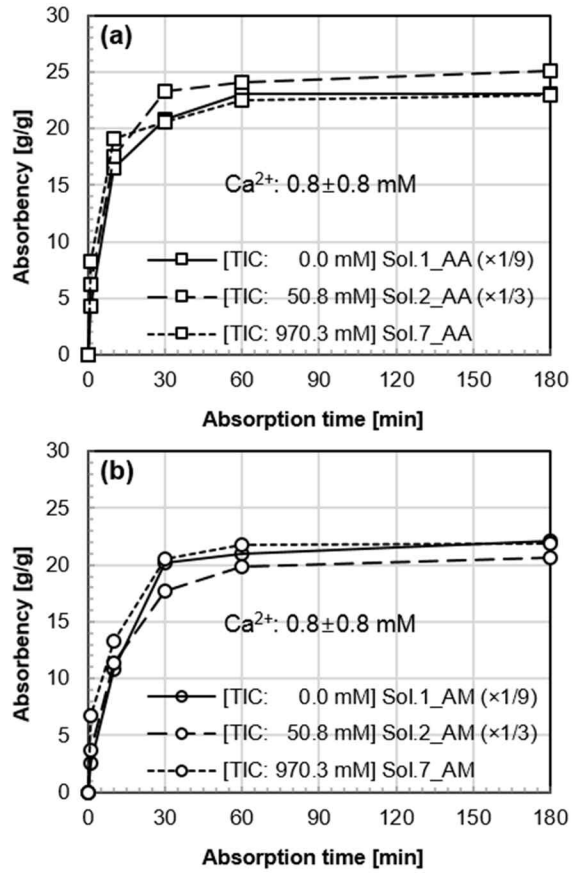


Fig. 3-13 Effect of the monovalent ion concentration (Na<sup>+</sup> and Cl<sup>-</sup>) on the absorbencies of SAP\_AA (a) and SAP\_AM (b): the absorbencies in Sol. 1 and Sol. 2 are scaled down by 1/9 and 1/3, respectively

### **3.2.3.3 Effect of cation charge number on the SAP absorbency**

The effect of the cationic charge number (1 or 2) on the absorptivity and absorption kinetics of SAP is presented in Fig. 3-14 at the given cation concentration ( $24.5 \pm 0.8$  mM). Certainly, the maximum absorbency decreased and the absorption kinetics changed by the increase of the charge number. The initial absorption speed up to 1 min is slightly decreased because the TIC of Sol. 3 increased by 40%, and the maximum absorbency after 1 min remarkably decreased because of the increased IS. In particular, unlike SAP\_AM, SAP\_AA shows a consistent swelling reduction after 10 min. This means that the absorption kinetics of SAP with a high density of anionic groups is sensitive to the cationic charge number, i.e., the absorption capacity of this type of SAP can be dramatically decreased by the effect of multivalent cations. The same trends were observed in the absorbency tests using both ionic solutions and cement filtrates (Zhu *et al.*, 2015; Pourjavadi *et al.*, 2013; Schröfl *et al.*, 2012).

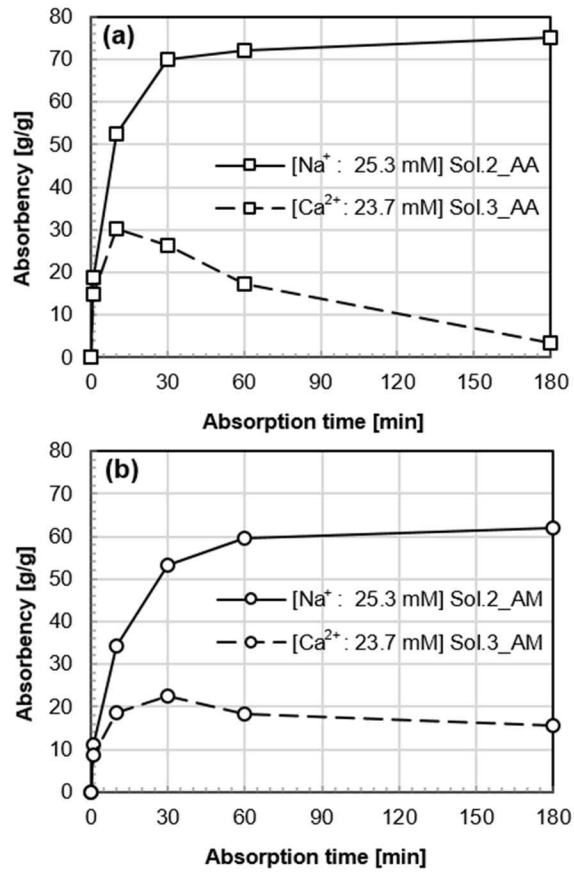


Fig. 3-14 Effect of the cation charge number (Na<sup>+</sup> vs. Ca<sup>2+</sup>) on the absorption kinetics of SAP\_AA (a) and SAP\_AM (b) at a cation concentration of 24.5±0.8 mM

#### **3.2.3.4 Effect of Ca<sup>2+</sup> concentration on the SAP absorbency at the given total ion concentration**

At the given TIC (982.5±12.3 mM), Fig. 3-15 shows the absorption kinetics of the SAP that depend on the Ca<sup>2+</sup> concentration. The Ca<sup>2+</sup> concentration to TIC ratio of Sol. 7 is 2.2%, which is 11 times higher than that of Sol. 7 (0.2%). Nevertheless, the two solutions are composed of mostly (> 97.8%) of monovalent ions (Na<sup>+</sup>, Cl<sup>-</sup>, and NO<sub>3</sub><sup>-</sup>). The initial absorbency at 1 min in the two solutions is similar because of the fixed TIC value.

However, 2% of the increase (from 0.2% to 2.2%) of the Ca<sup>2+</sup> concentration to the TIC ratio caused the change of the absorption kinetics because of the ionic cross-linking effect. The results in Fig. 3-15 show the change of the kinetics caused by the 20.3 mM increase of the Ca<sup>2+</sup> concentration. Both this change and the reduction of the absorption capacity were especially noticeable for SAP\_AA. After 30 min, this SAP could not absorb any additional solution, and from 60 min it released the absorbed solution by reducing the swelling. As a result, the absorbency at 180 min decreased by 57%. However, the absorbencies of SAP\_AM are similar in the two solutions up to 10 min, after which there is no distinct difference in the absorption capacity and kinetics between the two solutions, except at the point of maximum absorbency (60 min vs. > 180 min). The 180 min absorbency of SAP\_AM is only decreased by 6% because of the increase of the Ca<sup>2+</sup> concentration.

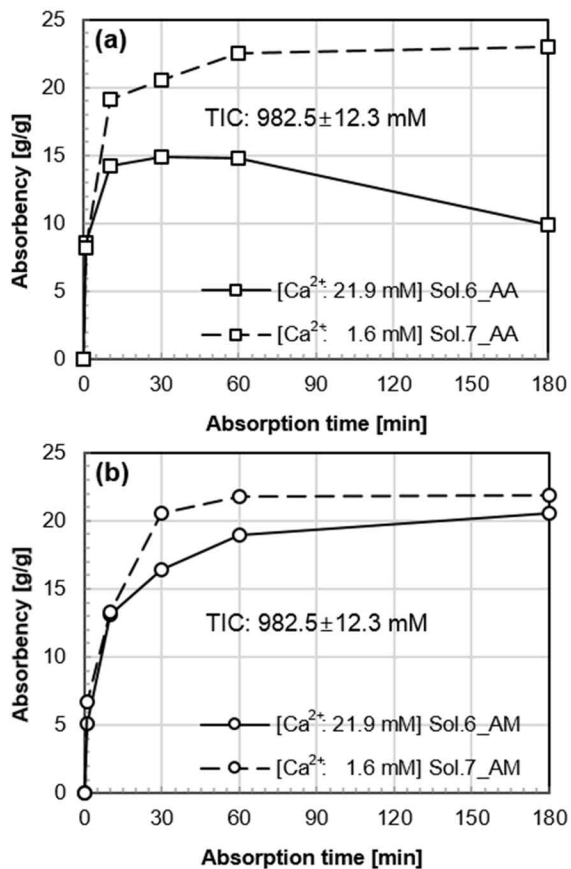


Fig. 3-15 Effect of  $Ca^{2+}$  concentration (1.6 mM vs. 21.9 mM) on the absorption kinetics of SAP at a total ion concentration of  $982.5 \pm 12.3$  mM

### **3.2.3.5 Effect of monovalent ion concentration on the SAP absorbency at a given Ca<sup>2+</sup> concentration**

The effect of the MIC on the absorption kinetics at a Ca<sup>2+</sup> concentration of 22.5±1.5 mM is shown in Fig. 3-16. Because the increase of the MIC has an effect on both the increases of TIC and IS, the initial absorption speed and the maximum absorbency are decreased, similar to that in Fig. 3-13. In addition, the swelling reduction is mitigated with respect to the TIC, as shown in Fig. 3-16. In particular, the reduction of SAP\_AA almost disappeared in Sol. 6, whose TIC and IS values are the highest among the four solutions (Sols. 3-6). The swelling reduction of SAP\_AM is also mitigated as the TIC increases. In Sol. 6, SAP\_AM absorbed even more solutions after 60 min. The mitigation trends of the SAPs are also observed in the cement filtrates (Filt. 1-4), whose Ca<sup>2+</sup> concentration levels are the same as the real cement pore solution (Fig. 3-17). These two figures experimentally verify the risks of the overestimation of initial absorbency and the underestimation of retention capacity from the use of artificial pore solutions with unrealistic ion concentrations and compositions.

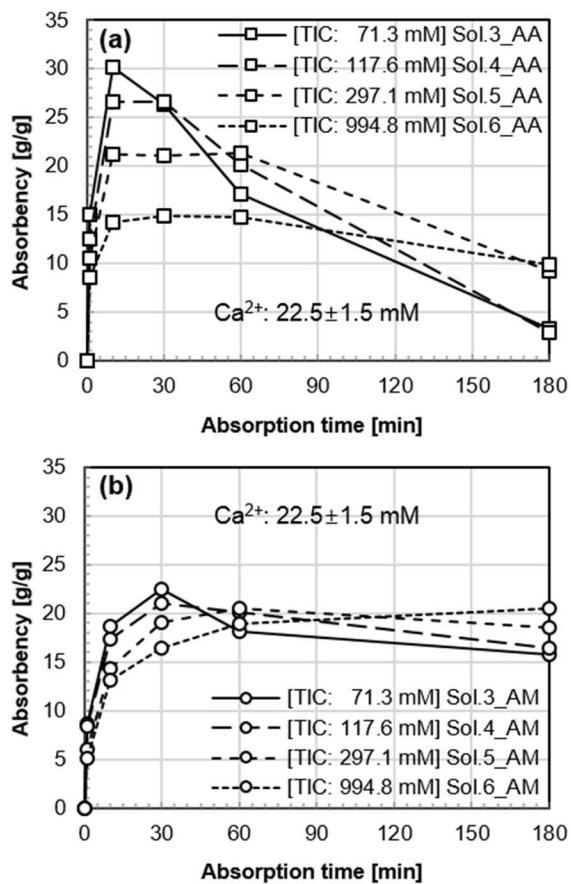


Fig. 3-16 Effect of the  $\text{Na}^+$  concentration on the absorption kinetics of SAP\_AA (a) and SAP\_AM (b) at a  $\text{Ca}^{2+}$  concentration of  $22.5 \pm 1.5$  mM in the solutions

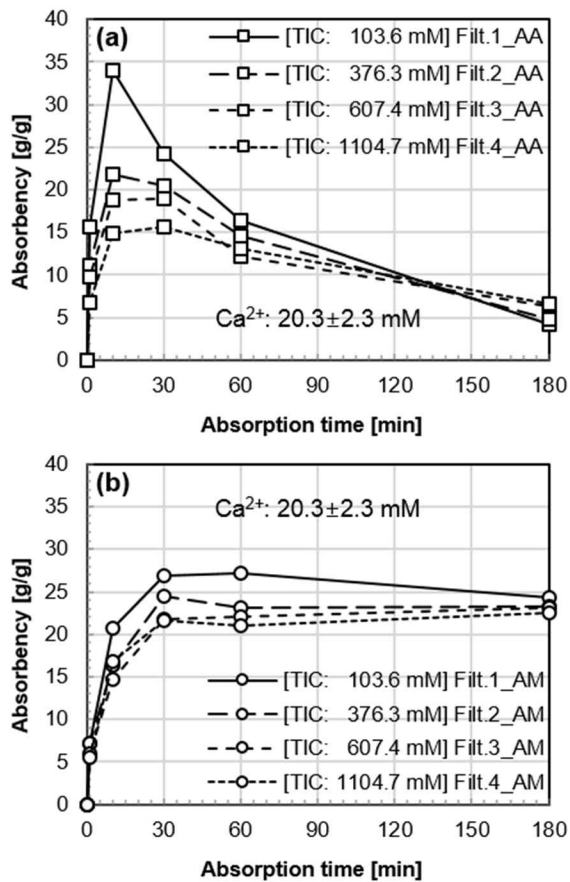


Fig. 3-17 Effect of the monovalent cation concentration on the absorption kinetics of SAP\_AA (a) and SAP\_AM (b) at a  $\text{Ca}^{2+}$  concentration of  $20.3 \pm 2.3$  mM in the cement filtrates

### **3.2.4 Discussion**

$\text{Ca}^{2+}$  generally has a decisive effect on the absorptivity and absorption kinetics of SAP in cement-based solutions (Kang *et al.*, 2016a; Zhu *et al.*, 2015; Schröfl *et al.*, 2012). This was theoretically reviewed in the previous section by the influences of its concentration on the TIC and IC as well as the cross-linking density. However, the results of this study show that this effect is not independent of the  $\text{Ca}^{2+}$  concentration only, but dependent on the concentrations of the other ions (monovalent cations and anions). Firstly, as the concentrations of the other ions increase, the driving force for SAP absorption is decreased. Thus, the absorbency at 1 min is proportionally decreased as TIC increases (Fig. 3-18). Next, the swelling reduction is mitigated with the decrease of the initial absorbency, which results in the improved water retention capacity of SAP. Therefore, an inverse relationship between the initial (10 min) and long-term (180 min) absorbencies can be determined (Fig. 3-19). This relationship indicates that the long-term absorbency, affected by the retention capacity, is related to the initial absorbency. In summary, although the same amount of  $\text{Ca}^{2+}$  is dissolved in an external solution, the ionic-cross linking effect that causes the swelling reduction is dependent on the TIS and IS of the solution. To clearly understand this dependency that has not been considered in previous studies, the influences of the TIC and IS on the initial and long-term absorbencies as well as the ionic cross-linking effect are investigated and discussed in this section.

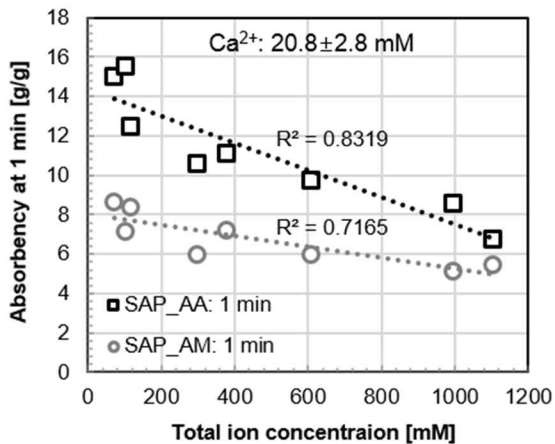


Fig. 3-18 SAP absorbency at 1 min at a Ca<sup>2+</sup> concentration of 20.8±2.8 mM as a function of the total ion concentration

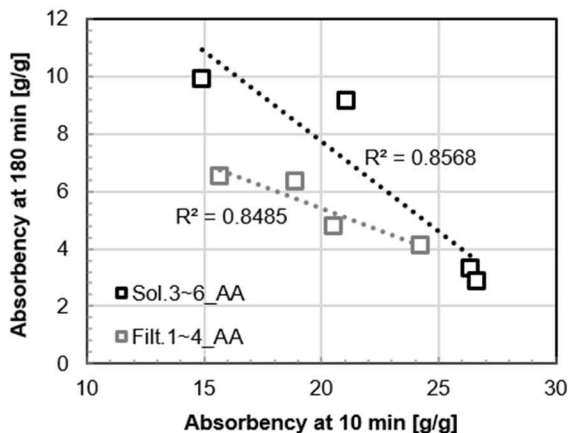


Fig. 3-19 Relationship between the initial (at 10 min) and long-term (at 180 min) absorbencies of SAP\_AA

### **3.2.4.1 Absorption speed of SAP as a function of total ion concentration**

At the given  $\text{Ca}^{2+}$  concentration, the influences of TIC on the initial and long-term absorption speeds are shown in Fig. 3-20. The initial and long-term absorption speeds are defined as the average absorption speed (AAS) between 0 and 10 min, and between 60 min and 180 min, respectively. In Fig. 3-20, the positive and negative signs of the absorption speed indicate the absorption and release of the solution by SAP, respectively. As TIC increases, the initial AAS tends to increase and the long-term AAS tends to decrease.

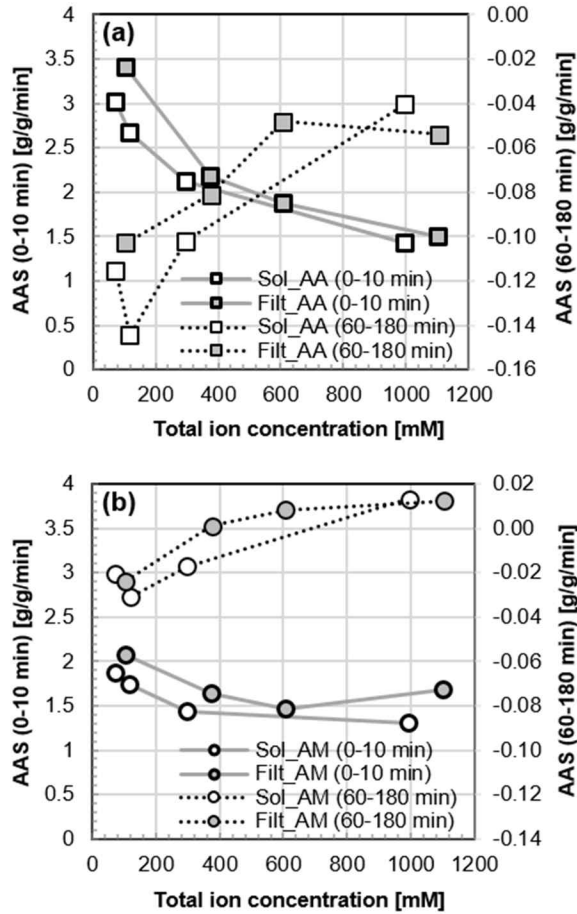


Fig. 3-20 Average absorption speed (AAS) between 0-10 min and 60-180 min of SAP\_AA (a) and SAP\_AM (b) as a function of the total ion concentration

However, the initial AAS of SAP\_AM is not affected by the TIC when TIC > 400 mM. This is because the charge screening effect that is attributed to weakening the electrostatic repulsion between the anionic groups (Pourjavadi *et al.*, 2013) is less sensitive in SAP\_AM (i.e., low anionic group density). Thus, the initial absorbency of this SAP is insensitive or not affected by the TIC

change of the cement pore solutions whose TICs are above 700 mM. Moreover, the long-term (60-180 min) water release speed of SAP\_AM approaches zero as TIC increases; in particular, the release changes to the absorption because of the high level of TIC (> 700 mM). Based on this investigation, an outstanding water retention capacity of SAP\_AM is expected in a concrete.

The trend of alleviated swelling reduction is more pronounced in SAP\_AA than in SAP\_AM. The severe swelling reduction is mitigated by the increase of TIC, i.e., the dewatering speed is nearly zero under the upper than 700 mM of TIC (a speed of zero means there is perfect water retention for SAP). Because of this alleviation trend, the swelling reduction of SAP\_AA disappeared in the two solutions (Sol. 6 and Filt. 4) that have the highest level of TIC (around 1,000 mM). The reductions of the initial absorption speed and the maximum absorbency influenced by TIC and IS can be understood by using the osmotic pressure and the charge screening effect. However, the alleviation trend that depends on TIC (which has not been reported yet) cannot be directly explained by these two factors. The swelling reduction of SAP is caused by the ionic cross-linking effect within the ionic solution containing the multivalent cations (Zhu *et al.*, 2015). This effect is attributed to the formation of new intermolecular complexes by irreversible ion exchanges between the multivalent ions (e.g.,  $\text{Ca}^{2+}$ ) and the anionic groups (Pourjavadi *et al.*, 2013; Shimomura & Namba, 1994). Thus, the measured ion exchange behavior will be discussed to explain the reason for this new result.

### **3.2.4.2 Cation uptake and release by SAP within an ionic solution**

To investigate the ion exchange behavior of SAP as a function of cation charge number (1 vs. 2), the ion concentrations of two solutions (Sol. 2 and Sol. 3) containing SAPs were measured with respect to the absorption time. The result is presented in Fig. 3-21. In the figure, the negative and positive changes created trapped and released cations by SAP, respectively. The measured ion exchange behavior corresponds to the absorption kinetics of SAP. In section 3, it was confirmed that the maximum absorbency decreased and the absorption kinetics changed as the charge number of the cation increased from 1 to 2 (Fig. 3-14). By relating this result to the ion exchange behavior, it is concluded that the swelling reduction occurs while  $\text{Ca}^{2+}$  ions are trapped by SAPs, like in Sol. 3. Assuming that SAP absorbs pure water even in an ionic solution, the ion concentration of the solution should be consistently increased along with the swelling of SAP. However, the ion concentration of Sol. 2 was constantly maintained despite a steady swelling. In addition, the ion concentration history was dependent on the charge number of the cations. These results clearly verify that cations are trapped in the SAP by absorbing not pure water, but ionic solutions.

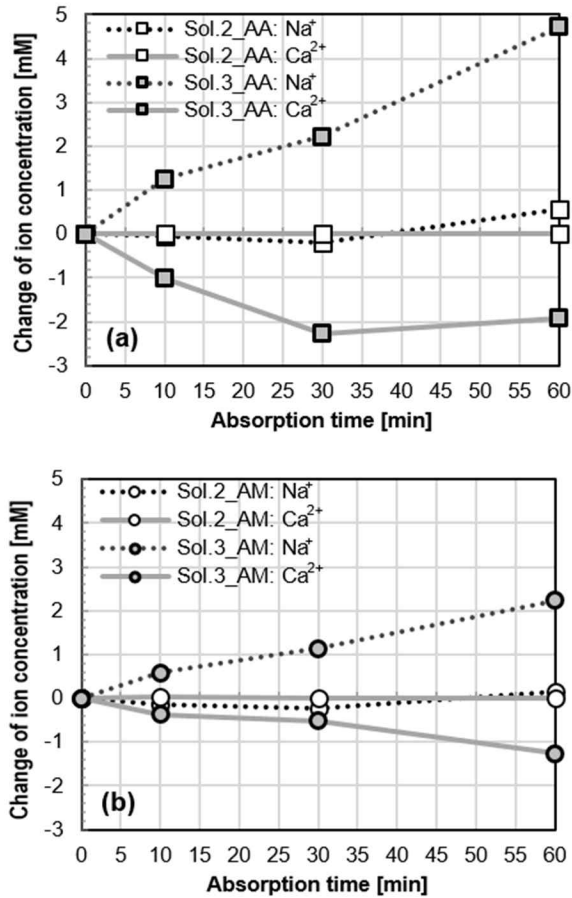


Fig. 3-21 Change of the ion concentration in solutions caused by ion trapping or releasing by SAP\_AA (a) and SAP\_AM (b)

The ion concentration history of the solutions containing SAP depends on the charge number of the cation. In Sol. 2, the ion concentration is maintained because SAP absorbs the ionic solution containing Na<sup>+</sup> without any swelling reduction. For Sol. 3, in contrast, the Ca<sup>2+</sup> concentration is decreased by the ion exchange behavior, whereas the Na<sup>+</sup> concentration is increased. This increase is caused by the release of Na<sup>+</sup> that was originally included in the dry SAP, as

### Chapter 3. Absorption kinetics and retention capacity of SAP in cementitious materials

confirmed from the ion concentration of Sol. 3 before the absorbency test (Table 3-4). The reason for this release is the irreversible ion exchange between  $\text{Ca}^{2+}$  and anionic groups of SAP. Other possible reasons are the simple dissolution of  $\text{Na}^+$  in a solution and its release by swelling reduction. However, a comparison of the ion concentration history and the absorption kinetics indicates that these are implausible. This is because there is no change of the  $\text{Na}^+$  concentration in Sol. 2 during the absorption time, and the  $\text{Na}^+$  concentration of Sol. 3 is increased during the swelling increase period, such as within 10 min of the absorption time. An additional new finding of this study is that the  $\text{Ca}^{2+}$  concentration is decreased in Sol. 3 despite the dewatering (10-30 min) of SAP\_AA, as evidenced by the irreversible ion exchange between  $\text{Ca}^{2+}$  and the anionic groups, such as carboxylate groups ( $-\text{COO}^-\text{Na}^+$ ).

As expected, the decreasing speed and rate of the  $\text{Ca}^{2+}$  concentration are higher in an ionic solution containing SAP\_AA than SAP\_AM. Because the dry SAP\_AA has more anionic groups ( $-\text{COO}^-\text{Na}^+$  and  $-\text{COO}^-\text{H}^+$ ) than the dry SAP\_AM (which contains a part of the nonionic groups, e.g.,  $-\text{NH}_2$  or  $-\text{CONH}_2$ ), both the released  $\text{Na}^+$  and trapped  $\text{Ca}^{2+}$  ions are larger in SAP\_AA than in SAP\_AM. Zue et al. confirmed that more  $\text{Ca}^{2+}$  ions are trapped by SAP until an equilibrium swelling state (at 240 min) as the ESR decreases because of the swelling reduction (Zhu *et al.*, 2015). In addition, we have confirmed that the absorption of  $\text{Ca}^{2+}$  and the release of  $\text{Na}^+$  proceeded simultaneously, and these began as soon as the dry SAP was in contact with the ionic solutions that include  $\text{Ca}^{2+}$ . This finding can additionally contribute to the understanding of the absorption kinetics of SAP in a concrete because it means that  $\text{Ca}^{2+}$  ions dissolved from cement at a very early age and can also be trapped by SAP at a

very early age. Moreover, the result of the  $\text{Na}^+$  release from dry SAP can also help provide an understanding of the pore solution of internally cured concrete because this release can be a reason for the additional change of the pore solution's ion concentration.

In particular, the verification of the irreversible  $\text{Ca}^{2+}$  exchange can decisively contribute to the research of self-sealing (Snoeck, Steuperaert, Van Tittelboom, Dubruel & De Belie, 2012; Lee, Wong & Buenfeld, 2010) or healing (Snoeck *et al.*, 2014b; Van Tittelboom & De Belie, 2013; Kim & Schlengen, 2010) cementitious materials that require the reabsorption capability of SAP. Because the cross-linking density of SAP is additionally increased by the exchange, SAP in a hardened concrete can lose this capability compared to its dry state. Thus, the anionic group density can be a critical factor for the selection of proper type of SAP for the self-healing or sealing applications.

#### **3.2.4.3 Conceptual model for the swelling behavior of polyacrylate hydrogels depending on the initial absorbency and ionic cross-linking density**

When SAP absorbs a cement-based solution, an irreversible ion exchange that causes the swelling reduction is expected to occur. The increases of the monovalent cations and anions weaken the driving force for absorption and accelerate the charge screening effect; thus, the initial and maximum absorbencies are decreased. The more  $\text{Ca}^{2+}$  ions that are trapped in SAP, the

more ionic-cross linkers are formed with a limited amount of anionic groups, which accelerates the swelling reduction. In contrast, at a given  $\text{Ca}^{2+}$  concentration of the cement pore solution (19-24 mM), as the initial absorbency is decreased by the monovalent cations and anions, the amount of trapped  $\text{Ca}^{2+}$  in SAP is decreased. Thus, the ionic-cross linking density is decreased and the swelling reduction is mitigated. In addition, SAP\_AM with a low anionic group density is insensitive to the effects of  $\text{Ca}^{2+}$  and the other ions.

This study suggests a conceptual model shown in Fig. 3-22 to explain the absorption kinetics and retention capacity of SAP that depends on the initial absorbency. By using the model, it is possible to understand the reason for the differences of kinetics and capacity for the cement filtrates (Fig. 3-22 (a)) and real cement pore solutions (Fig. 3-22 (b)). A low total concentration of the four major ions ( $\text{Na}^+$ ,  $\text{K}^+$ ,  $\text{SO}_4^{2-}$ , and  $\text{OH}^-$ ) in the cement filtrate (caused by the dilution effect) leads to a low TIC and IS. Thus, the SAP in the filtrate rapidly absorbs a large amount of solution along with the  $\text{Ca}^{2+}$  ions because of the strong osmotic pressure. Because the irreversible ion exchange by these  $\text{Ca}^{2+}$  ions makes the cross-linking density of SAP high, SAP has to release the absorbed solution without keeping it. However, due to the high level of TIC and IS in a real cement pore solution, SAP slowly absorbs a small amount of the solution along with the  $\text{Ca}^{2+}$  ions from the beginning of the absorption. This weakens the ionic-cross linking effect, and thus the swelling reduction is delayed and mitigated, i.e., the retention capacity is improved.

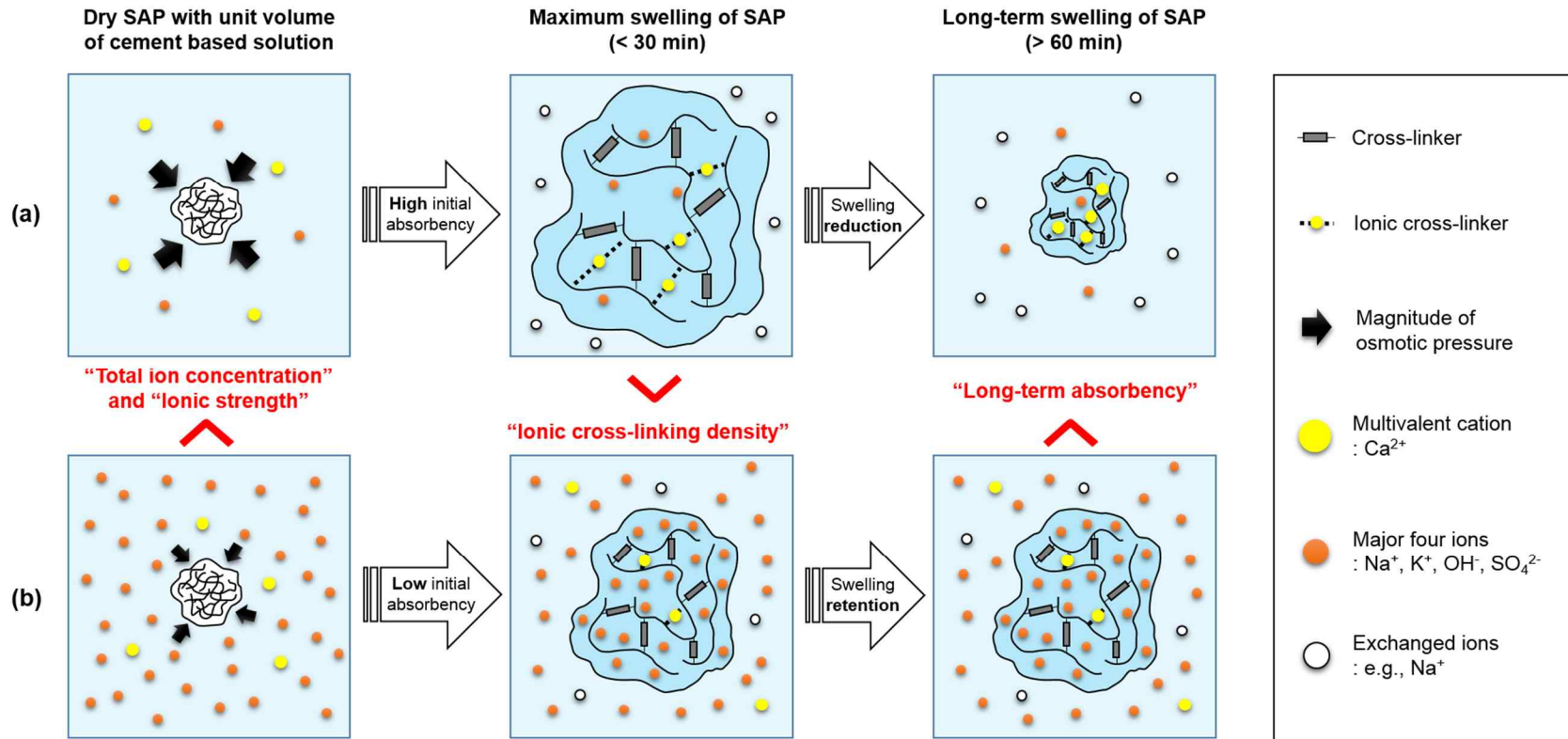


Fig. 3-22 Schematic of the initial absorbency-dependent ionic cross-linking effect and retention capacity of polyacrylate SAP in cement-based solutions: with a high initial absorbency (a) and with a low initial absorbency (b)

The retention capacity can be a more important factor than the maximum absorbency when considering the effectiveness of the concrete IC. By using the SAP with a relatively high retention capacity but a low absorption capacity, the designed IC of water can be provided in the low w/c concrete during a suitable period (e.g., after an initial setting or time zero of AS). However, if an SAP with an excellent absorption capacity but poor retention capacity is used for the IC, the water absorbed by SAP can be released much earlier than the suitable period. This will cause not only a strength reduction, but also an ineffective AS reduction. For instance, the maximum absorbency of SAP\_AA in Sol. 3 or Filt. 1 at 10 min is higher than 30 g/g, whereas the absorbency at 180 min is less than 5 g/g. If these absorption kinetics occurs in the low w/c concrete, the IC of water cannot be used to mitigate the AS. However, despite the relatively low maximum absorbency (e.g., 15), if SAP\_AA retains more than half of the maximum absorbency (e.g., 7-10) until 180 min in the concrete (like for Sol. 6 or Filt. 4), the absorbed water can be used for the IC. The TIC-sensitive swelling behavior of the polyacrylate hydrogel (SAP\_AA), which was verified in this study, helps us to understand its retention capacity in the concrete. Because of the high level of TIC in the concrete, this type of SAP can have an adequate water retention capacity to be used for an IC agent. In the next section, the water retention capacity of the hydrogel in the concrete and the effectiveness of the IC will be discussed.

#### **3.2.4.4 Water retention capacity of polyacrylate hydrogel in a cement pore solution**

Fig. 3-23 represents the TIC and IS of two cement pore solutions ( $w/c=0.4$  and  $0.5$ ) with respect to the curing ages (Lothenbach *et al.*, 2008; Lothenbach & Winnefeld, 2006). The histories of the TIC and IS were obtained using the concentrations of five ions ( $\text{Na}^+$ ,  $\text{K}^+$ ,  $\text{Ca}^{2+}$ ,  $\text{SO}_4^{2-}$ , and  $\text{OH}^-$ ). The TIC and IS are maintained at 700-850 mM and 600-700 mM, respectively, during the induction period ( $< 7\text{h}$ ). These are 6.8-8.2 and 5.0-5.8 times higher than those of cement filtrate ( $w/c=4$ ), Filt. 1. From 7 h to 24 h, the TICs of the pore solutions rapidly increase from the sudden rise of the concentrations of monovalent ions ( $\text{Na}^+$ ,  $\text{K}^+$ ,  $\text{OH}^-$ ). This rapid increase of TIC has been suggested as the driving force for desorption of SAP in a concrete because this increase can oppositely change the direction of the osmotic pressure (Wang *et al.*, 2015). Meanwhile, IS tends to decrease during this period. The decrease of the divalent ion concentrations ( $\text{Ca}^{2+}$  and  $\text{SO}_4^{2-}$ ) crucially attributed to this decrease, rather than the increase of the monovalent ion concentrations. Consequently, desorption of SAP during the acceleration period of cement hydration is mainly caused by the increase of the monovalent ion concentration because the osmotic pressure is influenced by the TIC rather than IS.

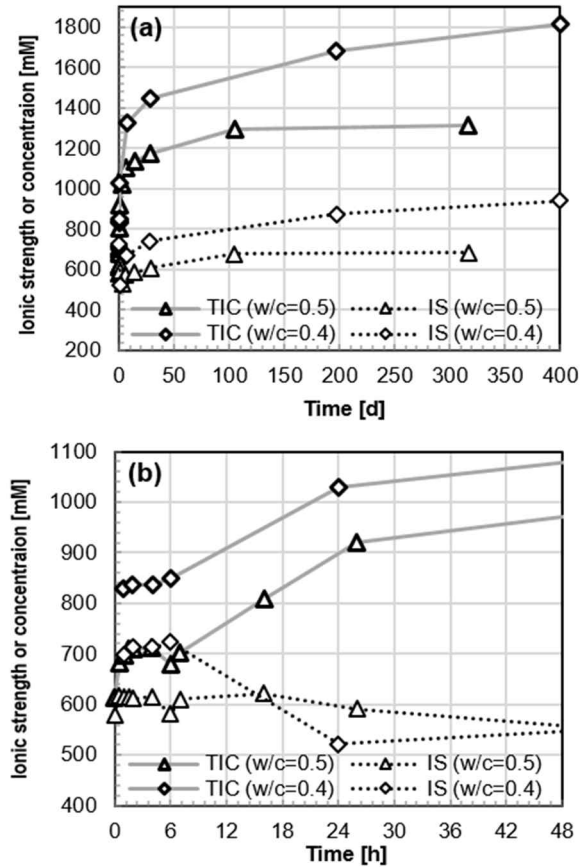


Fig. 3-23 Total ion concentration and ionic strength of cement pore solutions (w/c=0.4 and 0.5) during long-term (a) and early (b) ages based on five ions ( $\text{Na}^+$ ,  $\text{K}^+$ ,  $\text{Ca}^{2+}$ ,  $\text{SO}_4^{2-}$ , and  $\text{OH}^-$ )

(Lothenbach *et al.*, 2008; Lothenbach & Winnefeld, 2006)

The absorption kinetics and swelling behavior in cementitious materials can be simulated correctly by using an artificial pore solution, such as Sol. 6 or Fil. 4, in which the ion composition and concentration are realistically reflected. Although the TICs of the two solutions (1,000-1,100 mM) are higher compared to those of the cement pore solutions, TICs in the low w/c concrete are also

possibly higher than those of the pore solutions. As the w/c of the cement pore solutions is decreased by 0.1 (from 0.5 to 0.4), the average  $\text{Ca}^{2+}$  concentration during the induction period ( $< 7$  h) is slightly decreased (1.7 mM), but the average concentrations of the main four ions ( $\text{Na}^+$ ,  $\text{K}^+$ ,  $\text{SO}_4^{2-}$ , and  $\text{OH}^-$ ) are significantly increased by 52, 50, 22.6, and 26.9 mM, respectively. In addition to this, it has been reported that the IC using SAP can effectively mitigate the AS of the low w/c ( $< 0.3$ ) concretes (Justs *et al.*, 2015; Kang *et al.*, 2015; Mechtcherine & Reinhardt, 2012; Schröfl *et al.*, 2012; Jensen & Hansen, 2002). In summary, it is safely expected that not only the poly (acrylic acid-co-acrylamide) hydrogel (e.g., SAP\_AM), but also the polyacrylate hydrogel (e.g., SAP\_AA) possesses the water retention capacity in the low w/c concrete in which TIC is higher than 850 mM.

A lot of studies dealing with the IC of concrete have mentioned that SAPs have an outstanding absorption capacity (Hasholt *et al.*, 2015; Snoeck *et al.*, 2015a; Wang *et al.*, 2015; Zhu *et al.*, 2015; Snoeck *et al.*, 2014a; Snoeck *et al.*, 2014b; Schröfl *et al.*, 2012; Snoeck *et al.*, 2012) and that most ( $> 90\%$ ) of the SAPs are being used for disposable diapers (Mechtcherine & Reinhardt, 2012; Jensen & Hansen, 2001b). In particular, polyacrylate hydrogel has been commercially optimized for diapers (Mechtcherine & Reinhardt, 2012; Shimomura & Namba, 1994). Nevertheless, its retention capacity for the IC has been underestimated by showing an invalid retention capacity in cement-based solutions (Schröfl *et al.*, 2015; Schröfl *et al.*, 2012). However, SAP\_AA effectively can reduce AS of UHPC without having a loss of strength or flowability as will be presented in Section 5. These results indicate that there is no significant difference in the retention capacity between the two SAPs in the

concrete if properly designed. Similar to this, the acrylic acid-type SAP also showed an effectiveness as the IC agent in the high strength mortar ( $w/c=0.3$ ) (Schröfl *et al.*, 2012) and concrete ( $w/c=0.3$ ) (Mechtcherine *et al.*, 2014) by reducing their AS. Generally, the AS and self-desiccation become pronounced as the  $w/c$  of the concrete is decreased (Baroghel-Bouny, Mounanga, Khelidj, Loukili & Rafäi, 2006; Jiang *et al.*, 2005); thus as the  $w/c$  is lower, the IC by SAP is more effective. As discussed, the low  $w/c$  condition, such as 0.2-0.35 (Jensen & Hansen, 2001b) makes the TIC and IS of the concrete pore solution higher than the cement pore solutions ( $w/c=0.4-0.5$ ). Therefore, the IC by the polyacrylate hydrogel can be effectively used for the low  $w/c$  concrete, as confirmed previously, because of its sufficient retention capacity, as explained by the suggested model (Fig. 3-22).

### **3.2.5 Summary and concluding remarks**

In Section 3.2, the absorption kinetics and retention capacity of SAP were clearly investigated; both parameters vary with respect to the ion composition and the concentration of the cement-based solutions. The presence of  $Ca^{2+}$  in the solution decreases the retention capacity because of the irreversible ion exchange with the anionic groups of SAP. This ion exchange behavior was quantitatively analyzed by measuring the ion concentration history of the solution containing SAP. Immediately after contact with the solution, the anionic groups (e.g.,  $-COO^-Na^+$ ) exchanged their monovalent cations with the trapped  $Ca^{2+}$  ions. These monovalent cations, originally included in dry SAP,

were then released to the solution, regardless of the swelling reduction. As a result, the swelling reduction occurred by the ionic-cross linking effect, and the retention capacity decreased.

However, the swelling reduction is dependent on the concentrations of the monovalent cations and anions at a given  $\text{Ca}^{2+}$  concentration of the solution. In other words, as the concentrations of monovalent cations and anions are increased, the initial absorbency of SAP is decreased, whereas the long-term water retention capacity is improved. To explain the reason for this dependency in the swelling reduction, the conceptual model was proposed. Firstly, the TIC of the solution is increased by increasing the concentrations of the main four ions ( $\text{Na}^+$ ,  $\text{K}^+$ ,  $\text{SO}_4^{2-}$ , and  $\text{OH}^-$ ); because the driving force of SAP absorption (i.e., the osmotic pressure) is weakened by the TIC increase, the initial absorption speed and maximum absorbency are decreased. Next, the ionic cross-linking effect is diminished as the amount of absorbed solution including  $\text{Ca}^{2+}$  is decreased because a limited number of anionic groups of SAP can exchange their ions with the trapped  $\text{Ca}^{2+}$ . Finally, thanks to the diminished ionic cross-linking effect and the low maximum absorbency, the swelling reduction is alleviated and the retention capacity is improved.

Cement filtrates have been generally used for artificial pore solutions to predict the absorptivity of SAP in cementitious materials. However, compared with real cement pore solutions, the concentrations of the main four ions ( $\text{Na}^+$ ,  $\text{K}^+$ ,  $\text{SO}_4^{2-}$ , and  $\text{OH}^-$ ) except  $\text{Ca}^{2+}$ , are exceptionally low in the filtrates because of the dilution effect. The differences of the ion concentrations and compositions between the cement filtrates and pore solutions can provide the

reasons for the incorrect predictions of the absorptivity and the retention capacity. This can cause an incorrect estimation of the extra water for internally cured concrete. In particular, if this artificial solution is used for the prediction, certainly the retention capacity of polyacrylate hydrogel with a high anionic group density is underestimated because the TIC of the cement filtrate ( $w/c=4$ ) is just 14-17% that of the cement pore solutions ( $w/c=0.4-0.5$ ) and the swelling reduction for this type of SAP is accelerated.

Therefore, when manufacturing an artificial pore solution to simulate a real cement or concrete pore solution, it is necessary to reflect reasonable ionic factors (ion concentration and composition) to avoid the risks of potentially incorrect predictions. In addition, the suggested model provides a clear understanding of the reason that the polyacrylate hydrogel (SAP\_AA) could effectively reduce the AS of the low  $w/c$  concrete ( $w/c=0.215$ ) even though it shows a severe swelling reduction in cement filtrates. It is true that acrylic acid-co-acrylamide hydrogel (e.g., SAP\_AM) is more effective than the polyacrylate hydrogel (e.g., SAP\_AA) with respect to the IC performance, but the polyacrylate type can also be effectively and efficiently used for multifunctional cement admixtures with its additional merits of better productivity and price competitiveness.



## **Chapter 4. Hydration reaction and microstructure**

### **4.1 Introduction**

The main purpose of Section 4 is to examine and verify the effects of IC—by the addition of a superabsorbent polymer (SAP)—on the hydration reaction and pore structures of ultra-high performance concrete (UHPC). Based on this purpose, this chapter is divided into two main parts: investigating promotion of the hydration reaction (which depends on the released water from SAP); and analyses of the shape, distribution, and network of pores, formation of which are directly related to the swollen SAP particles.

The heat of hydration was measured and the effects of IC on the heat evolution of UHPC were discussed based on literature. However, this section does not include the results and discussion of the measurements because the hydration reaction—which is affected by the released water from SAP—is also associated with the self-desiccation or internal RH history of the concrete. The properties of the heat of hydration, internal RH (or the desiccation), and autogenous shrinkage of the internally cured UHPC (I-UHPC) are the main subjects of Section 5; thus, these IC-related properties will be rigorously compared and discussed in Section 5.

X-ray powder diffraction (XRD) analysis was conducted to confirm the variation in the hydration products due to IC. Crystalline phases that are newly created or disappear can be detected by this method. However, SAP particles

cannot react with other cementitious or supplementary materials such as cement and silica fume, and only the water released from them affects the hydration reaction. Therefore, the types of hydration products cannot be changed despite the addition of SAP and extra water; only the amount of the products can be changed. For this reason, previous studies have not performed XRD analysis as a primary tool to study the IC of concrete. Nonetheless, in this study, XRD analysis was performed to investigate the effect of IC on the amount of unhydrated cement clinkers in hardened UHPC.

Image analysis of UHPC was performed using a field emission scanning electron microscope (JSM-7800F Prime, JEOL Ltd.) to observe the pores induced by the swollen SAP particles (named SAP pores), and the shrunken SAP particles in the pores after releasing water. In addition, the change in the pore structure owing to SAP pores was systematically analyzed using 3D-computed tomography (CT). Lastly, the pore size distribution and total porosity of each sample were investigated using two different methods, mercury intrusion porosimetry (MIP) and 3D-CT. These two methods were selected for this investigation because the two methods can detect different ranges of pore sizes (Aligizaki, 2006). The MIP method is suitable for analyzing capillary pores (5 nm - 10  $\mu$ m) (Abell, Willis & Lange, 1999). In this method, a non-wetting liquid (i.e., mercury) with a contact angle of 90° or higher intrudes into the capillary of a solid (e.g., concrete) by pressure. The diameter of each pore can be determined by the relationship between the pressure and the diameter of the capillary, as shown in Eq. (4-1) (Abell *et al.*, 1999). The MIP method has been widely used to analyze the pore size distribution and porosity of cementitious materials because of its simplicity and ease. However, the pore

shape and void network cannot be studied by this method.

$$p = \frac{-4\gamma\cos\theta}{d} \quad (4-1)$$

where,  $p$ ,  $\gamma$ ,  $\theta$ , and  $d$  are the pressure, surface tension of the liquid, contact angle of the liquid, and diameter of the capillary, respectively.

On the other hand, pore structure analysis using 3D-CT is an image-based technique. Thus, the precision of the method and the detectable minimum size of void depend on the resolution of the images. This method is specifically suited to detect large-sized pores (1  $\mu\text{m}$  - 10 mm). Based on the pore ranges of hydrated cement paste shown in Fig. 4-1, these pores correspond to the entrained and trapped air voids (Mehta & Monteiro, 2006). Compared to other pore analysis methods (e.g., MIP and gas adsorption method), the advantage of the 3D-CT method is that the entire internal structure of a relatively large specimen (up to a 50 mm  $\times$  10 mm cylinder) can be analyzed nondestructively, and the 3D-pore network can be visually displayed as well.

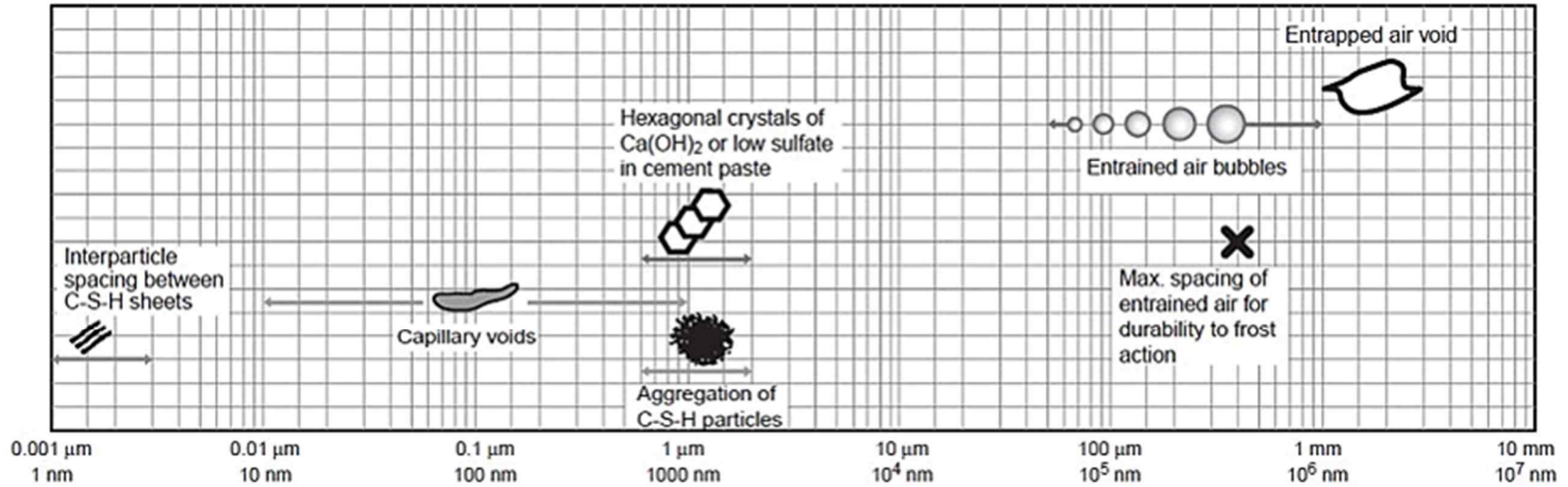


Fig. 4-1 Multi-scale pore network in a hydrated cement paste  
(Mehta & Monteiro, 2006)

## 4.2 Materials and methods

### 4.2.1 Sample preparation

Samples were prepared using identical raw materials, instruments (including a 5 L Hobart mixer), mix proportions (Table 4-1), mixing techniques as those used in the previous studies (Kang, Hong & Moon, 2016b, 2016c; Kang, Wang, Hong & Moon, 2016e; Kang *et al.*, 2015). As mentioned in Section 1 these were optimized by our preliminary experiment to develop the ordinary UHPC (O-UHPC). First, ordinary Portland cement, silica fume, silica power, and silica sand were blended homogeneously to prepare dry-mix powders. The chemical compositions and particle-size distributions of the dry materials are presented in Table 4-2 and Fig. 4-2, respectively. The silica sand is primarily composed (> 90%) of SiO<sub>2</sub> components. Once the dry-mix powder was prepared, the mixing water, which contained a polycarboxylate-type superplasticizer, was added to the powders and mixed. Finally, the steel fibers, which had a diameter, length, and tensile strength of 0.2 mm, 13 mm, and 2700 MPa, respectively, were added to the mixture and mixed. More detailed material images can be seen in Appendix A. All specimens used in this section were cured under the ambient curing condition (20 °C, RH 60%).

When the SAP was incorporated into the UHPC, it was homogeneously blended with the other dry materials during the preparation of the dry-mix powders. As presented in Table 4-1, two ordinary UHPCs (O-UHPCs), namely Ref\_0.215 and Ref\_0.255, and two internally cured UHPCs (I-UHPCs), with SAPs of AA\_0.255 or AM\_0.275, were planned. These samples have varying

w/c ratios, with the exception of Ref\_0.255 and AA\_0.255. The w/c ratios of the three samples (Ref\_0.215, AA\_0.255, and AM\_0.275) were determined to satisfy the target slump-flow diameter,  $750 \pm 50$  mm. Owing to the absorption capacity of the SAP, the w/c ratios of the I-UHPCs were inevitably increased to satisfy the aforementioned target. Thus, the extra water/cement ratios were determined to be 0.04 and 0.06 for AA\_0.255 and AM\_0.275, respectively. Based on the determined ratios, it can be predicted that at the time of the slump-flow test (10–15 min), the absorptivity of SAP\_AM ( $0.06/0.003=20$  g/g) in the UHPC is twice than that of SAP\_AA ( $0.04/0.004=10$  g/g). Another O-UHPC (Ref\_0.255) was additionally prepared to verify that the IC effect was due to the added SAP rather than the additionally increased w/c ratio.

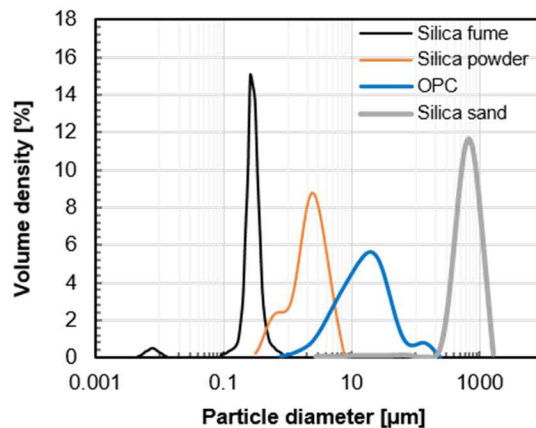


Fig. 4-2 Particle size distributions of raw materials used in developed UHPC

Table 4-1. Mix proportion of developed ultra-high performance concrete (UHPC)

Sample	Cement	Silica fume	Silica powder (flour)	Silica sand	Water to cement ratio	Super-plasticizer	SAP	Steel fiber (vol.% of UHPC)	Time zero [h]	Max. internal temp. [°C]
Ref_0.215					0.215		0		12	21.6
Ref_0.255	1	0.25	0.35	1.1	0.255	0.04	0	2	15	24.4
AA_0.255					0.255		0.004 (SAP_AA)		13	21.8
AM_0.275					0.275		0.003 (SAP_AM)		13	21.9

Table 4-2 Oxide compositions of raw materials (wt.%)

Chemical composition	SiO <sub>2</sub>	Al <sub>2</sub> O <sub>3</sub>	TiO <sub>2</sub>	Fe <sub>2</sub> O <sub>3</sub>	MgO	CaO	K <sub>2</sub> O	MnO	SO <sub>3</sub>	LOI	Total
Cement	20.80	4.82	0.29	3.33	3.30	61.74	0.90	0.09	1.86	2.50	99.63
Silica fume	96.90	0.29	0.01	0.15	0.18	1.54	0.64	0.03	-	0.02	99.97
Silica powder	97.70	0.49	0.08	0.05	0.21	1.37	0.02	0.01	-	0.02	99.99

## **4.2.2 Test methods**

### **4.2.2.1 Heat of hydration and X-ray powder diffraction (XRD)**

The heat flow was measured using isothermal calorimetry (TAM Air, TA Instruments). To start, 10 g of freshly mixed concrete paste (according to the mix design in Table 4-1 but without fine aggregate and steel fiber) was weighed into a glass vial. Then the vial was sealed and placed into the calorimeter and the heat flow was measured for 3 d. The calorimetry test was conducted twice to evaluate its reproducibility.

X-ray diffraction analysis was applied to all specimens at 28 d. The identical specimens used for hydration heat test, were also prepared for this analysis. At 28 d of curing, each sample was finely ground and placed into sample holder. A Cu x-ray source with 15 kV was used to cover 2 theta range from 10° to 80° with a step size of 0.01°. Quantitative analysis was achieved by using Highscore Plus Rietveld analysis software.

### **4.2.2.2 Scanning electron microscope (SEM) and pore structure analysis**

Scanning electron microscope (SEM) analysis was performed at 28 d to identify the microstructure of SAP-incorporated UHPC. A thin section of AM\_0.275 was prepared by the procedure that a slice of harden sample was dried and attached on a glass plate using an epoxy bond, and then it was grounded thinly (100 μm) and coated with carbon.

As a specimen for the 3D-CT analysis, the cylinder (50 mm diameter and 100 mm height) was prepared to visualize internal pore structure and fiber distribution, as well. This experiment was performed at 28 d using SkyScan 1173 CT scanner. The voltage of 130 kV and current of 60 uA were selected. Post processing work is called image-processing technique which extracts quantitatively meaningful information from the stack of 2D stack images which are the outcomes of CT experiments. Obtained 2D image has 2,240 x 2,240 pixel<sup>2</sup>. Image resolution was 35.15  $\mu\text{m}/\text{pixel}$ . 500 ms exposure time with rotational step of 0.2° takes almost 2 hours of scanning time for each sample. Total number of 2D images was around 2,000 per each sample. Because it is challenging and time consuming to deal with 2,000 images, 1,000 images were selected for image rendering and mathematical analysis.

MIP test was implemented using AutoPore IV 9500 (Micromeritics Instrument Corporation) to investigate the porosity and pore size distribution. At 28 d, spilt samples were selected and analyzed; during the test, mercury parameters were set to values of 485 erg/cm<sup>2</sup> (for the surface tension) and 130° (for the contact angle).

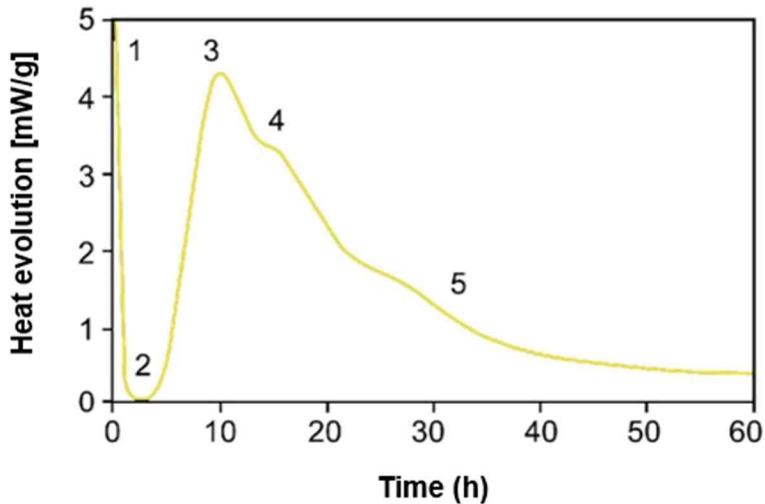
## 4.3 Results and discussion

### 4.3.1 Literature study on heat evolution by cement hydration

Fig. 4-3 explains typical hydration kinetics of regular cement paste. First phase there is a rapid initial process by dissolution of ions and initial hydration. In phase 2 (dormant period), the hydration is slow down. From phase 3-5, silicate and aluminate hydration cause acceleration of hydration. Lastly, phase 5 indicates the retardation period from sulphate depletion and slowing down of the hydration process.

Recently, isothermal calorimetry was used to study hydration heat flow of low w/b cement pastes with different dosages of SAP and extra water (Justs, Wyrzykowski, Winnefeld, Bajare & Lura, 2014). Water entrainment by means of SAP increased the degree of hydration at later hydration times in a manner similar to increasing the water-to-binder ratio. Addition of SAP also delayed the main calorimetric hydration peak compared to the reference pastes, however, in a less prominent manner than the increase in water-to-cement ratio. Early hydration is especially important in terms of the setting time and strength development. A retardation of the setting time may have consequences for the practical use of UHPC, as setting time is already delayed by the high SAP content of these mixtures and a further retardation may be acceptable. Moreover, a rapid strength development at an early age is often also fundamental for the application of UHPC, so that even if SAP are introduced into the mixture, they should not be overly detrimental for the early strength. As both SAP and additional water to saturate them are introduced into the mixtures with IC, it is

necessary in this analysis to separate the effect of the SAP on the early hydration from that of an increase in the w/c of the pastes.



Phase 1: Rapid initial process – dissolution of ions and initial hydration.

Phase 2: Dormant period – associated with a low heat evolution and slow dissolution of silicates.

Phase 3: Acceleration period – Silicate hydration.

Phase 4: Acceleration period – aluminate hydration.

Phase 5: Retardation period – sulphate depletion and slowing down of the hydration process. (sulphate is from gypsum)

Fig. 4-3 Typical hydration heat curve of cement paste

### 4.3.2 X-ray diffraction (XRD) analysis

As an example, the collected pattern for AA\_0.255 is shown in Fig. 4-4 (a). Rietveld analysis was applied for a quantitative analysis only for crystalline phases in the specimen. The results of all samples are presented in Fig. 4-4 (b) which relatively compares the proportions of crystalline phases except for amorphous phases such as calcium-silicate-hydrate (C-S-H) gel and silica fume. Thus, it should be noted that exact quantification for the amorphous phases were missing in this analysis, i.e., only qualitative analysis on different samples could be achieved. The cement used contained alite and belite dominantly (94%). In all samples, significant amounts of unreacted clinkers (i.e., alite and belite) were detected at 28 d of curing. Moreover, the portlandite contents in the samples, also give the evidence for incomplete pozzolanic reactions even at 28 d of hydration, whereas the absence of calcite indicates an insignificant carbonation in this specimen. It has been also reported that the degree of hydration of UHPC ( $w/c=0.2$ ) at 28 d is 57.5% (Loukili, Khelidj & Richard, 1999), which means 42.5% of cement is unreacted and remain just as fillers. Fig. 4-4 also confirms this incomplete cement hydration of the samples because of the insufficient water and space hydration reaction and products (Korpa, Kowald & Trettin, 2009).

In addition, all quarts found in this analysis, were from silica flour since there was no fine aggregate mixed for specimen for XRD and calorimetry tests. Given the fact that the initial amount of silica flour was fixed at about 19% including silica fume ( $0.35/[1+0.25+0.35+0.215+0.04]$ ) or 25% excluding amorphous silica fume ( $0.35/[1+(0.25\times 0.031)+0.35+0.215+0.04]$ ), a quartz

composition of over 40% indicates a significant amount of amorphous phase was produced during the hydration reaction. However, its presence could not be confirmed quantitatively by this method. Therefore, an accurate “quantitative” analysis like the ex-situ XRD experiment using an internal standard is additionally necessary.

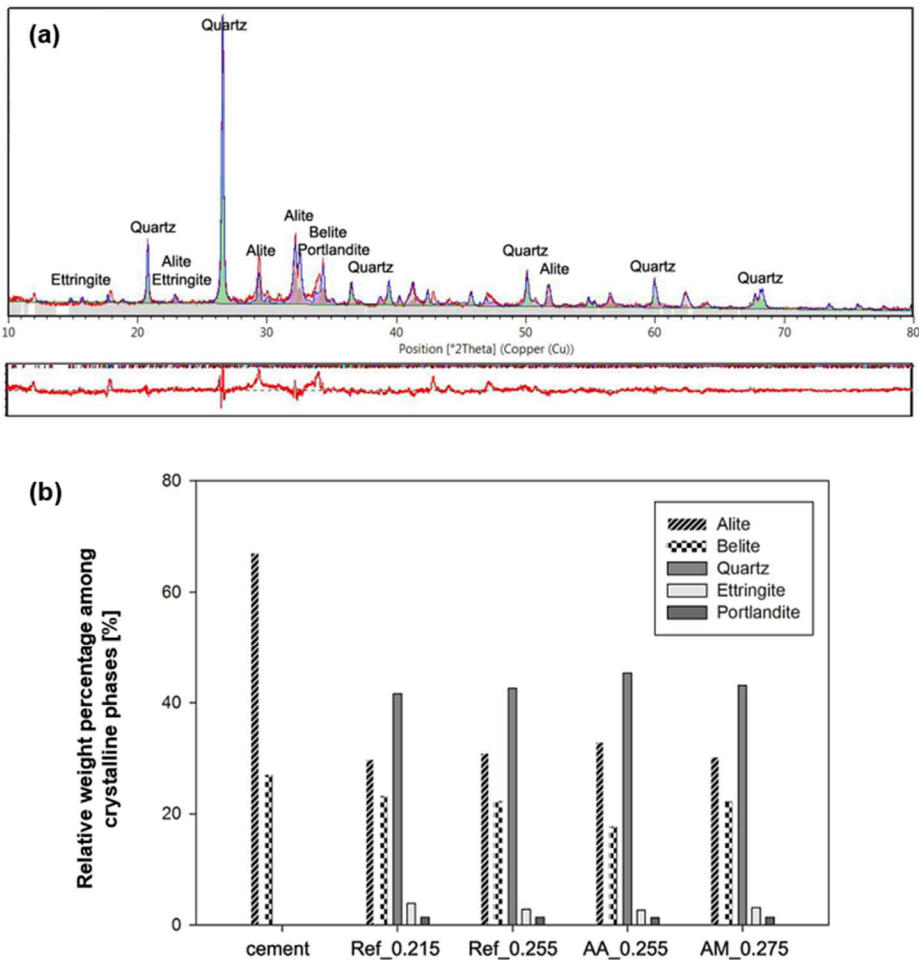


Fig. 4-4 Results of XRD analysis of cement and UHPC pastes: X-ray Rietveld analysis of AA<sub>0.255</sub> (a), and quantitative results of all samples (b)

### 4.3.3 Scanning electron microscope (SEM) analysis

SEM images in Fig. 4-5 show perfectly globular SAP pores of AM\_0.275; the pores can be clearly distinguished from the other pores due to their shape. Similar to the SAP particles that is presented in Section 2, the SAP pores have various sizes. The steel fibers and agglomerates of raw materials could be observed in the images. Finally, the dried SAP particles in the pores which were formed due to the previous swollen state SAP particles, could be observed. This dried SAP\_AM is expected to expand again if proper water is supplied. SEM images of other samples also can be seen in Appendix A.

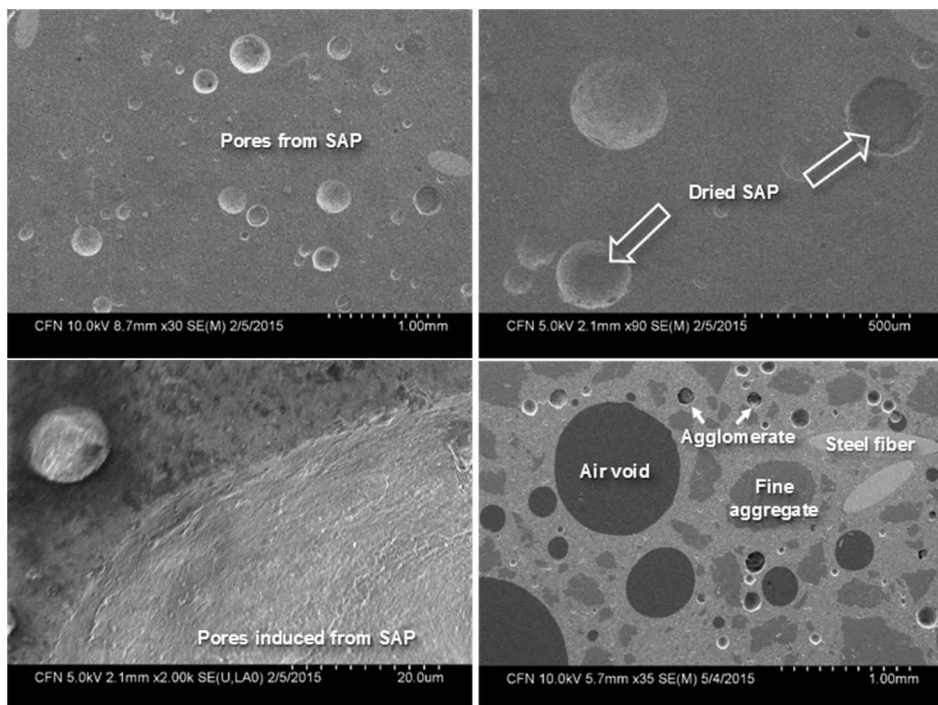


Fig. 4-5 SEM images of internally cured UHPC (AM\_0.275)

#### 4.3.4 Pore structure by 3D-computed tomography (CT) analysis

Fig. 4-6 shows the results of conducted CT experiment. From a high image contrast, identification of matrix (gray), pores (black), and steel fibers (white) was possible as shown in top-left image in Fig. 4-6. All image processing was done using AVIZO Fire image processing software. To differentiate pores, different threshold values of 25, 30, 35, and 40/256 were applied. Then small pores of a size of smaller than 10 voxel have been removed. These images show identified pores (or fibers in the last image with a threshold 100-211/256) depending on the threshold limits.

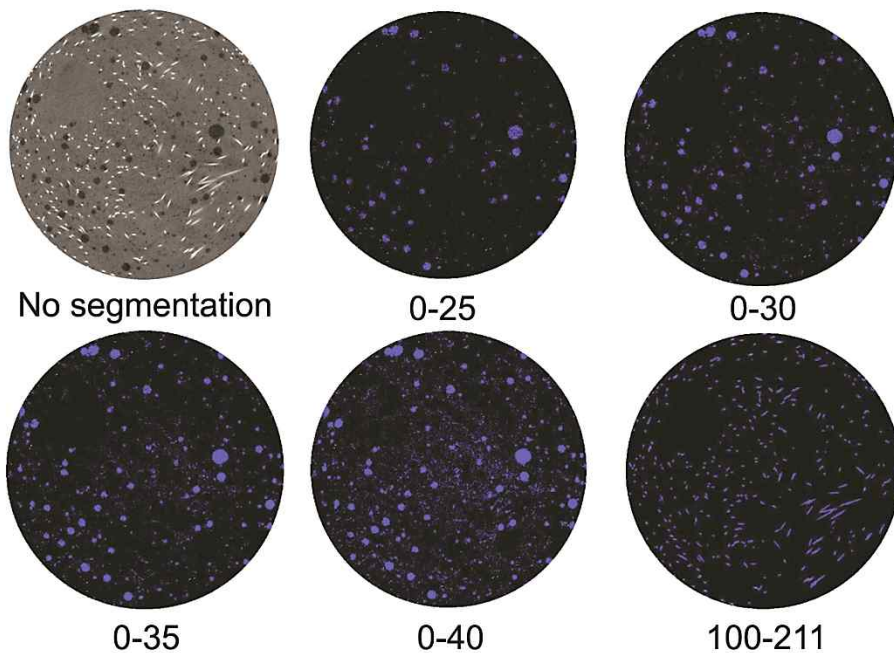


Fig. 4-6 2D-CT images with different threshold values

Fig. 4-7 shows three-dimensional rendering images of AM<sub>0.275</sub> before

and after the segmentation of pores (white) and steel fibers (blue). As expected, fibers and pores are successfully separated from the cement matrix due to the highly different image contrast obtained in the CT experiment. Based on the segmented pores, rigorous quantitative analysis was conducted to understand the characteristics of pore especially from the addition of SAP.

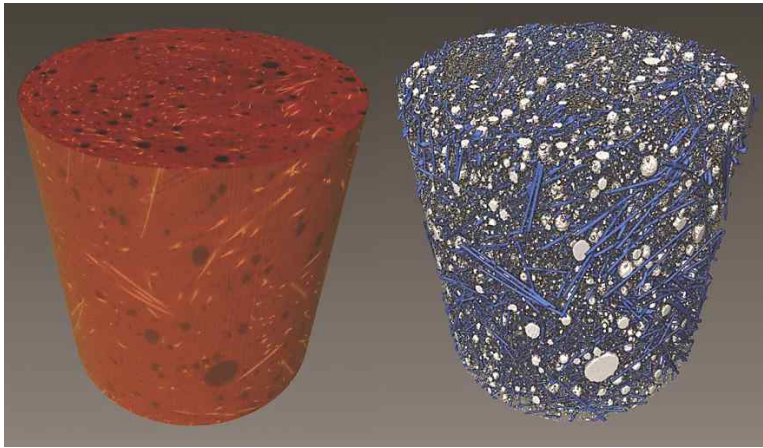


Fig. 4-7 3D-rendering images of UHPC with SAP (left) and pores/fibers segmentation (right)

Although it is not directly related to the subject of this study, another advantage of CT analysis is that it is possible to visually check the fiber distribution and orientation as well as a volume ratio of a fiber reinforced concrete. These distribution and orientation of UHPC (Ref\_0.215) was observed through CT experiment. Above all, the estimated fiber volume fraction was 2% of UHPC, which accurately matches with the mix proportion in Table 4-1. In addition, by analyzing the orientation of each steel fiber included, the angles ( $\phi$ ) on the vertical plane of the cylinder and the angles ( $\theta$ ) on the horizontal plane are expressed in 4-8 (a) and (b), respectively. As a result, the fiber distribution was focused on the circumference of the

cylindrical specimen since the fresh UHPC was poured aiming at the center of the mold. Then, the steel fibers were possibly moved perpendicularly into the surround area (Boulekbache, Hamrat, Chemrouk & Amziane, 2010). In the case of samples with a low viscosity, steel fibers, whose density is relatively large, can sink to the bottom. However, in this study, this was not observed due to the sufficient consistency of the mix design and possibly the effect of SAP.

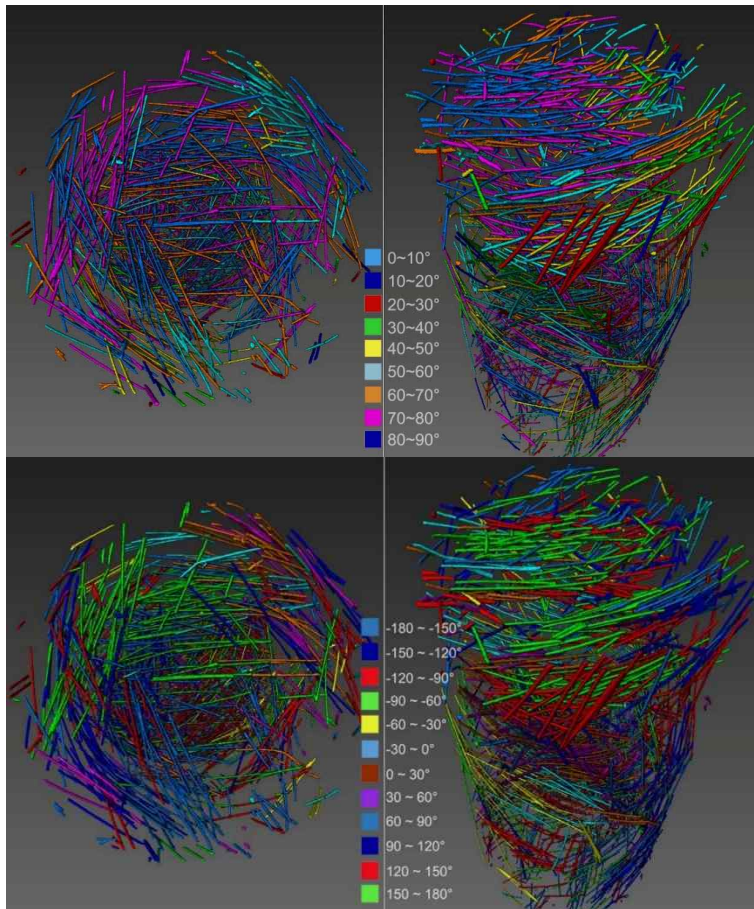


Fig. 4-8 Fiber orientation analysis of Ref\_0.215 on vertical (top) and horizontal (bottom) directions

The analysis results shown in Fig. 4-8 were used to statistically present the orientations of the steel fibers in the cylindrical specimen (Fig. 4-9). As presented in Fig. 4-9 (a), the steel fibers in the three samples (Ref\_0.215, AA\_0.255, and AM\_0.275) tended to be oriented at 45-90°, rather than 0-45°, relative to the vertical direction, whereas the fibers in Ref\_0.255 tended to be at 0-45°. In other words, the steel fibers in the three specimens and Ref\_0.255 tended to be oriented vertically and horizontally, respectively. To prepare the cylindrical specimen, the tube-shaped mold was filled with fresh UHPC by dropping it from an upper position. As the orientation of the fibers depends on the flow direction of fresh UHPC, they would be placed vertically with a short movement as soon as the concrete entered a narrow mold (diameter  $\leq 50$  mm). Then, they would be flattened again because of gravity and buoyancy. This positional change (i.e., the tendency to lie horizontally) was prominent only in Ref\_0.255, which is relatively fluid (due to high w/c without SAP); a similar tendency was not observed for the other specimens. The various plastic viscosities and yield stresses of the fresh UHPCs possibly contributed to the differences in the vertical orientations of the fibers. On the other hand, as shown in Fig. 4-9 (b), the fibers on the horizontal plane did not have a predominant orientation, i.e., all of them were randomly distributed. This is because the factors that affect the orientation in the vertical plane (e.g., gravity and buoyancy), were not relevant in the horizontal direction.

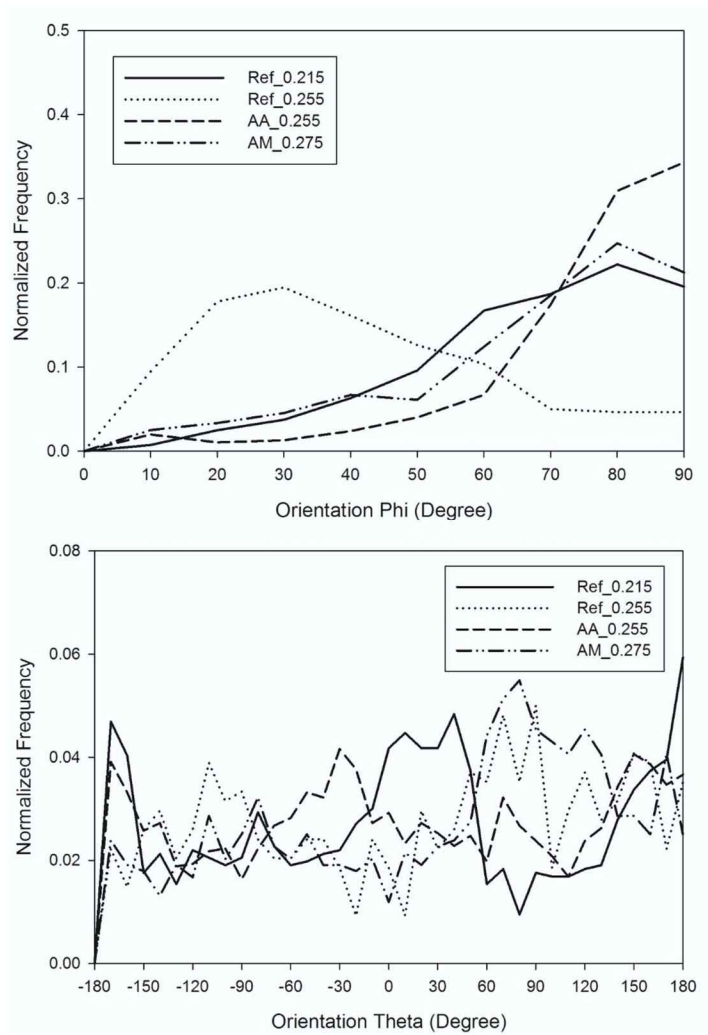


Fig. 4-9 Orientation of steel fibers on vertical (top) and horizontal (bottom) directions

Meanwhile, the results of 3D-CT analysis of two samples (Ref\_0.215 and AM\_0.275) were compared with each other to investigate the effect of the SAP addition on the pore structure of hardened UHPC. Firstly, porosity as a function of pore volumes was calculated with different threshold limits. Fig. 4-10 clearly shows that porosity curves are different between the two samples. Especially, it is quite significant starting from the pore volume of  $1 \times 10^8 \mu\text{m}^3$  regardless of

the threshold limits. Therefore, it can be safely suggested that the addition of SAP particles generates pores especially larger than that size. Of course, there should be ordinary entrapped pores with that size but the number of them is much smaller than that of SAP pores. It should be also mentioned that the two porosity curves follow an almost exact trajectory until they reach the size. Thus, it can be inferred that the measured two UHPC samples have similar “small size” pore system. With the threshold value of 40, the trend looks abnormal which can be due to the overestimation of pore size. Thus the threshold range of 0-35 was selected for further analysis. Fig. 4-11 summaries total porosity of the two samples with different threshold limit. As expected, total porosity is increased as a threshold limit is increased and with the addition of SAP. With the limit of 35, total porosity was measured as 6.0% and 2.5% for UHPC with and without SAP, respectively.

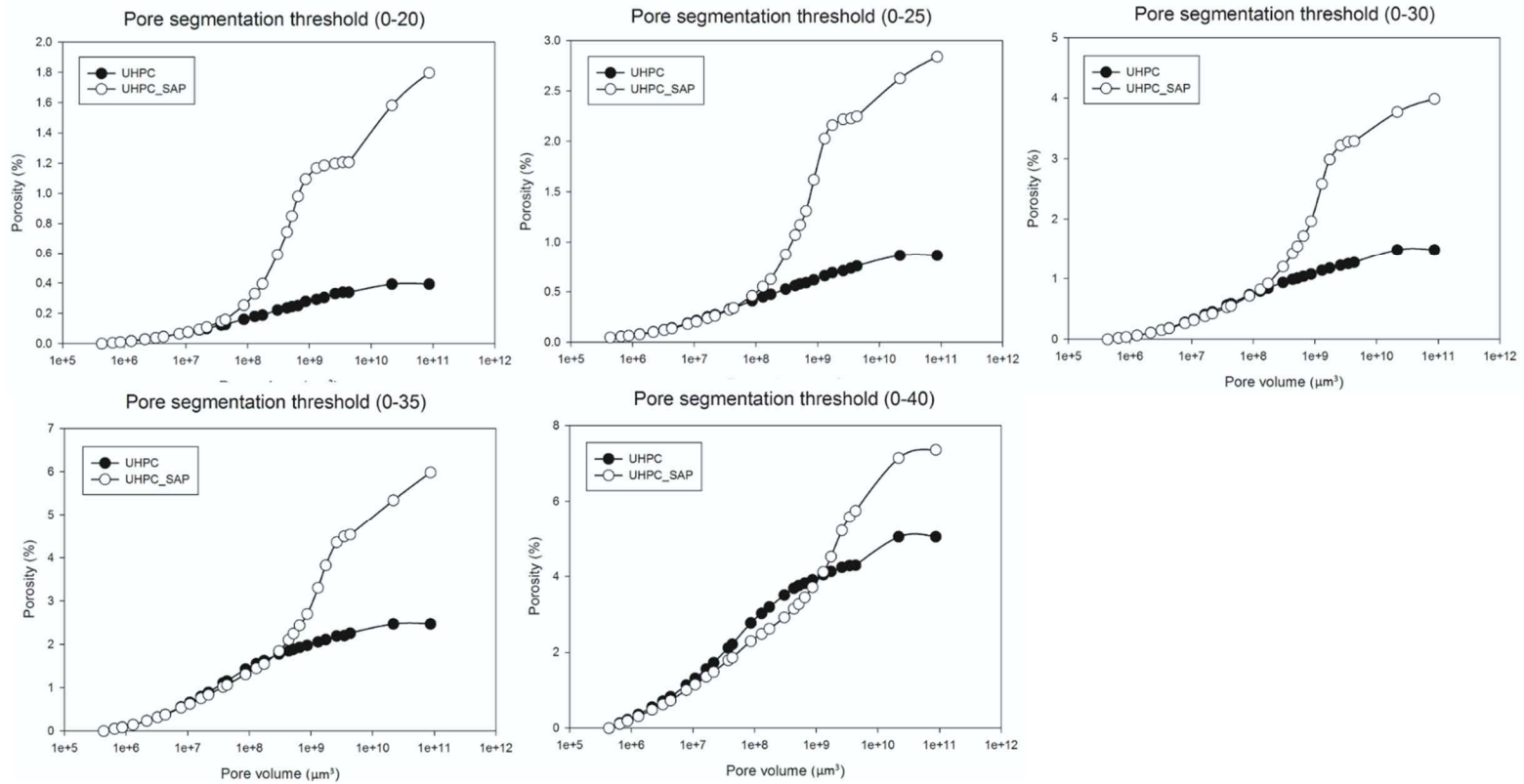


Fig. 4-10 Cumulative distributions of pore volumes with different threshold values (20, 25, 30, 35, and 40/256)

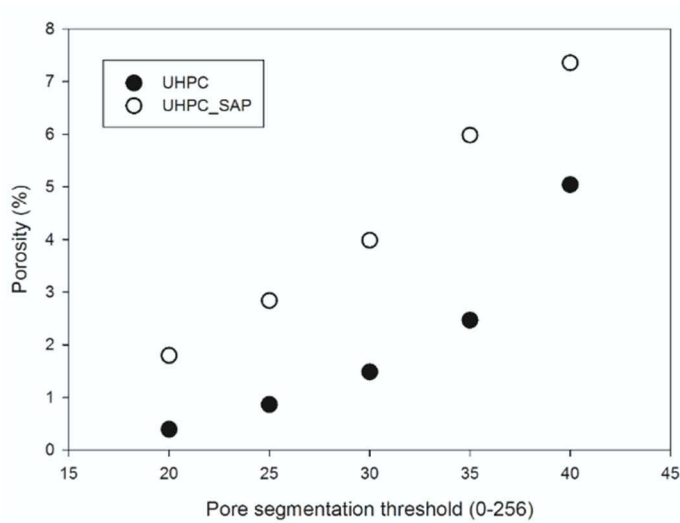


Fig. 4-11 Computed total porosity as a function of segmentation threshold

Fig. 4-12 shows histograms of the counted pores. It is surprising that the two samples have an almost identical number of pores. This result not only indicates that they have a similar number of small pores (as previously confirmed) but it can also confirm the accuracy of the conducted CT experiment and the consistency of UHPC sample preparation. In order to separate SAP pores from ordinary pores, the distribution of pores with respect to surface area and volume has been calculated (Fig. 4-13). Although they have similar trend in terms of pore count as a function of pore volume (Fig. 4-12), they have a quite different number of “big” pores. This difference can explain the total porosity result. The relatively small number of big pores can make a big difference in total porosity. Thus, in this study, we used a threshold limit of  $3 \times 10^8 \mu\text{m}^3$  to differentiate SAP pores from ordinary pores. That means pores larger than that size in AM\_0.275 were considered as pores induced from the volume expansion of the SAP. As discussed, there should be ordinary pores in

that range, but the number of them is negligible (Fig. 4-13). The separation result is shown in Fig. 4-14. The number of total pores in Ref\_0.215 is 123,559 while the number of separated SAP pores in AM\_0.275 is only 1,012.

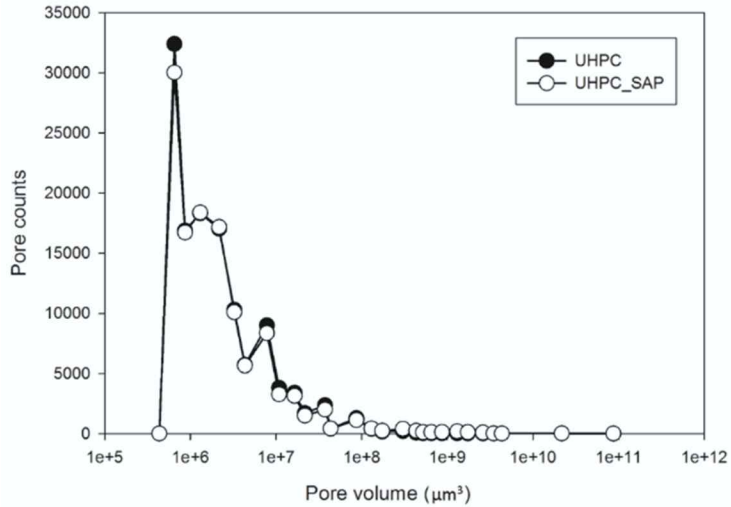


Fig. 4-12 Pore number as a function of volume

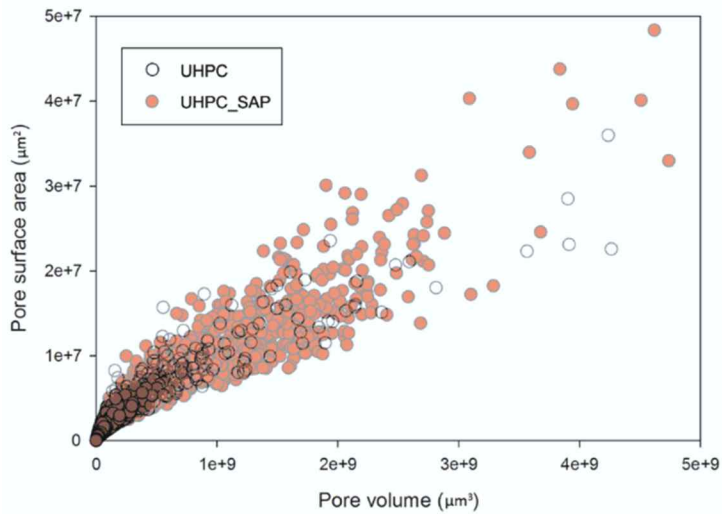


Fig. 4-13 Scatter distribution of measured surface areas and volumes from pores

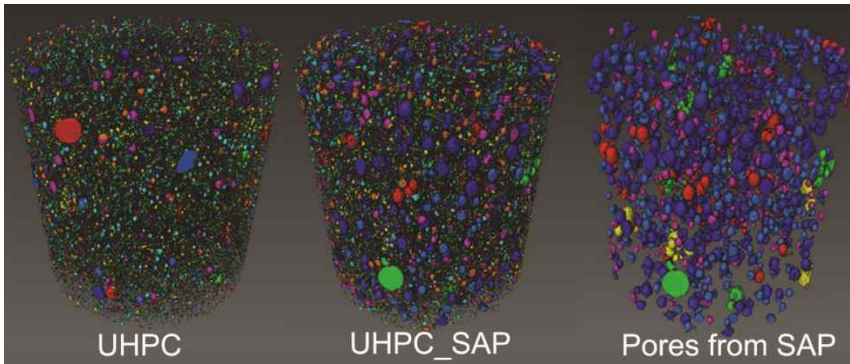


Fig. 4-14 3D-rendering images of Ref\_0.215 (UHPC), AM\_0.275 (UHPC\_SAP), and only SAP pores in AM\_0.275

Next, the mass properties of the pores were calculated by the inertia tensor method (Drach, Drach & Tsukrov, 2013). A 3 by 3 matrix ( $I$ ) can be defined as the moments of inertia of each pore in  $x$ ,  $y$ , and  $z$  coordinate system. Then, eigenvalues and eigenvectors of the matrix  $I$  are equal to the principal moments ( $I_{11}$ ,  $I_{22}$ ,  $I_{33}$ ) and principal reactions, respectively. The degree of anisotropy of each pore could be also formulated from Eq. 4-1.

$$\text{Degree of anisotropy} = 1 - \frac{I_{m \max}}{I_{m \min}} \quad (4-1)$$

Where,  $I_{m \max}$  and  $I_{m \min}$  are the maximum and minimum eigenvalue, respectively.

The principal moment data and corresponding anisotropy data are calculated for all identified pores. The the anisotropy of the two samples are shown in Fig. 4-15. Again, due to the large difference between the number of

pores and SAP pores, the data has been normalized. Anisotropy value of zero indicates perfectly isotropic circular shape. As can be seen, likewise the dry stage SAP particles, SAP pores are much more isotropic compared to all pores in the control sample. Thus, it can be suggested that the pore generation induced from SAP occurs hydrostatically inside the concrete. This result can be also confirmed by the following analysis. Fig. 4-16 shows the distribution of the ratio of the principal moments ( $I_{33}/I_{11}$  and  $I_{22}/I_{11}$ ) of all pores in Ref\_0.215 and SAP pores in AM\_0.275. While the distribution of ordinary pores is intensely focused on (0,0) point, that of SAP pores is fairly spread. Thus, it can be concluded that the pores from SAP\_AM have quite different shapes (more isotropic) compared to ordinarily entrapped pores in UHPC. Lastly, the closest distance of adjacent pores is computed for all pores in Ref\_0.215 and SAP pores in AM\_0.275. The computed results are shown in Fig. 4-17. The average value of the closest distance for all pores and SAP pores is 395.5  $\mu\text{m}$  and 1998.6  $\mu\text{m}$ , respectively. The size of SAP as well as the distance of pores are important factors that affect the degree of moisture diffusion for IC effect.

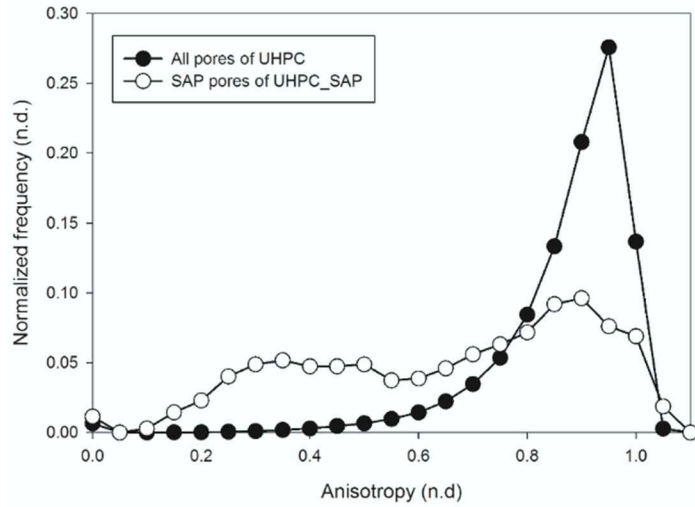


Fig. 4-15 Normalized distribution of computed pore anisotropy

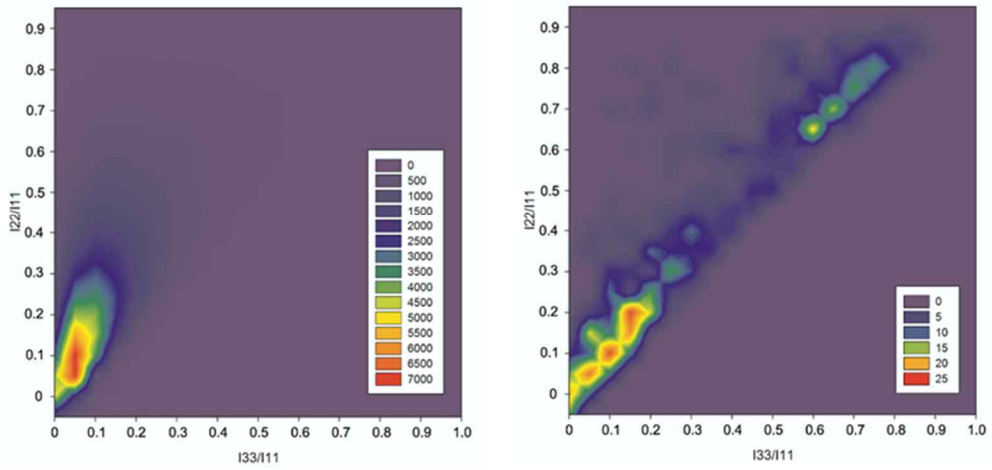


Fig. 4-16 Distribution of  $I_{22}/I_{11}$  and  $I_{33}/I_{11}$  of pores in Ref\_0.215 (left) and only SAP pores in AM\_0.275 (right)

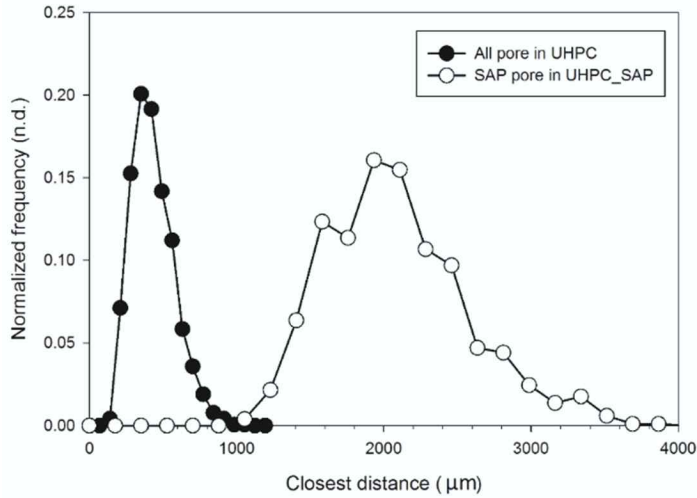


Fig. 4-17 Distribution of measured closest distance of all pores in Ref\_0.215 and SAP pores in AM\_0.275

#### 4.3.5 Pore-size distribution and total porosity by mercury intrusion porosimetry (MIP) and 3D-CT analysis

Fig. 4-18 (a) and (b) show the pore-size distributions of the samples by MIP and 3D-CT analyses, respectively. Although the same specimen was used for the two methods, the results of both methods were completely different. The MIP analysis provided the distribution of sub-micron size ( $< 1 \mu\text{m}$ ) pores, while 3D-CT provided the macro-size ( $> 50 \mu\text{m}$ ) pore distribution.

Fig. 4-18 (a) shows the variation of pore structure due to only the hydration reaction and the resulting hydration products, i.e., the effects of SAP pores were fully excluded. It is confirmed that the volume of the pores ( $> 10 \text{ nm}$ ) in Ref\_0.255 is much higher than the other samples. The increase in the volume

of capillary voids (Fig. 4-1) due to the increased w/c without SAP (from 0.215 to 0.255) caused this result. In particular, the distributions of the smaller pores ( $< 10$  nm) were remarkably different between the samples. These pores are classified as small capillary pores and gel-pores (Aligizaki, 2006). As explained in Section 2, the hydration reaction promoted by IC can increase the degree of hydration of low w/c concrete, which contributes to the additional formation of hydration products such as C-S-H gel and portlandite. Thus, the small capillary pores ( $> 7$   $\mu\text{m}$ ) of AM\_0.275 should be additionally filled with the products [12], which eventually leads to a volume increase of gel pores ( $< 7$   $\mu\text{m}$ ) because sizes of the capillary pores should be decreased. The analysis result of AA\_0.255 is also noticeable. That is, despite a 4% higher w/c, the pore volume of AA\_0.255 was almost equal (pore size  $> 10$  nm) or even lower (pore size  $< 10$  nm) than in Ref\_0.215. As in Ref\_0.255, the volume of capillary pores is increased only if w/c is increased without SAP. However, this volume was not increased in AA\_0.255, which also verifies that a part of the extra water was used in IC to promote the hydration reaction. Further evidence of this promotion is also found in the distributions of pores below a diameter of 10 nm. Although the size of pores was not decreased as in AM\_0.275, the volume of pores ( $< 10$  nm) in AA\_0.255 was lower than that of Ref\_0.215. This also could be caused by the additionally-formed hydration products. The MIP results of AM\_0.275 and AA\_0.255 clearly demonstrated the effectiveness of IC on hydration promotion.

The large-sized pore distributions measured by the 3D-CT method are shown in Fig. 4-18 (b). The pores consisted of entrapped and/or entrained air voids and SAP pores. First, by comparing Ref-0.215 and Ref\_0.255, the volume

change of air voids of O-UHPC was confirmed as a function of w/c, i.e., the air voids were increased as w/c increases. This is because the amount of air voids generated during mixing could be decreased due to the changed rheological properties (i.e., yield stress and plastic viscosity) as the amount of mixing water increased (Wallevik & Wallevik, 2011). Meanwhile, unlike the MIP analysis, only the 3D-CT method verified that the volume of these large voids in I-UHPCs was higher than that in O-UHPCs. This result was caused by the additionally formed SAP pores, as confirmed previously. In particular, the volume increase of AM\_0.275 (containing 0.3% SAP\_AM) was greater than AA\_0.255 (containing 0.4% SAP\_AA), which reveals that the volume increase by SAP pores is more dependent on the absorption capacity of SAP than the designed SAP to cement ratio. Thus, IC by SAP (especially possessing superior water absorption and retention capacities) can considerably increase both nano- (< 10 nm) and macro- sized (> 500  $\mu\text{m}$ ) pores in a concrete.

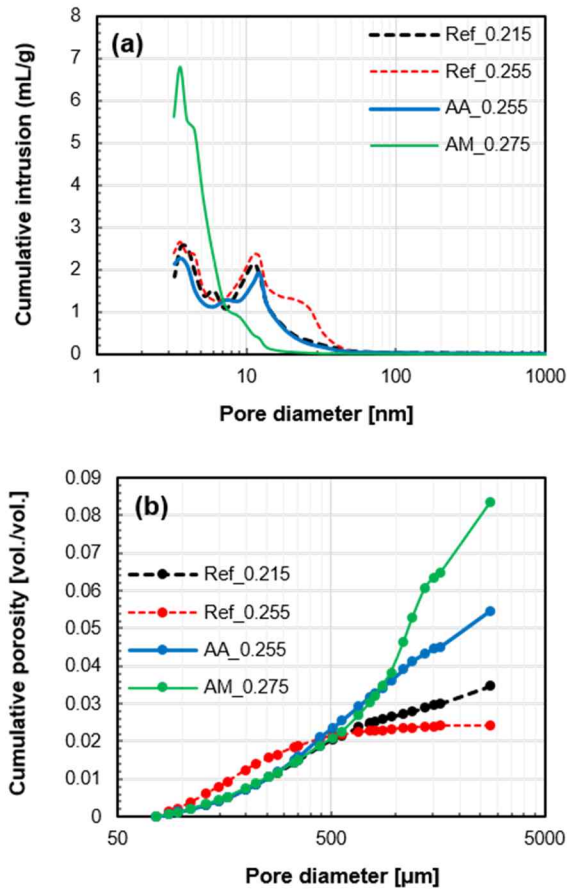


Fig. 4-18 Pore size distribution of UHPC by MIP (a) and 3D-CT (b) methods

The total porosities of the samples (comparing the analysis methods) are presented in Fig. 4-19 based on the results shown in Fig. 4-18. The porosities also reflect both the hydration reaction promoted by IC and the increase of large-sized SAP pores.

The green bars in Fig. 4-19 show the estimated total porosity by the MIP method. In the case of O-UHPCs (Ref\_0.215 and Ref\_0.255), the total porosity was increased by 28% ( $14.7\% / 11.5\% = 1.28$ ) as the w/c increased by 4%, due

to the volume increase of capillary pores (diameter > 10  $\mu\text{m}$ ). Compared to Ref\_0.215, the porosity of AA\_0.255 was almost identical (only 1% reduction,  $11.4\% / 11.5\% = 0.99$ ), whereas that of AM\_0.275 was the lowest among all samples despite having the highest w/c. Along with AA\_0.255 (1% reduction in total porosity), the 3.5% reduction in the porosity of AM\_0.275 ( $11.1\% / 11.5\% = 0.965$ ) again verifies that the hydration reaction is promoted by IC.

The total porosity by the 3D-CT method only reflected the effect of SAP pores excluding that of IC. The porosities of I-UHPC were significantly increased depending on the volume of swollen SAP particles in each concrete sample. In other words, the porosities of AA\_0.255 and AM\_0.275 were increased by 58% and 147%, respectively, relative to Ref\_0.215. However, the air voids of Ref\_0.255 decreased by 33% due to the changed rheology. The 3D-CT results verify that the addition of SAP totally changes the pore structure of UHPC, i.e., the structure of the UHPC is changed to a coarse system by the addition of SAP.

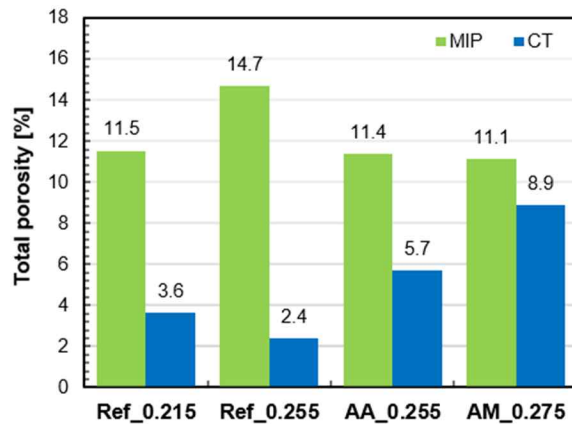


Fig. 4-19 Total porosity of UHPC by MIP and 3D-CT methods

## 4.4 Summary and concluding remarks

In this section, the effects of IC by SAP on the hydration characteristics and pore structure of UHPC were investigated and verified using various experimental methods. XRD analysis showed that a significant amount of unhydrated cement remained in the hardened UHPC, regardless of the addition of SAP. Therefore, it was found that a large portion of the mixed raw cement only functions as a filler; however, it can react with extra water supplied, contributing to an increase in the degree of hydration. Large-sized pores induced by the swollen SAP particles and shrunken SAPs in the pores were directly observed in SEM images. Unlike SEM analysis which only could provide 2D images at arbitrary areas, CT analysis provided clear 3D images of the entire internal structure of the cylindrical specimen. Based on this method, the network, volume, number, shape, and spacing of the SAP pores in UHPC could be accurately identified and estimated. The most notable results of this section were confirmed in the pore size distribution and total porosity analyses by MIP and 3D-CT. Sub-micron sized pore analysis by MIP verified that hydration products formed additionally by IC can decrease the volume of this size of pores. In addition, macro-sized pore analysis by 3D-CT verified that the pore structure of UHPC is completely changed by the additionally formed SAP pores. The analysis results of this section are the decisive evidence of the changed material properties of I-UHPCs, which will be discussed in the next section.

## **Chapter 5. Properties of internally cured ultra-high performance concrete (UHPC)**

### **5.1 Precast UHPC**

#### **5.1.1 Introduction**

To ensure outstanding performance at an early stage of curing ( $< 7$  d), UHPC members are commonly subjected to heat treatments (HT) for 24–48 h following their initial mixing (Association Française De Génie Civil (AFGC), 2013; Richard & Cheyrezy, 1995). During standard HT, members are exposed to treatment conditions ( $90\text{ }^{\circ}\text{C}$ , relative humidity (RH)  $> 90\%$ ) for 48 h (Selleng, Meng & Fontana, 2016; Association Française De Génie Civil (AFGC), 2013; Garas, Kurtis & Kahn, 2012; Heinz, Urbonas & Gerlicher, 2012; Korea Concrete Institute (KCI), 2012; Schachinger *et al.*, 2008; Japan Society of Civil Engineers (JSCE), 2004). In addition, during the manufacture of architectural precast elements, UHPC can also be subjected to moderate HT conditions ( $60\text{ }^{\circ}\text{C}$ ,  $95\%$  RH for 72 h) (National Precast Concrete Association (NPCA), 2013). Such moderate condition satisfies the HT regulations for normal precast concrete, in which the maximum temperature should be below  $70\text{ }^{\circ}\text{C}$  to avoid delayed ettringite formation (DEF) (Heinz & Ludwig, 2004; Taylor, Famy & Scrivener, 2001). This mitigated HT method, which is used for the manufacture of architectural UHPC, is advantageous because it can be performed using general precast concrete facilities that are used to manufacture normal concrete, rather than using special equipment to maintain a temperature of  $90\text{ }^{\circ}\text{C}$ . In

addition, the associated lower energy consumption and manufacturing costs are beneficial (Selleng *et al.*, 2016; Yazıcı, Deniz & Baradan, 2013).

During the HT, the hydration reaction consumes water and accelerates the self-desiccation (Maruyama & Teramoto, 2013; Jensen & Hansen, 1996); thus, the AS, directly related to the desiccation, increases (Maruyama & Teramoto, 2013; Jiang *et al.*, 2005). In addition, the reduction of the pore size causes an increase in capillary forces due to the self-desiccation (Snoeck *et al.*, 2015a; Lura *et al.*, 2001); therefore, the HT certainly further increases the AS of the UHPC. For instance, at 40 d, heat-treated UHPC exhibits a higher volumetric strain due to AS than that of ambient-cured UHPC; in particular, owing to the HT, the shrinkage rate is increased up to ten-fold (Graybeal, 2006).

When considering the risk of early-age cracking, the rate of shrinkage is known to be more critical than its magnitude (Shen, Wang, Cheng, Zhang & Jiang, 2016; Jiang *et al.*, 2014; Lura *et al.*, 2001). A higher curing temperature can increase the risk of cracking due to the increased rate of shrinkage strain (Jiang *et al.*, 2014; Lura *et al.*, 2001). In a previous study, compared with restrained specimens cured at below 20 °C, high-performance concrete specimens that were cured at over 30 °C exhibited a greater number of early cracks (Lura *et al.*, 2001). The risks of cracking and shrinkage-induced deformation can be underestimated unless the temperature history is accurately considered (Loukili *et al.*, 2000). Specifically, the actual curing temperature should be reflected to evaluate the associated risks and deformation accurately, especially when deformed bars are used to reinforce the concrete (Japan Society of Civil Engineers (JSCE), 2004). However, the majority of studies on the

shrinkage of UHPC have only considered room temperature conditions. There are few studies that focus on AS under HT because it is difficult to accurately measure the AS of UHPC. In addition, the associated experiments are complex, such as those that measure the heat of hydration or accurate AS under various temperatures. Therefore, the effect of HT on the magnitude and rate of shrinkage have not yet been elucidated, and suitable methods to overcome the cracking of heat-treated UHPC have not been established.

When considering the characteristics of UHPC with densely compacted fine particles ( $< 1$  mm) and low w/c (National Precast Concrete Association (NPCA), 2013; Richard & Cheyrezy, 1995), one of the potential methods used to mitigate AS can be IC using a superabsorbent polymer (SAP). Previous studies have confirmed that this method is effective for the reduction of AS and the risk of early-age cracking under ambient-curing conditions (Justs *et al.*, 2015; Snoeck *et al.*, 2015a; Jensen & Hansen, 2002, 2001b). As mentioned, the SAP releases the absorbed water gradually within the concrete, which maintains internal RH high during the self-desiccation period. In the same manner, this mechanism can be also applied to mitigate the accelerated shrinkage or self-desiccation of UHPC during the HT period. Therefore, the objectives of the Section 5.1 are to elucidate the shrinkage behavior of heat-treated UHPC and to evaluate the effectiveness of IC, with SAP, on the shrinkage reduction. The AS, drying shrinkage (DS), and thermal shrinkage were accurately measured under moderate HT conditions, followed by 2 d of ambient-curing conditions. The complex phenomena related to the shrinkage, strain rates, and hydration kinetics were discussed with regard to the effectiveness of the SAP as an IC admixture.

### **5.1.2 Experiment methods**

The heat flow of hydration was measured using an isothermal calorimeter (TAM Air, TA Instruments) to confirm the effect of the HT on the hydration reaction of the UHPC. In this measurement, 15 g of each paste was tested, which excluded the non-reactive materials such as the silica sand and steel fibers. First, heat curves were obtained under isothermal conditions of 20 °C for 48 h. Subsequently, the newly prepared pastes that had been subjected to curing at 20 °C for 48 h were tested under high temperature conditions (60 °C for 72 h or 90 °C for 48 h). Finally, each curve that was measured during the HT period was plotted alongside the associated previously measured early-age curve (48 h of curing at 20 °C). To perform isothermal calorimetry, the pastes were inserted when the calorimeter had attained its target temperature (20 °C, and 60 °C or 90 °C). Thus, the measurements were performed three times to obtain two sets of hydration histories for each UHPC specimen.

Prismatic steel molds of 40×40×160 mm<sup>3</sup> were prepared to measure the shrinkage of the heat-treated UHPC as shown in Fig. 5-1. Internally, the mold was lined with Teflon sheets to avoid frictional resistance between the mold and specimen. An embedded-type strain gauge (Tokyo Sokki Kenkyujo Co., Ltd.), used for concrete and mortar, was longitudinally positioned in the center of the mold using flexible steel wires. Additionally, a T-type thermocouple was positioned along with the gauge to measure the internal temperature (IT) history of the specimen. The fresh UHPC was poured into the mold, and subsequently, the top surface was sealed using polyester film; the specimen was then cured in a chamber. The chamber was programmed with the curing conditions presented

in Fig. 5-1. Considering the operating-temperature range of the gauge (-20–60 °C), the specimen was subjected to a moderate HT. The measured shrinkage was recorded using a data logger every 5 min from the time that AS commenced (known as “time zero”) to the 28<sup>th</sup> day.

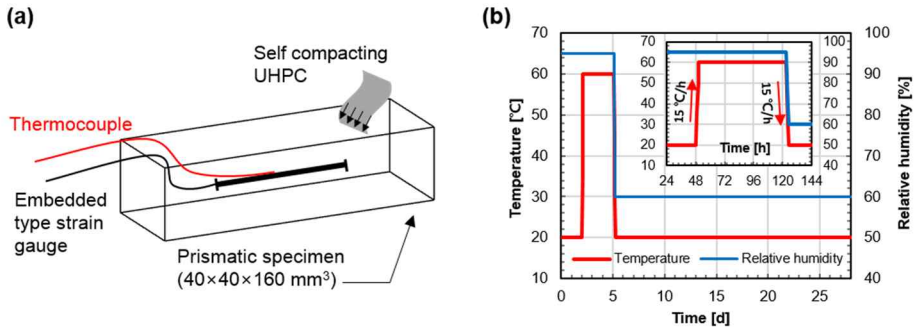


Fig. 5-1 Free strain measurement for shrinkage test (a) and curing program for heat treated UHPC (b)

‘Time zero’ can be determined using the ultra-pulse velocity (UPV) method. The UPV of the fresh concrete suddenly rises when the formation of the solid skeleton commences (Staquet, Boulay, Robeyst & De Belie, 2008). Using the FreshCon system (Reinhardt, Grosse & Herb, 2000), ‘time zero’, was determined by monitoring the UPV history as presented in Table 4-1. The test method and results also can be seen in Fig. 5-2. The determined time zero was considered as a point of strain normalization. Three specimens were prepared to perform shrinkage tests on each sample. To prevent moisture loss during the demolding process at around 48 h, and moisture uptake by steam owed to the HT, all the specimens were cured under sealed conditions for 7 d. Following their demolding at 7 d, two of the specimens were covered with adhesive aluminum tape to measure the AS. The surface of the other specimen was directly exposed to air-curing conditions (20 °C, RH 60%) to measure the TS.

The sealed shrinkage (SS) was determined to be an average of that of the two replicates, whereas TS was determined from the measurement results obtained for one specimen between 7 d and 28 d. As a common practice, other properties such as heat of hydration reaction and time zero were also determined by one measurement.

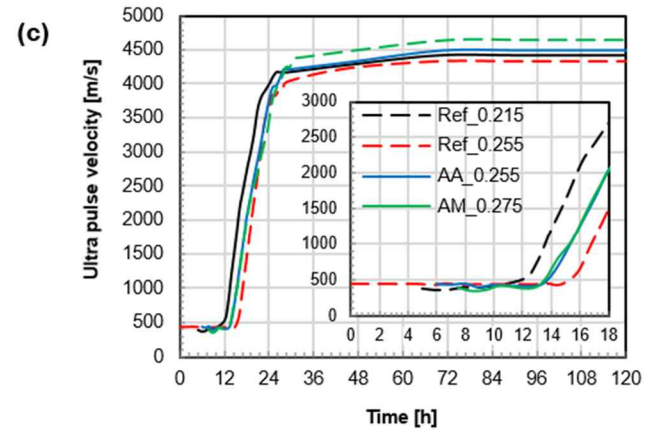
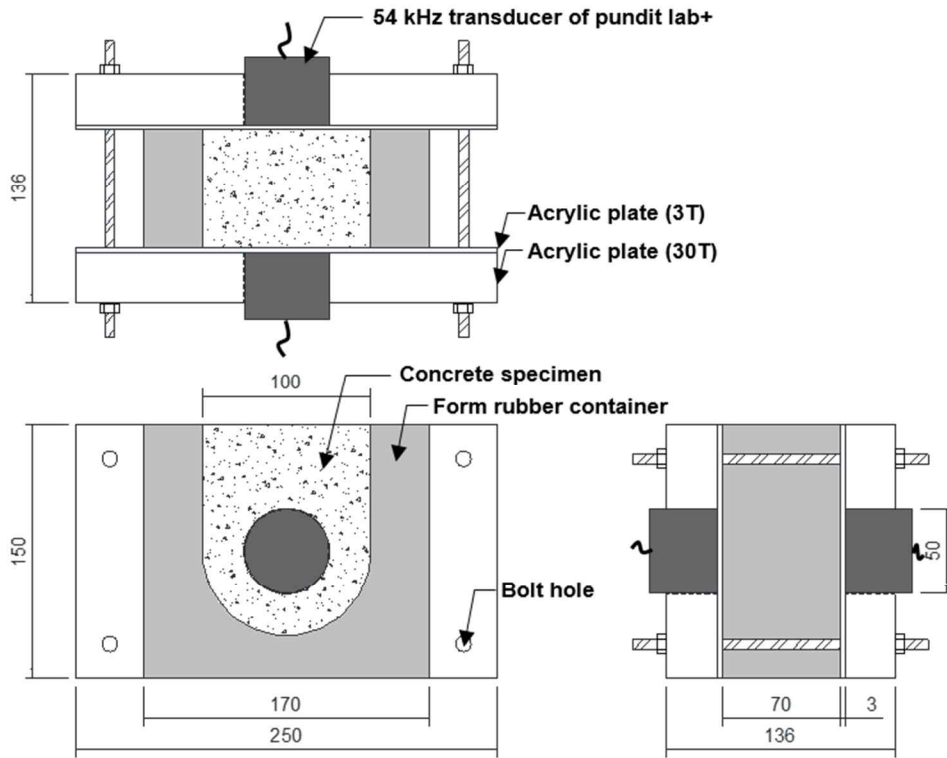


Fig. 5-2 Modified FreshCon system by this study (a), preparation of device for “time zero” (b), and measured UPV of sample over time (c)

In this study, SS, which is defined as the shrinkage under sealed conditions, including thermal deformation, was considered the predominant type of shrinkage with regard to the heat-treated UHPC. Under sealed conditions without loading, two types of shrinkage occur during the early-age volume change of concrete; namely AS, which is caused by the hydration reaction, and thermal shrinkage, caused by the change of the IT (Mounanga *et al.*, 2006). To determine the AS, the latter should be excluded from the measured SS. The driving force of the thermal shrinkage is owed to a change in the IT by the hydration heat or curing temperature; all these factors especially influence heat-treated UHPC prior to 7 d. This shrinkage is also dependent on the coefficient of thermal expansion (CTE) of concrete (Mehta & Monteiro, 2006). However, when determining AS, it is unreasonable to use a constant CTE to calculate the thermal deformation because this coefficient does not have a fixed value with regard to early-age concrete (Yang, Sato & Kawai, 2005). Between certain initial and final setting points, the CTE is dramatically decreased because solidification commences (Maruyama & Teramoto, 2013). Simultaneously, the AS strain of the concrete with a low w/c ratio (to be revised) also significantly increased over the same period. Moreover, the CTE also increases as a function of the curing temperature due to the accelerated self-desiccation (Maruyama & Teramoto, 2012). Similarly, the addition of SAP reduces the CTE because it increases the internal RH of concrete. Therefore, to investigate the shrinkage characteristics of heat-treated UHPC, it is better to analyze the SS rather than AS, which is estimated using a constant CTE (Wyrzykowski & Lura, 2013).

The DS was simply determined by excluding the SS from the TS.

Specifically, the difference between the two shrinkages is not identical to that of the shrinkage caused by drying (Zhang *et al.*, 2003); this is because the curing conditions used to measure these shrinkages are different. During the TS measurement, cement hydration can be disturbed due to moisture loss owed to the drying of specimen (Yang *et al.*, 2005). Specifically, the AS of the specimen can be underestimated because of the lack of a hydration reaction. However, heat-treated UHPC is cured under sealed or wet conditions throughout the HT, to prevent the loss of moisture or hydration. In addition, because almost all hydration reactions occur during the HT, underestimation is unlikely. Thus, accurate DS measurements can be obtained using the simple method.

### 5.1.3 Results and discussion

#### 5.1.3.1 Hydration reaction of heat-treated UHPC

Fig. 5-3 and Fig. 5-4 show the hydration heat curves of the UHPCs that were subjected to moderate (60 °C) and standard (90 °C) HTs, respectively. During the acceleration period (8–24 h), the hydration heats gradually increased, and the first hydration peak was formed at 24 h. Following the formation of the peak, the heat decreased during the post-acceleration period (> 24 h). The intensity of the hydration peak of the cement paste (w/c=0.2–0.3) increased as the w/c ratio increased (Justs *et al.*, 2015; Justs *et al.*, 2014). In particular, the intensity of hydration peak of the internally cured cement paste with SAP was determined to be between those of two reference cement pastes (with or without extra water), depending on the absorption and desorption capacity of the SAP (Justs *et al.*, 2015; Justs *et al.*, 2014). Similarly, the intensity of the hydration peak of AA\_0.255 was determined to be between those of Ref\_0.215 and Ref\_0.255 (Fig. 5-3). The intensity of the hydration peak of AM\_0.275 is remarkably close to that of Ref\_0.215. This result also confirms that SAP\_AM possesses outstanding absorption and retention capacities in UHPC, and can retain almost all extra water up to a certain point. SAP\_AA also absorbed and retained a portion of extra water up to a certain point. Thanks to these water-entrainment properties, the two internally cured samples showed greater hydration reactions during the post-acceleration period compared with those of the other reference samples.

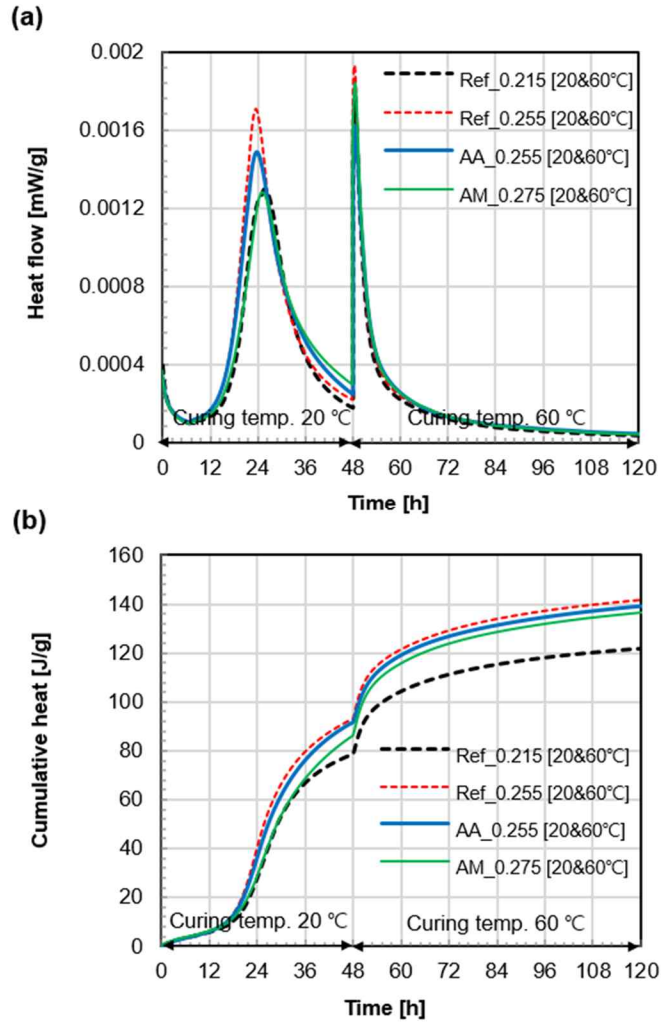


Fig. 5-3 Heat flow of hydration (a) and cumulative heat (b) of UHPC cured under 20 °C for 2 days then successively under 60 °C for 3 days

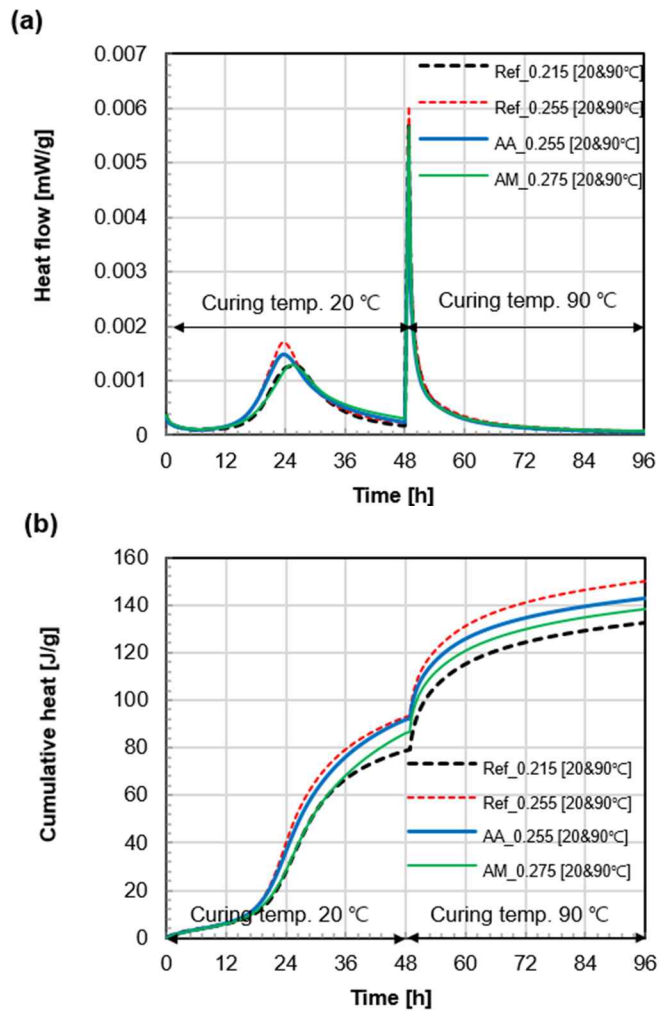


Fig. 5-4 Heat flow of hydration (a) and cumulative heat (b) of UHPC cured under 20 °C for 2 days then successively under 90 °C for 2 days

Cementitious material that is cured under room temperature exhibits one main hydration peak during its lifespan (Justs *et al.*, 2015; Kang *et al.*, 2015; Justs *et al.*, 2014; Wyrzykowski & Lura, 2013). However, this study revealed that heat-treated UHPCs have two main hydration peaks. Immediately after the HT (48 h) commenced, the hydration heat increased at a greater rate than that measured previously, causing a second peak to form within a period of 1 h (< 49 h). If the heating rate to the target temperature was controlled (e.g., 15 °C/h, identical to the conditions in the chamber), a second peak would form at a later stage. However, this strong second peak certainly indicates that the water consumption during the reaction was promoted by the HT (National Precast Concrete Association (NPCA), 2013). In particular, during the post-acceleration period (from 1 d to 7 d), it can be inferred that the accelerated pozzolanic reaction significantly contributes to the total hydration reaction along with the cement hydration (Korpa *et al.*, 2009). Previously, it has been experimentally confirmed that an intensified pozzolanic reaction is the primary reason for the improved performance of heat-treated UHPC (Selleng *et al.*, 2016; Heinz *et al.*, 2012). The hydration products, such as C-S-H, which are formed because of this reaction, result in a denser microstructure and finer pore structure (Snoeck *et al.*, 2015a; Heinz *et al.*, 2012). The pozzolanic reaction is a subsequent hydration reaction between the amorphous SiO<sub>2</sub> in the silica fume and the portlandite, which can be formed due to the cement hydration (Kasselouri, Kouloumbi & Thomopoulos, 2001; Richard & Cheyrezy, 1995). In the case of UHPC, the consumption of portlandite by the pozzolanic reaction is significant after 24 h (Korpa *et al.*, 2009), which lies within the post-acceleration period of our study. Thus, to effectively accelerate this second reaction, it is reasonable to commence HT on the second day (24-48 h),

following the formation of the first hydration product.

As mentioned in Section 1, reactive powder concrete, which is a well-known type of UHPC, is generally subjected to standard HT. Silica powder, which is also known as crushed quartz with regard to this concrete, was originally categorized as a reactive powder because it can potentially contribute to the pozzolanic reaction (Richard & Cheyrezy, 1995). However, following a study by Richard and Cheyrezy (Richard & Cheyrezy, 1995), it has been experimentally verified that this powder is a non-reactive material under conditions of  $< 150\text{ }^{\circ}\text{C}$  (Schachinger *et al.*, 2008; Reda, Shrive & Gillott, 1999; Zanni *et al.*, 1996). This suggests that the powder only functioned as a physical filler in our study. Therefore, the silica powder did not significantly influence the pozzolanic reaction to form the second peak. Fig. 5-5 compares the histories of the hydration heat during HT as a function of the curing temperature. Under the standard HT conditions ( $90\text{ }^{\circ}\text{C}$ ), the peak intensity was three times that measured under the moderate HT conditions ( $60\text{ }^{\circ}\text{C}$ ); this was because the increased temperature accelerated the pozzolanic reaction. However, the differences between the hydration heats measured under the two conditions ( $60\text{ }^{\circ}\text{C}$  vs.  $90\text{ }^{\circ}\text{C}$ ) are only significant during the initial 12 h. This subsequently indicates that the influence of the increase in temperature ( $+30\text{ }^{\circ}\text{C}$ ) on the reaction rapidly diminished with time. Specifically, the high temperature may not be beneficial after 60 h (48h + 12h). Based on the results of the accurately conducted hydration-heat tests, it can be inferred that the use of a standard HT over 48 h is less effective and economical compared with the HT used in this study (i.e., moderate HT for 72 h).

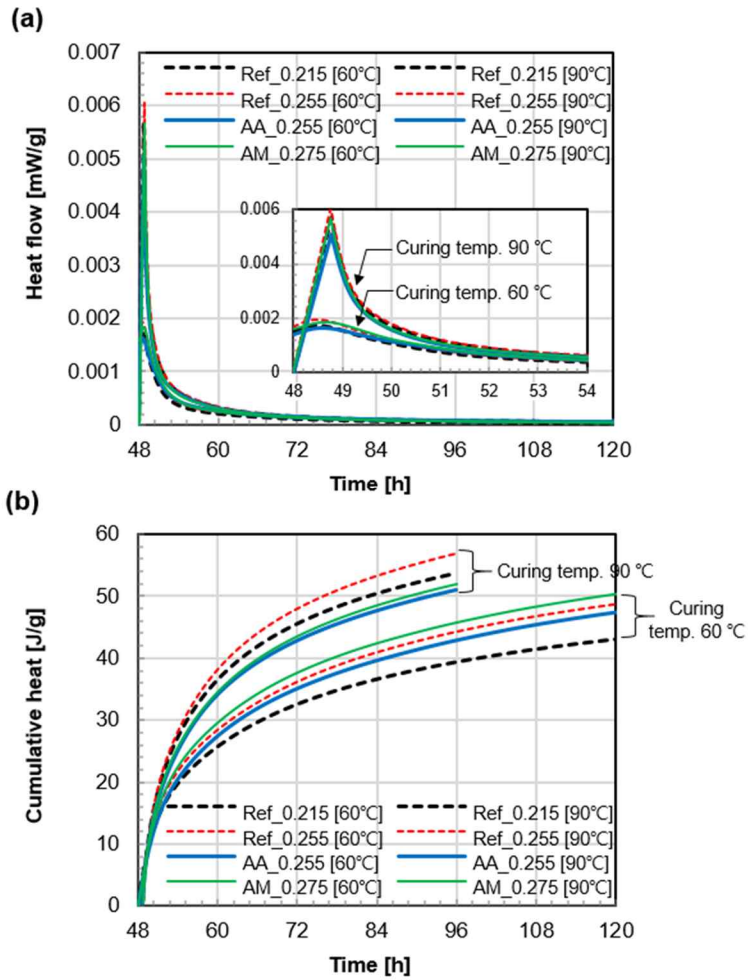


Fig. 5-5 Heat flow of hydration (a) and cumulative heat (b) of UHPC during heat treatment period

### **5.1.3.2 Shrinkage test method for heat treated UHPC**

Following the mixing of concrete, a volume change related to cement hydration occurs immediately (Loukili *et al.*, 2000). This phenomenon allows the measurement of early-age AS, which takes place before the concrete finally sets (Vande Voort *et al.*, 2008). Embedded-type strain gauges have been successfully used to measure the early-age shrinkage of concrete with low w/c ratios (Yoo *et al.*, 2015; Yoo, Min, Lee & Yoon, 2014; Yang *et al.*, 2005; Zhang *et al.*, 2003). For example, a vibrating, embedded-type gauge was used to measure the AS of heat-treated UHPC (Graybeal, 2006). If metals, electrical components, or polymers are incorporated in a shrinkage-measurement device, the high temperature or steam due to the HT can deteriorate the durability of the device and reduce the reliability of the test method. However, an embedded-type gauge that is sensitive and flexible (compared to concrete), which has a similar CTE to that of concrete, can behave simultaneously with the surrounding materials (e.g., concrete or mortar). The other electric devices used, such as data loggers and laptop computers, which are connected to the gauge by lead-wires, cannot be influenced by the curing conditions. The major factor that influences the accuracy of this method is the degree of compaction between the concrete and gauge. However, UHPC generally exhibits self-compacting properties because of polycarboxylate-type superplasticizers. Thus, the inside of the mold can be completely filled with fresh UHPC, which was confirmed by cutting the specimens after the shrinkage test (see Fig. 5-6).



Fig. 5-6 Section of specimen used for shrinkage test of UHPC

Meanwhile, it is crucial to determine ‘time zero’ to obtain the absolute shrinkage value of low w/c concrete, such as UHPC (Mechtcherine & Reinhardt, 2012), in which AS is a primary cause of shrinkage with regard to the TS. A low w/c concrete or mortar exhibits rigidity immediately after it initially sets (Darquennes, Staquet, Espion, Robeyst & De Belie, 2008); thus, AS commences at this time because the chemical shrinkage does not coincide with the external volume change (Zhang *et al.*, 2003). Therefore, a large proportion of the shrinkage value can be underestimated unless ‘time zero’ is determined accurately (Darquennes *et al.*, 2008). It is also difficult to accurately determine the initial setting time (Zhang *et al.*, 2003). The penetration resistance method is commonly used to determine the initial setting time (American Society for Testing and Materials (ASTM), 2008). However, the initial setting time determined by this method does not coincide with the initial point of self-desiccation, which is the driving force of AS; also, this method is not a scientifically accurate method for the determination of the ‘time zero’ (Chang-Wen, Qian, Wei & Jia-Ping, 2007). Moreover, once UHPC is exposed to air, its

surface becomes rigid over a short period of time as a result of drying (Fehling *et al.*, 2014); it is questionable whether the aforementioned method can represent the state of the entire volume of UHPC.

Based on physical phenomenon, setting represents the solidification of a plastic cement paste; thus, the initial setting indicates the commencement of solidification. Therefore, 'time zero' can be regarded as the time when a cementitious material initially becomes unworkable (Chang-Wen *et al.*, 2007). The UPV is very sensitive to changes in microstructure (Craeye, De Schutter, Desmet, Vantomme, Heirman, Vandewalle, Cizer, Aggoun & Kadri, 2010; Van Den Abeele, Desadeleer, De Schutter & Wevers, 2009), therefore, it is directly related to a dynamic Young's modulus (Heinz *et al.*, 2012). In summary, the UPV and the modulus of concrete suddenly rise when solidification commences. As a result, UPV has been used to successfully determine 'time zero' (Zhang, Zhang, She, Ma & Zhu, 2012; Craeye *et al.*, 2010; Darquennes *et al.*, 2008); the method that uses the FreshCon system (Reinhardt *et al.*, 2000) is known to be particularly reliable (Carette & Staquet, 2015; Lee, Lee, Kim, Yim & Bae, 2004). This method predicts the changes in microstructure more accurately than the penetration resistance method (Lee *et al.*, 2004). Thus, we adopted the method that employs the FreshCon system for the complicated shrinkage measurement under HT.

### **5.1.3.3 Sealed shrinkage**

#### **1) Ordinary UHPC (O-UHPC)**

Fig. 5-7 shows the SS, TS, and IT of the specimens. The reproducibility of the test method can be confirmed from the two results, SS\_1<sup>st</sup> and SS\_2<sup>nd</sup>. Test results are also presented in Fig. 5-8, specifically, to compare the shrinkage behavior that occurred during the early-age and HT periods. The O-UHPCs, namely Ref\_0.215 and Ref\_0.255, exhibited extremely rapid shrinkages during the 7 d of the sealed period. The first shrinkage, AS, commenced from the initial setting and it attained a value of approximately 400  $\mu\text{m}/\text{m}$  at 1 d. The AS mechanism is described in the following paragraphs. Chemical shrinkage by cement hydration results in a reduction of the concrete volume (Craeye *et al.*, 2010; Bentz & Jensen, 2004). Following the initial setting, the formation of a solid skeleton results in a restrained condition, therefore, the reduction in volume does not subsequently correspond with the change in the external volume. In addition, pores are formed within the concrete because of the internal volume reduction (Chang-Wen *et al.*, 2007; Lura *et al.*, 2003). The continuous hydration reaction reduces the internal RH of the pores, which causes self-desiccation (Bentz & Jensen, 2004). This RH loss is related to the development of capillary tension; therefore, the volume of the matrix finally decreases (Vande Voort *et al.*, 2008; Termkhajornkit, Nawa, Nakai & Saito, 2005; Lura *et al.*, 2003).

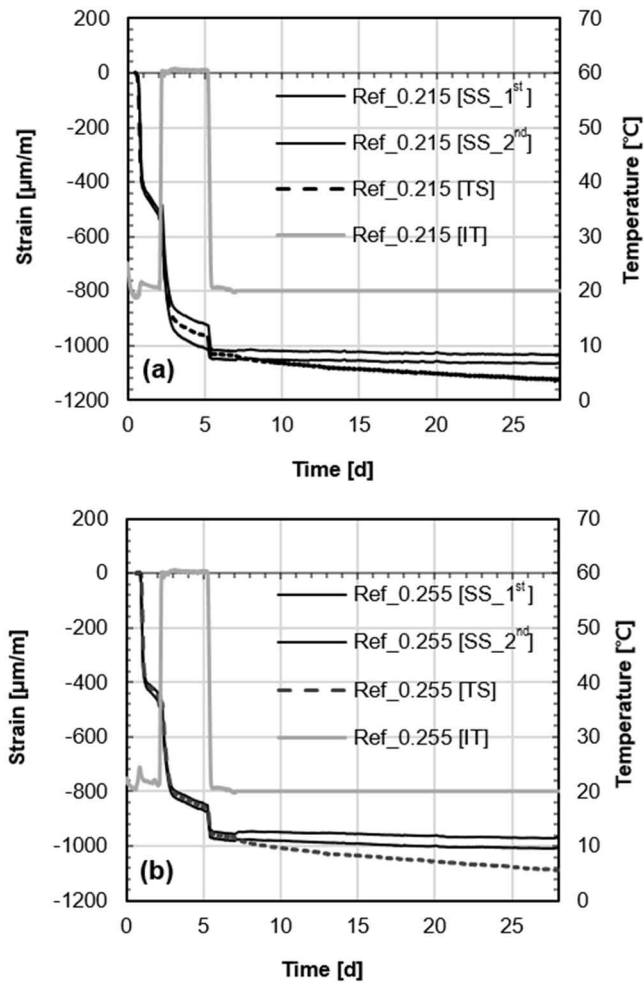


Fig. 5-7 Shrinkage behaviors of heat treated UHPC: Ref\_0.215 (a), Ref\_0.255 (b). TS before 7 d was determined by the average of SS\_1<sup>st</sup> and SS\_2<sup>nd</sup>.

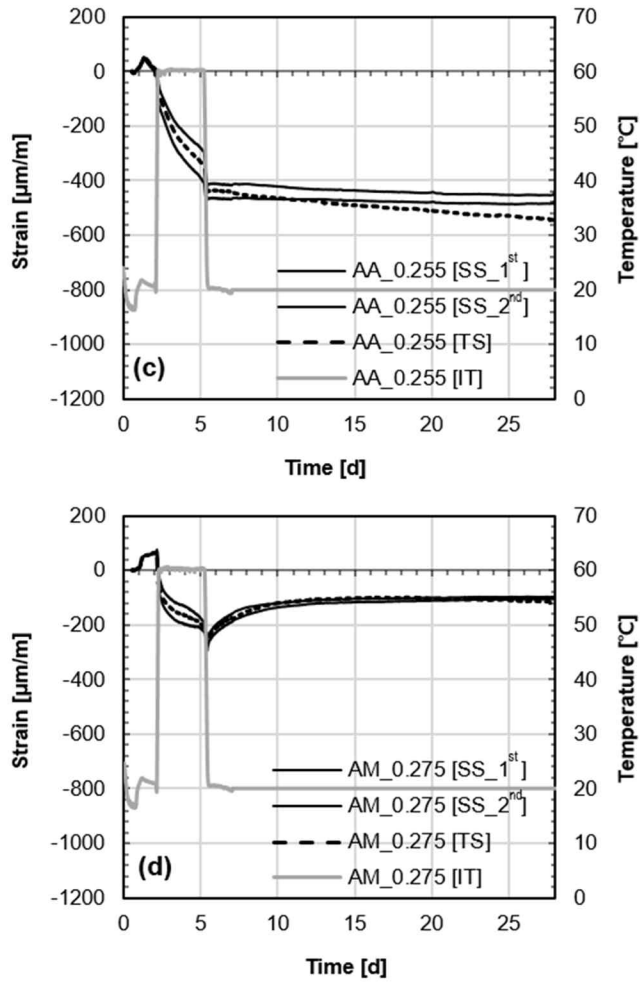


Fig. 5-7 (cont.) Shrinkage behaviors of heat treated UHPC: AA\_0.255 (c) and AM\_0.275 (d). TS before 7 d was determined by the average of SS\_1<sup>st</sup> and SS\_2<sup>nd</sup>.

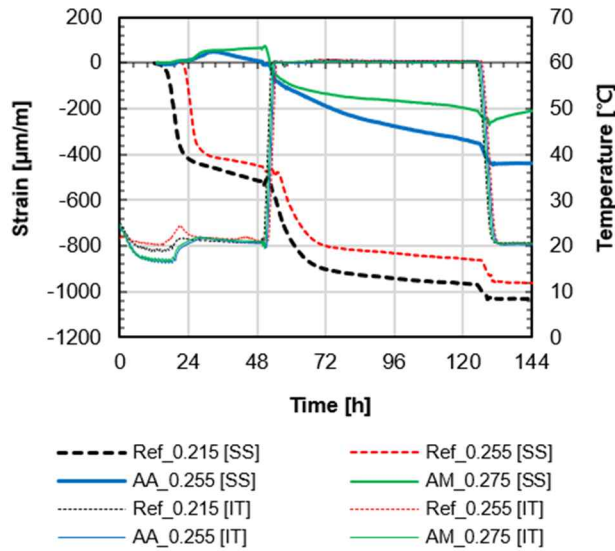


Fig. 5-8 Shrinkage behaviors of heat treated UHPC during the first 6 days

The rapid and severe AS of UHPC at an early age is directly related to the internal RH history because the AS is caused by self-desiccation. The AS encounters a turning point, also known as a knee point, when the RH is closed to 73–75% (Loukili *et al.*, 1999). Subsequently, the rate of AS suddenly decelerates and stabilizes (Vande Voort *et al.*, 2008). To explain the stabilization, two mechanisms have been considered. The first is that self-desiccation cannot proceed significantly once the internal RH drops below 75% (Jensen & Hansen, 2001a). The second is that a semi-rigid skeleton is formed by hydration products, such as C-S-H gel, which form a stress-resistant microstructure that can sustain AS (Mounanga *et al.*, 2006). This stabilization does not indicate the completion of the hydration and self-desiccation processes. Following the knee point, the internal RH gradually decreases because of the water consumption by the pozzolanic reaction (Loukili *et al.*, 1999).

In this state (following the knee point), the accelerated pozzolanic reaction due to the HT (or temperature increase) promotes self-desiccation via the consumption of water (Maruyama & Teramoto, 2013), and results in the formation of denser pore structures (Snoeck *et al.*, 2015a; Garas *et al.*, 2012). These fine pore structures lead to the generation of large capillary forces during self-desiccation, which causes severe AS (De La Varga *et al.*, 2012; Craeye *et al.*, 2010; Meddah & Tagnit-Hamou, 2009; Lura *et al.*, 2001). In addition, the HT can result in C-S-H shrinkage (Maruyama & Teramoto, 2013; Lura *et al.*, 2003). Both the increase in temperature and the accelerated reaction induce conditions of high temperature and low RH within the concrete. Under these conditions, the C-S-H tends to be dense and therefore there is a reduction in its volume (Maruyama & Teramoto, 2013). Furthermore, the increase in temperature can influence the self-desiccation and AS because the RH depends on the temperature (Wyrzykowski & Lura, 2013; Sant, 2012; Bentz & Jensen, 2004). Owing to these reasons, shrinkage, rather than expansion, was the dominant deformation mechanism despite the temperature rise during the HT (Fig. 5-7 and Fig. 5-8). During the temperature rise, expansion occurred about for 1 h (at 35 °C); subsequently, severe shrinkage occurred once more over 24 h. Remarkably, the shrinkage that occurred during the early stages of the HT (< 12 h) was especially rapid (Fig. 5-8); in addition, there was significant hydration heat generated during the first 12 h (Fig. 5-5). This indicates that the shrinkage due to the HT is related to the loss of internal RH, or changes in the microstructure or pore structure due to the accelerated pozzolanic reaction.

The second knee point was formed between 60 h and 72 h (or 12–24 h following the start of the HT); subsequently, the shrinkage speed decelerated

again. In a study by Graybeal, a knee point was also formed in the case of UHPC prepared under standard HT conditions (Graybeal, 2006). However, unlike our study this knee point was the first that was observed; another knee point had not formed before the HT commenced. One possible reason for this difference is that the HT commenced at an earlier instance (29 h) compared with that of our study (48 h). An earlier starting time can be used to avoid the formation of a knee point before treatment. The results of the two shrinkage tests verify that the knee point is formed under curing temperatures of 60–90 °C. The mechanism of the formation as well as the reason for the shrinkage stabilization were previously discussed in the second paragraph of this section.

The final occurrence of rapid shrinkage occurred due to thermal deformation, which also resulted in the formation of the third knee point. Owing to the temperature drop at the end of the HT, Ref\_0.215 and Ref\_0.255 shrunk by as much as 62  $\mu\text{m}/\text{m}$  and 73  $\mu\text{m}/\text{m}$ , respectively, over 160 min. Deformation due to thermal effects is reversible in hardened concrete (Zhang *et al.*, 2003). However, the thermal deformation of the UHPC due to the HT was not perfectly reversible because there were differences in the CTE values measured when the temperature increased and decreased. When the temperature both increased and decreased, the dominant deformation was owed to shrinkage, rather than expansion, which provides evidence of irreversible thermal deformation. Thus, thermal deformation due to the HT is another factor that accelerates the shrinkage of the heat-treated UHPC. The SS or AS of the UHPC converged to a constant value once the HT was complete (Fig. 5-7). Almost all the shrinkage of the UHPC occurs by the end of the HT (Graybeal, 2006) because the consumption of water and microstructural refinement due to the hydration

reaction continue until the HT is complete (Garas, Kahn & Kurtis, 2009). The lacks of water and available space to form new hydration products is related to the completion of the hydration reaction (Justs *et al.*, 2014; Powers & Brownyard, 1948); this could also explain the convergence of the shrinkage results.

Based on the test results, it can be concluded that HTs cannot be used to reduce the risk of shrinkage or cracking in UHPC because considerable shrinkage, similar to that of AS, occurs rapidly during the HT period. Thus, although no cracks could be observed on the UHPC surfaces at the time of demolding, the risk of cracking does not cease to exist with the application of post-process, HTs.

## **2) Internally cured UHPC (I-UHPC)**

Owing to the intended IC effect, AA\_0.255 and AM\_0.275 did not shrink before the HT commenced (Fig. 5-7). The dimensions of the two I-UHPCs were slightly increased owing to the expansion behavior (i.e., compensating AS) that occurred after ‘time zero’. Furthermore, it was observed that the mitigation of shrinkage by the IC was also effective during the HT period. In the case of the O-UHPC, severe shrinkage occurred during this period and a knee point was observed, whereas the I-UHPC exhibited alleviated shrinkage without the formation of the knee point. Although the shrinkage of the I-UHPC was also accelerated due to the HT, it was slow and gradual compared with that of the O-UHPC. At the start of the HT, the SAP in the UHPC still contained the available IC water despite the release of water during the early aging period (<

48 h). Just et al. reported that during the first 3 d, water release from SAP is effective with regard to low w/c concrete (w/c=0.2–0.3) (Justs *et al.*, 2015; Justs *et al.*, 2014). Thus, the remaining absorbed water can be effectively used to mitigate the self-desiccation due to the HT.

In the section 3.2, the driving force of SAP desorption in the concrete was discussed without the consideration of temperature effect; based on the equation of osmotic pressure (Eq. (3-1)), sudden increase in TIC of concrete pore solution can change the direction of osmotic pressure. In the same manner, sudden increase in an absolute temperature of a concrete can also contribute to the change of the direction. In other words, the temperature increase due to the start of HT at 2 d can accelerate desorption of SAP in which a part of extra water still remains. In reality, the difference of the pressure between inside of SAPs and surrounding solutions determines the direction and magnitude of ab-  
sor-desorption. The difference of the pressure by a temperature change also depends on the thermal conductions of a concrete and SAP. Therefore, it is inferred that rapid increases in internal temperature (40 K/160 min) of the internally cured UHPCs (as confirmed in Fig. 5-8) accelerated desorption of the remained water in SAP immediately after the HT commenced. On the other hand, without HT the internal temperature was increased only at an early age (< 24 h) due to hydration reaction. As can be seen in Table 4-1, the temperature rises of the samples (1.6-4.4 K) during this period were negligibly small compared with the rises due to HT; thus, the rises before HT have no noticeable impact on the osmotic pressure.

Meanwhile, during the HT it was determined that the shrinkage strains of

AA\_0.255 and AM\_0.275 were 347  $\mu\text{m}/\text{m}$  and 281  $\mu\text{m}/\text{m}$ , respectively (Fig. 5-9). These strains are 23% (or 103  $\mu\text{m}/\text{m}$ ) and 38% (or 169  $\mu\text{m}/\text{m}$ ) lower than that measured, 451  $\mu\text{m}/\text{m}$ , for Ref\_0.215. However, for the first time, it was experimentally determined that the effectiveness of the IC decreased during the HT period compared to that of the early-age period ( $< 48$  h). A possible reason for this is that the self-desiccation was not completely prevented because of the reduced quantity of IC water. Based on the measured shrinkage strains, the IC effect that occurred in the case of AM\_0.275 was superior to that of AA\_0.255 during both the early-age and HT periods. The absorption and water retention capacities of SAP\_AM were greater than those of SAP\_AA; thus, a greater amount of water was originally incorporated in SAP\_AM. The experiment in Section 3 also confirmed that the absorption capacity of SAP\_AM is greater than that of SAP\_AA in the case of low w/c concrete such as UHPC (Kang *et al.*, 2016a). Consequently, a greater quantity of moisture could be used to prevent self-desiccation in the case of AM\_0.275.

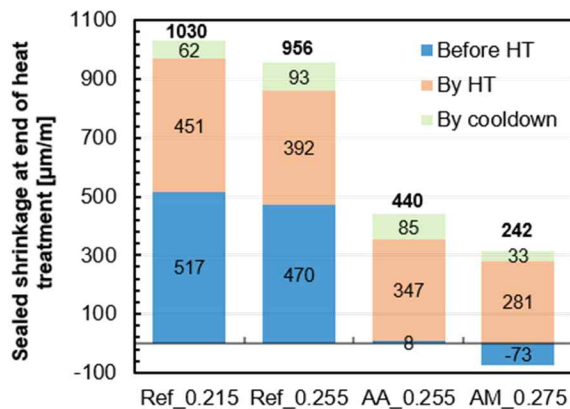


Fig. 5-9 Sealed shrinkage at the end of heat treatment (negative value indicates expansion)

Meanwhile, unlike the other specimens, specimen AM\_0.275 expanded by as much as 136  $\mu\text{m/m}$  for 7 d following the HT, and subsequently, the deformation converged. This led to a negligible shrinkage strain (approximately 100  $\mu\text{m/m}$ ). This expansion only occurred when a SAP was added to the UHPC; however, this depends on the type of SAP. Furthermore, by comparing the SS and TS of AM\_0.275, we could determine that the expansion is not a function of external RH (i.e., it is irrelevant to the drying of the UHPC). This phenomenon, the expansion of internally cured concrete following HT, has not been reported previously. In a study by Maruyama and Teramoto, a low water-to-binder ratio (0.15) cement paste, which contained silica fume, expanded for about 40 d (7–47 d) following a reduction in temperature (from 50–60 °C to 20 °C) (Maruyama & Teramoto, 2013). This expansion has not been observed when maximum temperatures of 20–40 °C are used. Although this phenomenon was not elucidated, the authors suggested that it was possible that DEF or the transformation of C-S-H via a temperature change occurred (Maruyama & Teramoto, 2013). Expansive reactions often occur in cementitious materials because of the growth of ettringite (Bentz & Jensen, 2004). In the case of precast concrete, it is necessary to monitor the growth during long-term aging following HT (Japan Society of Civil Engineers (JSCE), 2004). A structural UHPC element is potentially at risk from DEF because it is commonly exposed to temperatures of > 65 °C for many hours (Association Française De Génie Civil (AFGC), 2013). However, the risk of DEF occurring in UHPC is considered to be very low due to the lack of free water available following the HT (Association Française De Génie Civil (AFGC), 2013; Heinz & Ludwig, 2004; Japan Society of Civil Engineers (JSCE), 2004). However, this can

change when UHPC contains a hydrogel, such as SAP\_AM, which has outstanding absorption and retention capacities (Kang *et al.*, 2016a). Thus, additional studies are required to clearly determine the possibility of DEF occurring in I-UHPC by considering the presence of residual water following a standard HT (90 °C).

However, in this study, DEF can obviously be excluded as the reason for this expansion. This is because sample AM\_0.275 has not been subjected to temperatures over 65°C like normal precast concrete. Unlike SAP\_AA in AA\_0.255, SAP\_AM formed large and globular pores in AM\_0.275, depending on its shape and absorption capacity. The micro-CT analysis in Section 4 confirmed that the total porosity of AM\_0.275 (6.0%) is 4.5% higher than that of Ref\_0.215 (2.5%), because of the large pores induced by SAP\_AM (Kang *et al.*, 2016e). The number of SAP-pores was only 0.8% that of original pores in Ref\_0.215. Specifically, only a relatively small quantity of SAP-pores were responsible for the 4.5% increase in total porosity. Despite this increase, the 28 d compressive strength of AM\_0.275 (147.3 MPa) was 3.5% higher than that of Ref\_0.215 (142.3 MPa) (Kang *et al.*, 2016b; Kang *et al.*, 2016e; Kang *et al.*, 2015). According to a study by Beushausen and Gillmer, the pores induced by SAP (acrylic acid/acrylamide copolymers with a spherical shape similar to that of SAP\_AM in our study) tend to reduce the elastic modulus and improve the tensile relaxation of silica fume-containing cement mortars, which reduces the risk of cracking due to DS despite no noticeable difference in DS strain (Beushausen & Gillmer, 2014). The authors suggested that the reason for this reduction was owed to the enhanced deformability of the mortars due to the additional large pores.

In our current study, we first determined that the UHPC expanded following HT, especially with the use of an AM-type of SAP (not AA-type of SAP, nor O-UHPC). Considering the moderate temperature used in this HT, with respect to the expansion, we suggest that a physical effect (such as the improved deformability) occurs, rather than a chemical effect (such as DEF). Researchers that previously studied internally cured low w/b cementitious materials containing inverse-suspension- or suspension-polymerized spherical acrylic acid/acrylamide copolymers, did not observe this type of expansion (Kang *et al.*, 2015; Schröfl *et al.*, 2012; Jensen & Hansen, 2002). This is because these materials without SAP generally undergo rapid and severe AS at early age (before final setting) when a HT is not applied. However, materials that possess large SAP pores could not experience this shrinkage because of the IC effect by the polymer. In the current study, AM\_0.275 initially experienced shrinkage due to self-induced stress during the HT period. The accelerated stress due to the HT would certainly disappear following the HT. Subsequently, a proportion of this shrinkage could be offset because of the improved deformability of the material due to the porous internal structure.

### ***3) Strain rate***

The strain rates of the heat-treated UHPCs are presented in Fig. 5-10; these show the change in the shrinkage or expansion rates over time. The rate is defined as the change in strain per hour. Two of the O-UHPCs (Ref\_0.215 and Ref\_0.255) exhibited three shrinkage peaks and one expansion peak as the

temperature increased. Unlike the third shrinkage peak, which was caused by a reduction in temperature, the shapes of the other shrinkage peaks are similar to those of the two hydration-heat peaks (Fig. 5-3 (a)). This confirms again that the shrinkage is closely related to the hydration reaction. Considering the heat-flow curve (Fig. 5-3 (a)), the intensity of the second peak is greater than that of the first peak. However, considering the strain-rate curves (Fig. 5-10), the intensity of the first peak is greater than that of the second peak. Following the initial setting, the ability of the matrix to resist shrinkage improves because of the formation of the solid skeleton; this could explain the aforementioned differences. Consequently, the maximum shrinkage-strain rate occurred at early age ( $< 48$  h). This rate was more than twice the maximum rate that occurred during HT ( $> 48$  h).

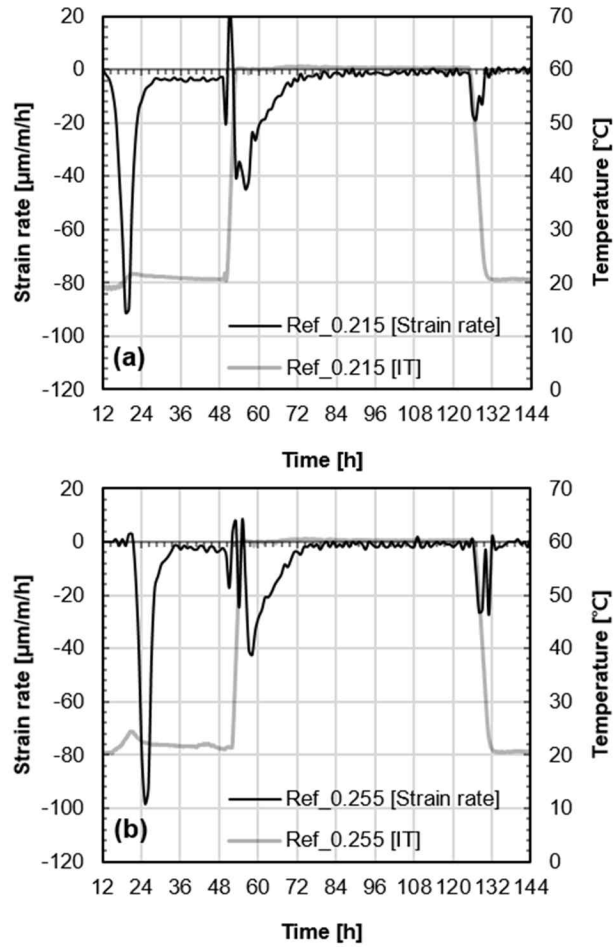


Fig. 5-10 Strain rates of heat treated UHPC during the first 6 days: Ref\_0.215 (a), Ref\_0.255 (b)

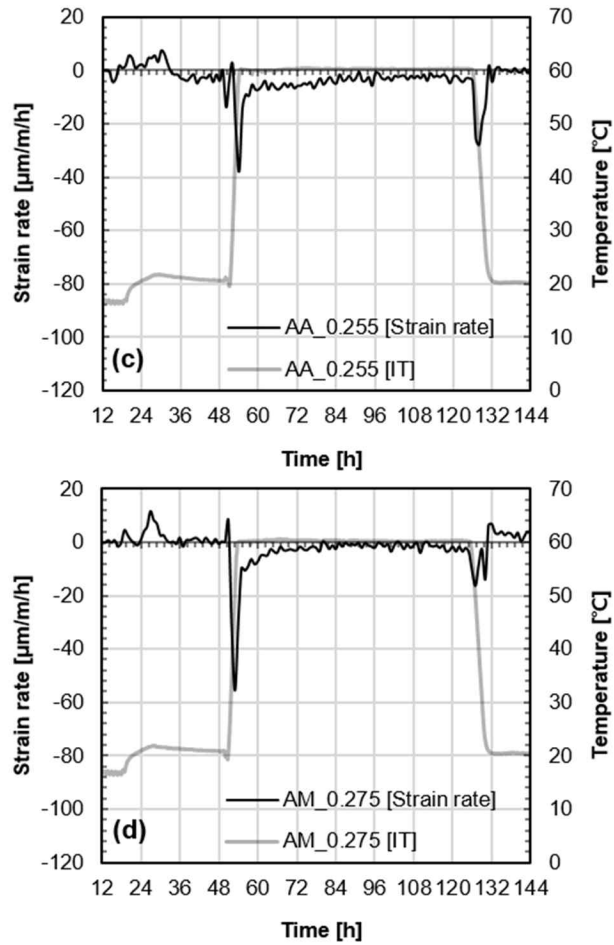


Fig. 5-10 (cont.) Strain rates of heat treated ultra-high performance concrete during the first 6 days: AA\_0.255 (c), and AM\_0.275 (d)

The first strain rate peak of Ref\_0.255 (99  $\mu\text{m}/\text{m}/\text{h}$ ) was slightly higher than that of Ref\_0.215 (91  $\mu\text{m}/\text{m}/\text{h}$ ). As shown in Fig. 5-3 (a), the intensity of the first hydration peak also increases as a function of the w/c ratio (Ref\_0.215 vs. Ref\_0.255). However, as shown in Fig. 5-9, the SS strain of Ref\_0.215 is higher than that of Ref\_0.255, because of the wider width of the strain-rate peak. Furthermore, the intensity of the second peak of Ref\_0.215 (45  $\mu\text{m}/\text{m}/\text{h}$ ) is slightly greater than that of Ref\_0.255 (42  $\mu\text{m}/\text{m}/\text{h}$ ). This indicates that the densification of the pore structure, due to the reduction of the w/c ratio, can lead to rapid shrinkage. In the case of I-UHPC, the maximum shrinkage-strain rate occurred during the HT period. Prior to the HT, the shrinkage peaks had not formed; only several expansion peaks had formed due to the IC effect. Immediately after HT commenced, shrinkage peaks were also observed in the case of the I-UHPCs. The peak intensities measured for samples AA\_0.255 and AM\_0.275 were 38  $\mu\text{m}/\text{m}/\text{h}$  and 55  $\mu\text{m}/\text{m}/\text{h}$ , respectively. Although the IC by SAP could not reduce these intensities, it was certainly effective with regard to reducing the width of the peak, which contributed to a reduction in the shrinkage strain due to the HT. Following the HT, sample AM\_0.275 exhibited an expansive peak once more, as discussed in a previous section, but the peak intensity tended to decrease with time.

#### **5.1.3.4 Drying and total shrinkages**

When the specimens were exposed to air-drying conditions (20°C, RH 60%), the DS strain increased with time (Fig. 5-7). While moisture in a concrete evaporates into unsaturated air (Neville, 1981), tensile stress is generated via

evaporation within the capillary pores (Vande Voort *et al.*, 2008). This causes the volume reduction of the concrete. In the case of UHPC, DS can be largely prevented because of its dense microstructure (Vande Voort *et al.*, 2008). Thus, the DS to TS ratios were only 7% and 9% in the case of Ref\_0.215 and Ref\_0.255, respectively (Fig. 5-11). Specifically, almost all (> 90%) of the shrinkage that occurs in heat-treated UHPC occurs under sealed conditions. The 2% difference in the ratio between the two specimens can be explained by the fact that there was a reduction and increase in the SS and DS strains, respectively, as the w/c ratio was increased by 4%.

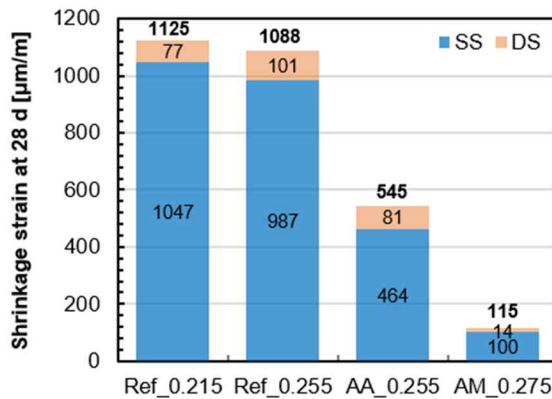


Fig. 5-11 Sealed and drying shrinkages of UHPC at 28 days (bold numbers on the chart mean total shrinkages)

In the case of the I-UHPCs, the DS to TS ratios are greater than those of the O-UHPC (Fig. 5-11). This indicates that the DS strain does not increase due to the SAP addition, but the SS strain decreases due to the IC effect. The strain due to DS did not increase when the SAP was incorporated into the UHPC. Based on the experimental results, it can be concluded that the IC due to the

SAP had no (or negligible) effect on the DS of the heat-treated UHPC. In addition, the TS of the UHPC was reduced by 52% and 90% with the incorporation of SAP\_AA and SAP\_AM, respectively. Thus, IC is certainly an effective method to reduce the shrinkage of heat-treated UHPC; this method can obviously mitigate the primary shrinkage (SS) of UHPC.

#### **5.1.4 Summary and concluding remarks**

Typically, UHPC elements are subjected to HT to ensure the outstanding mechanical properties and durability at an early stage (< 7d). Herein, the shrinkage characteristics of heat-treated UHPC and the effect of IC on the UHPC were studied.

The heat-treated UHPC experienced rapid and severe shrinkage three times during the curing period. The first shrinkage, namely AS, occurred during the early age period (< 48 h) under a constant curing temperature (20 °C). This was caused by self-desiccation following the initial setting. The second shrinkage was owed to SS, which is AS under a temperature change condition. This shrinkage was caused by the accelerated pozzolanic reaction due to the temperature increase during HT. The second shrinkage was as severe as the first one. The final shrinkage occurred because of the thermal deformation that occurred when the temperature decreased as the HT was completed. As well as concrete, UHPC can potentially crack during the cooling process due to the temperature difference between its surface and interior. Thus, it is desirable to reduce the cooling rate.

Almost all ( $> 90\%$ ) of the TS of the UHPC was owed to SS, which occurred before the end of the HT. One advantage of heat-treated UHPC is that the influence of shrinkage after HT can be neglected. Specifically, this is limited to the shrinkage that occurs under sealed conditions, because the DS gradually increases under post-treatment drying conditions. However, this study verified that the degree of long-term DS ( $> 7$  d) is relatively small compared with the SS ( $< 7$  d).

It is known that low w/c concrete that contains silica fume has a high risk of cracking at an early age; however, this preconception can be changed with the use of internally cured UHPC, especially with the application of HT. The IC did not increase the degree of DS of UHPC, which was originally very low. In addition to this, the IC was able to mitigate the AS (or SS), the primary type of shrinkage of UHPC. Moreover, the IC was effective under both ambient and high-temperature curing conditions. The TS strains recorded for the UHPCs that contained SAP\_AA and SAP\_AM were  $545 \mu\text{m/m}$  and  $115 \mu\text{m/m}$  at 28 d, respectively. These TS strains are lower than half of that in an ordinary UHPC, and even lower than that of normal concrete, which commonly has a DS of  $> 1,000 \mu\text{m/m}$  for several years or decades. The UHPC that contained SAP\_AM exhibited extremely low shrinkage; the expansion that occurred before and after HT contributed to this. In particular, for a week after the treatment, an expansion of  $136 \mu\text{m/m}$  occurred in the UHPC, which has not been reported by previous researchers. Although more investigation is necessary, this study suggests that a physical effect occurs, such as the improvement of the deformability as a result of the additionally formed large pores; this could provide a possible reason for this new phenomenon.

## **5.2 Field-cast UHPC**

### **5.2.1 Introduction**

As mentioned in Section 1, UHPC features outstanding strength, flowability, ductility, and very low permeability (Tayeh, Bakar & Johari, 2013; Brühwiler & Denarié, 2008). However, the material cost is dozens of times higher than that of normal concrete. Thus, this material should be used only where these superior properties are needed (Brühwiler & Denarié, 2008; Habel, Denarié & Brühwiler, 2006). One of the most reasonable and effective ways is to use UHPC for composite structural members as a thin overlay layer (commonly 30–40 mm) in old concrete structures (Bastien-Masse & Brühwiler, 2016a; Noshiravani & Brühwiler, 2013a, 2013b; Tayeh *et al.*, 2013; Brühwiler & Denarié, 2008). If the surfaces of old concrete structure are overlaid with UHPC, the resistance capacities of the structure against extreme environments, such as mechanical (or structural) performance and durability, can be greatly improved (Brühwiler & Denarié, 2008). The compact internal structure and metallic fibers of the UHPC based overlay can improve watertightness and the crack-resistance capacity of the surfaces, respectively (Bastien-Masse & Brühwiler, 2016b; Brühwiler & Denarié, 2008). Besides, owing to the small-diameter rebars that are generally reinforced in the new layer, the tensile strength and ductility of the structural members can be further improved along with the added strain hardening behavior (Bastien-Masse & Brühwiler, 2016a, 2016b; Brühwiler & Denarié, 2013; Noshiravani & Brühwiler, 2013a, 2013b). Therefore, this is a promising method to improve the structural safety of old concrete structures conveniently, without any notable increase in the thickness

of old members (Brühwiler & Denarié, 2008). The most suitable structural members in which this method can be successfully applied are typically bridge decks and floor slabs (including flat slabs for punching shear resistance) (Bastien-Masse & Brühwiler, 2016b; Noshiravani & Brühwiler, 2013a). In addition, the jacketing technique using UHPC is also an effective method to improve the energy absorption capacity of a building structure (especially the beam, column, or beam-column joint) in a seismic area. (Lampropoulos, Paschalis, Tsioulou & Dritsos, 2016). From the economic perspective, this overlay method is economical as it takes into account the construction cost as well as the life cycle cost, including reduction of traffic congestion (Brühwiler & Denarié, 2008).

When an old concrete substrate is overlaid with a new repair concrete, not only the performance of the new material but also the compatibility between the two concretes are crucial factors that should be considered in advance (Bentz, Jones, Peltz & Stutzman, 2015). Under the restrained conditions due to the hardened concrete substrate or deformed bars in UHPC, early-age shrinkage of the repair material can lead to interface stress between the substrate and the new layer, and in turn to premature cracking; this debonding problem can even prevent performance improvement (Bentz *et al.*, 2015; Brühwiler & Denarié, 2008). The shrinkage-related problem is crucial, especially in UHPC, because severe AS occurs at an early age (Kang *et al.*, 2016d; Vande Voort *et al.*, 2008; Japan Society of Civil Engineers (JSCE), 2004). The debonding problem in the composite structure is an indication that the effectiveness of UHPC as an overlay material is over. Thus, the early-age shrinkage or debonding problem is the preferential factor that is surveyed and solved.

The driving force of AS is the self-desiccation that occurs in low-water-to-cement-ratio (w/c) cementitious materials such as UHPC. The desiccation and resulting AS are directly related to the decrease in internal relative humidity (RH) (Maruyama & Teramoto, 2013; De La Varga *et al.*, 2012; Kosmatka *et al.*, 2011; Jiang *et al.*, 2005; Lura *et al.*, 2001). However, it is very challenging to diffuse water into the UHPC layer by using the traditional external curing method because the layer has a very low permeability (Justs *et al.*, 2015). In the case of high-performance concrete for bridge deck structures, IC by porous lightweight aggregate has been effectively and economically used (Cusson *et al.*, 2010). However, the average diameter of the aggregate is larger than the maximum particle size of UHPC ( $< 1$  mm) (Kang *et al.*, 2016d; Kang *et al.*, 2015; Richard & Cheyrezy, 1995). When considering the compact composition of UHPC (Richard & Cheyrezy, 1995), IC by superabsorbent polymer (SAP) is the most promising way to solve the shrinkage and debonding problems of the UHPC overlay (Justs *et al.*, 2015; Snoeck *et al.*, 2015a; Jensen & Hansen, 2002, 2001b). A low-w/c (0.3) concrete showed the decrease in internal RH (up to 75%) due to the self-desiccation, whereas the concrete with SAP maintained more than 95% of internal RH, under the sealed curing condition (Lura, Durand, Loukili, Kovler & Jensen, 2006; Jensen & Hansen, 2002). Maintaining a high internal RH also coincides with the purpose of the traditional external or water-curing method, which is performed to ensure the design strength of normal concrete (Di Bella, Griffa, Ulrich & Lura, 2016; Kosmatka *et al.*, 2011; ACI Committee 308, 2001). Likewise, IC by SAP can increase the degree of hydration of low-w/c concrete, which also helps increase the strength (Justs *et al.*, 2015; Kang *et al.*, 2015; Soliman & Nehdi, 2011).

As mentioned earlier, early-age shrinkage of low-w/c concrete can be mitigated by maintaining a high internal RH using SAP under the sealed condition (Justs *et al.*, 2015; Snoeck *et al.*, 2015a; Jensen & Hansen, 2002, 2001b). However, this condition is not always beneficial for concrete structures. For instance, a high level of moisture contents is disadvantage in concrete slabs of building structures; these slabs are commonly covered with decorative finishing materials. Because adhesive finishing materials are moisture sensitive, a sufficient drying period is required to install the finishing materials within a construction schedule (Cement Concrete & Aggregates Australia (CCAA), 2007). If the finishing materials are installed in an insufficiently dried slab, the floor covering can become detached later (Cement Concrete & Aggregates Australia (CCAA), 2007). Furthermore, considering the field-cast condition and construction procedure of a repair or retrofitting project, the UHPC layer for overlay or jacketing cannot be sealed for a long period (Bastien-Masse & Brühwiler, 2016b; Tayeh *et al.*, 2013). In other words, unlike precast UHPC (Kang *et al.*, 2016d), this layer should be exposed to a dry condition; in this case, the internal moisture content inevitably decreases by evaporation on the wide and thin layer (Soliman & Nehdi, 2011; Henkensiefken, Nantung & Weiss, 2009). In addition, the variable moisture content also crucially affects the mechanical properties of hardened cement paste or concrete (Di Bella *et al.*, 2016; Wittmann, 1973). In general, the compressive strength of concrete decreases linearly as the moisture content increases (Di Bella *et al.*, 2016; Chen, Huang & Zhou, 2012; Shoukry, William, Downie & Riad, 2011). It has been observed that the air-dried concrete at the test day has 20%–25% higher compressive strength compared with the water-saturated concrete (Mehta & Monteiro, 2006; Jensen & Hansen, 2002; Bartlett & Macgregor, 1995). The

surface energy and disjoining pressure of cement paste are involved in this phenomenon (Di Bella *et al.*, 2016; Mehta & Monteiro, 2006; Soroka, 1979; Wittmann, 1973). Mechanical properties such as compressive strength are highly dependent on the surface energy of the hydration product, and the energy decreases as the RH increases (Wittmann, 1973). Moreover, the low internal RH of concrete can contribute to strengthening the capillary forces in the pore fluid of the solid structure (Lura *et al.*, 2006).

Theoretically, it is possible to use IC by SAP without compressive strength loss (Hasholt *et al.*, 2012). On the other hand, previous studies have shown inconsistent test results. IC has two opposite effects on the concrete strength (Hasholt, Jespersen & Jensen, 2010; Jensen & Hansen, 2001b). First, the additionally formed pores by the SAP particles are large enough to be comparable to the entrained air void of concrete; these pores are well known to be the reason for strength reduction (Jensen & Hansen, 2001b). In general, a 1% increase in air void leads to a 5% loss in the compressive strength of concrete (Jensen & Hansen, 2001b; Powers & Brownyard, 1948); further, the strength of UHPC can be expressed as functions of w/c and air content, as well (Wille *et al.*, 2011). Second, IC can increase the maximum degree of hydration, which is closely related to the strength gain (Hasholt *et al.*, 2010; Jensen & Hansen, 2001b). Because these two complementary factors affect the strength simultaneously, strength reduction can be prevented (Kang *et al.*, 2016b; Jensen & Hansen, 2001b). Nevertheless, strength loss due to SAP addition has been reported (Craeye *et al.*, 2011). After this report, however, it has also been proposed that one another reason for the strength loss is the excessive amount of extra water added with SAP; i.e., if a larger amount of extra water than the

absorption capacity of SAP is added to a concrete with SAP, the real w/c ratio of concrete increases; thus, the compressive strength can decrease (Kang *et al.*, 2016a; Hasholt *et al.*, 2012). Aside from the case of excessively designed extra water, another possible reason for the strength loss is the high internal RH by SAP addition (Hasholt *et al.*, 2010; Jensen & Hansen, 2001b). At room temperature (20 °C) without external drying of concrete, strength loss due to SAP addition has been reported in the low-w/c cementitious materials: 2%–12% in a high-performance concrete (HPC) (w/c=0.33) (Shen, Wang, Chen, Wang & Jiang, 2015), 19% in a high-performance mortar (HPM) (Jensen & Hansen, 2002), 7%–13% in a HPC (w/c=0.35) (Piérard, Pollet, Cauberg, Jensen, Lura & Kovler, 2006), and 15%–20% in HPMs (w/c=0.25–0.35) (Esteves, Cachim & Ferreira, 2007). In particular, the HPMs did not show strength loss when they were cured under the external dry condition (RH 30%–50%) (Esteves *et al.*, 2007). Along with the large pores by SAP, this confirms the possibility of another reason (i.e., high internal RH by IC) for the loss of strength. In a low-w/c concrete or mortar that has low permeability, self-desiccation can occur at early age, even possibly under water curing; thus, its internal RH is far lower than the concrete or mortar with SAP (Jensen & Hansen, 2001b). In other words, the difference in moisture content on the test day can affect the compressive strength, especially negatively in the concrete or mortar with SAP (Jensen & Hansen, 2002). If the compressive strength is measured under a similar internal RH condition (e.g., 75%), IC definitely has no negative effect on the strength (Lura *et al.*, 2006; Jensen & Hansen, 2002). Therefore, the necessity of a strength test under similar moisture contents has been proposed for the accurate evaluation of the effect of IC by SAP on the strength (Lura *et al.*, 2006; Jensen & Hansen, 2002).

Although the internal RH is a decisive factor for the influence of IC on the strength, most previous studies consider only the effects of porosity and the hydration reaction, without considering the effects of the moisture content or internal RH. In fact, it is challenging to accurately measure the RH or to ensure similar internal RH conditions (or moisture content) in concretes. For instance, the internal RH of UHPC with or without SAP was recently reported (Justs *et al.*, 2015). However, there was no information on the early-age RH (during the first 24–48 h) and the long-term-age RH (> 5–7 d) in the study (Justs *et al.*, 2015); these ages are the critical periods for self-desiccation and strength development, respectively. Thus, the interdependent effect of the RH on the compressive strength and early-age shrinkage behavior has not been fully understood yet. To use IC for field-cast UHPC successfully, the internal RH should be rigorously investigated under the air-dry condition, because this has a decisive impact on both the volume change and compressive strength. Accordingly, this study investigated the effect of IC on UHPC under two curing conditions: air-dry and water-curing conditions. The internal RH histories of UHPCs were measured to understand the effect of variation in moisture content on the volumetric change (i.e., shrinkage) and compressive strength. The measured shrinkage and strength of internally cured UHPC (I-UHPC) were compared with those of ordinary UHPC (O-UHPC). Lastly, the characteristics of compressive strength of I-UHPC were interpreted from its interdependent relationship with the moisture content.

## **5.2.2 Experiment methods**

### **5.2.2.1 Specimen preparation**

The material properties of UHPC such as shrinkage, strength, and internal RH, the specimens were measured. Two O-UHPCs and I-UHPCs were respectively prepared on the basis of the mix proportions listed in Table 4-1. As soon as the mixing was finished, fresh UHPC was poured into the prepared molds; the top surface of UHPC was sealed with 0.1-mm-thick polyester film. The specimens were cured under two different curing programs. Taking into consideration the field-cast condition, the first was the air-dry curing (20 °C and RH 60%) program; the specimens were demolded at 7 d without an additional seal. The American Concrete Institute also recommends a minimum of 7 d curing for the concrete of Portland cement type I (ACI Committee 308, 2001). The second curing program was the water-curing program, which reflects the laboratory test conditions (American Society for Testing and Materials (ASTM), 2016); after 1 d of moist curing (20 °C and RH > 95%), the specimens were demolded and submerged in 20 °C water until the test.

### **5.2.2.2 Experimental procedure**

The compressive strength of each sample was determined as an average of three replicates using 50 mm × 50 mm × 50 mm size cubes. To obtain the day-compressive strength relationships, the cubes were loaded with a speed of 1 MPa/s using a hydraulic testing machine at 1, 3, 7, and 28 d. During the test, the water on the specimen surface was wiped (if necessary), and the specimens

were loaded within 1 h as soon as the specimens were moved from the curing chambers. This was to prevent unintended moisture loss of specimens due to the dry laboratory condition (RH < 60%).

To measure the internal RH histories, cylindrical specimens ( $\Phi$  100 mm $\times$ 200 mm size) were also cured employing the same curing programs used with the cubic specimens. Previous studies used the method to measure the histories of concretes; i.e., using a plastic tube, a hole was made in a specimen from the surface to the center, and the hole was sealed after inserting an RH sensor (Shen *et al.*, 2015; Han, Zhang, Luosun & Hao, 2014; Wang *et al.*, 2009). Unlike this, our method used a portable RH sensor (dimensions 20 mm $\times$ 20 mm $\times$ 100 mm) with a data logger and battery, which was directly embedded in UHPC owing to its outstanding self-compacting ability. Immediately after the casting of UHPC including the sensor, the internal RH at the center of the cylindrical specimens was recorded every 5 min. To avoid any blocking of the measuring point of the sensor by fresh UHPC, the surroundings of the point were covered with polyethylene and polypropylene fine mesh which permitted moisture to pass, but not fresh UHPC. Once the cylindrical specimen was demolded, the perimeter of the protruding wire (necessary for connecting to a computer) on the top surface of the specimen was sealed using waterproof bond. Thus, inflow of water or outflow of moisture through the gap between the wire and UHPC could be blocked. Before embedding the sensor in the specimen, its accuracy was checked by a method in which four identical sensors were operated at 5 min. interval for 56 d, under variable RH conditions (40–70%) of a room; the result was that the maximum standard variation among the sensors was 1%. The test method and the result of accuracy check are presented in Fig.

5-12 (a) and (b), respectively. Based on this result, accuracy of the method could be verified. Thus, it was concluded that the used method for the RH history has a reproducibility. The history of each sample was determined using one sensor in the specimen considering the efficiency of the measurement and the relatively high price of the disposable sensor.

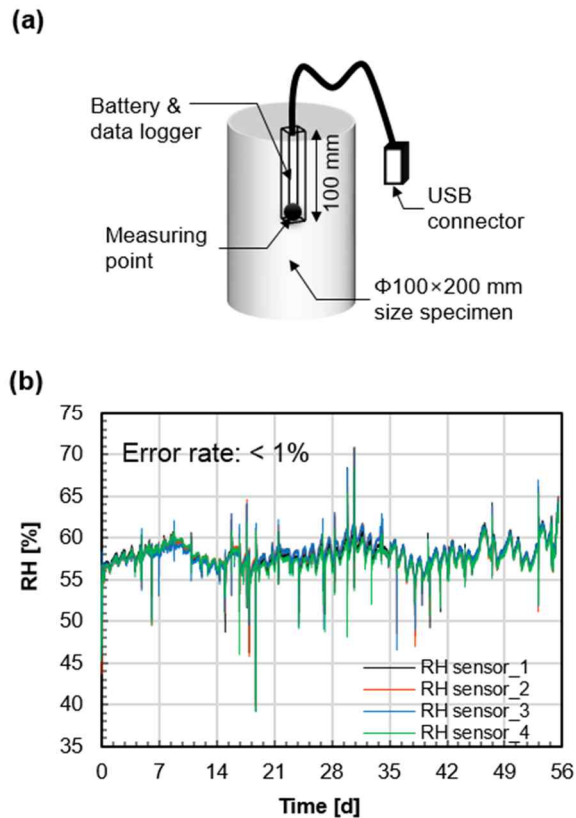


Fig. 5-12 Specimen for internal RH of UHPC (a) and accuracy test of RH sensor (b)

The AS and total shrinkage (TS) were measured using the same method employed in the Section 3.1. Every 5 min, free strains of all specimens were simultaneously recorded. Because the real elements made using UHPC are thinner than other types of concrete members (Eppers & Müller, 2008), the

cross section (dimensions 40 mm×40 mm) of the specimen is a suitable size. The shrinkage strain was recorded immediately after UHPC was poured into the mold (approximately 10 min after the end of mixing), but the strain was normalized to the starting point of AS, also known as time zero. Hence, previous data from the points was excluded when determining the magnitude and rate of shrinkage. Three identical specimens were prepared for the shrinkage test of each sample. They were cured only under the air-dry condition (20 °C and RH 60%). In accordance with the air-dry curing program, one of them was stripped at 7 d and exposed to the dry air for another days, whereas the other two specimens were sealed again at 7 d using adhesive aluminum tape to measure AS. The strain under water-curing program was not performed because it is an uncommon condition for a shrinkage test.

To determine AS strains precisely, strain due to the internal temperature change of the sealed specimens should be removed from the measured free strains. However, it is difficult to estimate this thermal deformation accurately because the coefficient of thermal expansion of concrete is dramatically changed at an early age (Maruyama & Teramoto, 2013; Wyrzykowski & Lura, 2013; Yang *et al.*, 2005), when the temperature is also variable (Kang *et al.*, 2016d). Moreover, as can be seen in Table 4-1, the maximum variation between external (20 °C) and internal temperatures (21.6–24.4 °C) after time zero was not significant (Snoeck *et al.*, 2015a); based on this, it was assumed that thermal deformation of a thin UHPC specimen has no significant impact on the AS strain. Thus, in this study, the measured free strains were not revised by using a constant coefficient; i.e., a minor thermal strain was included in the AS strains. The AS strain of each sample was determined by averaging two replicates,

whereas the TS strain was obtained from one unsealed specimen. The strain due to drying shrinkage (DS) was simply determined by subtracting the AS strain from TS (Kang *et al.*, 2016d).

### **5.2.3 Results and discussion**

#### **5.2.3.1 Hydration heat and internal RH history**

Fig. 5-13 and Fig. 5-14 show the histories of hydration heat and internal RH, respectively. These histories have been generally used for internally cured concrete in order to confirm the promotion of the hydration reaction and the mitigation of self-desiccation by IC, respectively (Kang *et al.*, 2016d; Justs *et al.*, 2015; Kang *et al.*, 2015; Justs *et al.*, 2014; Wyrzykowski & Lura, 2013). Mostly in low-w/c (0.2–0.3) cementitious materials, the height of the main hydration peak increases as the w/c ratio increases (Justs *et al.*, 2015; Justs *et al.*, 2014). Therefore, when SAP is added in the materials without extra water, the height decreases depending on the absorption capacity of the SAP (Kang *et al.*, 2016d; Justs *et al.*, 2014). This trend is actually confirmed in the peaks between Ref\_0.255 and AA\_0.255 (Fig. 5-13 (a)). Because of the SAP's ability to absorb and retain water, the available water for hydration reaction was reduced, which in turn decelerated the hydration reaction during the initial stage of cement hydration (< 24 h). The remarkable result is that even though the largest amount of water was included in AM\_0.275, the height was the lowest along with Ref\_0.215, which had the lowest amount of water among all the samples. This result confirms that the amount of extra water for IC was accurately designed in AM\_0.275 considering the SAP's capacity in UHPC.

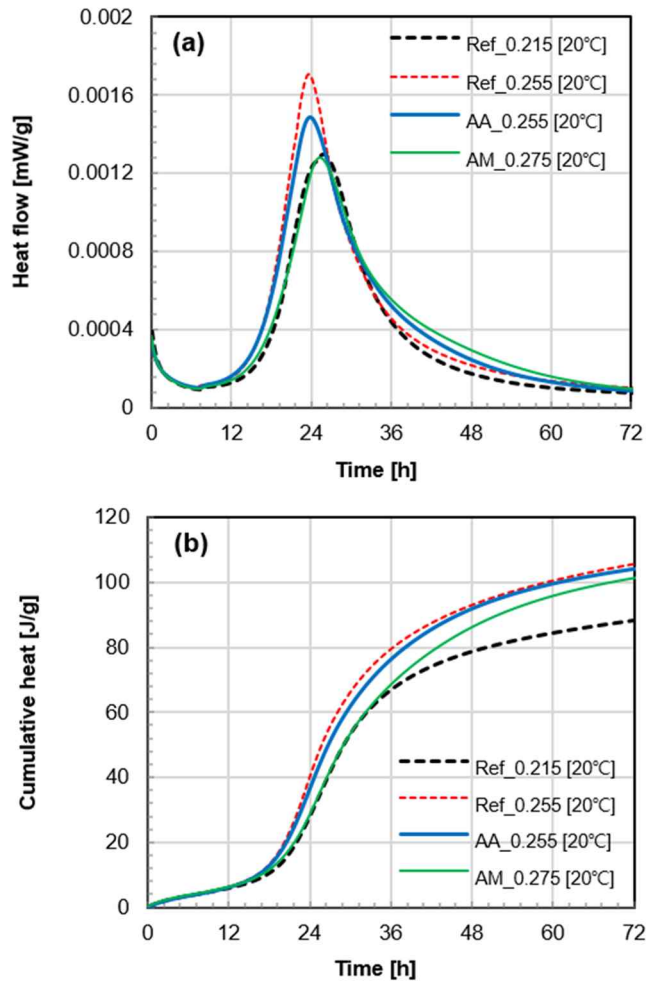


Fig. 5-13 Heat flow (a) and cumulative heat of hydration (b)

It has been reported that the promotion of the hydration reaction by IC is effective during the deceleration period of cement hydration (Wyrzykowski & Lura, 2013). The extra water absorbed by the SAP begins to be released to the surrounding concrete (Kang *et al.*, 2016a; Wang *et al.*, 2015), due to the dramatic change of ion concentration in the concrete pore solution during the acceleration period (Lothenbach *et al.*, 2008; Lothenbach & Winnefeld, 2006). This released water or moisture can be consumed to accelerate the hydration reaction during the deceleration period. Compared with Ref\_0.255, the hydration reaction of AA\_0.255 was decelerated at the initial stage (< 27 h), but accelerated after this stage (27–60 h). Accordingly, the cumulative hydration heats of the two samples were almost the same after 60 h (Fig. 5-13 (b)). Similar results have also been shown in low-w/c (0.183–0.25) cementitious composites (Justs *et al.*, 2015; Justs *et al.*, 2014). In these composites, a SAP whose shape and manufacturing method is identical to those of SAP\_AA, but whose particle size is less than 63  $\mu\text{m}$ , was added without extra water. Two composites with or without SAP showed almost the same cumulative hydration heats at 3 d; the hydration promotion by SAP during the deceleration period contributed to the result. On the basis of this result, it has been reported that almost all the water that was absorbed by SAP is released during the first 3 d (Justs *et al.*, 2015; Justs *et al.*, 2014). However, the hydration promotion by SAP\_AM (another type of SAP) began from 30 h, and was also effective after 3 d. This can be confirmed by the fact that the cumulative heat of AM\_0.275 at 3 d was lower than that of other samples having a w/c of 0.255. The outstanding long-term water retention and desorption characteristics of SAP\_AM (Kang *et al.*, 2016a) resulted in the slow but long-term (> 3 d)

promotion of the additional hydration reaction in AM\_0.275.

Fig. 5-14 (a) and (b) show the internal RH histories of the air-dried and water-cured samples, respectively. These histories were closely related to the evolution of hydration heat. However, it is first revealed in this study that there is a gap between the times when self-desiccation begins to abate (14–17 h depending on the sample) owing to the moisture released by SAP, and when the hydration reaction began to be promoted by IC (> 24 h). After the initial setting (12–15 h depending on the sample), the ion concentration of the concrete pore solution was dramatically changed owing to the accelerated cement hydration (Fig. 5-13) (Lothenbach *et al.*, 2008; Lothenbach & Winnefeld, 2006), which caused SAP to release the absorbed water (Kang *et al.*, 2016a; Wang *et al.*, 2015). The self-desiccation that began at 14–17 h was mitigated by this release, i.e., the IC effect (Fig. 5-14). However, the deceleration period when the promotion of the hydration reaction was effective, began 7–9 h after the start time of self-desiccation. In other word, the moisture released by SAP was consumed for the promotion, not instantly but after several hours. The start time of this promotion also corresponds to that of the pozzolanic reaction in UHPC. This water-consuming reaction between portlandite of the first hydration products and amorphous SiO<sub>2</sub> in silica fume occurs in UHPC after 24 h (Korpa *et al.*, 2009; Loukili *et al.*, 1999).

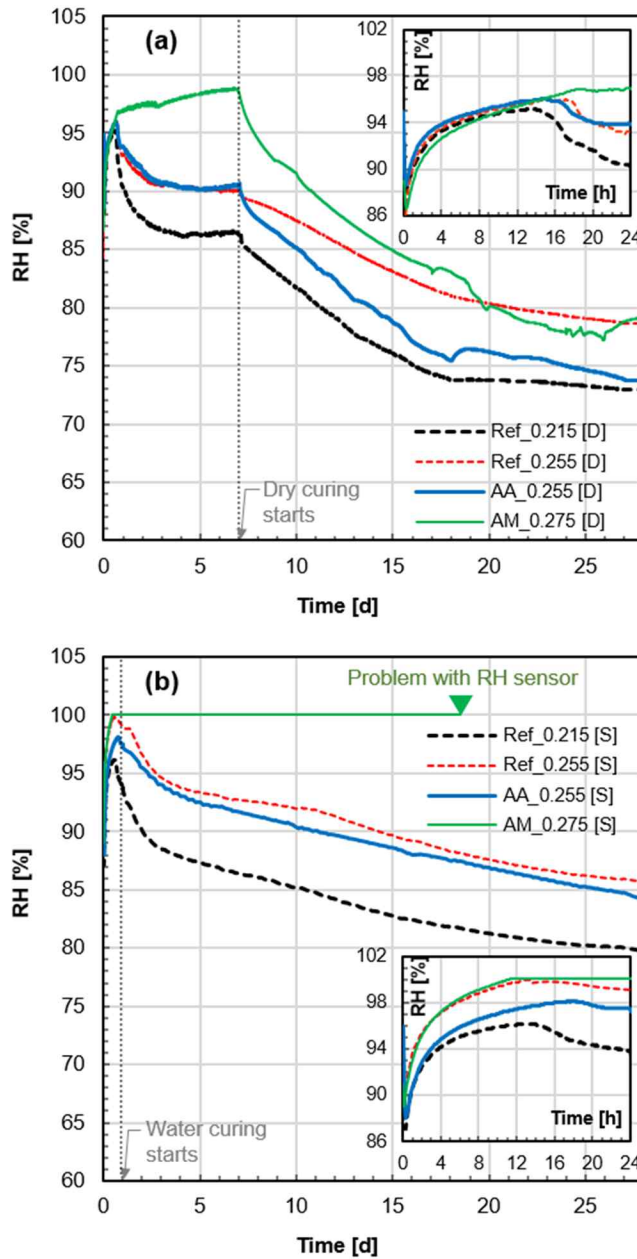


Fig. 5-14 Internal RH histories of UHPC under air-dry curing condition (20 °C and RH 60%) (a), and water curing condition (20 °C) (b)

During the first 7 d, it is also confirmed that the internal RH of the water-cured specimen was higher than that of the sealed specimen under the air-dry condition. At an early age ( $< 1$  d), the internal structure of UHPC is relatively less dense. Previous pore structure analysis using mercury intrusion porosimetry supports this fact. In UHPC ( $w/c=0.2$ , silica fume/cement ratio ( $sf/c=0.25$ ), the volume of large capillary pores ( $> 50$  nm in diameter) was lowly maintained over the entire lifetime owing to the filling effect by silica fume particles; however, the volume of small capillary pores (10–50 nm in diameter) was especially higher at an early age compared to the other period (Loukili *et al.*, 1999). Because of the pozzolanic reaction after 1 d, the main peak (at 30 nm) height of the pore size distribution decreased by 87% between 1 d and 7 d (Loukili *et al.*, 1999). Therefore, moist or water curing of fresh UHPC at a very early age (especially before initial setting) can increase the internal RH by absorption of external moisture, and likewise partially or fully hardened normal concrete. On the basis of the comparison between Fig. 5-14 (a) and (b), the increase in internal RH by moist curing was pronounced. Thus, it can be safely inferred that Ref\_0.215 is the most compact and has the lowest permeability among the samples, because the difference in internal RHs between the two conditions was the smallest, as can be seen in Fig. 5-14.

On the basis of the results of Fig. 5-13 and Fig. 5-14 (a), it is also shown that IC cannot facilitate an increase in the internal RH before self-desiccation. This is because the driving force for desorption of SAP, such as the change in ion concentration, does not occur before initial setting or during the dormant period. After the initial setting of 14–17 h, however, the RHs of samples started

to decrease, except for AM\_0.275, then self-desiccation began to occur. Although the self-desiccation of AA\_0.255 was slightly reduced compared with that of O-UHPCs during the first 3 d, the desiccation was not completely prevented. Possible reason is that at the stage of mix design, this sample did not satisfy the required amount of extra water to prevent self-desiccation. The required extra water-to-cement ratio is estimated as 3.87% according to the design equation by Jensen and Hansen (Jensen & Hansen, 2001b); AA\_0.255 satisfied the requirement at first. However, this ratio is increased to 6% when considering the change of chemical shrinkage by silica fume addition (Assmann, 2013; Lura, 2003). Based on this, there should be the desiccation in AA\_0.255, whereas AM\_0.275 satisfied the requirement considering incorporated silica fume. However, it is questionable whether the amount of released water after the beginning of the desiccation was identical to the designed extra water. Previously, we studied about the amount of absorbed water by SAP at the beginning point. In the study, SAP\_AM retained the entire amount of extra water (more than 6% by wt.% of cement) at that point, while SAP\_AA was likely to release a part of absorbed water before the point (Kang *et al.*, 2016a). Consequently, not only the estimation of extra water at the design stage but also the water retention capacity of SAP should be considered for the effectiveness of IC. Test results of previous study also support the importance of the absorption capacity. Internal RHs of an O-UHPC ( $w/c=0.15$  and  $sf/c$  ratio=0.1) and two I-UHPCs which satisfied the required extra water-to-cement ratio ( $> 3.3\%$ ) were measured (Justs *et al.*, 2015). After 1 d 1 day of casting, the internal RHs consistently decreased owing to self-desiccation and the RH of the O-UHPC reached to 89% at 5 d (Justs *et al.*, 2015). The addition of SAP (same type of SAP\_AA as mentioned before) to the O-UHPC mitigated the reduction

of the RH depending on the  $w/c$  ratios, but self-desiccation occurred despite the addition. However, SAP\_AM in the current study increased the RH of UHPC after the starting point of self-desiccation; thus, AM\_0.275 maintained a saturated state despite smaller amounts of added SAP particles (i.e., greater distances between the particles in the concrete) than AA\_0.255. Therefore, complete prevention of self-desiccation was possible by using the IC method, that greatly affected by the water retention capacity of SAP.

Based on the results on Fig. 5-14 (b), it was firstly verified by conducted experiment herein that the self-desiccation of UHPC cannot be prevented by an external curing method such as water curing. AA\_0.255, which was cured in water, also showed self-desiccation due to the relatively low water retention capacity of SAP\_AA. This desiccation also confirms the waterproofing performance of I-UHPC, similar to O-UHPC. Unlike AA\_0.255, the internal RH of AM\_0.275 was maintained as 100% during the water-curing period. Once the external drying or evaporation was blocked, the internal RH of UHPC with SAP\_AM went up to 100% RH (Fig. 5-14 (a)). However, during the test, this long-term wet state caused a corrosion problem in the embedded sensor (specifically in the battery) thus the sensor in AM\_0.275 stopped at 18 d.

However, the addition of SAP accelerated the drying of specimens under the air-dry curing condition (Fig. 5-14 (a)). Previously we confirmed that large-size pores were additionally formed in AA\_0.255 and AM\_0.275 (Kang *et al.*, 2016e; Kang *et al.*, 2015). The total porosity of AM\_0.275 (6%) was increased by 3.5% compared with that of Ref\_0.215 (2.5%) (Kang *et al.*, 2016e). This porous structure can be a factor that accelerates the drying of concrete. At the

point of demolding and removal of sealing, the internal RH of AA\_0.255 was almost equal to that of Ref\_0.255; however, at 28 d, the RH of AA\_0.255 was 5% lower than Ref\_0.255 and even identical with Ref\_0.215. As mentioned in the Introduction Section, this rapid decline in the internal RH is of beneficial when taking into account the finishing processes of the concrete floor as well as its mechanical performance. In general, a normal concrete ( $w/c=0.5$ ) slab requires about 3 months for drying, and the concrete ( $w/c > 0.6$ ) is extremely difficult to dry (Cement Concrete & Aggregates Australia (CCAA), 2007). If the drying time has to be reduced in a construction project, using low- $w/c$  concrete can be a solution (Cement Concrete & Aggregates Australia (CCAA), 2007). However, this concrete is vulnerable to early-age shrinkage and resulting cracks (Kang *et al.*, 2016d; Hasholt *et al.*, 2012; Schröfl *et al.*, 2012; Jensen & Hansen, 2001b). IC by SAP can be reasonably and effectively used in these applications, because the internally cured concrete can be dried rapidly with the reduced early shrinkage and cracking risk under the field curing condition. In particular, the drying speed of AM\_0.275, which had the largest amount of moisture at the start time of drying, was the fastest among all samples. Although the  $w/c$  ratio and the internal RH at 7 d (starting point of drying) of AM\_0.275 were 2% and 10% higher, respectively than those of Ref\_0.255, their internal RHs at 28 d were almost the same. However, the 28 d RH of AM\_0.275 was 5% higher than that of Ref\_0.215 or AA\_0.255. The outstanding retention capacity of SAP\_AM contributed to the 5% higher internal RH.

### 5.2.3.2 Shrinkages under drying or sealed condition

Fig. 5-15 shows free strains of the sealed specimens during the first 24 h, before taking any normalization. During the first 4 h, all fresh specimens (at fluid state) shrank as much as approximately 100  $\mu\text{m}/\text{m}$ . This was possibly caused by the internal temperature drop of the specimens, as also shown in the previous studies (Kang *et al.*, 2016d; Yoo *et al.*, 2014). After 4 h, there were no volume change in the specimens up to the time zero point. However, immediately after the point, severe AS occurred in the O-UHPCs because of the self-desiccation. In other words, after the initial setting (presented in Table 4-1), this desiccation began (see Fig. 5-14) in the pores that had been formed with the restrained conditions due to the formation of solid skeleton (Chang-Wen *et al.*, 2007; Lura *et al.*, 2003). The results presented in Fig. 5-15 also confirm the accuracy of the UPV method used herein to find the starting point of AS, i.e., time zero.

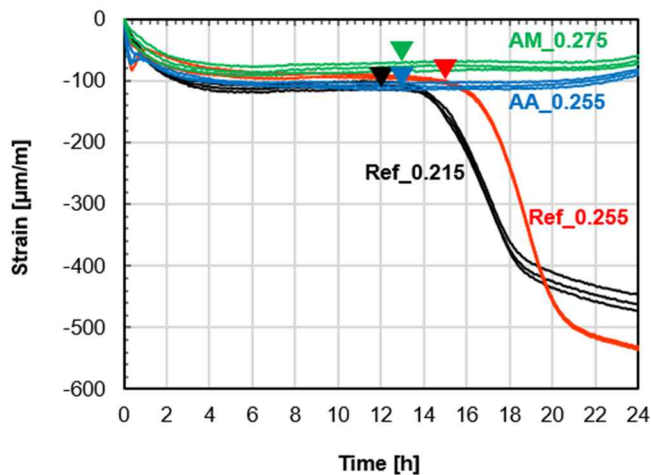


Fig. 5-15 Early-age shrinkage behavior of three replicates for each specimen ( $\nabla$  symbols indicate defined time zero points from UPV measurement)

In the time zero-normalized strain results, two O-UHPCs showed unpredictable results (Fig. 5-16 (a) and (b)). In general, the AS of low-w/c concrete increases as the w/c ratio decreases, and vice versa (Soliman & Nehdi, 2011; Holt & Leivo, 2004; Zhang *et al.*, 2003). However, in this study, even though the w/c ratio of O-UHPC decreased from 0.255 to 0.215, the AS did not increase. Similar results often have been reported in the low-w/c concrete containing silica fume: UHPCs (w/c=0.22 and 0.25) (Soliman & Nehdi, 2011), UHPCs (w/c=0.23 and 0.26) (Eppers & Müller, 2008), and HPCs (w/c=0.3 and 0.34) (Zhang *et al.*, 2003). In particular, a reason for this unpredictable result can be found in extremely low-w/c and high-sf/c conditions, as in UHPC. As the degree of agglomeration of silica fume in the concrete increases, the resulting porosity can also increase (Soliman & Nehdi, 2011). Meanwhile, these O-UHPCs were encountering the so-called knee point at an early age. At this point, AS is drastically slowed down because a semirigid skeleton (stress-resistance microstructure) was formed to resist the shrinkage (Mounanga *et al.*, 2006). Although it was slowed down, AS did not stop but proceed after the point owing to self-desiccation. Cement hydration is only possible in a saturated space (e.g., RH > 80%) (Kosmatka *et al.*, 2011; Mehta & Monteiro, 2006; ACI Committee 308, 2001). If the internal RH of cement paste drops below 80%, the hydration reaction that is the driving force of self-desiccation can barely proceed. Besides, it was reported that self-desiccation is not found when the RH is lower than 75% (Jensen & Hansen, 2001a). Under the water-curing condition, the RH of Ref\_0.215 reached 80% at 28 d (Fig. 5-14 (b)), and AS tended to stop at the same time (Fig. 5-16 (a)). On the other hand, the RH of Ref\_0.255 was 86% at 28 d (Fig. 5-14 (b)), and AS was continuously increased.

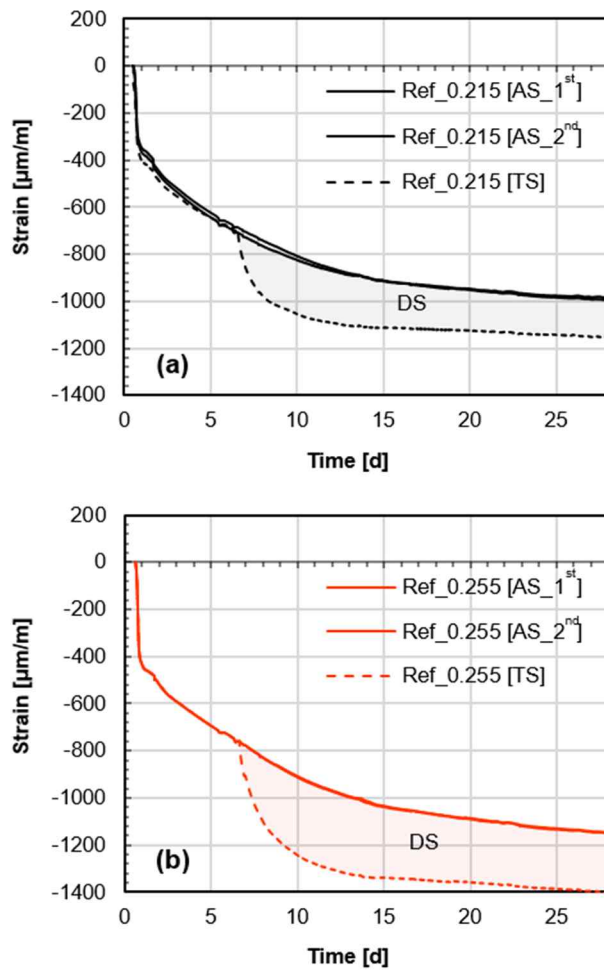


Fig. 5-16 Total and autogenous shrinkages of designed UHPC: Ref\_0.215 (a), Ref\_0.255 (b)

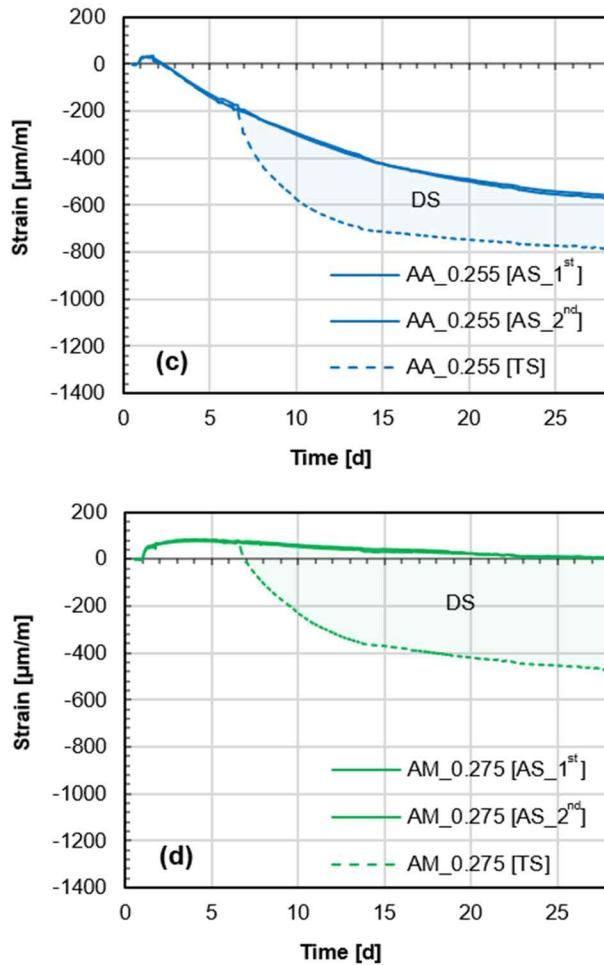


Fig. 5-16 (cont.) Total and autogenous shrinkages of designed UHPC: AA\_0.255 (c), and AM\_0.275 (d)

AA\_0.255 showed unexpected shrinkage behavior at an early age (Fig. 5-16 (c)). Although the IC by SAP\_AA promoted the hydration reaction and slightly (or negligibly) mitigated self-desiccation during the deceleration period between 1 d and 3 d, the self-desiccation of AA\_0.255 was not completely prevented. However, it is interesting to note that a slight expansion was (up to 40  $\mu\text{m/m}$ ) observed. It can be seen from Fig. 5-16 (c) that this expansion was effective during the first 2 d, and then shrinkage occurred due to self-desiccation, as in O-UHPC. The first 2 d is the most effective period to mitigate the early-age shrinkage of UHPC, because significant AS occurs most rapidly during this period. In the case of O-UHPCs, the AS strain at 2 d was approximately 45% of that at 28 d (Fig. 5-16). However, this significant portion was prevented by SAP\_AA during 2 d, which contributed to the 43% reduced AS strains of AA\_0.255 compared to that occurring in Ref\_0.215 at 28 d.

Due to IC by SAP\_AM, AM\_0.275 continued to remain in the saturated state without any self-desiccation (Fig. 5-14); thus, AS was completely prevented under the sealed curing condition (Fig. 5-16 (d)). Rather than shrinkage, an expansion occurred (up to 80  $\mu\text{m/m}$ ) during the first 7 d, as in AA\_0.255. As a possible reason for early-age expansion of low-w/c (0.3) cement paste, partial reabsorption of bleeding water by cementitious materials has been proposed (Snoeck *et al.*, 2015a). However, it is hard to believe the reabsorption occurs within a UHPC system because bleeding is almost impossible owing to the extremely low-w/c condition; this condition also causes the rapid drying of the UHPC surface when it is exposed to dry air (Fehling *et al.*, 2014). On the other hand, this situation can be reconsidered in

internally cured UHPC; i.e., SAP in UHPC releases the absorbed water after initial setting, which can make the reabsorption of IC water possible depending on the absorption and retention capacity of SAP. In the case of this study, cementitious materials in UHPC could reabsorb water during 2 d (with SAP\_AA) or more than 3 d (with SAP\_AM). It can be inferred that the reabsorbed water could be consumed to promote the hydration reaction as shown in Fig. 5-13. In addition, this reabsorption due to IC can be a possible reason for the unexpected shrinkage behavior of AA\_0.255 in which only expansion occurred in spite of self-desiccation. Lura has mentioned about the expansion phenomenon that the reabsorption of bleeding water affects an early-age deformation (i.e., expansion) of concrete, which is not related to the change of internal RH; this independent expansion is eventually diminished due to the self-desiccation or AS (Lura, 2003). The previous experiment has also shown the possibility of reabsorption and resulting expansion; i.e., an I-UHPC ( $w/c=0.2$ ) containing solution polymerized SAP showed reduction in internal RH between 2 d and 3 d, but the concrete was expanded during the same period (Justs *et al.*, 2015). The authors mentioned that water release by SAP was effective during the first 3 d, but the reason for the expansion was not explained (Justs *et al.*, 2015). However, on the basis of these experimental reviews, the current study describes a new phenomenon related to expansion of internally cured concrete, and suggests a likely reason for the discrepancy between the expansion and the desiccation, especially when using acrylic acid (or solution polymerized) SAP.

Meanwhile, the magnitude of AS under the drying condition can be different from that under the sealed condition (Zhang *et al.*, 2003). Fig. 5-1

confirms this difference. The air-dry curing condition shortened the time to reach a low internal RH (e.g. 75–80%), which can stop the AS. Therefore, the measured AS under the sealed condition can overestimate AS compared to the actual AS occurrence in field conditions. Obviously, the actual DS-to-TS ratio under field conditions will be higher than that shown in Fig. 5-16. Although there is a possibility of overestimation of the AS-to-TS ratio, Fig. 5-17 shows that a considerable part of the shrinkage in TS is AS in the case of UHPC at 28 d. The AS-to-TS ratio decreases as the w/c ratio increases (Ref\_0.215 vs. Ref\_0.255) or when SAP is included (Ref\_0.255 vs. AA\_0.255 or AM\_0.275). The DS strain tended to increase as the w/c ratio increased, but the addition of SAP at a given w/c ratio reduced the DS strain slightly (Ref\_0.255 vs. AA\_0.255). The DS strain of AA\_0.255 was 30  $\mu\text{m}/\text{m}$  (or 13%) lower than that of Ref\_0.255, although more water in AA\_0.255 dried more rapidly than Ref\_0.255 during the air-dry curing period. This is because only a part of the extra water was consumed to promote the hydration reaction, and the remaining water evaporated (Reinhardt & Assmann, 2010). In other word, the extra water released by SAP can never be entirely used to promote the hydration reaction or to mitigate self-desiccation under the air-dry condition; thus, the DS of AA\_0.255 or AM\_0.275 was inevitably higher than that of Ref\_0.215. Other studies also have shown the increased DS of internally cured concrete when exposed to the drying condition (Assmann & Reinhardt, 2013; Soliman & Nehdi, 2011; Mechtcherine, Dudziak, Schulze & Staehr, 2006; Piérard *et al.*, 2006). Noticeably, it has been reported that IC by SAP is ineffective even in reducing the TS of low-w/c concretes when the concrete is exposed to dry air immediately after demolding (commonly at 1 d) (Soliman & Nehdi, 2011;

Mechtcherine *et al.*, 2006; Piérard *et al.*, 2006). On the other hand, in our study, the TS at 28 d was decreased by 32% in AA\_0.255 and 59% in AM\_0.275 compared with Ref\_0.215, because the reduction in AS by IC during the sealed period (first 7 d) contributed to the reduction of the TS.

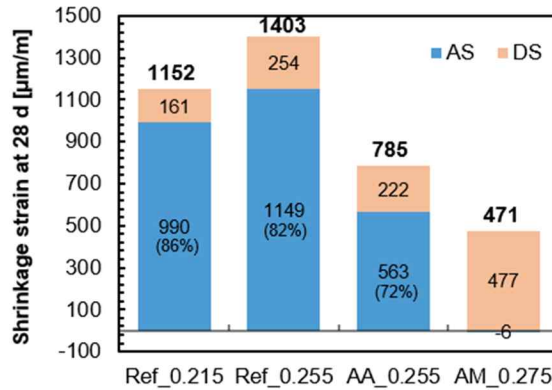


Fig. 5-17 Autogenous and drying shrinkages of UHPC at 28 days under air-dry curing condition (bold numbers on each chart mean total shrinkages)

Fig. 5-18 shows the variation of the strain rate, which is defined as the strain change in every 1 h. The strain rate is more important than the magnitude considering the risk of shrinkage related cracking (Shen *et al.*, 2016; Jiang *et al.*, 2014; Lura *et al.*, 2001). At an early age, the risk is exceptionally high because concrete has the lowest tensile strain capacity during the entire period (Holt & Leivo, 2004). Hence, in the case of low-w/c concrete such as UHPC, the risk due to internal drying (related to AS) is considerably higher than that by external drying (related to DS). Moreover, the risk due to DS can be mitigated depending on the long-term relaxation rate of a concrete (Jensen & Hansen, 2001b). This study experimentally verified that the serious problem, i.e., the risk of cracking at an early age, can be completely solved using IC by SAP, and this method was also effective in reducing the risk of cracking due to

DS that occurred during the first 2 d (7-9 d) of the drying period (Fig. 5-18). The changed pore structure due to the addition of SAP could contribute to the decrease in the strain rate due to DS. Accordingly, this also supports that IC is one of the most effective and efficient ways to reduce the risk of cracking for field-cast UHPC.

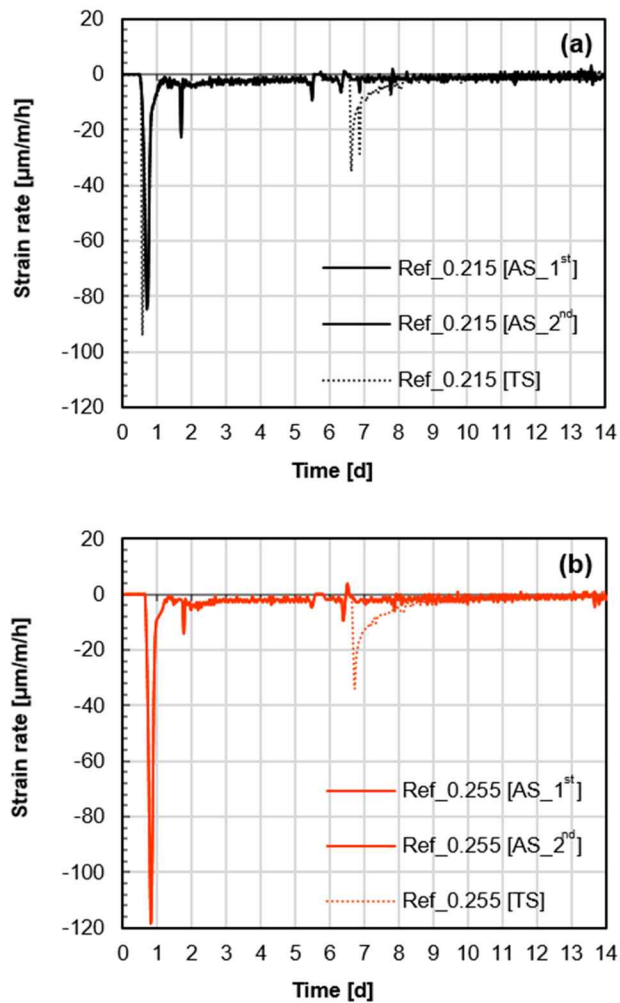


Fig. 5-18 Strain rates of UHPC: Ref\_0.215 (a), Ref\_0.255 (b)

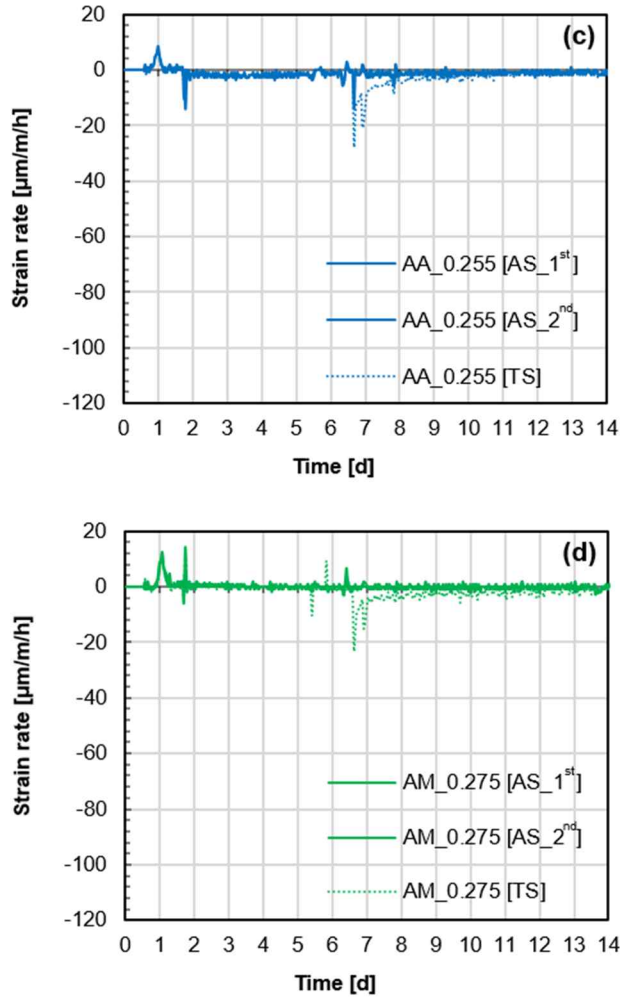


Fig. 5-18 (cont.) Strain rates of UHPC: AA\_0.255 (c), and AM\_0.275 (d)

### 5.2.3.3 Compressive strength depending on moisture content

The compressive strength of the specimens as a function of curing days is presented in Fig. 5-19. The results are separated on the basis of two different curing programs: air-dry and water curing. Above all, unlike O-UHPC, the strength of I-UHPC significantly decreased due to the water curing (Fig. 5-19

(a) vs. (b)). However, the decreased strength could be recovered during the period of 7–28 d. In particular, the recovery of AM\_0.275, which showed the most substantial reduction in the internal RH during the drying period (Fig. 5-14 (a)), was the most pronounced as shown in Fig. 5-19 (a). The strength change and recovery were investigated using Fig. 5-20 in more detail.

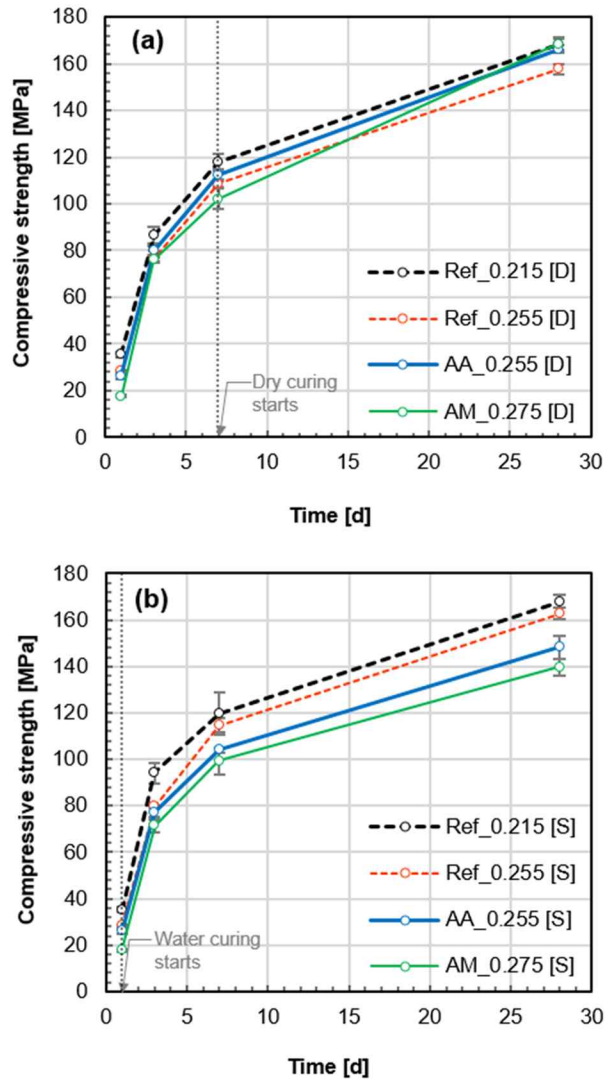


Fig. 5-19 Compressive strength development of UHPC under air-dry curing condition (20 °C and RH 60%) (a), and water curing condition (20 °C) (b)

The strengths of all water-cured specimens were increased by 40–43% between 7 d and 28 d (blue bars in Fig. 5-20 (a)); i.e., there were no remarkable differences in the rate of increase among the samples. Likewise, the strength of only air-dried O-UHPC was increased by 43–45% (green bars in Fig. 5-20 (a)). On the basis of two curing methods, the 3% difference between the increase rate for each specimen (40% vs. 43% in Ref\_0.215 or 42% vs. 45% in Ref\_0.255) was attributed to the decreased 7 d strength, i.e., not the increased 28 d strength, under the air-dry condition. However, as can be seen in Fig. 5-20 (b), the benefit of water curing for the strength was disappeared over time; finally, the strengths of Ref\_0.215 at 28 d were the same under the both curing methods. In general, the strength of O-UHPC decreased as the w/c ratio increased regardless of curing methods or ages. This decrease was exceptionally pronounced before 7 d, but was mitigated later.

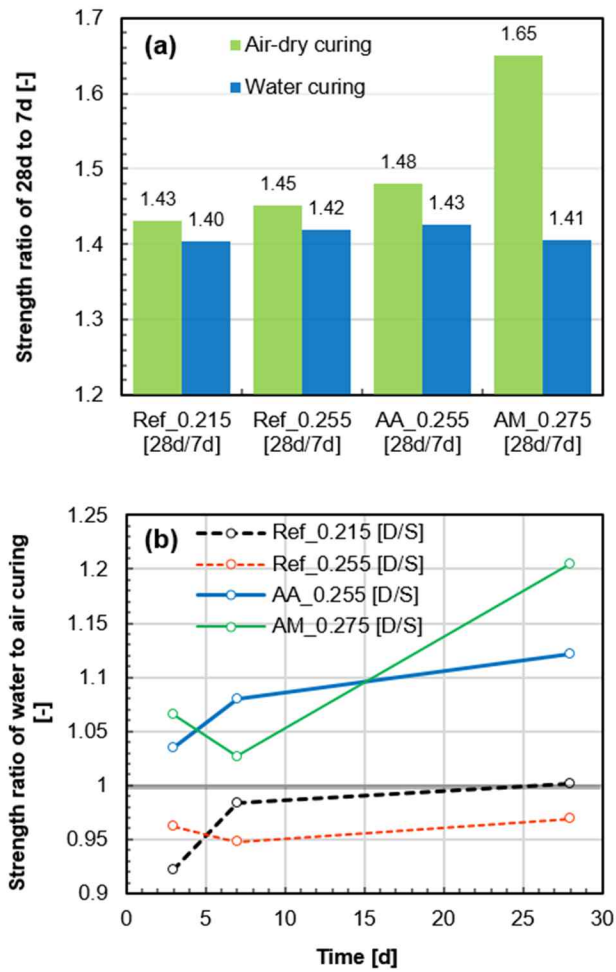


Fig. 5-20 Compressive strength ratios of 28 d to 7 d (a), air-dry curing to water curing (b)

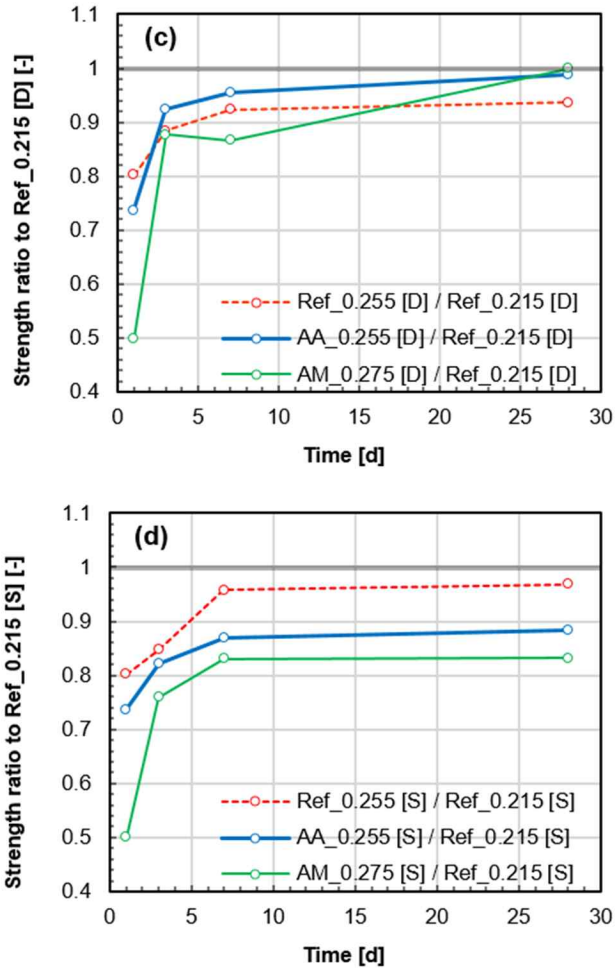


Fig. 5-20 (cont.) Compressive strength ratios of other samples to reference sample (Ref\_0.215) with air-dry curing (c) and water curing (d)

However, the strength of air-dried I-UHPCs was increased by 48–65% during the drying period (green bars in Fig. 5-20 (a)). This outstanding increase means the air-dry curing is beneficial for the strength development of I-UHPC. Compared with the water-cured specimen, the 28 d strength of the air-dried specimen was 12–21% higher (Fig. 5-20 (b)). Due to the drying of internal moisture, the strength of I-UHPC even reached that of Ref\_0.215 at 28 d despite the considerably higher w/c ratio. It is common practice for SAP to be included with extra water to ensure flowability; thus, to investigate the effect of IC by SAP on the strength. Therefore it is reasonable to compare internally cured concrete with concrete without SAP as well as extra water such as Ref\_0.215 (Jensen & Hansen, 2001b). From this comparison, the strength ratio of samples to Ref\_0.215 was presented in Fig. 5-20 (c) and 8 (d) by separating each sample with a curing program.

Certainly, the addition of SAP could increase the strength of UHPC at a given w/c ratio (e.g., 0.255) as long as it was subjected to the air-dry condition (Fig. 5-20 (c)). However, as can be seen in Fig. 5-20 (d), the 28 d strength of I-UHPC decreased by 12–17% under the water-curing condition, and even the strength was lower than that of Ref\_0.255 during the entire period. These results clearly show that the water curing that is beneficial for traditional concrete, can a negative factor in the strength of internally cured concrete.

In UHPC, plenty of non-reacted clinkers remain owing to the low-w/c condition (Selleng *et al.*, 2016); maintaining the long-term saturated stage (internal RH > 80%) can be a crucial factor that increases the strength because

this can help the further reaction of the clinkers and the pozzolanic reaction. In addition, according to basic principles, the effect of IC by SAP on the strength of low-w/c ( $< 0.4$ ) concrete can be summarized as follows (Hasholt *et al.*, 2012; Jensen & Hansen, 2001b). IC increases the final degree of hydration and in turn the gel-space ratio of the concrete, which plays a positive role in the strength development. On the other hand, SAP makes large-sized pores in the concrete depending on its shape and absorption capacity, which is a negative factor in the strength performance. Because these two factors are effective in concrete simultaneously, its effect on strength can be complicated (Hasholt *et al.*, 2012; Jensen & Hansen, 2001b).

However, AM\_0.275 showed a substantial strength loss under water curing condition even though this specimen maintained a perfect saturated condition (internal RH=100%) due to IC by SAP\_AM. The reduced strength was increased again after the specimen was dried. According to Griffith's theory, the strength of a solid such as concrete decreases as the moisture content increases (Soroka, 1979). In the case of concrete, as the moisture content or the internal RH increases, cohesive force decreases because the absorption of water vapor by the materials weakens the van der Waals attraction; this reduces the surface energy or bonds between the gel particles, and consequently the strength decreases (Mehta & Monteiro, 2006; Soroka, 1979; Wittmann, 1973).

When a UHPC is exposed to dry air, evaporation (external drying) occurs along with self-desiccation (internal drying) (Soliman & Nehdi, 2011). This accelerates the reduction of internal moisture. Although this reduction could delay or prevent the hydration reaction (Kosmatka *et al.*, 2011), the drying of

I-UHPC after 7 d was certainly beneficial for the strength. Maintaining the saturated condition longer than 7 d is not advantageous but disadvantageous from a practical standpoint, unless the hydration reactions of UHPC are accelerated by other methods such as heat treatment. The lack of available water and space in which hydration products are newly formed influences the hydration termination of concrete, but the end of hydration reaction in low w/c concrete such as UHPC is more dominantly controlled by the second factor, lack of available space (Justs *et al.*, 2015; Jensen & Hansen, 2001b). This means that the promotion of the hydration reaction by keeping the high internal RH (or saturated condition) is not beneficial any longer for the strength of I-UHPC after the end of hydration reaction. This effective period of IC can be determined by an isothermal calorimetry test as in Fig. 5-13 (e.g., 3 d for AA\_0.255 or > 3 d for AM\_0.275). Conservatively, 7 d is suitable for IC by considering the variety type and mixing ratio of UHPC or SAP.

Nevertheless, the compressive strengths of internally cured concrete or mortars did not decrease under sealed or water curing condition without an air-dry period: an HPC (w/c=0.35) (Hasholt *et al.*, 2010) and HPMs (w/c=0.315–0.32) (Lura *et al.*, 2006). In particular, the second study has reported inconsistent results regarding the effect of 1 month air-dry curing (RH 75%) on the 56 d strength of cement paste (w/c=0.3 and sf/c=0 or 0.2). Regardless of the SAP addition, the strength of the paste without silica fume increased due to the last 1 month of drying curing, but the strength with silica fume decreased (Lura *et al.*, 2006). The authors have attributed the inconsistent results to the formation of additional micro cracks due to loss of moisture content in the presence of silica fume; these cracks can affect the strength (Lura *et al.*, 2006).

However, these results can be reinterpreted: the strength of dried paste consistently increases if the effect of micro cracks is excluded.

Unlike this cement paste, UHPC possesses outstanding tensile strength and crack-resistance capacity due to the bridging action of the fibers (Noshiravani & Brühwiler, 2013a, 2013b; Markovic, 2006). Only 1% steel fiber by UHPC volume (half the ratio used in this study) can reduce 10–15% of AS by this action (Eppers & Müller, 2008). Therefore, the effect of micro cracks due to the drying of the specimens could be reasonably excluded in this study. The strength loss due to the increase of moisture contents is more pronounced in a mortar or concrete than in a paste because the attraction influenced by the moisture content is mostly effective between aggregate and paste (Mehta & Monteiro, 2006; Wittmann, 1973). Although the moisture content or internal RH was not measured in the previous studies where the strength increase due to SAP under the sealed condition were reported (Hasholt *et al.*, 2010; Lura *et al.*, 2006), the sealed specimens should maintain a higher internal RH due to the water entrainment (Jensen & Hansen, 2001b). The internally cured specimens would show increased strength if they had the same level of moisture contents as other specimens in which self-desiccation occurred without the entrainment.

Fig. 5-21 clearly shows the effect of the external drying on the compressive strength of internally cured UHPC. In Fig. 5-21 (a), the relationship between the decreased internal RH and the increased strength was presented by considering only the effect of evaporation. The air-dry condition provided a low internal RH, especially after 7 d, which is an unfavorable

condition for the degree of hydration. On the other hand, the water-cured specimens contained more moisture on the test day, which is also an unfavorable condition for the mechanical properties. Along with these disadvantages, Fig. 5-21 shows that the moisture content is a crucial factor confirming that the drying of I-UHPC after 7 d is obviously effective in increasing the strength. The decreased internal RH due to evaporation was negligibly low (4–7%) in O-UHPCs, and the increased strength (1–2 MPa) was also negligible. On the other hand, the decreased internal RH of I-UHPCs was remarkable (9–20%), which caused a significant increase in the strength (10–26 MPa). Fig. 5-21 (b) shows the difference between the 28 d strength of air- and water-cured specimens as a function of the increased internal RH. As a similar trend with Fig. 5-21 (a), this figure also revealed the severe strength loss (18–29 MPa) of water-cured I-UHPCs, unlike the strength increase (up to 5 MPa) of water-cured O-UHPCs.

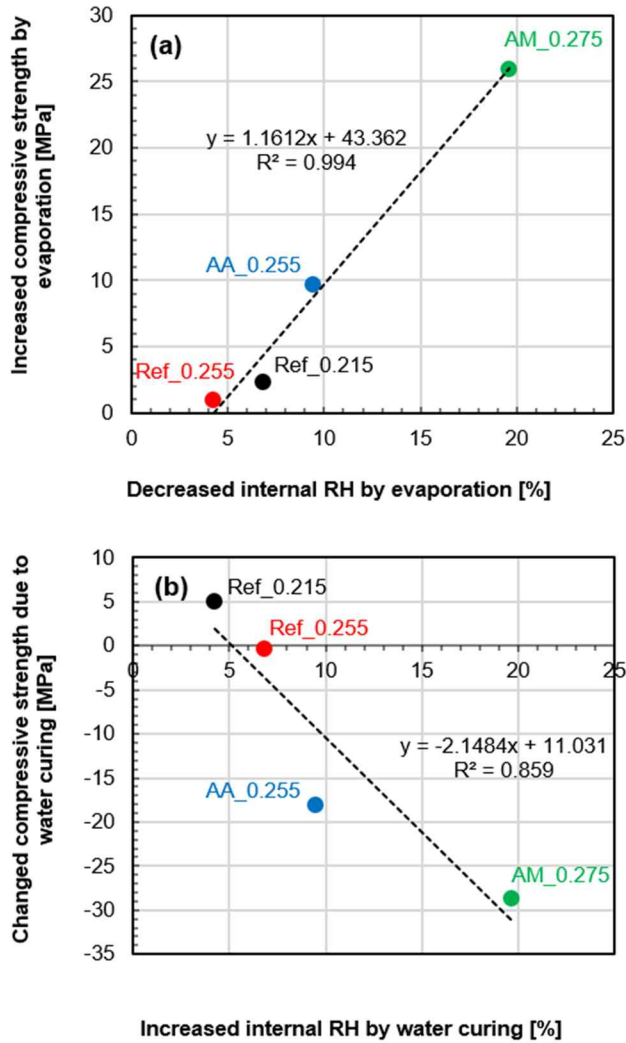


Fig. 5-21 Compressive strength change based on decreased internal RH by evaporation between 7 d and 28 d (a) and increased internal RH by water curing (b)

### **5.2.4 Summary and concluding remarks**

The severe early-age shrinkage and resulting cracking problems have to be preferentially resolved to widely use UHPC as overlay materials for old concrete structures. To verify one of the most promising solutions to this problem, this study investigated the effect of IC by SAP on the shrinkage and compressive strength of UHPC by considering the field curing condition. The field-cured UHPC (air-dried after 7 d of sealed curing) was compared with the water-cured UHPC to understand these properties as a function of the moisture content. In particular, the promotion of the hydration reaction, mitigation of self-desiccation, volume change, and the characteristics of compressive strength were clearly explained on the basis of the internal RH history.

Because of the water absorption and retention capacities of SAP, the cement hydration of UHPC was decelerated, lowering the height of the hydration peak. However, the water absorbed by SAP was released to the surrounding concrete after the acceleration period, and in turn the reaction was promoted during the deceleration period of cement hydration. The end time of this promotion was dependent on the type of SAP, especially its absorption capacities. The end time of SAP\_AA was less than 72 h, but that of SAP\_AM was greater than 72 h.

The history of the internal RH provided evidence of hydration promotion and the mitigation of self-desiccation. The RH history showed that the self-desiccation of UHPC cannot be prevented by external water curing owing to its extremely dense structure and low permeability. The IC by SAP had no

influence on the RH history before the start of self-desiccation, but it was significantly effective in increasing the internal RH once self-desiccation began. In particular, AM\_0.275 maintained the saturated condition without any internal drying, under the sealed or water-curing condition. However, as soon as UHPC was exposed to dry air, the addition of SAP accelerated the drying of internal moisture due to the changed pore structure. This rapid drying characteristic of the internally cured concrete, which is firstly discovered in this study, can be of benefit for overlay application. For instance, a short drying period is beneficial, especially to cover floor slabs with a decorative finish using an adhesive bond. The use of SAP can be also considered to accelerate drying of new concrete slabs for the same purpose.

The mitigation of self-desiccation by IC led to the prevention of AS, especially during the first 2 d. Thus, the reduced AS during the first 7 d of the sealed period predominantly contributed to the reduction in TS at 28 d. Because SAP is commonly included with extra water in concrete, it has proved impossible to reduce the DS of UHPC by IC. However, because the increased DS strain was much smaller than the decreased AS strain, IC was significantly effective in reducing the TS strain under the field curing condition. In addition, this method was more effective in reducing the strain rate, which is a more critical factor than the magnitude of strain in the risk of cracking. At an early age, when the risk is the highest within the lifetime of a low-w/c concrete, the possibility of cracking in UHPC was completely eliminated by IC. When UHPC was exposed to dry air, the strain rate suddenly increased during the first 2 d, but IC also effectively reduced the strain rate due to DS.

By using IC by SAP, the shrinkage-related problems of a field-cast low-w/c concrete can be solved without strength loss. The 28 d compressive strength of I-UHPC did not decrease with the 21 d of air-dry curing after 7 d. In other words, I-UHPCs had the same strength as the O-UHPC (Ref\_0.215) in which SAP and extra water was not included. However, the water curing affected the strength depending on whether UHPC contains SAP or not. The water curing conferred on O-UHPC the high internal RH condition, which is beneficial for the hydration reaction; as a result, the 28 d strength was slightly increased or maintained. On the other hand, the 28 d strength of I-UHPC remarkably decreased under the water-curing condition owing to the high moisture content as well as the changed pore structure. However, along with the rapid drying characteristic, the level of the content could reach that of O-UHPC within 2 weeks of the drying period, which facilitated complete recovery of the decreased strength.

From this study, it can be concluded that the mechanical properties of I-UHPC can be underestimated if it is cured not under the air-dry (field curing) condition but under the water (laboratory) curing condition. It was also confirmed that the addition of SAP accelerates the drying of a concrete. The first 7 d of sealed curing can ensure the benefits of IC, but more than 7 d of sealed curing can adversely affect the strength. Along with the outstanding mechanical properties, durability, and watertightness of UHPC, the new findings of this study support the use of I-UHPC as a promising overlay material for existing concrete structures.

## Chapter 6. Conclusions

Internally cured UHPC was successfully developed by water entrainment using SAP. This development was possible because the mix proportion of UHPC including SAP was designed optimally, and the designed concrete was mixed and cured appropriately. In addition, the water absorption and release behaviors of SAP in concrete, which has not been understood to date, was clearly explained.

A modified teabag method using a cement-based solution was proposed to measure the absorption capacity of SAP in concrete. Using this method, the capacity was accurately measured compared to the previous method because the excess solution which lowers the accuracy of the experiment, could be removed by a centrifugal process. Not only the excess solution, but the ion concentration and composition of the solutions used in the teabag method also contribute decisively to the accuracy of the measurement. The ion composition and concentration of the cement filtrate, which is the most commonly used solutions in the method to simulate a real cement pore solution for cement based materials, was measured. As a result, it was pointed out that this filtrate is unsuitable for the measurement of the capacity of SAP because the ion conditions of the filtrate are different with those of the pore solution. In other word, the w/c of this filtrate is significantly higher than the actual pore solution; while decreasing the concentrations of other ions, i.e., monovalent ions, this high w/c condition increases the concentration of calcium ion that affects the absorption capacity decisively. Particularly, these changes in ion concentrations

crucially affect to reduce the absorption capacity of polyacrylate SAP, which is the most widely used type for a commercial purpose. Therefore, the measurement of absorbency using conventional method and solution certainly underestimates the capacity of this type SAP. This underestimation problem was solved by compensating the diluted monovalent ions. In other words, by using the modified cement filtrate in which sodium hydroxide and potassium hydroxide were additionally dissolved, it was verified that the absorbency of this SAP is actually increased compared with that by the previous method in which pure cement filtrate is used. Because the ion condition of this modified filtrate is similar to that of the actual cement pore solution, it can be easily and reasonably used to measure the absorbency, absorption behavior and water retention capacity of the SAP in concrete.

Using the modified teabag method, the absorption behavior and water retention capacity of polyacrylate SAP were investigated in more detail. A new principle was established by this investigation, which clearly explains the variation of the retention capacity depending on the ion concentration and composition of a solution. This principle and phenomenon were experimentally verified. In summary, the concentration of the major ions (monovalent ions) in a cement pore solution determines the initial absorbency of SAP, thus, and the amount of the calcium ions trapped by SAP is influenced based of the initial absorbency, i.e., when the concentrations of monovalent ions are low, the osmotic pressure (driving force of absorption of SAP) increases, which increases the concentration of multivalent cation inside of SAP. Eventually, this increase in the concentration of multivalent cation additionally increases the cross-link density of SAP, which in turn reduces water retention and long-term

absorption capacities. This new discovery is a more evolutionary theory than the existing theory that has been reported the absorption capacity of SAP depends solely on the concentration of multivalent ions.

The variation of pore structure of UHPC as a function of IC using SAP was clearly confirmed by 3D-CT and MIP analysis. The promotion of the hydration reaction by IC made the pore structure denser within sub-micron size range. On the other hand, due to the large sized pores ( $> 0.5 \text{ mm}$ ) induced by swollen SAP particles, the total porosity of UHPC was significantly increased, which completely changed the pore structure.

The IC or water entrainment is a promising method that can completely solve the problems such as shrinkage by self-desiccation and the resulting cracking risk of both precast UHPC including heat treatment and field-cast UHPC. Because the heat treatment promoted the hydration reaction, the self-desiccation and autogenous shrinkage of UHPC was also accelerated. However, these were alleviated due to the additionally supplied water by SAP, which was effective in both ambient and high-temperature curing conditions. In the case of field-cast UHPC, as expected, the shrinkage and cracking risk were also completely eliminated by the addition of SAP. In particular, this study firstly verified that this method does not cause the loss of mechanical performance of UHPC under field curing conditions. To verify this, the internal RH history of UHPC was measured. Based on the test results, we pointed out that maintaining a high level of internal RH ( $> 80\%$ ) or saturation condition by the water entrainment for long periods, may be effective to reduce the self-desiccation and shrinkage, but is the cause of strength loss. However, due to the changed

pore structure by SAP particles, the drying speed of the concrete was accelerated under the field conditions. Therefore, the strength loss due to the increases in the total porosity and internal RH could be certainly solved. Considering the practical field curing condition as well as the drying period, the time to remove molds or seals of the internally cured field-cast UHPC was determined as the 7<sup>th</sup> day after casting concrete.

---

## References

Abell, A., Willis, K. & Lange, D. 1999. Mercury intrusion porosimetry and image analysis of cement-based materials. *Journal of colloid and interface science*, 211(1):39-44.

ACI Committee 308. 2001. *Guide to curing concrete*. Farmington Hills, Michigan, USA: American Concrete Institute.

Addari, D., Elsener, B. & Rossi, A. 2008. Electrochemistry and surface chemistry of stainless steels in alkaline media simulating concrete pore solutions. *Electrochimica Acta*, 53(27):8078-8086.

Aligizaki, K.K. 2006. *Pore structure of cement-based materials: testing, interpretation and requirements*. Abingdon, Oxfordshire, UK: Taylor & Francis.

American Concrete Institute. 2013. *ACI concrete terminology (ACI CT-13)*. Farmington Hills, Michigan, USA: American Concrete Institute.

American Society for Testing and Materials (ASTM) 2008. C 403/403M, Standard test method for time of setting of concrete mixtures by penetration resistance. West Conshohocken, USA: ASTM International.

American Society for Testing and Materials (ASTM) 2016. C 192/192M, Standard practice for making and curing concrete test specimens in the laboratory. West Conshohocken, USA: ASTM International.

Andersson, K., Allard, B., Bengtsson, M. & Magnusson, B. 1989. Chemical composition of cement pore solutions. *Cement and Concrete Research*, 19(3):327-332.

Assmann, A. 2013. *Physical properties of concrete modified with superabsorbent polymers*. Stuttgart, Germany: Stuttgart University.

Assmann, A. & Reinhardt, H.-W. 2013. The use of superabsorbent polymers to mitigate shrinkage of concrete. Proceedings of the 9th International Conference on Creep, Shrinkage, and Durability Mechanics (CONCREEP-9). Cambridge, Massachusetts, USA.

Association Française De Génie Civil (AFGC). 2013. *Ultra high performance fibre-reinforced concrete-Recommendations (Revised edition)*. Paris, France.

ASTM 2014. Standard specification for flow table for use in tests of hydraulic cement (C230/C230M-14). West Conshohocken, Pennsylvania, USA: ASTM International.

ASTM C1611 / 1611m 2014. Standard test method for slump flow of self-consolidating concrete. West Conshohocken, Pennsylvania, USA: ASTM international.

Azarijafari, H., Kazemian, A., Rahimi, M. & Yahia, A. 2016. Effects of pre-soaked super absorbent polymers on fresh and hardened properties of self-consolidating lightweight concrete. *Construction and Building Materials*,

113:215-220.

Bache, H.H. 1981. Densified cement ultra-fine particle-based materials.

Baroghel-Bouny, V., Mounanga, P., Khelidj, A., Loukili, A. & Rafaï, N. 2006. Autogenous deformations of cement pastes: part II. W/C effects, micro–macro correlations, and threshold values. *Cement and Concrete Research*, 36(1):123-136.

Bartlett, F.M. & Macgregor, J.G. 1995. Cores from high-performance concrete beams. *Materials Journal*, 91(6):567-576.

Bastien-Masse, M. & Brühwiler, E. 2016a. Composite model for predicting the punching resistance of R-UHPFRC–RC composite slabs. *Engineering Structures*, 117:603-616.

Bastien-Masse, M. & Brühwiler, E. 2016b. Experimental investigation on punching resistance of R-UHPFRC–RC composite slabs. *Materials and Structures*, 49(5):1573-1590.

Bentz, D.P. & Jensen, O.M. 2004. Mitigation strategies for autogenous shrinkage cracking. *Cement and Concrete Composites*, 26(6):677-685.

Bentz, D.P., Jones, S.Z., Peltz, M.A. & Stutzman, P.E. 2015. Mitigation of autogenous shrinkage in repair mortars via internal curing. *Concrete in Australia*, 41(4):35-39.

Bentz, D.P. & Weiss, W.J. 2011. *Internal curing: a 2010 state-of-the-art review*. US Department of Commerce, National Institute of Standards and Technology.

Beushausen, H. & Gillmer, M. 2014. The use of superabsorbent polymers to reduce cracking of bonded mortar overlays. *Cement and Concrete Composites*, 52:1-8.

Bonen, D. & Sarkar, S.L. 1995. The superplasticizer adsorption capacity of cement pastes, pore solution composition, and parameters affecting flow loss. *Cement and Concrete Research*, 25(7):1423-1434.

Boulekbache, B., Hamrat, M., Chemrouk, M. & Amziane, S. 2010. Flowability of fibre-reinforced concrete and its effect on the mechanical properties of the material. *Construction and Building Materials*, 24(9):1664-1671.

Brühwiler, E. & Denarié, E. 2008. Rehabilitation of concrete structures using ultra-high performance fibre reinforced concrete. Proceedings of the 2nd International Symposium on UHPC,. Kassel, Germany.

Brühwiler, E. & Denarié, E. 2013. Rehabilitation and strengthening of concrete structures using ultra-high performance fibre reinforced concrete. *Structural Engineering International*, 23(4):450-457.

Buchholz, F.L. 1994. Preparation methods of superabsorbent polyacrylates. ACS symposium series.

Buchholz, F.L. 1996. Superabsorbent polymers: An idea whose time has come. *Journal of chemical education*, 73(6):512-515.

Carette, J. & Staquet, S. 2015. Monitoring the setting process of mortars by ultrasonic P and S-wave transmission velocity measurement. *Construction and Building Materials*, 94:196-208.

Cement Concrete & Aggregates Australia (CCAA) 2007. Moisture in concrete and moisture-sensitive finishes and coatings. Sydney, Australia: Cement Concrete & Aggregates Australia.

Chang-Wen, M., Qian, T., Wei, S. & Jia-Ping, L. 2007. Water consumption of the early-age paste and the determination of “time-zero” of self-desiccation shrinkage. *Cement and Concrete Research*, 37(11):1496-1501.

Chem Tech Co. Ltd., A.K. 2003. Process for preparing bead-typed hydrogel (in korean). *Korean Intellectual Property Office*:1-10.

Chen, X., Huang, W. & Zhou, J. 2012. Effect of moisture content on compressive and split tensile strength of concrete. *Indian Journal of Engineering & Materials Sciences*, 19(6):427-435.

Craeye, B., De Schutter, G., Desmet, B., Vantomme, J., Heirman, G., Vandewalle, L., Cizer, Ø., Aggoun, S. & Kadri, E. 2010. Effect of mineral filler type on autogenous shrinkage of self-compacting concrete. *Cement and Concrete Research*, 40(6):908-913.

Craeye, B., Geirnaert, M. & De Schutter, G. 2011. Super absorbing polymers as an internal curing agent for mitigation of early-age cracking of high-performance concrete bridge decks. *Construction and Building Materials*, 25(1):1-13.

Cusson, D., Lounis, Z. & Daigle, L. 2010. Benefits of internal curing on service life and life-cycle cost of high-performance concrete bridge decks – A case study. *Cement and Concrete Composites*, 32(5):339-350.

Darquennes, A., Staquet, S., Espion, B., Robeyst, N. & De Belie, N. 2008. Autogenous shrinkage development and setting monitoring of slag cement concrete. Proceedings of the 8th International Conference on Creep, Shrinkage and Durability of Concrete Structures.

De La Varga, I., Castro, J., Bentz, D. & Weiss, J. 2012. Application of internal curing for mixtures containing high volumes of fly ash. *Cement and Concrete Composites*, 34(9):1001-1008.

De Larrard, F. & Sedran, T. 1994. Optimization of ultra-high-performance concrete by the use of a packing model. *Cement and Concrete Research*, 24(6):997-1009.

Di Bella, C., Griffa, M., Ulrich, T. & Lura, P. 2016. Early-age elastic properties of cement-based materials as a function of decreasing moisture content. *Cement and Concrete Research*, 89:87-96.

Drach, B., Drach, A. & Tsukrov, I. 2013. Characterization and statistical

modeling of irregular porosity in carbon/carbon composites based on X-ray microtomography data. *ZAMM-Journal of Applied Mathematics and Mechanics/Zeitschrift für Angewandte Mathematik und Mechanik*, 93(5):346-366.

Dudziak, L. & Mechtcherine, V. 2008. Mitigation of volume changes of ultra-high performance concrete (UHPC) by using super absorbent polymers. Second international symposium on ultra high performance concrete, . Kassel.

Eppers, S. & Müller, C. 2008. Autogenous shrinkage strain of ultra-high-performance concrete (UHPC). Proceedings of the 2nd International Symposium on UHPC,. Kassel, Germany.

Esteves, L.P. 2010. On the absorption kinetics of superabsorbent polymers. International RILEM conference on use of superabsorbent polymers and other new additives in concrete. Lyngby.

Esteves, L.P. 2015. Recommended method for measurement of absorbency of superabsorbent polymers in cement-based materials. *Materials and Structures*, 48(8):2397-2401.

Esteves, L.P., Cachim, P. & Ferreira, V.M. 2007. Mechanical properties of cement mortars with superabsorbent polymers. *Advances in Construction Materials*. Springer, .

Fehling, E., Schmidt, M., Walraven, J., Leutbecher, T. & Fröhlich, S. 2014. *Ultra-high performance concrete UHPC: Fundamentals, design, examples*.

John Wiley & Sons, .

Flory, P.J. 1953. *Principles of polymer chemistry*. Ithaca, United States: Cornell University Press.

Garas, V., Kurtis, K. & Kahn, L. 2012. Creep of UHPC in tension and compression: Effect of thermal treatment. *Cement and Concrete Composites*, 34(4):493-502.

Garas, V.Y., Kahn, L.F. & Kurtis, K.E. 2009. Short-term tensile creep and shrinkage of ultra-high performance concrete. *Cement and Concrete Composites*, 31(3):147-152.

Graybeal, B.A. 2006. Material property characterization of ultra-high performance concrete. McLean, Virginia, USA: Federal Highway Administration, US Department of Transportation.

Habel, K., Denarié, E. & Brühwiler, E. 2006. Structural response of elements combining ultra high-performance fiber-reinforced concretes and reinforced concrete. *Journal of Structural Engineering*, 132(11):1793-1800.

Han, Y., Zhang, J., Luosun, Y. & Hao, T. 2014. Effect of internal curing on internal relative humidity and shrinkage of high strength concrete slabs. *Construction and Building Materials*, 61:41-49.

Hasholt, M.T., Jensen, O.M., Kovler, K. & Zhutovsky, S. 2012. Can superabsorbent polymers mitigate autogenous shrinkage of internally cured

concrete without compromising the strength? *Construction and Building Materials*, 31:226-230.

Hasholt, M.T., Jensen, O.M. & Laustsen, S. 2015. Superabsorbent Polymers as a Means of Improving Frost Resistance of Concrete. *Advances in Civil Engineering Materials*, 4(1):237-256.

Hasholt, M.T., Jespersen, M.H.S. & Jensen, O.M. 2010. Mechanical properties of concrete with SAP. Part I: Development of compressive strength. *Use of Superabsorbent Polymers and Other New Additives in Concrete*.

Heinz, D. & Ludwig, H.-M. 2004. Heat treatment and the risk of DEF delayed ettringite formation in UHPC. 1st International Symposium on Ultra-High Performance Concrete Kassel, Germany.

Heinz, D., Urbonas, L. & Gerlicher, T. 2012. Effect of heat treatment method on the properties of UHPC. 3rd International Symposium on Ultra High Performance Concrete and Nanotechnology for High Performance Construction Materials. Kassel, Gemany.

Henkensiefken, R., Nantung, T. & Weiss, J. 2009. Internal curing-from the laboratory to implementation. 26th Annual International Bridge Conference. Pittsburgh, Pennsylvania, USA.

Hewlett, P. 2010. *Lea's chemistry of cement and concrete*, 4. Oxford, UK: Butterworth-Heinemann.

Holt, E. & Leivo, M. 2004. Cracking risks associated with early age shrinkage. *Cement and Concrete Composites*, 26(5):521-530.

Japan Society of Civil Engineers (JSCE). 2004. *Recommendations for design and construction of ultra high-strength fiber-reinforced concrete structures-Draft (in Japanese)*. Tokyo, Japan.

Jensen, O.M. 2013. Use of superabsorbent polymers in concrete. *Concrete international*, 35(1):48-52.

Jensen, O.M. & Hansen, P.F. 1996. Autogenous deformation and change of the relative humidity in silica fume-modified cement paste. *ACI Materials Journal*, 93(6):539-543.

Jensen, O.M. & Hansen, P.F. 2001a. Autogenous deformation and RH-change in perspective. *Cement and Concrete Research*, 31(12):1859-1865.

Jensen, O.M. & Hansen, P.F. 2001b. Water-entrained cement-based materials: I. Principles and theoretical background. *Cement and Concrete Research*, 31(4):647-654.

Jensen, O.M. & Hansen, P.F. 2002. Water-entrained cement-based materials: II. Experimental observations. *Cement and Concrete Research*, 32(6):973-978.

Jiang, C., Yang, Y., Wang, Y., Zhou, Y. & Ma, C. 2014. Autogenous shrinkage of high performance concrete containing mineral admixtures under

---

different curing temperatures. *Construction and Building Materials*, 61:260-269.

Jiang, Z., Sun, Z. & Wang, P. 2005. Autogenous relative humidity change and autogenous shrinkage of high-performance cement pastes. *Cement and Concrete Research*, 35(8):1539-1545.

Jignesh H. Trivedi, W.M., Young Huang and Harikrishna C. Trivedi. 2015. Photo-induced sodium salt of partially carboxymethylated psyllium-g-polyacrylonitrile: II. Synthesis, characterization and swelling behaviour of its superabsorbent hydrogel. *International Journal of Scientific and Research Publications (IJSRP)*, 5(5):14.

Justs, J., Wyrzykowski, M., Bajare, D. & Lura, P. 2015. Internal curing by superabsorbent polymers in ultra-high performance concrete. *Cement and Concrete Research*, 76:82-90.

Justs, J., Wyrzykowski, M., Winnefeld, F., Bajare, D. & Lura, P. 2014. Influence of superabsorbent polymers on hydration of cement pastes with low water-to-binder ratio. *Journal of Thermal Analysis and Calorimetry*, 115(1):425-432.

Kang, S.H., Gyephel, T., Hong, S.G. & Moon, J. 2015. Effect of water-entraining admixtures on the hydro-mechanical properties of ultra-high performance concrete. 14th International Congress on the Chemistry of Cement, Beijing, China.

Kang, S.H., Hong, S.G. & Moon, J. 2016a. Absorption kinetics of superabsorbent polymer (SAP) in various cement based solutions, in submit to the journal of Cement and Concrete Research.

Kang, S.H., Hong, S.G. & Moon, J. 2016b. Influence of internal curing by superabsorbent polymer on mechanical properties of ultra high performance concrete. 4th International Symposium on Ultra-High Performance Concrete and High Performance Materials. Kassel, Gemany.

Kang, S.H., Hong, S.G. & Moon, J. 2016c. Influence of internal curing on autogenous and drying shrinkages of ultra-high performance concrete considering heat treatment. fib Symposium 2016. Cape Town, South Africa.

Kang, S.H., Hong, S.G. & Moon, J. 2016d. Shrinkage characteristics of heat treated ultra-high performance concrete and its mitigation using superabsorbent polymer based internal curing method, in submit to the journal of Cement and Concrete Composites.

Kang, S.H., Wang, Z., Hong, S.G. & Moon, J. 2016e. Micro-computed tomography study on the pore structure of ultra-high performance concrete containing water-entraining admixture. 4th International Symposium on Ultra-High Performance Concrete and High Performance Materials. Kassel, Gemany.

Kasselouri, V., Kouloumbi, N. & Thomopoulos, T. 2001. Performance of silica fume-calcium hydroxide mixture as a repair material. *Cement and Concrete Composites*, 23(1):103-110.

Kendall, K., Howard, A., Birchall, J., Pratt, P., Proctor, B. & Jefferis, S. 1983. The relation between porosity, microstructure and strength, and the approach to advanced cement-based materials [and discussion]. *Philosophical Transactions of the Royal Society of London A: Mathematical, Physical and Engineering Sciences*, 310(1511):139-153.

Kiatkamjornwong, S. 2007. Superabsorbent polymers and superabsorbent polymer composites. *Sci. Asia*, 33(s1):39-43.

Kim, J. & Schlangen, E. 2010. Super absorbent polymers to simulate self healing in ECC. 2nd International Symposium on Service Life Design for Infrastructures.

Korea Concrete Institute (KCI). 2012. *Design recommendations for K-UHPC (in Korean)*. Seoul, Korea.

Korpa, A., Kowald, T. & Trettin, R. 2009. Phase development in normal and ultra high performance cementitious systems by quantitative X-ray analysis and thermoanalytical methods. *Cement and Concrete Research*, 39(2):69-76.

Kosmatka, S.H., Kerkhoff, B. & Panarese, W.C. 2011. *Design and control of concrete mixtures*. Portland Cement Association, .

Lampropoulos, A., Paschalis, S.A., Tsioulou, O. & Dritsos, S.E. 2016. Strengthening of reinforced concrete beams using ultra high performance fibre reinforced concrete (UHPFRC). *Engineering Structures*, 106:370-384.

Lankard, D.R. 1984. Slurry infiltrated fiber concrete (SIFCON): properties and applications. *MRS Proceedings*.

Larbi, J., Fraay, A. & Bijen, J. 1990. The chemistry of the pore fluid of silica fume-blended cement systems. *Cement and Concrete Research*, 20(4):506-516.

Lee, H., Lee, K., Kim, Y., Yim, H. & Bae, D. 2004. Ultrasonic in-situ monitoring of setting process of high-performance concrete. *Cement and Concrete Research*, 34(4):631-640.

Lee, H.X.D., Wong, H.S. & Buenfeld, N. 2010. Self-sealing cement-based materials using superabsorbent polymers. *Proceedings of International RILEM Conference on Use of Superabsorbent Polymers and Other New Additives in Concrete*, Lyngby, Denmark.

Lesti, M., Ng, S. & Plank, J. 2010. Ca<sup>2+</sup>-mediated interaction between microsilica and polycarboxylate comb polymers in a model cement pore solution. *Journal of the American ceramic society*, 93(10):3493-3498.

Lothenbach, B., Le Saout, G., Gallucci, E. & Scrivener, K. 2008. Influence of limestone on the hydration of Portland cements. *Cement and Concrete Research*, 38(6):848-860.

Lothenbach, B. & Winnefeld, F. 2006. Thermodynamic modelling of the hydration of Portland cement. *Cement and Concrete Research*, 36(2):209-226.

Lothenbach, B., Winnefeld, F. & Figi, R. 2007. The influence of superplasticizers on the hydration of Portland cement. Proceedings of the 12th International Congress on the Chemistry of Cement, . Montreal.

Loukili, A., Chopin, D., Khelidj, A. & Le Touzo, J.-Y. 2000. A new approach to determine autogenous shrinkage of mortar at an early age considering temperature history. *Cement and Concrete Research*, 30(6):915-922.

Loukili, A., Khelidj, A. & Richard, P. 1999. Hydration kinetics, change of relative humidity, and autogenous shrinkage of ultra-high-strength concrete. *Cement and Concrete Research*, 29(4):577-584.

Lura, P. 2003. *Autogenous deformation and internal curing of concrete*. Delft, Nederland: TU Delft, Delft University of Technology.

Lura, P., Durand, F., Loukili, A., Kovler, K. & Jensen, O.M. 2006. Compressive strength of cement pastes and mortars with superabsorbent polymers. International RILEM Conference on Volume Changes of hardening concrete: Testing and Mitigation.

Lura, P., Jensen, O.M. & Van Breugel, K. 2003. Autogenous shrinkage in high-performance cement paste: An evaluation of basic mechanisms. *Cement and Concrete Research*, 33(2):223-232.

Lura, P., Lothenbach, B., Miao, C., Ye, G. & Chen, H. 2010. Influence of pore solution chemistry on shrinkage of cement paste. The 50-year Teaching

and Research Anniversary of Prof. Sun Wei on Advances in Civil Engineering Materials. Nanjing.

Lura, P., Van Breugel, K. & Maruyama, I. 2001. Effect of curing temperature and type of cement on early-age shrinkage of high-performance concrete. *Cement and Concrete Research*, 31(12):1867-1872.

Markovic, I. 2006. *High-performance hybrid-fibre concrete: development and utilisation, PhD dissertation*. Delft University of Technology.

Maruyama, I. & Teramoto, A. 2012. Effect of water-retaining lightweight aggregate on the reduction of thermal expansion coefficient in mortar subject to temperature histories. *Cement and Concrete Composites*, 34(10):1124-1129.

Maruyama, I. & Teramoto, A. 2013. Temperature dependence of autogenous shrinkage of silica fume cement pastes with a very low water-binder ratio. *Cement and Concrete Research*, 50:41-50.

Mechtcherine, V., Dudziak, L., Schulze, J. & Staehr, H. 2006. Internal curing by super absorbent polymers (SAP) – Effects on material properties of self-compacting fibre-reinforced high performance concrete. International RILEM Conference on Volume Changes of Hardening Concrete: Testing and Mitigation. Lyngby, Denmark.

Mechtcherine, V., Gorges, M., Schroefl, C., Assmann, A., Brameshuber, W., Ribeiro, A.B., Cusson, D., Custódio, J., Da Silva, E.F. & Ichimiya, K. 2014. Effect of internal curing by using superabsorbent polymers (SAP) on

---

autogenous shrinkage and other properties of a high-performance fine-grained concrete: Results of a RILEM round-robin test. *Materials and Structures*, 47(3):541-562.

Mechtcherine, V. & Reinhardt, H.-W. 2012. *Application of super absorbent polymers (SAP) in concrete construction: State-of-the-art report prepared by Technical Committee 225-SAP*. Springer, .

Mechtcherine, V., Secieru, E. & Schröfl, C. 2015. Effect of superabsorbent polymers (SAPs) on rheological properties of fresh cement-based mortars-development of yield stress and plastic viscosity over time. *Cement and Concrete Research*, 67:52-65.

Meddah, M.S., Suzuki, M. & Sato, R. 2011. Influence of a combination of expansive and shrinkage-reducing admixture on autogenous deformation and self-stress of silica fume high-performance concrete. *Construction and Building Materials*, 25(1):239-250.

Meddah, M.S. & Tagnit-Hamou, A. 2009. Pore structure of concrete with mineral admixtures and its effect on self-desiccation shrinkage. *ACI Mater J*, 106(3):241-250.

Mehta, P.K. & Monteiro, P.J. 2006. *Concrete-microstructure, properties and materials*. New York, USA: McGraw-Hill.

Mönnig, S. 2009. *Superabsorbing additions in concrete: applications, modelling and comparison of different internal water sources*. Stuttgart,

Germany: University of Stuttgart.

Moragues, A., Macias, A. & Andrade, C. 1987. Equilibria of the chemical composition of the concrete pore solution. Part I: Comparative study of synthetic and extracted solutions. *Cement and Concrete Research*, 17(2):173-182.

Mounanga, P., Baroghel-Bouny, V., Loukili, A. & Khelidj, A. 2006. Autogenous deformations of cement pastes: Part I. Temperature effects at early age and micro–macro correlations. *Cement and Concrete Research*, 36(1):110-122.

Nagorski, H. 1994. Characterization of a new superabsorbent polymer generation. ACS symposium series.

Narayanan, S. 2016. How to guarantee design life of concrete structures? *The Masterbuilder India: The Masterbuilder*

National Precast Concrete Association (NPCA) 2013. Ultra high performance concrete (UHPC): Guide to manufacturing architectural precast UHPC elements. Carmel, USA.

Neville, A.M. 1981. *Properties of concrete*. London, UK: Pitman Press.

Noshiravani, T. & Brühwiler, E. 2013a. Experimental investigation on reinforced ultra-high-performance fiber-reinforced concrete composite beams subjected to combined bending and shear. *ACI Structural Journal*, 110(2):251-

261.

Noshiravani, T. & Brühwiler, E. 2013b. Rotation capacity and stress redistribution ability of R-UHPFRC–RC composite continuous beams: an experimental investigation. *Materials and Structures*, 46(12).

Page, C. & Vennesland, Ú. 1983. Pore solution composition and chloride binding capacity of silica-fume cement pastes. *Matériaux et Construction*, 16(1):19-25.

Piérard, J., Pollet, V., Cauberg, N., Jensen, O., Lura, P. & Kovler, K. 2006. Mitigating autogenous shrinkage in HPC by internal curing using superabsorbent polymers. International RILEM Conference on Volume Changes of Hardening Concrete: Testing and Mitigation. Lyngby, Denmark.

Plank, J., Schroeﬂ, C., Gruber, M., Lesti, M. & Sieber, R. 2009. Effectiveness of polycarboxylate superplasticizers in ultra-high strength concrete: The importance of PCE compatibility with silica fume. *Journal of Advanced Concrete Technology*, 7(1):5-12.

Pourjavadi, A., Fakoopoor, S.M., Hosseini, P. & Khaloo, A. 2013. Interactions between superabsorbent polymers and cement-based composites incorporating colloidal silica nanoparticles. *Cement and Concrete Composites*, 37:196-204.

Pourjavadi, A. & Mahdavinia, G.R. 2006. Superabsorbency, pH-sensitivity and swelling kinetics of partially hydrolyzed chitosan-g-poly

(acrylamide) hydrogels. *Turkish Journal of Chemistry*, 30(5):595-608.

Pourjavadi, A., Soleyman, R., Ghasemzadeh, H. & Salimi, H. 2010. CMC/celite superabsorbent composites: Effect of reaction variables on saline-absorbency under load. *Iranian Polymer Journal*, 19(8):571-579.

Powers, T. & Brownyard, T. 1948. *Studies of the physical properties of hardened Portland cement paste*. Research Laboratories of Portland Cement Association, .

Rechenberg, W. & Sprung, S. 1983. Composition of the solution in the hydration of cement. *Cement and Concrete Research*, 13(1):119-126.

Reda, M., Shrive, N. & Gillott, J. 1999. Microstructural investigation of innovative UHPC. *Cement and Concrete Research*, 29(3):323-329.

Reinhardt, H.-W. & Assmann, A. 2010. The effect of SAPs on drying shrinkage, porosity and setting of concrete. International RILEM Conference on Material Science. Aachen, Germany.

Reinhardt, H.-W., Grosse, C. & Herb, A. 2000. Ultrasonic monitoring of setting and hardening of cement mortar-a new device. *Materials and Structures*, 33(9):581-583.

Richard, P. & Cheyrezy, M. 1995. Composition of reactive powder concretes. *Cement and Concrete Research*, 25(7):1501-1511.

Sant, G. 2012. The influence of temperature on autogenous volume changes in cementitious materials containing shrinkage reducing admixtures. *Cement and Concrete Composites*, 34(7):855-865.

Schachinger, I., Hilbig, H. & Stengel, T. 2008. Effect of curing temperature at an early age on the long-term strength development of UHPC. 2nd International Symposium on Ultra High Performance Concrete. Kassel, Germany.

Schmidt, M. & Fehling, E. 2005. Ultra-high-performance concrete: Research, development and application in Europe. *ACI Special publication*, 228:51-78.

Schroefl, C., Mechtcherine, V., Vontobel, P., Hovind, J. & Lehmann, E. 2015. Sorption kinetics of superabsorbent polymers (SAPs) in fresh Portland cement-based pastes visualized and quantified by neutron radiography and correlated to the progress of cement hydration. *Cement and Concrete Research*, 75:1-13.

Schröfl, C., Mechtcherine, V. & Gorges, M. 2012. Relation between the molecular structure and the efficiency of superabsorbent polymers (SAP) as concrete admixture to mitigate autogenous shrinkage. *Cement and Concrete Research*, 42(6):865-873.

Selleng, C., Meng, B. & Fontana, P. 2016. Phase composition and strength of thermally treated UHPC. 4th International Symposium on Ultra-High

Performance Concrete and High Performance Materials. Kassel, Gemany.

Shen, D., Wang, T., Chen, Y., Wang, M. & Jiang, G. 2015. Effect of internal curing with super absorbent polymers on the relative humidity of early-age concrete. *Construction and Building Materials*, 99:246-253.

Shen, D., Wang, X., Cheng, D., Zhang, J. & Jiang, G. 2016. Effect of internal curing with super absorbent polymers on autogenous shrinkage of concrete at early age. *Construction and Building Materials*, 106:512-522.

Shimomura, T. & Namba, T. 1994. Preparation and application of high-performance superabsorbent polymers. ACS symposium series.

Shoukry, S.N., William, G.W., Downie, B. & Riad, M.Y. 2011. Effect of moisture and temperature on the mechanical properties of concrete. *Construction and Building Materials*, 25(2):688-696.

Siriwatwechakul, W., Siramanont, J. & Vichit-Vadakan, W. 2010. Superabsorbent polymer structures. International RILEM conference on use of superabsorbent polymers and other new additives in concrete. Lyngby.

Siriwatwechakul, W., Siramanont, J. & Vichit-Vadakan, W. 2012. Behavior of superabsorbent polymers in calcium-and sodium-rich solutions. *Journal of Materials in Civil Engineering*, 24(8):976-980.

Snoeck, D., Jensen, O.M. & De Belie, N. 2015a. The influence of superabsorbent polymers on the autogenous shrinkage properties of cement

---

pastes with supplementary cementitious materials. *Cement and Concrete Research*, 74:59-67.

Snoeck, D., Schaubroeck, D., Dubruel, P. & De Belie, N. 2014a. Effect of high amounts of superabsorbent polymers and additional water on the workability, microstructure and strength of mortars with a water-to-cement ratio of 0.50. *Construction and Building Materials*, 72:148-157.

Snoeck, D., Steuperaert, S., Van Tittelboom, K., Dubruel, P. & De Belie, N. 2012. Visualization of water penetration in cementitious materials with superabsorbent polymers by means of neutron radiography. *Cement and Concrete Research*, 42(8):1113-1121.

Snoeck, D., Van Tittelboom, K., Steuperaert, S., Dubruel, P. & De Belie, N. 2014b. Self-healing cementitious materials by the combination of microfibres and superabsorbent polymers. *Journal of Intelligent Material Systems and Structures*, 25(1):13-24.

Snoeck, D., Velasco, L., Mignon, A., Van Vlierberghe, S., Dubruel, P., Lodewyckx, P. & De Belie, N. 2015b. The effects of superabsorbent polymers on the microstructure of cementitious materials studied by means of sorption experiments. *Cement and Concrete Research*, 77:26-35.

Soliman, A. & Nehdi, M. 2011. Effect of drying conditions on autogenous shrinkage in ultra-high performance concrete at early-age. *Materials and Structures*, 44(5):879-899.

Soroka, I. 1979. *Portland cement paste and concrete*. Great Britain: The Macmillan Press Ltd.

Staquet, S., Boulay, C., Robeyst, N. & De Belie, N. 2008. Ultrasonic monitoring of setting and autogenous shrinkage development of high performance concrete. Proc. 8th International Conference on Creep, Shrinkage and Durability of Concrete and Concrete Structures (CONCREEP 8).

Sugano, S. 2008. Application of High-Strength and High-Performance Concrete in Seismic Regions. 8th HSC/HPC Symposium, Tokyo.

Tayeh, B.A., Bakar, B.A. & Johari, M.M. 2013. Characterization of the interfacial bond between old concrete substrate and ultra high performance fiber concrete repair composite. *Materials and Structures*, 46(5):743-753.

Taylor, H., Famy, C. & Scrivener, K. 2001. Delayed ettringite formation. *Cement and Concrete Research*, 31(5):683-693.

Termkhajornkit, P., Nawa, T., Nakai, M. & Saito, T. 2005. Effect of fly ash on autogenous shrinkage. *Cement and Concrete Research*, 35(3):473-482.

Toutlemonde, F. & Delort, M. 2016. The newly enforced French standard for UHPFRC specification, performance, production, and conformity. 4th International Symposium on Ultra-High Performance Concrete and High Performance Materials. Kassel, Germany.

Trtik, P., Münch, B., Weiss, W., Herth, G., Kaestner, A., Lehmann, E., Lura,

P. & Brameshuber, W. 2010. Neutron tomography measurements of water release from superabsorbent polymers in cement paste. International RILEM conference on material science. Aachen.

Tue, N.V., Ma, J. & Orgass, M. 2008. Influence of addition method of superplasticizer on the properties of fresh UHPC. Proceedings of Second International Symposium on Ultra High Performance Concrete, University of Kassel, Germany.

Van Den Abeele, K., Desadeleer, W., De Schutter, G. & Wevers, M. 2009. Active and passive monitoring of the early hydration process in concrete using linear and nonlinear acoustics. *Cement and Concrete Research*, 39(5):426-432.

Van Tittelboom, K. & De Belie, N. 2013. Self-healing in cementitious materials—A review. *Materials*, 6(6):2182-2217.

Vande Voort, T.L., Suleiman, M.T. & Sritharan, S. 2008. Design and performance verification of ultra-high performance concrete piles for deep foundations. Iowa State University.

Wallevik, O.H. & Wallevik, J.E. 2011. Rheology as a tool in concrete science: The use of rheographs and workability boxes. *Cement and Concrete Research*, 41(12):1279-1288.

Wang, F., Yang, J., Cheng, H., Wu, J. & Liang, X. 2015. Study on mechanism of desorption behavior of saturated superabsorbent polymers in concrete. *ACI Materials Journal*, 112(3):463-470.

Wang, F., Zhou, Y., Peng, B., Liu, Z. & Hu, S. 2009. Autogenous shrinkage of concrete with super-absorbent polymer. *ACI Materials Journal*, 106(2):123-127.

Wille, K., Naaman, A.E. & Parra-Montesinos, G.J. 2011. Ultra-high performance concrete with compressive strength exceeding 150 MPa (22 ksi): A simpler way. *ACI Materials Journal*, 108(1):46-54.

Wittmann, F. 1973. Interaction of hardened cement paste and water. *Journal of the American ceramic society*, 56(8):409-415.

Wyrzykowski, M. & Lura, P. 2013. Controlling the coefficient of thermal expansion of cementitious materials – A new application for superabsorbent polymers. *Cement and Concrete Composites*, 35(1):49-58.

Yang, Y., Sato, R. & Kawai, K. 2005. Autogenous shrinkage of high-strength concrete containing silica fume under drying at early ages. *Cement and Concrete Research*, 35(3):449-456.

Yazıcı, H., Deniz, E. & Baradan, B. 2013. The effect of autoclave pressure, temperature and duration time on mechanical properties of reactive powder concrete. *Construction and Building Materials*, 42:53-63.

Yoo, D.-Y., Banthia, N. & Yoon, Y.-S. 2015. Effectiveness of shrinkage-reducing admixture in reducing autogenous shrinkage stress of ultra-high-performance fiber-reinforced concrete. *Cement and Concrete Composites*, 64:27-36.

Yoo, D.-Y., Min, K.-H., Lee, J.-H. & Yoon, Y.-S. 2014. Shrinkage and cracking of restrained ultra-high-performance fiber-reinforced concrete slabs at early age. *Construction and Building Materials*, 73:357-365.

Zanni, H., Cheyrezy, M., Maret, V., Philippot, S. & Nieto, P. 1996. Investigation of hydration and pozzolanic reaction in reactive powder concrete (RPC) using  $^{29}\text{Si}$  NMR. *Cement and Concrete Research*, 26(1):93-100.

Zhang, M., Tam, C. & Leow, M. 2003. Effect of water-to-cementitious materials ratio and silica fume on the autogenous shrinkage of concrete. *Cement and Concrete Research*, 33(10):1687-1694.

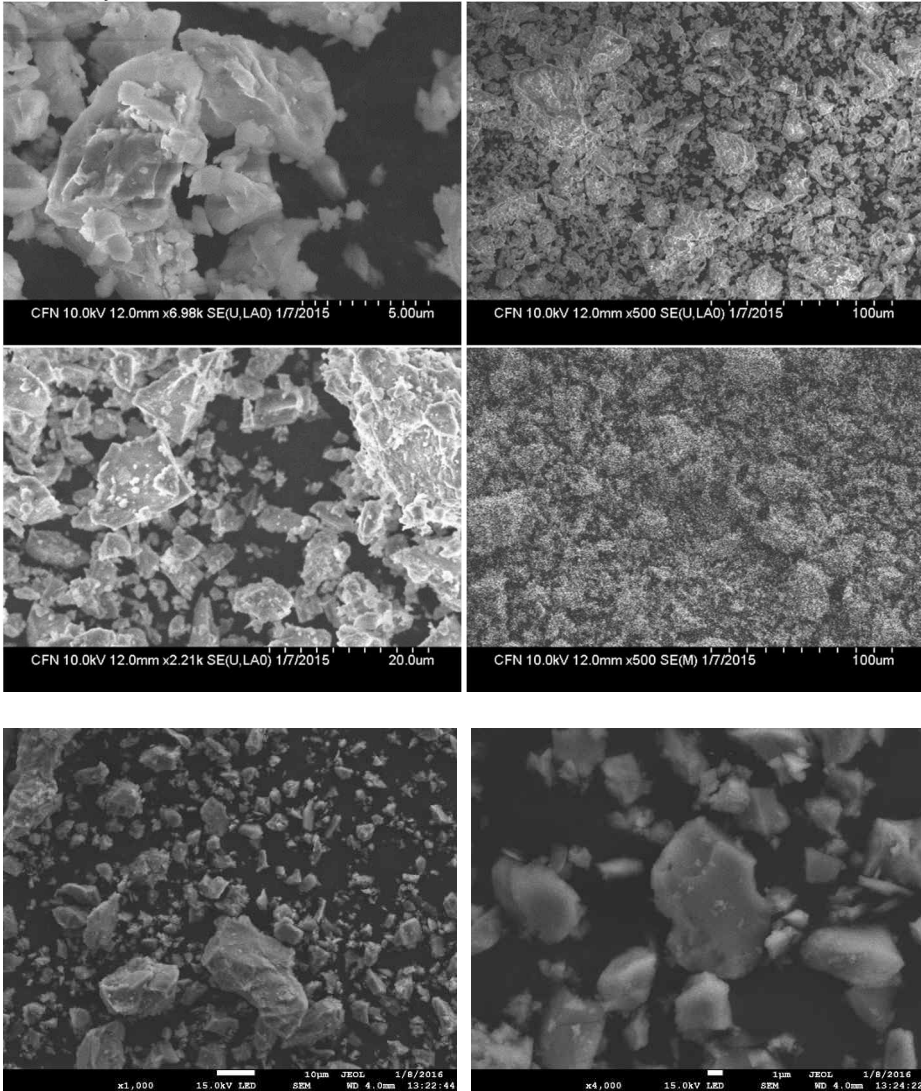
Zhang, Y., Zhang, W., She, W., Ma, L. & Zhu, W. 2012. Ultrasound monitoring of setting and hardening process of ultra-high performance cementitious materials. *NDT & E International*, 47:177-184.

Zhu, Q., Barney, C.W. & Erk, K.A. 2015. Effect of ionic crosslinking on the swelling and mechanical response of model superabsorbent polymer hydrogels for internally cured concrete. *Materials and Structures*, 48(7):2261-2276.

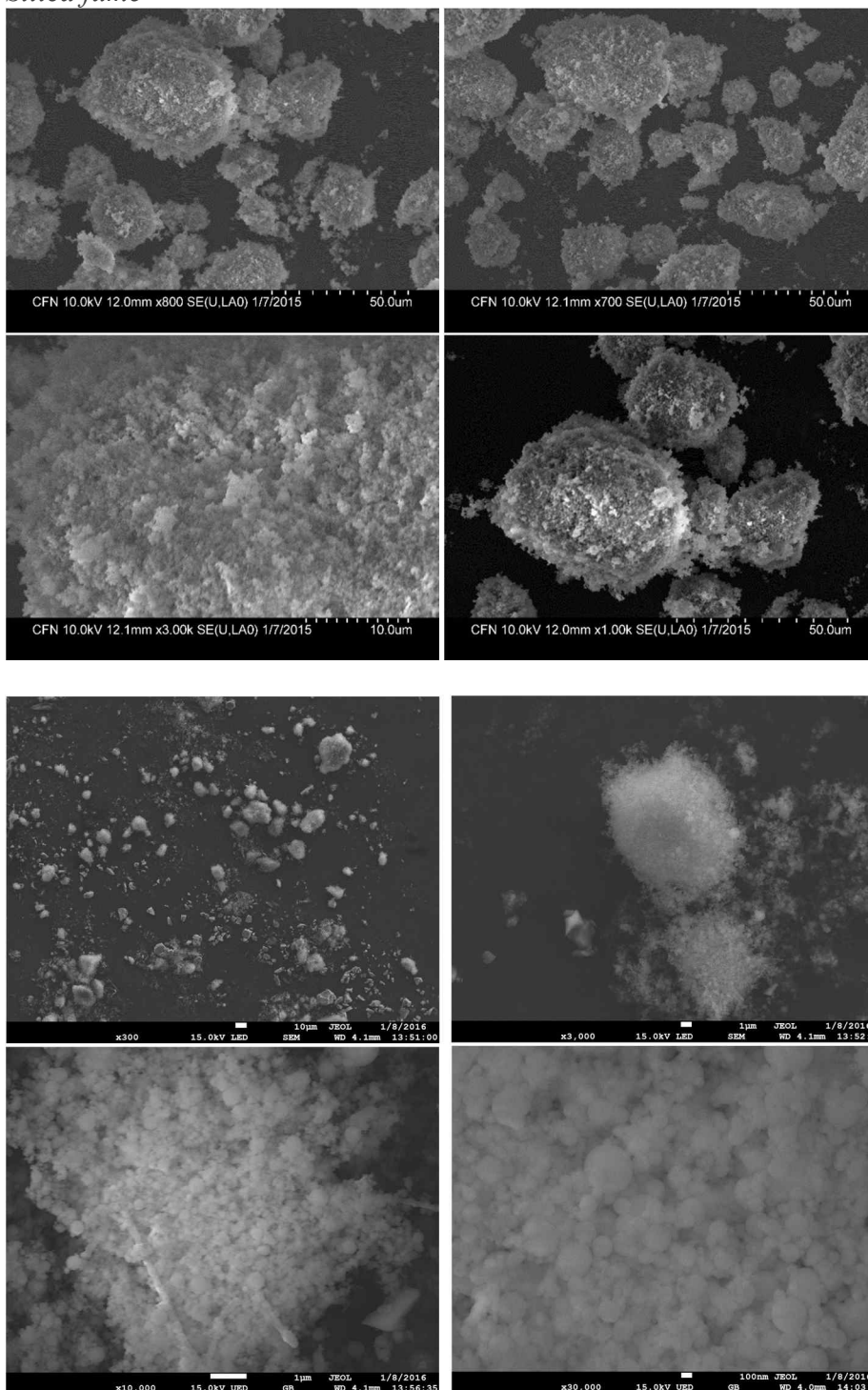
Zohuriaan-Mehr, M.J. & Kabiri, K. 2008. Superabsorbent polymer materials: A review. *Iranian Polymer Journal*, 17(6):451-477.

## Appendix A. SEM images of raw materials and UHPC samples

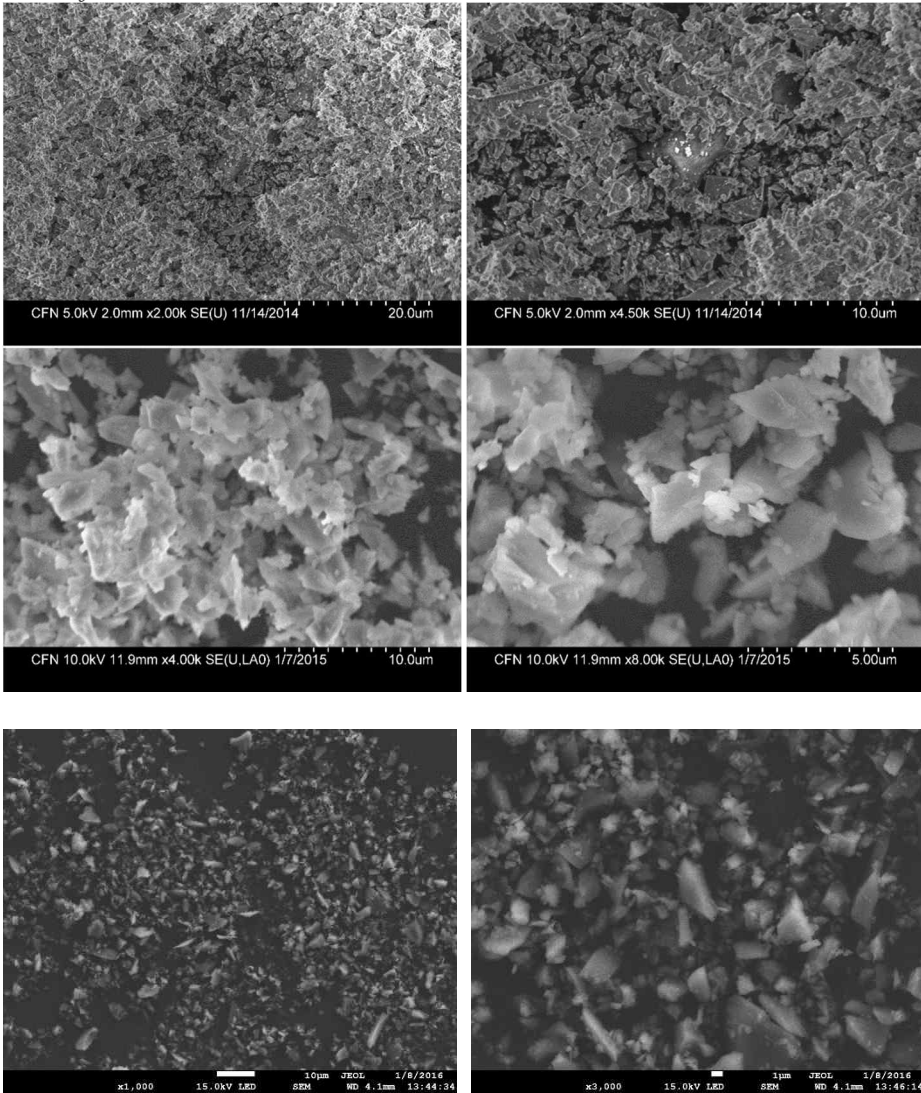
### *Ordinary Portland cement*



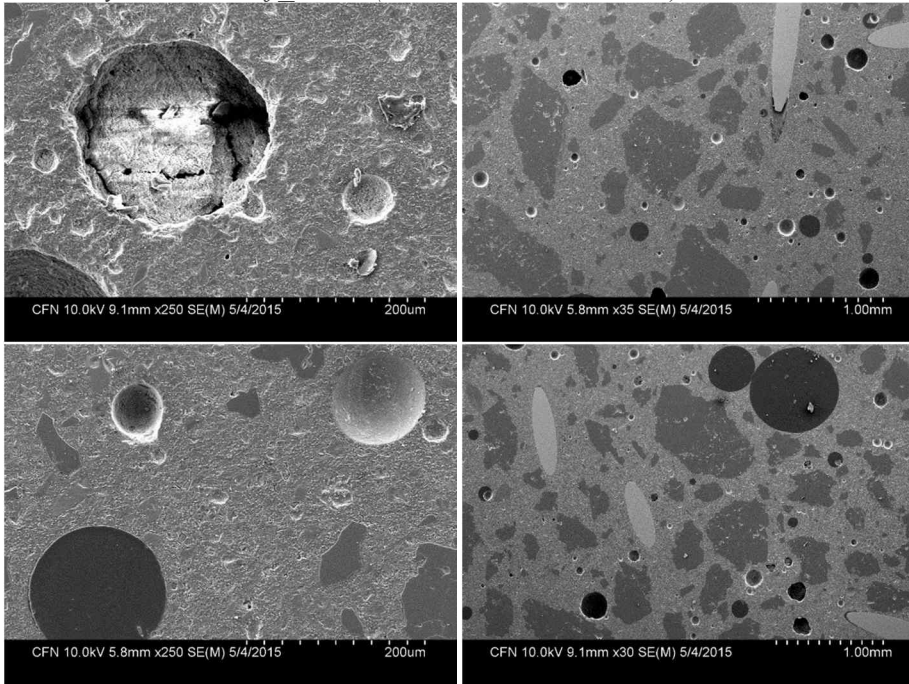
*Silica fume*



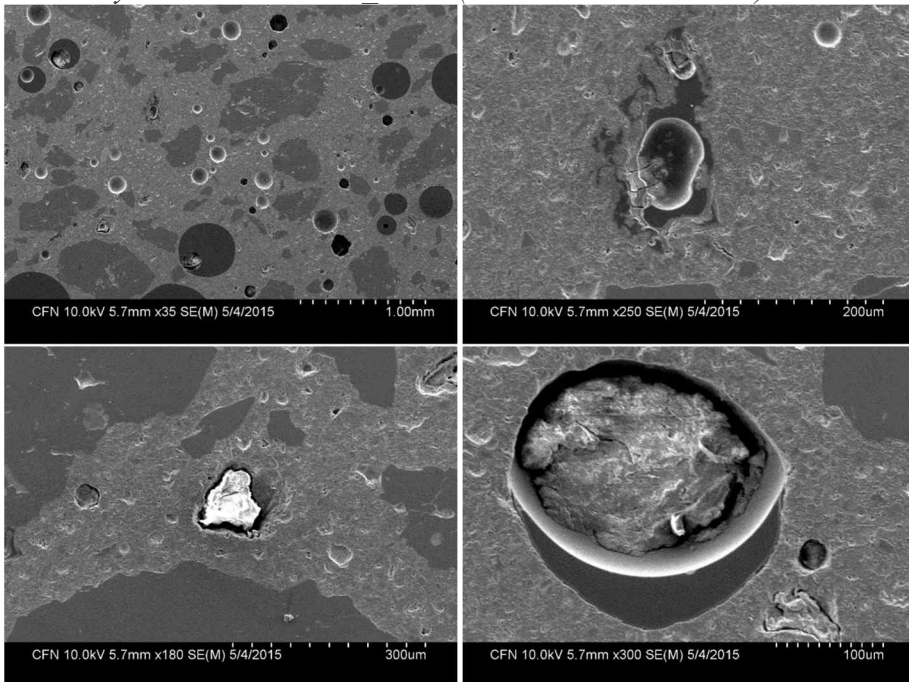
*Silica flour*



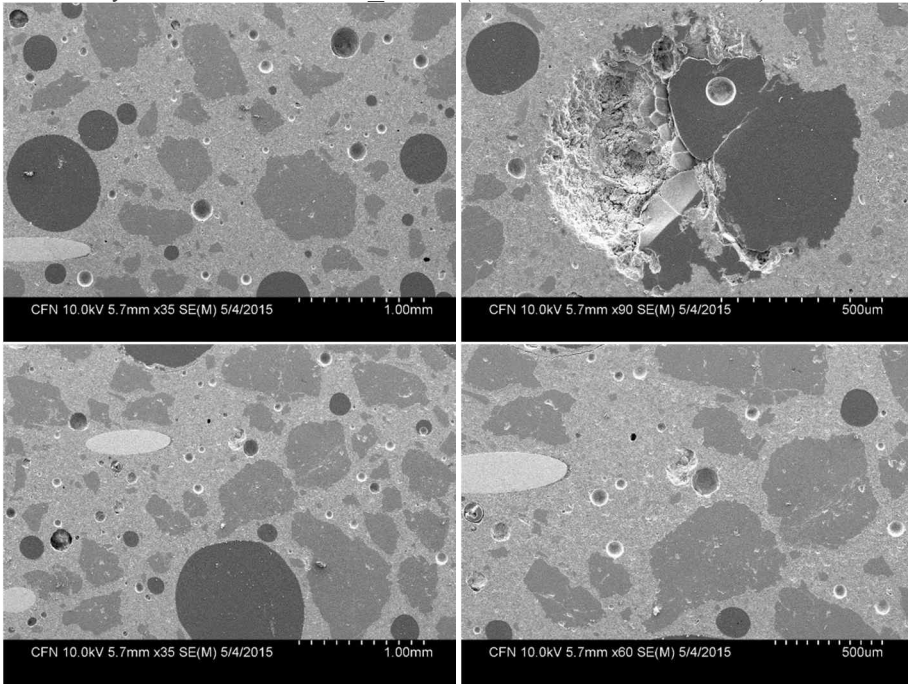
*Ordinary UHPC: Ref 0.215 (without heat treatment)*



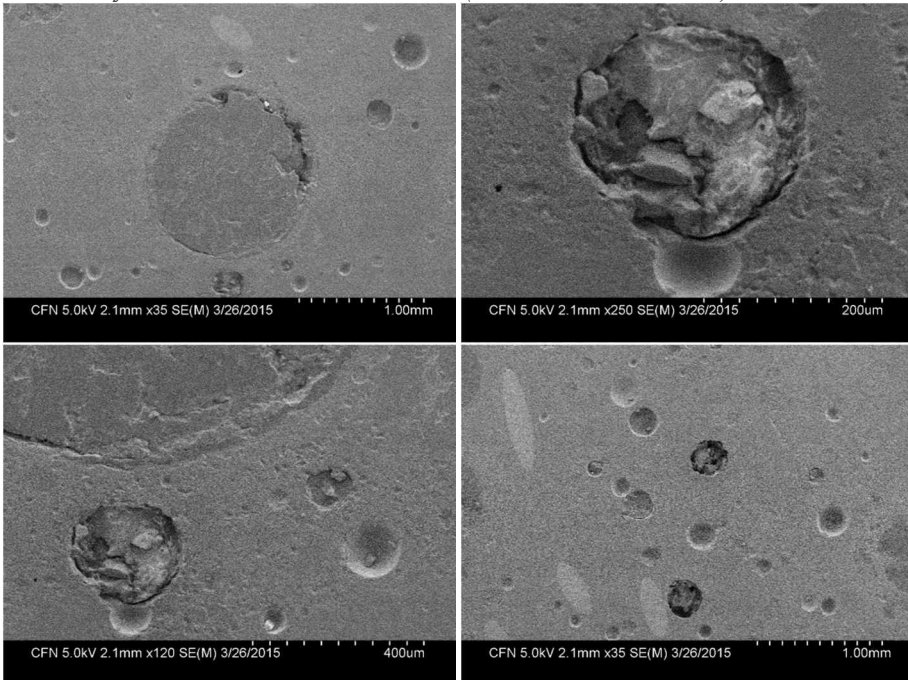
*Internally cured UHPC: AA 0.255 (without heat treatment)*



*Internally cured UHPC: AM 0.275 (without heat treatment)*



*Internally cured UHPC: AM 0.275 (with heat treatment)*



## 초 록

이 연구를 통해 고흡수성 수지 (SAP)를 이용하여 내부 양생된 초고성능 콘크리트 (UHPC)가 개발되었다. SAP은 뛰어난 흡수능력뿐만 아니라 가격 경쟁력에서의 장점 덕분에 낮은 물-시멘트 비 콘크리트의 수축저감제로서 주목 받고 있다. 개발된 콘크리트는 SAP과 같은 수분저장소를 자체적으로 포함하고 있기 때문에, 외부적인 양생(수중양생 또는 살수양생) 없이도 그것의 심각한 자기건조와 이로 인한 자기수축이 차단된다. 그러나, SAP은 물 또는 용액을 흡수하면서 체적이 건조상태 대비 각각 수백 또는 수십 배까지 증가한다. 따라서, 이러한 콘크리트 내부에는 수분저장소 뿐만 아니라, 강도감소의 원인이 되는 큰 공극들이 추가로 형성된다. 그럼에도 불구하고, 실제로 강도가 감소가 발생하지 않는다. 그 이유는 저장소로부터 방출되는 추가적인 수분에 의해 수화반응이 촉진되고, 이는 강도 증가에 기여하기 때문이다. 이러한 추가적인 수분방출은 이 콘크리트의 수분함량 또는 내부습도를 증가시키며, 이는 자기건조와 자기수축을 차단시키는 원인이다. 따라서, UHPC의 수축으로

인한 균열위험성은 제거될 수 있다. 그러나, 콘크리트의 높은 내부습도는 강도와 같은 역학적 성능감소에 기여하는 또 다른 요인이다. 이러한 요인에 의한 강도감소 역시 막을 수 있는데, 왜냐하면 SAP 혼입에 의해 바뀐 공극구조 때문에 내부수분이 건조되는 속도가 더 빨라지기 때문이다.

자기건조를 막기 위해 SAP과 함께 혼입되어야 하는 추가적인 물을 추가수라고 하며, 필요한 양은 기존 이론에 의해 설계될 수 있다. 그러나, 콘크리트의 유동성과 강도 손실 없이 균열위험성이 완전히 제거될 수 있는 이상적인 결과는, 콘크리트 내부에서 SAP이 정확히 설계된 추가수만을 흡수할 경우에만 가능하다. 다시 말해, 만약 SAP이 설계된 물 보다 더 적거나 더 많은 양의 물을 흡수한다면, 역학적 성능과 유동성이 각각 감소하는 상황으로 이어진다. 따라서, 먼저 기존 이론에 의해 추가수의 양이 설계된 상황에서, SAP 혼입율이 최적으로 결정되어야 하는데, 이것은 콘크리트 내부 환경에서 SAP의 흡수 및 수분 유지능력이 완벽히 이해되어야 가능하다. 이것을 이해하는 것은 현재까지 충분히 설명되고 있지 않은, 낮은 물-시멘트 비 콘크리트 내부에서의 SAP의 흡수 및 수분방출 거동을 설명하기 위해서도 반드시 필요하다. 이번 연구를 통해 이러한 복잡한 거동들이 밝혀졌다.

이를 위한 첫 번째 단계로, 다양한 시멘트 기반 용액들 내부에 위치한 SAP의 흡수력을 측정할 수 있는 방법이 제안되었다. 이 방법은 원심분리 탈수법을 포함하고 있으며, 흡수력 결정에 있어 심각한 오차의 원인으로 기여하는 SAP 입자들 사이에 갇힌 물이 이 방법에 의해 제거될 수 있다. 일정한 2가 양이온 농도 조건에서, 1가 이온들의 농도에 의존하여 SAP의 흡수거동은 확실하게 변한다. 이러한 결과를 기반으로 SAP의 흡수력이 과소평가 될 수 있는 가능성을 제기하였다. 이 연구에서 제안한 흡수력 측정법과 시멘트 기반 용액들은 SAP의 혼입율을 결정하기 위한 예비실험에 합리적이고 효율적으로 활용 될 수 있다. 더욱이, 연구에서 확인된, 용액의 이온 환경에 의존하는 SAP의 흡수거동은 그것의 특성을 이해하는데 도움을 줄 수 있을 뿐만 아니라, 콘크리트를 위한 전용 SAP 제품을 개발 하는데도 기여 할 수 있다.

이와 더불어, 시멘트 기반 용액의 이온 농도 및 조합에 의존하여 달라지는 SAP의 수분 유지능력도 체계적으로 조사되었다. 이온농도 이력과 SAP의 흡수력을 측정하여, 용액 속 칼슘 이온과 SAP 내부의 음이온간 비 가역 이온교환이 발생하는 것, 그리고 동시에 장기흡수력이 감소하는 현상이

검증되었다. 따라서, 칼슘이온 농도는 SAP의 흡수력뿐만 아니라 수분 유지능력에도 결정적인 영향을 미치는 주요 요인이다. 그러나, 칼슘 뿐만 아니라 나머지 1가 이온들의 농도 역시 흡수력과 수분유지능력에 중대한 영향을 미치는 것으로 확인되었다. 즉, 총 이온농도의 증가와 함께 수분유지 능력도 증가하였는데, 여기에는 1가 이온들의 농도 증가가 결정적으로 기여한다. 그리고 용액의 이온농도 증가는 SAP의 흡수 유발 요인인 삼투압을 감소시키므로, 최대흡수력과 함께 SAP으로 흡수되는 칼슘 이온농도가 감소된다. 따라서 결국 수분유지 능력은 향상된다. 이와 같은 검증 덕분에 시멘트 기반 용액의 이온구성에 의존하는 복잡한 SAP의 흡수거동이 이해 될 수 있다.

SAP에 의해 내부 양생된 UHPC의 공극구조 특성이 수은압입법 (MIP)과 3차원 CT 해석에 의해 광범위하게 조사되었다. 우선, CT 해석에 의해 SAP 입자들에 의해 형성된 UHPC 내부의 공극들이 다른 공극들 (간헐 공기, 연행된 공기 등)과 성공적으로 분리 되었다. 그 결과, SAP의 혼입 유무에 따라 UHPC의 총 공극률은 각각 6.0%와 2.5%로 확인되었고, 이는 추가로 형성된 큰 공극들에 의해 UHPC의 총 공극율이 극적으로 증가되는 것을 보여준다.

이러한 공극률 증가는 압축강도와 같은 역학적 성능 감소의 원인이 될 수 있다. 그러나, MIP 해석에 의해 이와 같은 강도감소 요인이 보상될 수 있는 가능성이 확인되었다. 즉, 내부양생에 의해 수화생성물이 추가로 발생하는데, 이것이 강도와 관계되는 모세관 공극률을 감소시켰다. 사용된 두 방법들이 공극률에 관해 서로 다른 결과를 보여준 이유는 각 방법에 의해 확인 될 수 있는 공극 크기가 서로 다르기 때문이다. 이러한 두 방법들을 사용함으로써, 내부양생에 의한 수화반응 촉진과, 물을 흡수하고 부푼 SAP 입자들에 의해 형성된 큰 크기의 공극들 모두가 확인될 수 있었다.

확인된 결과들 (SAP의 흡수거동 및 수분유지 능력, SAP을 이용한 내부양생이 수화반응 정도와 공극구조에 미치는 영향)을 기반으로 하여, 개발된 UHPC의 수화 반응성, 수축, 내부 습도 및 역학적 성능이 SAP 포함 여부를 주요 변수로 두고 조사되었다. 특히, UHPC의 현실적인 활용 현황을 고려하여 이와 같은 조사는 열처리를 포함하는 프리캐스트 UHPC와 그것을 포함하지 않는 현장타설 UHPC로 구분하여 진행되었다. 우선, 열처리된 UHPC의 수축특성이 밝혀졌고, 열처리 기간 동안의 수축균열 위험성이 내부양생으로 해결 될 수 있다는 사실을 확인하였다. 즉, 열처리 구간 동안의

고온양생 조건이 수화반응과 이로 인한 자기건조를 가속화시키고, 따라서 자기수축 역시 급격하게 증가하였다. 그러나, SAP에 의한 수분방출은 열처리 기간 동안에도 유효하며, 따라서 이 기간 동안의 심각한 자기건조와 자기수축이 완화되는 사실이 확인되었다. 이러한 새로운 검증 덕분에 SAP을 이용한 내부양생이 열처리된 UHPC의 수축저감 방법으로 활용 될 수 있다.

이 방법은 현장타설 UHPC의 수축 및 균열저감에도 역시 탁월한 효과를 보였다. 이러한 검증을 위해 콘크리트의 수화열, 내부습도 이력, 압축강도 및 수축변형이 시간에 따라 정확하게 측정되었다. 특히, 내부양생에 의존하는 UHPC의 내부습도가 이 실험에서 주요변수로 고려되었다. 실제로, 수화반응 촉진과 자기건조의 완화는 내부습도 이력과 밀접하게 연관된 것으로 확인되었다. 또한, 내부습도를 높게 유지하는 것이 강도감소의 요인이 되는 것을 확인하였다. 그러나, 이러한 강도감소 요인은 SAP을 포함하는 UHPC가 현장타설 조건에서 양생 될 경우 효력을 미치지 못했다. 그 이유는 SAP 혼입에 의해 변경된 공극 구조는 콘크리트 내부습도의 건조속도를 가속화시켰기 때문이다. 내부습도에 의해 상반적인 영향을 받는 수축 및 강도 모두를 고려할 때, 합리적인 밀봉기간은 초기 7일로

제안되었다. 이 조건은 일반적으로 시방서에 명시된 현장타설 콘크리트의 양생조건과도 일치한다.

UHPC의 심각한 수축과 이로 인한 균열위험성은 SAP을 이용한 내부양생을 이용하여 완전히 해결될 수 있다. 이 방법은 실용성과 가격경쟁력 모두에 있어 부정적인 영향을 미치지 않는다. 새롭게 제시된 실험방법들 (즉, 콘크리트 내부에서 SAP의 흡수거동, 고온양생을 포함하는 UHPC의 수축, 그리고 UHPC의 내부습도의 측정방법)은 다른 연구들의 새로운 실험결과 도출에도 기여할 수 있다. 또한, 최초로 발견된 실험결과들 (낮은 물-시멘트 비 콘크리트 내부에서 SAP의 흡수 및 수분유지 거동, 열처리 된 UHPC의 심각한 수축특성, SAP 혼입에 의해 가속화된 수분건조 속도 및 이로 인한 강도회복)은 실험적 증거로서, 콘크리트 분야에서 실제로 내부양생이 널리 활용 될 수 있도록 기여할 수 있다.

**주요어 :** 초고성능 콘크리트, 내부양생, 수분연행, 고흡수성 수지, 자기건조, 자기수축

**학 번 :** 2010-30158